From local to global scale - Marine emissions of the climate relevant sulfur gases carbonyl sulfide, carbon disulfide and dimethyl sulfide

Dissertation
zur Erlangung des Doktorgrads
der Mathematisch-Naturwissenschaftlichen Fakultät
der Christian-Albrechts Universität zu Kiel
vorgelegt von

Sinikka T. Lennartz

Kiel, 2017

From local to global scale - Marine emissions of the climate relevant sulfur gases carbonyl sulfide, carbon disulfide and dimethyl sulfide

Dissertation
zur Erlangung des Doktorgrads
der Mathematisch-Naturwissenschaftlichen Fakultät
der Christian-Albrechts Universität zu Kiel
vorgelegt von

Sinikka T. Lennartz

Kiel, 2017

Referentin: Prof. Dr. Christa A. Marandino
Koreferent: Prof. Dr. Hermann W. Bange

Tag der mündlichen Prüfung: 28.07.2017
Zum Druck genehmigt: 28.07.2017

Gez. Prof. Dr. Natascha Oppelt, Dekanin

Eidesstattliche Erklärung

Hiermit erkläre ich,

Sinikka T. Lennartz,

dass ich diese Doktorarbeit selbstständig verfasst sowie alle wörtlichen und inhaltlichen Zitate als solche gekennzeichnet habe.

Die Arbeit wurde unter Einhaltung der Regeln guter wissenschaftlicher Praxis der Deutschen Forschungsgemeinschaft verfasst.

Sie hat weder ganz noch in Teilen einer anderen Stelle im Rahmen eines Prüfungsverfahrens vorgelegen.

Kiel, den 16.05.2017

Abstract

Sulfur containing trace gases have gained attention due to their impact on the Earth's radiative budget and, thus, the climate on our planet. The ocean is a major natural source of the gases carbonyl sulfide (OCS), carbon disulfide (CS_2) and dimethyl sulfide (DMS). Understanding and quantifying their oceanic emissions is critical to decipher their present and future contribution to aerosol formation in the stratosphere (OCS) and troposphere (DMS, CS_2). These aerosols exert a natural cooling effect on surface temperatures and therefore counteract global warming. In addition, a well known atmospheric budget of OCS helps to constrain processes in the carbon cycle, in particular the terrestrial CO_2 uptake (gross primary production). This is needed to assess the response of the terrestrial biosphere to changing climate conditions. Both, climate predictions and constraining the carbon cycle using OCS, require well quantified sources and sinks of these gases in the atmosphere. However, especially the marine emissions are still associated with considerable uncertainties. A large gap in the atmospheric budget of OCS currently impedes conclusions about trends in stratospheric aerosol formation or gross primary production on a global level. Tropical oceanic emissions of OCS and its precursor gas CS_2, potentially also DMS, have been suggested to account for the missing source. In this thesis, newly developed measurement systems as well as numerical models were used in three studies to quantify marine emissions of OCS, CS_2 and DMS on local, regional and global scale in order to reduce existing uncertainties.

In the first study, the optimal representation of oceanic emissions in atmospheric models was systematically assessed. Atmospheric chemistry climate models provided with accurate boundary conditions are powerful tools to assess present and predict future climate. Such boundary conditions include emissions of gases from the ocean. The optimal method to represent these emissions in global atmospheric chemistry climate models was investigated by comparing a set-up with prescribed water concentrations and online calculation of emissions to a prescribed static flux climatology. The results indicated that simulated atmospheric mixing ratios agreed best with observations if emissions were calculated

online from prescribed sea surface concentration maps for gases that are concentrated close to equilibrium in the surface ocean. Gases further away from equilibrium concentrations were less sensitive towards online calculation of emissions.

While global DMS surface concentration maps are available in monthly resolution, oceanic measurements of OCS and CS_2 are still very scarce. Therefore, measuring and modeling sea surface concentrations of OCS, the latter both regionally in the tropics and globally, was the goal of the second study. A novel underway measurement system was developed to measure the trace gas OCS continuously and autonomously during two research cruises. The study areas focused on tropical regions with respect to the missing source of atmospheric OCS. Two contrasting regions, an oligotrophic region in the Indian Ocean as well as the highly productive eastern tropical South Pacific, were chosen to obtain a wide range of concentration variability. The new observations from the tropical regions were used in conjunction with existing data to derive a parameterization for marine photoproduction of OCS, which, for the first time, combines data from three major ocean basins. The parameterization was used to simulate global sea surface concentrations for OCS and derive a global emission estimate of 130 (±80) Gg S yr^{-1}. Results prove the dominant role of marine emissions in the atmospheric budget of OCS, which are nonetheless too low to account for the missing source. Emission estimates of the two other precursor gases complemented the inventory. Despite larger uncertainties in their contributions to the OCS budget, they are also unlikely to fill the gap in the atmospheric budget of OCS.

Characterizing the marine biogeochemical cycling of CS_2 and OCS in the water column to reduce these uncertainties was subject of the third study. For the first time, both gases were simultaneously measured in the water column of the highly productive eastern tropical South Pacific. A newly developed 1D water column model within the modeling framework GOTM/FABM was used to systematically assess their marine cycling. Model simulations for OCS agreed well with measurements in and below the mixed layer. Additionally, a new parameterization for OCS light-independent production was derived, which confirmed a temperature dependency stable across different biogeochemical regimes. Simulations for CS_2 profiles provided first field evidence for a significant subsurface degradation process. A stable ratio in the apparent quantum yield between OCS and CS_2 across different biogeochemical regimes is promising for future modeling studies.

In total, the results of this thesis improve the understanding of marine emissions of climate relevant sulfur gases and, thus, reduce uncertainties in their atmospheric budget. The outcome sets the base for future model implementations in order to assess global questions concerning the Earth's climate.

Zusammenfassung

Schwefelhaltige Spurengase haben durch ihren starken Einfluss auf das Strahlungsbudget der Erde, und damit auf das Klima unseres Planeten, große Aufmerksamkeit erlangt. Der Ozean ist eine bedeutende Quelle der Spurengase Karbonylsulfid (OCS), Kohlenstoffdisulfid (CS_2) und Dimethylsulfid (DMS). Das Verständnis und die Quantifizierung dieser Emissionen aus dem Ozean sind wichtig, da sie zur Aerosolbildung in der Stratosphäre (OCS) und Troposphäre (DMS, CS_2) beitragen. Sie üben daher einen natürlichen Kühlungseffekt auf die Oberflächentemperatur der Erde aus, welcher der globalen Erwärmung entgegenwirkt. Zusätzlich kann über das atmosphärische OCS-Budget die nicht direkt messbare pflanzliche CO_2 Aufnahme (Bruttoprimärproduktion) indirekt abgeleitet werden. Ein besseres Verständnis der Bruttoprimärproduktion ist notwendig, um die Reaktion der terrestrischen Biosphäre auf wechselnde Klimabedingungen abzuschätzen. Daher sind exakt quantifizierte Quellen und Senken von OCS, CS_2 und DMS notwendig, da letztere in der Atmosphäre zu OCS reagieren können. Eine große Lücke im atmosphärischen Budget von OCS erschwert momentan Rückschlüsse auf die Bildung von stratosphärischen Aerosolen, sowie auf die Bruttoprimärproduktion auf globaler Ebene. In diesem Zusammenhang haben die ozeanischen Emissionen von OCS und seinen Ausgangsstoffen an Aufmerksamkeit gewonnen, da Emissionen aus tropischen Ozeanregionen als fehlende Quelle angenommen werden. In der vorliegenden Dissertation wurden neu entwickelte Messsysteme sowie numerische Modelle in drei Studien eingesetzt, um die marinen Emissionen der Spurengase OCS, CS_2 und DMS lokal, regional und global zu quantifizieren.

In der ersten Studie wurde systematisch ausgewertet, wie Ozeanemissionen optimal in atmosphärische Klimamodelle eingebunden werden können. Diese sind wichtige Werkzeuge für die Erforschung des gegenwärtigen Klimas und die Vorhersage zukünftiger Trends, sofern sie mit sinnvollen Rahmenbedingungen ausgestattet werden. Solche Rahmenbedingungen sind unter anderem die Ozeanemissionen von Spurengasen. In dieser Studie wurden Modellläufe mit vorgeschriebenen Wasserkonzentrationen und einer interaktiven Berechnung der Emissionen mit Modellläufen mit statisch vorgeschriebenen Emissionskli-

matologien verglichen. Die Ergebnisse zeigen, dass simulierte Atmosphärenkonzentrationen am besten mit Beobachtungsdaten übereinstimmen, wenn die Emissionen während der Simulation interaktiv berechnet werden. Das gilt insbesondere für Gase, die im Ozean nahe am Lösungsgleichgewicht konzentriert sind. Gase, deren Wasserkonzentrationen weiter vom Lösungsgleichgewicht entfernt sind, waren weniger sensitiv gegenüber der interaktiven Emissionsberechnung.

Während für DMS globale Ozeankonzentrationen in monatlicher Auflösung vorliegen, sind für OCS und CS_2 relativ wenig Messdaten vorhanden. Deshalb war das Ziel der zweiten Studie, OCS im Oberflächenwasser des tropischen Ozeans zu messen, sowie dessen Oberflächenkonzentrationen auf regionaler und globaler Ebene zu simulieren. Dazu wurde ein neues Messsystem entwickelt, mit dem OCS kontinuierlich und automatisiert während zwei Forschungsfahrten gemessen wurde. Vor dem Hintergrund der fehlenden atmosphärischen Quelle von OCS wurde der Fokus auf tropische Regionen gelegt, da hier die Datenlage bisher unzureichend war. Zwei sehr unterschiedliche tropische Gebiete – eine oligotrophe Region im Indischen Ozean sowie eine hochproduktive Region im östlichen Südpazifik – wurden ausgewählt, um einen großen Bereich der Variabilität der Oberflächenkonzentrationen abzudecken. Mit den neu erhaltenen Daten wurde eine neue Parametrisierung für die marine Photoproduktion von OCS aufgestellt, die erstmalig Informationen aus allen drei großen Ozeanen kombiniert. Diese Parametrisierung wurde zur Berechnung globaler Oberflächenkonzentrationen von OCS verwendet. Die Abschätzung direkter globaler Emissionen beläuft sich auf 130 ± 80 Gg S a^{-1}. Die Ergebnisse belegen die wichtige Rolle ozeanischer Emissionen, sind jedoch zu niedrig, um die Lücke im atmosphärischen Budget von OCS zu schließen. Auch indirekte OCS-Emissionen durch die Ausgangsstoffe CS_2 und DMS können die Lücke wahrscheinlich nicht schließen.

Die Charakterisierung mariner Stoffkreisläufe von OCS und CS_2 waren daher Gegenstand der dritten Studie. Erstmalig wurden Konzentrationsprofile beider Gase in der Wassersäule im biologisch hochproduktiven tropischen Südostpazifik gemessen. Ein neu entwickeltes 1D-Wassersäulenmodell in der Modellumgebung GOTM/FABM wurde verwendet, um die biogeochemischen Prozesse beider Gase systematisch zu untersuchen. Mit dem neu entwickelten Modell konnten die Messungen von OCS in der Wassersäule sehr gut reproduziert werden. Zusätzlich wurde eine neue Parametrisierung für die lichtunabhängige OCS-Produktion entwickelt. Simulationen der CS_2-Profile geben Hinweise auf einen Abbauprozess unterhalb der Mischungsschicht, für den bisher kein Reaktionsprozess bekannt ist. Der für die Bestimmung der Photoproduktionsrate wichtige *apparent quantum yield* beider Gase zeigte über verschiedene biogeochemische Regionen hinweg ein stabiles Verhältnis, was vielversprechend für zukünftige kombinierte Modellstudien ist.

Insgesamt wurde in dieser Dissertation das Verständnis der Emissionen klimarelevanter Schwefelgase verbessert und die Unsicherheiten ihrer atmosphärischen Budgets verringert. Die Ergebnisse liefern eine Grundlage für weitere Modellimplementierungen, um globale Fragen bezüglich des Klimas der Erde zu beantworten.

Manuscript contributions

This dissertation is based on the following manuscripts:

1. **Lennartz, S. T.**, Krysztofiak, G., Marandino, C. A., Sinnhuber, B. M., Tegtmeier, S., Ziska, F., Hossaini, R., Krüger, K., Montzka, S. A., Atlas, E., Oram, D. E., Keber, T., Bönisch, H., and Quack, B.: **Modelling marine emissions and atmospheric distributions of halocarbons and dimethyl sulfide: The influence of prescribed water concentration vs. Prescribed emissions**, published in: Atmos. Chem. Phys., 15, 11753-11772, 10.5194/acp-15-11753-2015, 2015.
   My contribution: I designed the study together with GK, CAM, BMS, BQ and KK, performed the simulations together with GK, analysed the data together with GK, and wrote the manuscript with contributions from all authors.

2. **Lennartz, S. T.**, Marandino, C. A., von Hobe, M., Cortes, P., Quack, B., Simo, R., Booge, D., Pozzer, A., Steinhoff, T., Arevalo-Martinez, D. L., Kloss, C., Bracher, A., Röttgers, R., Atlas, E., and Krüger, K.: **Direct oceanic emissions unlikely to account for the missing source of atmospheric carbonyl sulfide**, published in: Atmos. Chem. Phys., 17, 385-402, 10.5194/acp-17-385-2017, 2017.
   My contribution: I designed the study with CAM and MvH, developed the measurement system, performed shipboard measurements and OCS model studies, and wrote manuscript with contributions from all authors.

3. **Lennartz, S.T.**, Marandino, C.A., von Hobe, M., Fischer, T., Bittig, H., Booge, D., Goncalves-Araujo, R., Ksionzek, K., Koch, B.P., Bracher, A., Röttgers, R., Quack, B.: **Production and Consumption processes of OCS and CS_2 in the Eastern Tropical South Pacific**, manuscript in preparation for JGR.
   My contribution: I designed the study together with CAM, performed shipboard measurements and sampling, developed the GOTM/FABM module together with HB, and wrote the manuscript with contributions from all authors.

In addition, I have contributed to the following manuscripts and publications:

1. Campbell, E., Kesselmeier, J., Yakir, D., Berry, J. A., Peylin, P., Belviso, S., Vesala, T., Maseyk, K., Seibt, U., Chen, H., Whelan, M., Hilton, T., Montzka, S., **Lennartz, S.T.**, Kuai, L., Wohlfahrt, G., Wang, Y., Blake, N., and Blake, D.: Assessing a new clue to how much carbon plants store, EOS Earth and Space Science News, 2017, *in press.*

2. Schlundt, C., Marandino, C. A., Tegtmeier, S., **Lennartz, S. T.**, Bracher, A., Cheah, W., Krüger, K., and Quack, B.: Oxygenated volatile organic carbon in the western pacific convective centre: Ocean cycling, air-sea gas exchange and atmospheric transport, Atmos. Chem. Phys. Discuss., 2017, 1-29, 10.5194/acp-2017-9, 2017.

3. Falk, S., Sinnhuber, B. M., Krysztofiak, G., Jöckel, P., Graf, P., and **Lennartz, S. T.**: Brominated VSLS and their influence on ozone under a changing climate, Atmos. Chem. Phys. Discuss., 2017, 1-24, 10.5194/acp-2017-34, 2017.

4. Whelan, M. and COSANOVA Team: Synthesis on Carbonyl Sulfide as a tracer for terrestrial gross primary production. Manuscript, 2017.

Acknowledgments

First and foremost, I would like to thank Prof. Dr. Christa Marandino for supervising my thesis, for sharing her contagious enthusiasm for science, and for keeping the perfect balance between guidance and freedom to let me pursue my own scientific ideas. I am very grateful to Dr. Birgit Quack for her commitment, for her thorough feedback throughout my thesis and for asking the right questions at the right time. Furthermore, I highly appreciated the assistance of Dr. Marc von Hobe, who not only trusted me in deploying his precious OCS analyzer on ships in the middle of the ocean, but also for sharing his great knowledge and experience in measuring and modeling OCS. I also would like to thank the members of my ISOS-committee, Christa, Birgit, Dr. Irene Stemmler and Prof. Dr. Andreas Oschlies, for their valuable input during discussions in my semiannual committee meetings, which always provided me with a new perspective.

The members of the Marine Chemistry Department have immensely contributed to making my time as a PhD student productive and enjoyable. A huge 'Thank you!' to Alex and Dennis (the Golden T.C. Racing Team I), who hold a major share in making my PhD time unforgettable. Especially for you: Thank you for the music! A special 'Thank you!' to the current and former members of the HPA (and beyond), who were always open for questions, moral support and Friday afternoon beer: Alina, Anna, Annette, Cathleen, Damian, Helmke, Jimmy, Katharina, Kathrin, Meike, Melf, Roberto, Steffen, Tobi (x2). I am very grateful for the friendships that developed during this time. Also, I highly acknowledge the support of Damian and Tobi, for their technical help during two cruises in solving seemingly impossible-to-solve problems with their experience and inexhaustible pool of emergency lab material. Tim is thanked for his incredible patience in making physical oceanography understandable to me. Thanks to Nils for valuable IT support in exchange for burgers. I would also like to thank the TLZ, namely Wiebke, René, Rudi, and Uwe, for transforming my crazy ideas into deployable systems.

I acknowledge funding of my research from the BMBF (ROMIC-THREAT) and Prof. Dr. Christa Marandino's Helmholtz Young Investigators Group TRASE-EC.

Last but not least, I am particularly grateful to my family and Jonas, for their loving support, their unlimited encouragement and their irrevocable belief in me. You have been a major source of strength and without you I would not be where I am now.

Contents

List of Figures

List of Tables

1 Introduction

1.1 Sulfur and its role in climate

The climate of the Earth critically depends on the interaction between atmosphere, ocean, ice and land masses to absorb and redistribute solar energy. The atmosphere plays a key role in this context, as its composition strongly influences the radiative budget of the Earth. The concentration of trace gases and aerosols in the atmosphere determines the reflection, absorption and transformation of incoming solar radiation, and thus influences the temperature of the planet. Sulfur containing trace gases play an important role in defining the radiative balance of the Earth with both warming and cooling effects. Sulfate aerosols, which form by oxidation of precursor gases such as carbonyl sulfide (OCS) and sulfur dioxide (SO_2), reflect solar radiation and thus increase Earth's albedo in the stratosphere and the troposphere (Boucher et al., 2013; Kremser et al., 2016). Secondary aerosols from biogenic trace gases such as dimethyl sulfide (DMS) might alter the formation and lifetime of clouds with an impact on albedo as well, although still associated with high uncertainty (Andreae & Crutzen, 1997). Besides the cooling effect, some sulfur gases (OCS, CS_2) also act as greenhouse gases with a warming effect (Brühl et al., 2012). Describing the radiative budget in our current as well as in future climate scenarios requires both, an accurate process understanding of the mechanisms that alter solar radiation in the atmosphere, as well as an exact quantification of the atmospheric budget, i.e. the sources and sinks, of sulfur containing trace gases. The atmospheric sulfur budget is fed by both natural and anthropogenic sources. Natural biogenic sulfur emissions include a variety of reduced gases (DMS, OCS, CS_2, H_2S, dimethyl sulfide) from oceanic emissions (Andreae, 1986; Liss et al., 2014), wetlands and soils (Bates et al., 2004)(Fig. 1.1). Emissions from volcanoes and, to a smaller amount, from dust storms, appear less regular and often only for a short time,

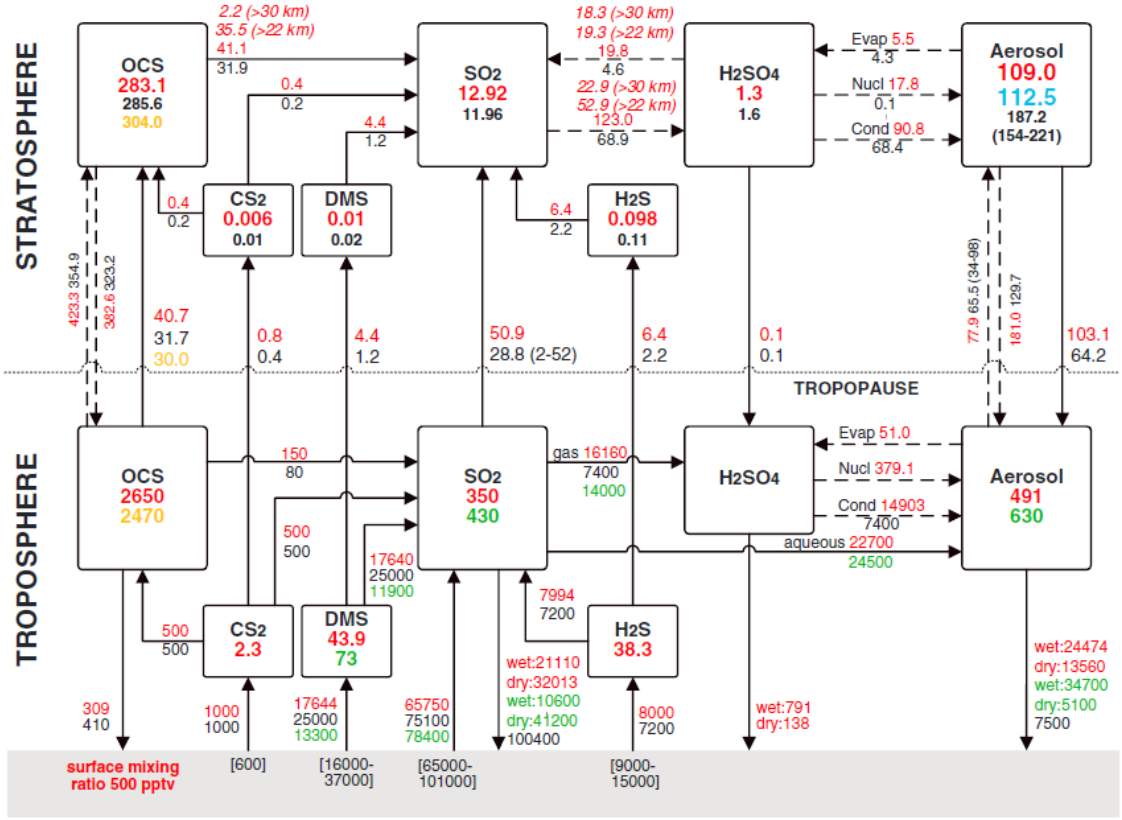

Figure 1.1: Global budget of atmospheric sulfur compounds from Sheng et al. (2015). Boxes represent reservoirs (Gg S) and arrows the direction of net fluxes (Gg S yr^{-1}. Numbers are color coded to indicate results from different model simulations or observations (black: AER-2D with sensitivity results in parenthesis, measurements in brackets from SPARC (2006), red: SOCOL-AER, green: tropospheric GOCART from Chin& Davis 2000, blue: SAGE-2 derived aerosol mass (Arfeuille 2013), orange: Chin & Davis (1995)).

but can introduce substantial amounts of sulfur gases such as SO_2 up to the stratosphere (Kremser et al., 2016). Besides these natural emissions, the atmospheric sulfur reservoir is strongly affected by human activities (Brimblecombe et al., 1989; Rodhe, 1999). Rodhe (1999) estimated the human emissions of sulfur to the atmosphere to be as large as 2-3 times the magnitude of natural emissions. This is because of emissions of SO_2 from coal and petroleum burning, and leads to a continuous rise of atmospheric sulfuric acid (H_2SO_4) since the beginning of the Industrial Revolution, which is even detectable in ice cores (Mayewski et al., 1990). Higher atmospheric concentrations of H_2SO_4 increase the acidity of rainwater with serious negative environmental effects (Likens & Bormann, 1974). The atmospheric sulfur cycle is thus a complex superposition of natural biogenic sulfur emissions, irregular volcanic eruptions and strong human perturbations. In order to understand this complexity, it is crucial to separate the single natural processes from the anthropogenic impact and reduce uncertainties in the fluxes between reservoirs.

High turnover rates make the atmospheric sulfur cycle react quickly to changes in environmental conditions and emissions. This close connection between source fluxes and effects can lead to feedback mechanisms with mitigating or amplifying effects on global warming (Boucher et al., 2013). Aerosol-climate feedbacks including secondary aerosols from biogenic sulfur gas emissions occur through changes in source strength of aerosols or their precursors (Boucher et al., 2013). For example, DMS has been suggested to be involved in a feedback mechanism (Charlson et al., 1987, see section 1.1.3), but the overall effect is currently associated with only a medium level of confidence (Boucher et al., 2013). Hence, quantifying the source strength of sulfur containing trace gases is important to assess the magnitude of such feedback mechanisms.

Despite the importance of atmospheric sulfur gases, their effects, budgets and fluxes between reservoirs carry high uncertainties. While aerosols provide an important natural counterpart to anthropogenic global warming, their overall effect on the radiative balance of the Earth still displays large uncertainty even in the direction of the impact (Fig. 1.2), resulting among others from uncertainty in effects and source strength of aerosol precursors. For global atmospheric sulfur budgets, estimated total emission of sulfur ranges between 82.5 Tg S yr^{-1} and 108.3 Tg S yr^{-1}, with resulting differences of approximately 30% (Chin et al., 2000; Sheng et al., 2015). Relative uncertainties in the source strength of single sulfur species are much higher. For example, emissions of OCS and CS_2 are associated with uncertainties of a factor of 2-4 for OCS (Kremser et al., 2016), and are even less well constrained for CS_2. Although the source strength of OCS and CS_2 on the order of several hundreds of Gg S per year is much smaller than the total atmospheric sulfur source strength in the teragram range, there are specific effects particular to these gases that require their

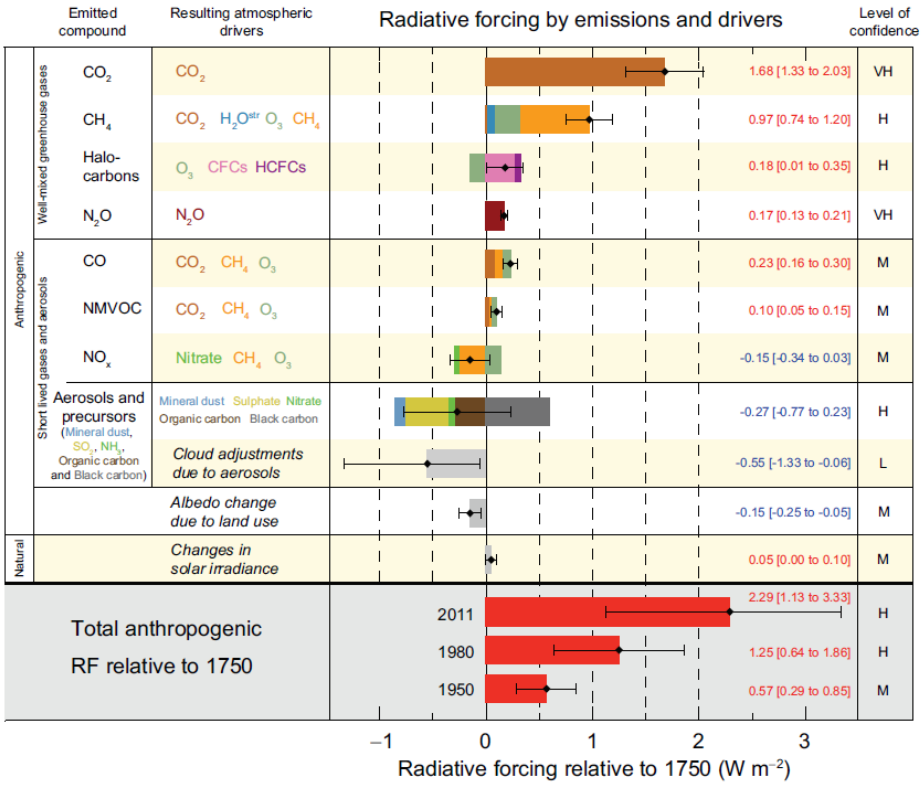

Figure 1.2: Globally averaged radiative forcing and aggregated uncertainties from 2011 in relation to 1750 (IPCC AR5). Black diamonds are best estimates together with uncertainty range and the level of confidence given at the last column of the table (VH - very high, H - high, M - medium, L - low.

budgets to be well constrained (see section 1.1.1 and 1.1.2). For example, CS_2 is the most important precursor of OCS, and OCS the major supplier of the stratospheric aerosol layer in volcanically quiescent periods (Kremser et al., 2016). Stratospheric aerosols have increased since 2000 with a small but significant impact on global surface temperatures (Solomon et al., 2011). Neglecting the variations in the global stratospheric aerosol layer can lead to an overestimation of global warming (Solomon et al., 2011). Therefore, accurately quantifying the individual contributions of major suppliers to stratospheric aerosols is important to identify reasons for the temporal variations in the stratospheric aerosol layers. Understanding the atmospheric sulfur budget and quantifying the fluxes in and out of the atmosphere as well as understanding the driving processes is crucial for assessment and prediction of climate in present and future. The ocean plays a major role as one of the largest sulfur emitters (Liss et al., 2014). Oceanic sulfur emissions represent the largest natural flux of sulfur to the atmosphere (Chin et al., 2000). Sulfur gases emitted by the

ocean are mainly reduced compounds, and include in descending order of the amount of annual emissions, DMS ≫ methyl mercaptane (CH_3SH) > OCS, CS_2 > H_2S (Liss et al., 2014). In this thesis, the focus is set on the gases OCS and CS_2, as especially the marine contribution of their emissions is associated with uncertainties of up to a factor of four of global annual emissions (see below). DMS is quantitatively the most important compound to transport sulfur from the ocean to the atmosphere, and its emissions are reasonably well quantified based on measurements and model studies (see e.g. Kloster et al., 2006; Lana et al., 2011). This thesis builds upon the previous knowledge by using DMS climatologies to assess how to best represent marine sulfur emissions in stand-alone atmospheric climate models, to provide a tool for dynamically including oceanic sulfur emissions for global climate assessment.

1.1.1 Carbonyl Sulfide (OCS) in the atmosphere

Carbonyl sulfide (OCS) is the most abundant sulfur gas in the atmosphere with an annual mean mixing ratio of approximately 500 ppt (Liss et al., 2014; Sheng et al., 2015). OCS is emitted to the atmosphere from the oceans by both direct and indirect emissions of the precursor gas CS_2 (and potentially DMS, see below), as well as from biomass burning and other anthropogenic sources. Sinks of atmospheric OCS are dominated by vegetation uptake, and uptake by soils and destruction by the OH radical are smaller but still significant (Chin & Davis, 1993; Kremser et al., 2016; Watts, 2000)(Fig. 1.3).

Spatial and temporal variations of atmospheric OCS mixing ratios occur on several scales. Although interannual variability on decadal timescales is low, a pronounced seasonal cycle leads to variations of ~100 ppt within one year, with a minimum in late summer and a maximum in spring (Montzka et al., 2007). Variations in atmospheric mixing ratios are stronger on millennial time scales. As inferred from firn ice and ice core measurements dating back ca. 55000 years B.P., atmospheric mixing ratios in Antarctica were as low as 160-210 ppt at the beginning of the Holocene (Aydin et al., 2016). On the spatial scale, several lines of evidence indicate a latitudinal gradient for atmospheric mixing ratios of OCS at least in some locations (Krysztofiak et al., 2015; Kuai et al., 2015). Ground based stations from the NOAA-ESRL (Earth System Research Laboratory) show constant air mixing ratios in the southern hemisphere (3 stations) and the tropics, but a decline in atmospheric volume mixing ratios towards high latitudes in the northern hemisphere, reflecting the uptake of OCS by vegetation in boreal latitudes (Montzka et al., 2007). The atmospheric lifetime of OCS is estimated between 2 and 7 years, which is long enough for mixing in the two hemispheres and to enable entrainment into the stratosphere, where OCS is rapidly photolysed (Kremser et al., 2016).

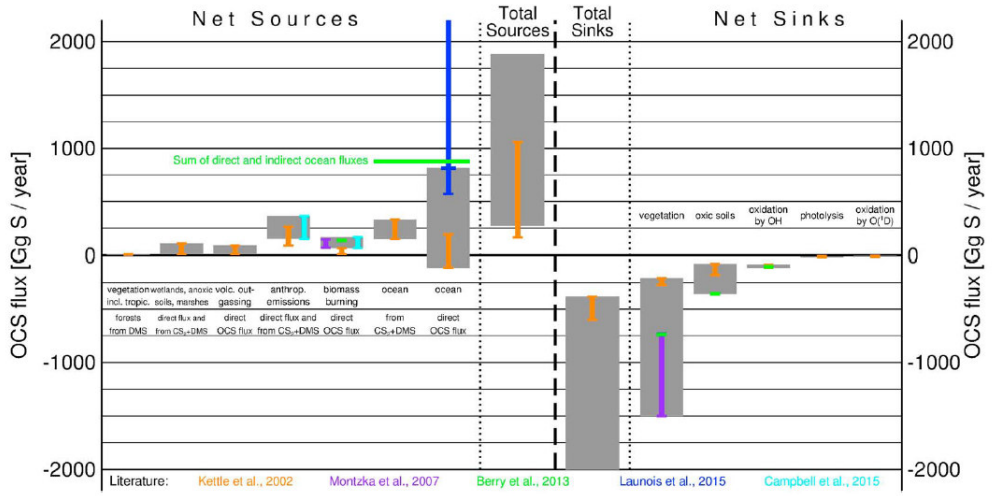

Figure 1.3: Uncertainties in the atmospheric budget of carbonyl sulfide (Kremser et al., 2016).

A well explained atmospheric budget is required for two reasons: First, OCS is a climate relevant trace gas and accurate fluxes are needed to derive an accurate atmospheric budget to assess its effect on climate. Second, OCS has shown potential as a proxy to constrain terrestrial gross primary production (Berry et al., 2013; Campbell et al., 2008), for which a well defined budget is needed to apply this proxy on the global scale (Beer et al., 2010).

Climate relevance of OCS

OCS is relevant to global climate in several ways with counteracting warming and cooling effects (Brühl et al., 2012). In the troposphere, OCS acts as a greenhouse gas with a direct radiative forcing efficiency 724 times that of CO_2 (Brühl et al., 2012). However, the much lower atmospheric mixing ratio of OCS (ppt) compared to CO_2 (ppm) reduces the overall warming effect considerably relative to other greenhouse gases such as CO_2. Due to its long lifetime, OCS can be transported to the stratosphere, where it acts as a precursor to stratospheric sulfate aerosols (Crutzen, 1976; Kremser et al., 2016). In volcanically quiescent periods, the upward transport of OCS controls the aerosol loading of the Junge layer in the stratosphere (Brühl et al., 2012). There, OCS is photolysed to SO_2 which reacts with OH to form H_2SO_4, yielding sulfate aerosols (Kremser et al., 2016). These sulfate aerosols reflect sunlight and thus increase Earth's albedo (Junge et al., 1961), therefore resulting in a cooling effect on global temperatures. Brühl et al. (2012) showed that the warming and the cooling effect balance each other on a global scale, but can lead to local differences. The net effect can potentially vary with changes in source strength and location

of emissions as well as atmospheric circulation over time. In contrast, Solomon et al. (2011) showed that model simulations overestimate global warming, if the cooling effect of the stratospheric aerosol layer supplied by OCS is not considered. A better understanding of sources and sinks of tropospheric OCS is needed to improve future climate prediction (Kremser et al., 2016).

Besides the cooling effect, the stratospheric aerosols also influence ozone depletion, as they support the formation of polar stratospheric clouds (Solomon et al., 2015). The ozone content in the polar atmosphere has been shown to be very sensitive to the aerosol loading (Solomon et al., 2015), as these aerosols provide the surfaces for heterogeneous reactions that accelerate ozone depletion. A change in carbonyl sulfide loading, aerosol formation and consequently ozone depletion could have potential feedbacks in the coupled system of ocean and atmosphere.

Currently, atmospheric chemistry climate models often use prescribed mixing ratios of OCS in the boundary layer instead of seasonally varying boundary fluxes (Brühl et al., 2012; Sheng et al., 2015). Simulations would benefit from temporally and spatially resolved boundary fluxes of sulfur containing trace gases to dynamically take into account variations in emissions and sulfur loading of the atmosphere (Kremser et al., 2016). At the moment, such simulations hampered by a poorly constrained atmospheric budget of OCS, in which known sinks exceed known sources of OCS to the atmosphere, so model simulations can not spin up to equilibrium.

Constraining gross primary production with OCS

In addition to its climate relevance, OCS recently regained attention as a CO_2 analog to constrain terrestrial gross primary production (GPP, Berry et al., 2013; Campbell et al., 2008). The global application of using OCS as a proxy for GPP was discovered as CO_2 and OCS both show a remarkable covariance in their seasonal cycle at ground based time series stations (Montzka et al., 2007) and airborne data (Campbell et al., 2008). Constraining processes in the biological part of the carbon cycle is crucial for climate projections, as one of the major uncertainties in climate forcing results from uncertainties in the terrestrial biosphere, i.e. photosynthetic uptake (Arneth et al., 2010). The representation of GPP in global climate models shows a large spread, and the trend as well as the interannual variability in carbon uptake from 1990-2009 is not represented consistently among observation-based datasets and process-oriented models (Anav et al., 2015). Using OCS as a proxy for GPP might thus be a promising tool to better constrain these uncertainties (Asaf et al., 2013; Beer et al., 2010).

The basic idea of this concept relies on inferring the CO_2 uptake by plants from the

uptake by OCS and the uptake ratio of both gases. GPP cannot be measured directly and thus relies on indirect methods of quantification (Anav et al., 2015). OCS can help quantifying terrestrial CO_2 uptake, as it is taken up by plants in a similar pathway as CO_2 (Sandoval-Soto et al., 2005). However, unlike CO_2, it is not concurrently emitted by respiration, but degraded within the leaf. This makes the OCS a one-way flux into the leaf, whereas the CO_2 flux into the leaf is masked by the concurrent release by respiration (Asaf et al., 2013). With a known uptake ratio of OCS and CO_2, the CO_2 uptake or GPP can be inferred (Asaf et al., 2013).

The global application of this proxy is encouraged because at least in the northern hemisphere, the seasonal cycle of atmospheric mixing ratios for both OCS and CO_2 is driven by vegetational uptake (Montzka et al., 2007; Suntharalingam et al., 2008). In addition, the atmospheric lifetime of OCS is advantageous, because it is long enough to be well mixed in the atmosphere, but short enough to react to changes in sources and sinks (Campbell et al., 2017). However, an uncertain atmospheric budget currently hampers the application of the OCS proxy technique on a global scale (Beer et al., 2010). To separate the flux of GPP from other fluxes in the seasonal cycle of OCS, all other atmospheric sources and sinks of OCS need to be adequately quantified. This is currently not the case, as a large missing source was identified by inverse modeling approaches with satellite and FTIR data (Glatthor et al., 2015; Kuai et al., 2015; Wang et al., 2016), leaving the atmospheric budget of OCS unclosed.

The missing source of atmospheric OCS

Known sinks exceed known sources of OCS to the atmosphere by ca. 600-800 Gg S each year (Fig. 1.3). As atmospheric mixing ratios of OCS are relatively constant on the timescale of decades (Montzka et al., 2007), an unidentified additional missing source of OCS has been suggested. The ocean plays a key role in this context, as it has been suggested that oceanic emissions might account for the missing source (Berry et al., 2013; Glatthor et al., 2015; Kuai et al., 2015).

In 2002, the atmospheric budget of OCS had been closed within the range of uncertainties (Kettle, 2002), although the cumulative uncertainties of 185 Gg S yr^{-1} were still large. The budget was brought out of balance by an upward revision of the vegetational uptake of OCS from the atmosphere. This revision was based on (i) a new bottom-up estimates for OCS uptake on the leaf scale (Sandoval-Soto et al., 2005) and (ii) a top-down approach to better fit the observed seasonality in ground based stations (Berry et al., 2013; Suntharalingam et al., 2008). With new satellite data for OCS becoming available from the Aura-TES and the Envisat-MIPAS instruments, the magnitude of the missing source has been increased to

600-800 Gg S yr^{-1} (Glatthor et al., 2015; Kuai et al., 2015). Based on a simple inversion approach increasing the total marine emissions of OCS, the missing source was suggested to be located in the tropical oceans, with a hot spot in the Pacific warm pool region (Kuai et al., 2015). It should be noted however, that the two satellite data sets are currently not fully consistent, with deviations of ca. 100 ppt in the tropopause (Glatthor et al., 2016). As inverse modeling approaches are very sensitive towards their forcing data, such an inconsistency might have implications for the atmospheric budget in top-down estimates.

A bottom-up modeling study by Launois et al. (2015) simulated oceanic concentrations in the 3D global ocean model NEMO-PISCES that corroborate the magnitude of the missing source with direct oceanic OCS emissions of 813 Gg S yr^{-1}. However, this would require concentrations in the range of annual mean concentrations of ca. 100-300 pmol L^{-1} in the tropics, which is not consistent with previous measurements (e.g. Kettle et al., 2001). While Launois et al. (2015) simulate a maximum of OCS concentrations in the tropics, other model studies found highest emissions in high latitudes (Kettle, 2000; Preiswerk & Najjar, 2000). The fact that top-down approaches cannot differentiate between direct OCS emissions and emissions of short-lived precursor gases further complicates the problem. The discrepancy between bottom-up and top-down budget estimates is currently not resolved, and hampers both the assessment of the climate effect and influence on the stratospheric aerosol layer with model simulations based on surface boundary fluxes, and using OCS as a proxy for gross primary production on the global scale. Spatially and temporally resolved emission estimates from the oceans are required to (i) assess whether the ocean can account for the missing source and (ii) provide models with accurate boundary fluxes of a key compound in atmospheric sulfur chemistry.

1.1.2 Carbon Disulfide (CS_2): the short-lived precursor of OCS

In contrast to OCS, CS_2 has a much shorter atmospheric lifetime (Bandy et al., 1981; Khalil & Rasmussen, 1984), and atmospheric volume mixing ratios have been reported to vary between 0.4 and 50 ppt at various locations in the Atlantic and Pacific Oceans in the marine boundary layer (Bandy et al., 1993; Cooper & Saltzman, 1991; Kim & Andreae, 1987; Kim & Andreae, 1992). The main loss process of CS_2 in the atmosphere is the reaction with OH (Eq. 1.1-1.2) (Chin & Davis, 1993).

$$CS_2 + OH + M \rightleftharpoons CS_2OH + M \tag{1.1}$$

$$CS_2OH + O_2 \longrightarrow \text{products} \tag{1.2}$$

It is generally agreed that the major reaction products from OH radical reaction with CS_2 are OCS and SO_2 (Hynes et al., 1988; Jones et al., 1982; Stickel et al., 1993). In a three-step reaction, an adduct is formed (CS_2-OH), where the OH radical is most likely added to one of the S atoms (Zeng et al., 2017). The S-adduct is either decomposed by the inverse reaction or further reacts in a bimolecular rection with O_2 (Jones et al., 1983; Stickel et al., 1993) yielding end products like OCS and SO_2.

While it is assumed that there is one major reaction channel producing OCS and another major reaction channel producing SO_2, the exact mechanism is not known (Stickel et al., 1993). Stickel et al. (1993) listed more than 26 possible exothermic reaction channels. OCS is generally considered as the major reaction product with reported molar conversion factors from CS_2 of 0.81 (Chin & Davis, 1993) and 0.83±0.08 (Stickel et al., 1993). Therefore, CS_2 is considered as a major source for OCS (Chin & Davis, 1993; Kettle, 2002; Watts, 2000). The adduct reaction constant of CS_2 and OH which yields OCS increases drastically with decreasing temperature (Hynes et al., 1988), potentially leading to faster conversion and thus a shorter atmospheric lifetime in higher latitudes. Other reaction processes in the atmosphere include reaction with O^3P (Hattori et al., 2012) and photooxidation (Wine et al., 1981), but seem to be quantitatively less important compared to the reaction with OH.

Although CS_2 is a greenhouse gas itself, its impact on tropospheric warming is small due to its low atmospheric mixing ratio and its short lifetime (Brühl et al., 2012). The major importance of CS_2 arises from being the main precursor of atmospheric OCS and thus indirectly affecting the stratospheric sulfur layer. However, the atmospheric budget of CS_2 is very poorly constrained, and this uncertainty directly translates into an uncertain budget for OCS. Due to the scarcity of data, top-down constraints for the atmospheric budget of CS_2 are highly uncertain. The ocean is believed to be a major source due to photochemical and biological production of CS_2 (Chin & Davis, 1993; Watts, 2000), but only few measurements (ca. 1000) exist from the sea surface. A better process understanding would help to reduce uncertainties in seasonality and magnitude of CS_2 emissions to the atmosphere, which is needed to quantify its impact within the atmospheric sulfur cycle.

1.1.3 Dimethyl sulfide (DMS): the major natural sulfur flux to the atmosphere

Dimethyl sulfide is a very short-lived sulfur gas with a lifetime in the order of hours to days due to its rapid oxidation in the atmosphere (Barnes et al., 2006; Osthoff et al., 2009). It is the major biogenic sulfur source to the atmosphere (Liss et al., 2014), and by

far the most is emitted from the ocean (Lana et al., 2011). The atmospheric oxidation of DMS to other gases makes an exact quantification of the DMS flux also important for the budgets of other sulfur containing trace gases. DMS is oxidized in the atmosphere by OH, following one of two possible reaction pathways: i) the addition pathway, which is favored at higher temperatures and includes reactions with OH, NO_3 and Cl, and ii) the H-abstraction pathway which is favored at lower temperatures and includes reactions with OH and Br (see e.g. Hoffmann et al., 2016, for a detailed summary). The abstraction pathway yields H_2SO_4 as an end product, which can form new aerosol particles (Kreidenweis & Seinfeld, 1988), so called non-sea-salt SO_4^{2-} or nss-SO_4^{2-}. Other oxidation products include dimethyl sulfoxide (DMSO) and methanesulfonic acid (MSA), the latter also being involved in formation and growing of aerosols (Hoffmann et al., 2016; Saltzman et al., 1983). An oxidation of DMS to OCS has been suggested previously (Barnes et al., 1994) and since then included in the budgets of OCS (Kettle, 2000; Watts, 2000), but severe doubts concerning the exact mechanism and the occurrence of this process under natural conditions have been raised (Whelan & COSANOVA-Team, 2017). The conversion of DMS to OCS had been derived from atmospheric chamber experiments with precursor levels far above natural conditions and only with a restricted pressure and temperature range, and their validity under environmental conditions is thus questionable.

The discovery of the formation of aerosols from DMS led to the postulation of the CLAW hypothesis (CLAW for Charlson, Lovelock, Andreae and Warren Charlson et al., 1987) which describes a possible feedback loop between marine DMS emissions and climate. Marine produced DMS is emitted to the atmosphere, where it forms nss-SO_4^{2-} which serve as cloud condensation nuclei (CCN). The concentration of cloud droplets then increases the scattering of solar radiation and thus increases albedo. Lower incoming radiation at the surface decreases temperature and solar irradiance below clouds, which was then postulated to feedback on marine phytoplankton and thus DMS production. The postulation of this hypothesis initiated a large number of field observations (overview in Lana et al., 2011), process studies (e.g. Simo et al., 2002) and modeling studies (Kloster et al., 2006; Six et al., 2013). Ayers & Gillett (2000) showed, that in remote locations such as the Southern Ocean, DMS is indeed a central player for a variety of important atmospheric processes.

The CLAW hypothesis has been systematically challenged by Quinn & Bates (2011). Points of criticism were 1) correlation between CCN and DMS/nss-SO_4^{2-} neither rules out other CNN sources nor indicates any sensitivity of CCN numbers to changes in DMS emissions, 2) other CCN sources might be more important, and 3) a spatial decoupling between source and effect might interrupt the feedback loop.

The exact magnitude of the climate effect of DMS is thus still debated, but the intensive

studies following the CLAW hypothesis make DMS the best studied compound of the trace gases described here.

1.2 Air-sea gas exchange

When a trace gas in the surface ocean is super- or undersaturated with respect to the overlying marine boundary layer, the compound is exchanged across the air-sea interface to reach equilibrium. With the air-sea interface covering 71% of the Earth's surface, air-sea exchange is a crucial component of many biogeochemical cycles. Accurately quantifying the fluxes across this interface is especially important for climate relevant trace gases, as the amount of gases entering or leaving the atmosphere through this boundary defines their impact on climate. Oceanic emissions play a major role for the sulfur gases discussed in this thesis (Chin & Davis, 1993; Lana et al., 2011; Watts, 2000).

A simple but useful conceptual model to describe air-sea exchange was proposed by Liss & Slater (1974), which characterizes the interface as the boundary between two diffusive sublayers where turbulence is suppressed and the exchange of mass depends on molecular diffusion (Donelan et al., 2002; Liss & Slater, 1974)(Fig. 1.4a). These layers provide the largest resistance for gases when crossing the interface (Donelan et al., 2002). For insoluble gases like OCS and CS_2, the resistance of the air-side diffusive sublayer is several orders of magnitude lower than the water-side resistance, and is thus often neglected in air-sea exchange calculations. For more soluble gases as e.g. DMS, the air-side resistance can become significant at low sea surface temperatures and moderate wind speeds (McGillis et al., 2001).

Air-sea exchange is defined as the product of the concentration gradient across the interface Δc and the transfer velocity k (eq. 1.3).

$$F = k \cdot \Delta c \tag{1.3}$$

While Δc describes the saturation state of the respective compound and thus the direction of the flux, i.e. the thermodynamical component, k determines the rate of the exchange, i.e. the kinetic component (the inverse of the air- and waterside resistance).
A widely used method to calculate air-sea fluxes is the bulk method, where fluxes are calculated from the measured concentration gradient across the surface and a parametrization of the transfer velocity k. This method relies on measurements of the gas in the surface ocean (usually around 5-10m depth) and the marine boundary layer (usually 10-30m height) for Δ c and a parametrization of the transfer velocity, mostly dependent on meteorological

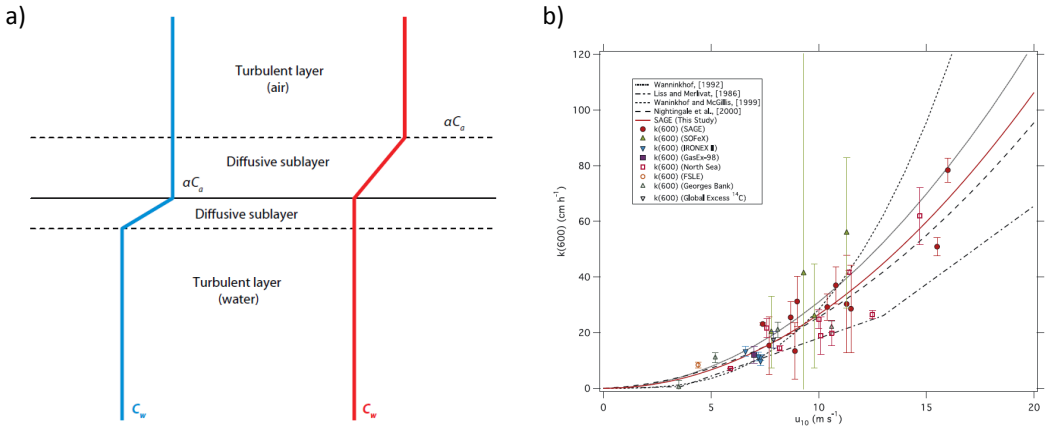

Figure 1.4: a) Conceptual model of air sea exchange (from: Wanninkhof et al. (2009)), b) different parameterizations of water-side transfer velocities and spread in measurements with the dual tracer technique (from: (Ho et al., 2006))

parameters such as wind speed. While the method has been extensively tested and generally validated for various gases (see e.g. Garbe et al., 2014; Wanninkhof et al., 2009), it should be noted that both terms, Δ c and k, rely on assumptions that may not always be valid:

- **The concentration gradient Δc:** When measuring Δc, concentrations as deep as 6 m in the mixed layer as well as several meters above sea level are taken as representative of the concentration gradient across the air-sea interface. While OCS is generally well mixed in the upper layers of the ocean and the marine boundary layers, it has been shown that this approach has its limitation if strong concentration gradients occur near the surface. Such gradients have previously been inferred for DMS (Kieber et al., 1996; Marandino et al., 2008) and N_2O (Kock et al., 2012). Walker et al. (2016) showed by comparison of direct flux measurements and emissions calculated with the bulk method, that production or enrichment of DMS near the surface can occur under certain meteorological and biological (i.e. blooms of DMS producing plankton species) conditions. In this context, the sea surface microlayer regained attention, as any loss or production occurring there directly influences air-sea exchange, but may be overlooked by the bulk method. The sea surface microlayer may differ from the underlying water in several aspects (Cunliffe et al., 2013) and has been shown to be enriched with chromophoric dissolved organic matter (CDOM) (Wurl et al., 2009), with implications for photochemically produced gases (Zhou & Mopper, 1997), such as OCS and CS_2.

- **The transfer velocity *k*:** The transfer velocity is governed by several physical

processes including turbulence, waves, sea spray formation and bubbles, but to date the key parameter and its dependency on k has not been fully characterized. As wind induces turbulence which in turn determines the transfer velocity, k has been found to correlate with wind speed (Liss & Slater, 1974; Wanninkhof et al., 2009). Therefore, most of the parameterizations for k rely on the wind speed at 10 m height. These parameterizations have been determined using different techniques such as dual tracer release and eddy covariance and have been tested in wind wave tanks as well as at sea, but uncertainties still exist both in the functional form (linear, quadratic, cubic) and the overall magnitude. Especially at high wind speeds above 10 m s^{-1}, k values differ by up to a factor of ~5 (Fig. 1.4b). The scatter in fig. 1.4b indicates that parameters other than wind speed substantially influence the air-sea exchange. A variety of different studies thus investigated the effects of rain (Ho et al., 2004), bubble enhanced gas transfer (Asher & Wanninkhof, 1998; Zhang et al., 2006), surfactants (Frew et al., 1990; Tsai & Liu, 2003) and boundary layer stability (Erickson, 1993). Additionally, it has been questioned that there is only one functional dependence of wind speed and k (i.e. linear, cubic) for all gases, as field measurements point towards differences between e.g. DMS and CO_2 at wind speeds above 11 m s^{-1}, potentially because of their different solubilities (Bell et al., 2013).

In summary, although the air-sea exchange is a molecular process occurring on vertically very small scales, the horizontal extent of the air-sea interface makes this process globally extremely relevant. Any reduction of uncertainties of the air-sea exchange directly translates into a reduced uncertainty in global marine emission estimates. Increasing our understanding of air-sea exchange is thus crucial for the atmospheric budget of climate relevant trace gases. In addition, the physical and biogeochemical drivers of air-sea fluxes will vary with changing climate, hence an accurate quantification is needed to quantify present and future trace gas emissions and potential feedback mechanisms.

1.3 Marine biogeochemistry of volatile organic sulfur compounds

The ocean plays a major role in the atmospheric budget of the three gases DMS, OCS and CS_2 (Chin & Davis, 1993; Liss et al., 2014), and it is thus important to accurately quantify their marine emissions in order to assess their influence on climate and atmospheric chemistry. This involves two aspects: First, measurements of the concentration gradient between atmosphere and surface ocean across various oceanic regimes are needed to

determine the order of magnitude of the flux. Second, the key parameters of the marine cycling have to be well understood to upscale observations to a global level. Models with verified parameterizations of production and consumption processes are useful tools for the quantification of emissions. In the following, the current level of understanding of marine production and consumption processes as well as sea surface concentration measurements is reviewed.

1.3.1 Carbonyl sulfide (OCS)

Carbonyl sulfide is present in the surface water of the oceans in the lower picomolar range with strong temporal and spatial variations. Temporal variations on a diurnal as well as on a seasonal scale can vary between super- and undersaturation, with highest concentrations usually shortly after local noon (Kettle, 2000; von Hobe et al., 2003) and during summer (Ulshöfer et al., 1995). Spatial variations are not fully understood due to the limited spatial coverage of previous measurements, but some common patterns seem to emerge. OCS concentrations are usually higher in coastal areas compared to the open ocean (Cutter & Radford-Knoery, 1993), and higher latitude waters show higher concentrations than tropical or temperate latitudes (e.g. Kettle, 2000; Staubes & Geogrii, 1993). To facilitate the measurements of both spatial and temporal variability of concentrations, automated and continuous measurement systems are needed, which will be addressed within this thesis in chapter 2.

The processes that determine the concentration of OCS in the surface waters have been described previously and include hydrolysis as a loss term, photoproduction and light-independent production as source terms, and air-sea exchange acting as a source or a sink depending on the saturation. Hydrolysis involves the reaction of OCS with either H_2O or OH^- (reaction 1.4 and 1.5):

$$OCS + H_2O \rightleftharpoons H_2S + CO_2 \tag{1.4}$$

$$OCS + OH^- \rightleftharpoons HS^- + CO_2 \tag{1.5}$$

Hydrolysis rates have been investigated in laboratory and field studies (see section 2.3.1), showing that hydrolysis is strongly temperature dependent. In warm, tropical waters, hydrolysis determines the lifetime of OCS on the order of several hours, whereas in colder waters, lifetime due to hydrolysis can be several days (Elliott et al., 1989).

A photochemical production of OCS was first suggested by Ferek & Andreae (1984) because diurnal variations in the supersaturation of OCS in surface waters follow a similar temporal pattern as solar radiation. The photoproduction of OCS is dependent on the

radiation, the concentration of the precursor and the apparent quantum yield (often also termed *in-situ* photoproduction rate constant). Flöck et al. (1997) identified cysteine, a common amino acid, as a precursor of OCS in incubation studies, but neither other precursors nor the distribution of these precursors in the ocean is sufficiently well known for modeling purposes. Although several studies used simple models to determine the photoproduction rate constant for specific locations (Uher & Andreae, 1997; von Hobe et al., 2003), no globally valid relationship has been established to date. Incubation experiments at different wave lengths indicated that the apparent quantum yield (AQY) of OCS is strongest in the UV wavelength range (Weiss et al., 1995). However, the variation between published AQYs from the open Pacific ocean (Weiss et al., 1995), the North Sea, and the Gulf of Mexico (Zepp & Andreae, 1994), the Sargasso Sea (Cutter et al., 2004) vary across two orders of magnitude. The inadequate description of photoproduction rates is a shortcoming of previous modeling studies, which hampers an accurate quantification of global marine emissions of OCS.

Light-independent production (also called dark production) has been suggested because OCS concentrations in the absence of light stabilize above the detection limit, indicating that a production process occurs at the same time as the hydrolysis loss process. Experimental studies showed significant production of OCS in the absence of UV light and identified glutathione as a potential precursor (Flöck & Andreae, 1996; Flöck et al., 1997). Currently, two hypotheses exist: a biological process, e.g. microbial activities (Cutter et al., 2004; Flöck et al., 1997) and/or radical reactions, as Pos et al. (1998) show that in theory, radical formation from metal complexes can lead to the formation of carbonyl sulfide. Dark production has been shown to vary with temperature and CDOM content, but currently only one parameterization describing dark production is available, which is based on data from several cruises to the Atlantic ocean (Von Hobe et al., 2001).

Under- and supersaturation of OCS has been detected in surface waters (Kettle, 2000; Ulshöfer et al., 1995), which implies that exchange of OCS across the air-sea interface occurs in both directions. Uncertainties related to this process are similar to other trace gases whose emissions are derived with the bulk method (see section 1.2).

In total, the production and loss processes for OCS are reasonably well described to narrow down the key parameters influencing surface concentrations and thus emissions. However, insufficient quantification of both production processes has still introduced considerable uncertainty in global modeling efforts to simulate global sea surface concentrations and emissions of OCS.

1.3.2 Carbon disulfide (CS_2)

Process understanding and the number of previous measurements for CS_2 in the surface ocean is even lower than for OCS. Observations show sea surface concentrations of CS_2 in the lower picomolar range (Kettle et al., 2001; Xie et al., 1999a), even though concentrations as high as 510 pmol L^{-1} have been reported in estuaries (Kim & Andreae, 1987). Surface concentrations of CS_2 decrease from estuary to coastal to open ocean (Kim & Andreae, 1987). In total, measurements are too scarce to reliably describe temporal and diurnal variability, but the variations seem to be similar to the ones of OCS.

Diurnal cycles have been reported (Kettle et al., 2001), although not as clearly pronounced as for OCS. In wavelength-resolved incubation studies, photochemical reactions involving CDOM have been shown to produce CS_2 (Xie et al., 1998). Therein, the quantum yield for CS_2 was found to be highest at wavelengths of 290-340nm, and correlates well with the absorption of CDOM at 350nm. The authors suggest an AQY four times smaller than that measured simultaneously for OCS. Furthermore, Xie et al. (1998) suggest that important precursors of CS_2 might be sulfur containing amino acids such as cysteine and cystine, and a potential influence of OH. However, production rates from other regions or from other precursors have not been reported.

In addition, there is evidence for a biological production of CS_2, as e.g. depth profiles of CS_2 concentrations in the North Atlantic typically exhibit a maximum at a depth close to the chlorophyll maximum, which the authors attributed to a possible link between biological production and CS_2 production (Xie et al., 1999a). In an incubation study with phytoplankton cultures, CS_2 production has been shown for some, but not all tested phytoplankton species (Xie et al., 1999b). Among the species tested, main producers were *Chaetocerus calcitrans*, *Phaeodactylum tricornutum* and *Phaeocystis sp.* However, the species specific production rates of CS_2, which can vary by a factor of 10 among species, challenge the global extrapolation of biological CS_2 production.

Other than air-sea exchange, no significant sinks for CS_2 in the surface ocean has been described, although indications for such a sink exist. Elliott (1990) tested for chemical degradation processes involving H_2O_2 and other radicals, but only found slow sinks on the time scales of 10s of days or more. With an inverse fit based on measurements during two Atlantic transects, Kettle (2000) determined degradation rates in the order of 8-13 days, but did not specify any underlying reaction mechanisms. Therefore, emission to the atmosphere is currently thought to be the major sink for CS_2 (Kettle, 2000). In total, the level of process understanding for CS_2 needs to be increased by laboratory studies and field experiments over a range of different biogeochemical regimes to enable extrapolations on

a broader scale.

1.3.3 Dimethyl sulfide (DMS)

DMS cycling and sea surface concentrations have been extensively studied and will be briefly summarized here. Lana et al. (2011) updated a global monthly climatology by Kettle (2000) based on more than 40000 measurements. DMS is typically present in concentrations of 1-7 nmol L^{-1} in the global ocean (Lana et al., 2011), and shows hot spots in high latitudes, e.g. the Southern Ocean. Regions such as the Southern Ocean and the Indian ocean are strongly undersampled.

DMS is naturally produced from its precursor dimethyl sulfoniopropionate (DMSP). DMSP is produced by phytoplankton, and two hypotheses exist for its physiological use in phytoplankton cells. According to the anti-oxidant hypothesis, DMSP can scavenge hydroxyl radicals and is produced in higher amounts by phytoplankton when subjected to oxidative stressors such as UV radiation (Sunda et al., 2002). In contrast, Stefels (2000) hypothesized that DMSP is produced in an overflow mechanism to cope with excess energy and reduced compounds. As of now, a lack of reported UV radiation in available studies prevents this issue from being solved (Liss et al., 2014). Key factors controlling DMSP production include the species community present as well as their physiological state, which depends on abiotic factors such as salinity, light, temperature and the availability of nutrients (Stefels et al., 2007). Intracellular DMSP that is released to the free water column by e.g. lysis or grazing is then enzymatically degraded following one of two competing pathways. Through the demethylation pathway, DMSP is converted into reduced compounds such as methanethiol during assimilatory metabolic reactions, which are then incorporated as amino acids in biomass (Kiene et al., 2000). Within the cleavage pathway, DMS and acrylate are generated. As the demethylation pathway is predominant, only 1 to 10 % of the DMSP is estimated to end up as DMS in the atmosphere (Bates et al., 1994; Liss et al., 2014).

Several loss processes reduce the concentration of DMS in the surface water. Bacterial consumption plays a dominant role, where DMS is oxidized by enzymes such as monooxygenases and dehydrogenases (Bentley & Chasteen, 2004; Stefels et al., 2007). DMS is also photochemically oxidized to DMSO and other compounds, mainly at wavelengths between 380 and 460 nm (Brimblecombe & Shooter, 1986; Kieber et al., 1996). DMS that is neither mixed downwards, nor chemically or biologically degraded is outgassed to the atmosphere and represents the largest biogenic flux of sulfur to the atmosphere. The quantification of the production and removal processes led to model simulations of DMS concentrations in 3D global ocean and coupled ocean-atmosphere models in time-slice (Bopp et al., 2003) and transient climate experiments (Kloster et al., 2006). Only a small

negative global feedback towards higher atmospheric CO_2 concentrations has been found, but large regional differences occurred. In total, DMS is the compound with the highest level of knowledge of the three gases focused on in this thesis, as i) more than 40000 sea surface measurements are available, ii) processes are analysed at the molecular, cell and organism level, and iii) biogeochemical models that simulate oceanic DMS concentrations have been developed and validated.

1.4 Objectives and Research Questions

Volatile organic sulfur compounds impact the radiative budget of the Earth, and an exact quantification of their climate impact is thus crucial for climate predictions. The magnitude of the climate impact is determined the amount of gases present. However, substantial uncertainty exists in the budgets of OCS and CS_2, especially the role of the oceanic emissions, as well as in the way how to best represent their marine emissions in atmospheric chemistry climate models. Therefore, the overarching goal of this thesis is to better constrain natural marine sulfur emissions of OCS, CS_2 and DMS, with a focus on the first two gases which carry the largest uncertainties. The question of the importance of marine sulfur for our climate needs to be addressed globally, and climate models are powerful tools in this context. However, they require accurate boundary conditions, such as the in- and outflux of climate relevant trace gases. The thesis focuses thus on 1) how to best represent marine emissions in atmospheric chemistry climate models, 2) providing surface concentration inventories for the use in global models and estimate source strengths of the gases, and 3) improving process understanding of the marine cycling of the sulfur gases OCS and CS_2. To achieve these goals, a range of methods from process studies and field observations at the local scale to upscaling by regional and global biogeochemical models were developed (Fig. 1.5). The methods include novel measurement and sampling systems, a new database compilation of seawater measurements of the sulfur compounds, as well as model development and application from 0D to 3D models (see chapter 2). To improve emission estimates of marine sulfur compounds, three questions are addressed and presented in the following chapters and publications:

I **What is the best method to model marine emissions in atmospheric stand-alone 3D models?**
Coupled ocean-atmosphere models provide a powerful tool to calculate oceanic emissions consistent with both the marine boundary and the ocean mixed layer. Such a coupled calculation also allows for feedbacks of atmospheric mixing ratio changes on the concentration gradient and the flux. However, coupled models require high

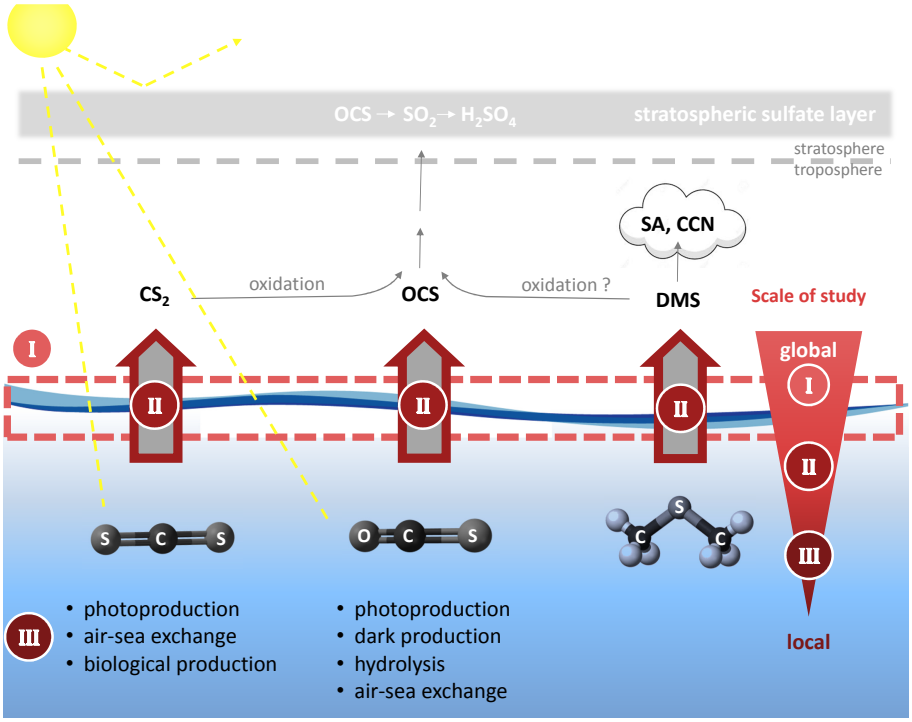

Figure 1.5: Research questions addressed in this thesis. Roman numbers refer to research questions defined in section 1.4. SA=secondary aerosols, CCN=cloud condensation nuclei.

computational power and thus, 3D stand-alone atmospheric models are often used instead. Therein, oceanic emissions are usually prescribed boundary conditions and hence not consistent with changes in atmospheric concentrations at the ocean surface. A submodule of calculating emissions online is used here to systematically test the difference between prescribed concentrations and prescribed emissions in the 3D atmospheric chemistry model EMAC (EHCAM5/MESSy2 atmospheric climate model) for DMS and 3 halocarbons.

This chapter is based on the following manuscript:

Lennartz, S. T., Krysztofiak, G., Marandino, C. A., Sinnhuber, B. M., Tegtmeier, S., Ziska, F., Hossaini, R., Krüger, K., Montzka, S. A., Atlas, E., Oram, D. E., Keber, T., Bönisch, H., and Quack, B.: Modeling marine emissions and atmospheric distributions of halocarbons and dimethyl sulfide: The influence of prescribed water concentration vs. prescribed emissions, Atmos. Chem. Phys., 15, 11753-11772, 10.5194/acp-15-11753-2015, 2015.

II **What is the global marine source strength of OCS?**

The global marine source strength of OCS is discussed against the background of its uncertain budget and missing tropical source, which inverse modeling studies have located in the tropical oceans (see section 1.1.1). CS_2 and potentially DMS contribute to the atmospheric budget of OCS. So far, top-down studies do not consider actual concentrations of OCS or its precursor gases in the surface ocean. Shipbased measurements of sea surface concentrations as well as atmospheric mixing ratios in the marine boundary layers are used to calculate emissions for two tropical regions and to fine-tune a model simulating OCS in the mixed layer, which is then applied globally to estimate the global source strength. This approach is complemented by global source estimates of the gases CS_2 and DMS.

The chapter is based on the following manuscript:

Lennartz, S. T., Marandino, C. A., von Hobe, M., Cortes, P., Quack, B., Simo, R., Booge, D., Pozzer, A., Steinhoff, T., Arevalo-Martinez, D. L., Kloss, C., Bracher, A., Röttgers, R., Atlas, E., and Krüger, K.: Direct oceanic emissions unlikely to account for the missing source of atmospheric carbonyl sulfide, Atmos. Chem. Phys., 17, 385-402, 10.5194/acp-17-385-2017, 2017.

III **Which processes drive the marine biogeochemical cycling of OCS and CS_2?**

Compared to DMS, little is known on the production processes for CS_2 and OCS. For OCS, the major processes are described, but only few quantitative parameterizations exist. For CS_2, detailed knowledge of production processes and drivers of the variations in marine concentrations are still lacking. Surface measurements and depth profiles of the two gases and several fractions of the dissolved organic matter pool are used here to further constrain and quantify the cycling of these two gases. A 1D model for OCS and CS_2 is developed for the physical and biogeochemical model framework GOTM/FABM, to assess yet unknown production and consumption processes from residual analyses. In particular, the influence of environmental parameters such as dissolved organic matter and oxygen is addressed, as the study site covered an upwelling system adjacent to a large oxygen minimum zone.

This chapter is based on the following manuscript:

Lennartz, S.T., Marandino, C.A., von Hobe, M., Fischer, T., Bittig, H., Booge, D., Goncalves-Araujo, R., Ksionzek, K., Koch, B.P., Bracher, A., Röttgers, R., Quack, B.: OCS and CS_2 production and loss processes in the eastern tropical South Pacific. Manuscript in preparation.

References

Anav, A.; Friedlingstein, P.; Beer, C.; Ciais, P.; Harper, A.; Jones, C.; Murray-Tortarolo, G.; Papale, D.; Parazoo, N. C.; Peylin, P.; Piao, S.; Sitch, S.; Viovy, N.; Wiltshire, A. & Zhao, M. (2015): Spatiotemporal patterns of terrestrial gross primary production: A review. *Reviews of Geophysics*.

Andreae, M. O. & Crutzen, P. J. (1997): Atmospheric aerosols: Biogeochemical sources and role in atmospheric chemistry. *Science* **276** (5315): 1052–1058.

Andreae, M. (1986): The ocean as a source of atmospheric sulfur compounds. *The role of air-sea exchange in geochemical cycling*. Springer,: 331–362.

Arneth, A.; Harrison, S. P.; Zaehle, S.; Tsigaridis, K.; Menon, S.; Bartlein, P. J.; Feichter, J.; Korhola, A.; Kulmala, M.; O'Donnell, D.; Schurgers, G.; Sorvari, S. & Vesala, T. (2010): Terrestrial biogeochemical feedbacks in the climate system. *Nature Geoscience* **3** (8): 525–532.

Asaf, D.; Rotenberg, E.; Tatarinov, F.; Dicken, U.; Montzka, S. A. & Yakir, D. (2013): Ecosystem photosynthesis inferred from measurements of carbonyl sulphide flux. *Nature Geoscience* **6** (3): 186–190.

Asher, W. E. & Wanninkhof, R. (1998): The effect of bubble-mediated gas transfer on purposeful dual-gaseous tracer experiments. *Journal of Geophysical Research: Oceans* **103** (C5): 10555–10560.

Aydin, M.; Campbell, J. E.; Fudge, T. J.; Cuffey, K. M.; Nicewonger, M. R.; Verhulst, K. R. & Saltzman, E. S. (2016): Changes in atmospheric carbonyl sulfide over the last 54,000years inferred from measurements in Antarctic ice cores. *Journal of Geophysical Research-Atmospheres* **121** (4) Aydin, M. Campbell, J. E. Fudge, T. J. Cuffey, K. M. Nicewonger, M. R. Verhulst, K. R. Saltzman, E. S.,: 1943–1954.

Ayers, G. & Gillett, R. (2000): DMS and its oxidation products in the remote marine atmosphere: implications for climate and atmospheric chemistry. *Journal of Sea Research* **43** (3): 275–286.

Bandy, A. R.; Maroulis, P. J.; Shalaby, L. & Wilner, L. A. (1981): Evidence for a short tropospheric residence time for carbon disulfide. *Geophysical Research Letters* **8** (11): 1180–1183.

Bandy, A. R.; Thornton, D. C. & Johnson, J. E. (1993): Carbon Disulfide Measurements in the Atmosphere of the Western North Atlantic and the Northwestern South Atlantic Oceans. *Journal of Geophysical Research* **98** (D12): 23449–23457.

Barnes, I.; Becker, K. H. & Patroescu, I. (1994): The tropospheric oxidation of dimethyl sulfide: A new source of carbonyl sulfide. *Geophysical Research Letters* **21** (22): 2389–2392.

Barnes, I.; Hjorth, J. & Mihalopoulos, N. (2006): Dimethyl Sulfide and Dimethyl Sulfoxide and Their Oxidation in the Atmosphere. *Chemical Reviews* **106** (3): 940–975.

Bates, T. S.; Lamb, B. K.; Guenther, A.; Dignon, J. & Stoiber, R. E. (2004): Sulfur emissions to the atmosphere from natural sourees. *Journal of Atmospheric Chemistry* **14**: 1–4.

Bates, T. S.; Kiene, R. P.; Wolfe, G. V.; Matrai, P. A.; Chavez, F. P.; Buck, K. R.; Blomquist, B. W. & Cuhel, R. L. (1994): The cycling of sulfur in surface seawater of the northeast Pacific. *Journal of Geophysical Research: Oceans* **99** (C4): 7835–7843.

Beer, C.; Reichstein, M.; Tomelleri, E.; Ciais, P.; Jung, M.; Carvalhais, N.; Rödenbeck, C.; Arain, M. A.; Baldocchi, D. & Bonan, G. B. (2010): Terrestrial gross carbon dioxide uptake: global distribution and covariation with climate. *Science* **329** (5993): 834–838.

Bell, T. G.; De Bruyn, W.; Miller, S. D.; Ward, B.; Christensen, K. H. & Saltzman, E. S. (2013): Air-sea dimethylsulfide (DMS) gas transfer in the North Atlantic: evidence for limited interfacial gas exchange at high wind speed. *Atmospheric Chemistry and Physics* **13** (21): 11073–11087.

Bentley, R. & Chasteen, T. G. (2004): Environmental VOSCs––formation and degradation of dimethyl sulfide, methanethiol and related materials. *Chemosphere* **55** (3): 291–317.

Berry, J.; Wolf, A.; Campbell, J. E.; Baker, I.; Blake, N.; Blake, D.; Denning, A. S.; Kawa, S. R.; Montzka, S. A.; Seibt, U.; Stimler, K.; Yakir, D. & Zhu, Z. (2013): A coupled model of the global cycles of carbonyl sulfide and CO_2: A possible new window on the carbon cycle. *Journal of Geophysical Research: Biogeosciences* **118** (2): 842–852.

Bopp, L.; Aumont, O.; Belviso, S. & Monfray, P. (2003): Potential impact of climate change on marine dimethyl sulfide emissions. *Tellus B* **55** (1): 11–22.

Boucher, O.; Randall, D.; Artaxo, P.; Bretherton, C.; Feingold, G.; Forster, P. M.; Kerminen, V.-M.; Kondo, Y.; Liao, H.; Lohmann, U.; Rasch, P. J.; Satheesh, S.; Sherwood, S.; Stevens, B. & Zhang, X. (2013): Clouds and Aerosols. *Climate Change 2013: The Physical Science Basis. Contribution of Working Group I to the Fifth Assessment Report of the Intergovernmental Panel on Climate Change*. Ed. by T. Stocker; D. Qin; G.-K. Plattner;

M. Tignor; S. Allen; J. Boschung; A. Nauels; Y. Xia; V. Bex & P. Midgley. Cambridge, United Kingdom and New York, NY, USA: Cambridge University Press.

Brimblecombe, P.; Hammer, C.; Rodhe, H.; Ryaboshapko, A. & Boutron, C. F. (1989): Human influence on the sulphur cycle. *Evolution of the global biogeochemical sulphur cycle,*: 77–121.

Brimblecombe, P. & Shooter, D. (1986): Photo-oxidation of dimethylsulphide in aqueous solution. *Marine Chemistry* **19** (4): 343–353.

Brühl, C.; Lelieveld, J.; Crutzen, P. J. & Tost, H. (2012): The role of carbonyl sulphide as a source of stratospheric sulphate aerosol and its impact on climate. *Atmos. Chem. Phys.* **12** (3): 1239–1253.

Campbell, E.; Kesselmeier, J.; Yakir, D.; Berry, J. A.; Peylin, P.; Belviso, S.; Vesala, T.; Maseyk, K.; Seibt, U.; Chen, H.; Whelan, M.; Hilton, T.; Montzka, S.; Lennartz, S.; Kuai, L.; Wohlfahrt, G.; Wang, Y.; Blake, N. & Blake, D. (2017): Assessing a New Clue to How Much Carbon Plants Store. *EOS Earth and Space Science News.*

Campbell, J. E.; Carmichael, G. R.; Chai, T.; Mena-Carrasco, M.; Tang, Y.; Blake, D. R.; Blake, N. J.; Vay, S. A.; Collatz, G. J.; Baker, I.; Berry, J. A.; Montzka, S. A.; Sweeney, C.; Schnoor, J. L. & Stanier, C. O. (2008): Photosynthetic Control of Atmospheric Carbonyl Sulfide During the Growing Season. *Science* **322** (5904): 1085–1088.

Charlson, R. J.; Lovelock, J. E.; Andreae, M. O. & Warren, S. G. (1987): Oceanic phytoplankton, atmospheric sulfur, cloud albedo and climate. *Nature* **326** (6114): 655–661.

Chin, M. & Davis, D. D. (1993): Global sources and sinks of OCS and CS_2 and their distributions. *Global Biogeochemical Cycles* **7** (2): 321–337.

Chin, M.; Rood, R. B.; Lin, S.-J.; Müller, J.-F. & Thompson, A. M. (2000): Atmospheric sulfur cycle simulated in the global model GOCART: Model description and global properties. *Journal of Geophysical Research: Atmospheres* **105** (D20): 24671–24687.

Cooper, D. & Saltzman, E. (1991): Measurements of Atmospheric Dimethylsulfide and Carbon Disulfide in the Western Atlantic Boundary Layer. *Journal of Atmospheric Chemistry* **12**: 153–168.

Crutzen, P. J. (1976): The possible importance of CSO for the sulfate layer of the stratosphere. *Geophysical Research Letters* **3** (2): 73–76.

Cunliffe, M.; Engel, A.; Frka, S.; Gasparovic, B.; Guitart, C.; Murrell, J. C.; Salter, M.; Stolle, C.; Upstill-Goddard, R. & Wurl, O. (2013): Sea surface microlayers: A unified physicochemical and biological perspective of the air–ocean interface. *Progress in Oceanography* **109**: 104–116.

Cutter, G. A.; Cutter, L. S. & Filippino, K. C. (2004): Sources and cycling of carbonyl sulfide in the Sargasso Sea. *Limnology and Oceanography* **49** (2): 555–565.

Cutter, G. A. & Radford-Knoery, J. (1993): Carbonyl sulfide in two estuaries and shelf waters of the western North Atlantic Ocean. *Marine Chemistry* **43** (1–4): 225–233.

Donelan, M. A.; Drennan, W.; Saltzman, E. & Wanninkhof, R. (2002): *Gas transfer at water surfaces—concepts and issues*. Gas transfer at water surfaces. Washington DC: American Geophysical Union.

Elliott, S. (1990): Effect of hydrogen peroxide on the alkaline hydrolysis of carbon disulfide. *Environmental Science & Technology* **24** (2): 264–267.

Elliott, S.; Lu, E. & Rowland, F. S. (1989): Rates and mechanisms for the hydrolysis of carbonyl sulfide in natural waters. *Environmental Science & Technology* **23** (4): 458–461.

Erickson, D. J. (1993): A stability dependent theory for air-sea gas exchange. *Journal of Geophysical Research: Oceans* **98** (C5): 8471–8488.

Ferek, R. & Andreae, M. O. (1984): Photochemical production of carbonyl sulphide in marine surface waters. *Letters to Nature* **1984**: 148–150.

Flöck, O. & Andreae, M. O. (1996): Photochemical and non-photochemical formation and destruction of carbonyl sulfide and methyl mercaptan in ocean waters. *Marine Chemistry* **54**: 11–26.

Flöck, O. R.; Andreae, M. O. & Dräger, M. (1997): Environmentally relevant precursors of carbonyl sulfide in aquatic systems. *Marine Chemistry* **59** (1–2): 71–85.

Frew, N. M.; Goldman, J. C.; Dennett, M. R. & Johnson, A. S. (1990): Impact of phytoplankton-generated surfactants on air-sea gas exchange. *Journal of Geophysical Research: Oceans* **95** (C3): 3337–3352.

Garbe, C. S.; Rutgersson, A.; Boutin, J.; De Leeuw, G.; Delille, B.; Fairall, C. W.; Gruber, N.; Hare, J.; Ho, D. T. & Johnson, M. T. (2014): Transfer across the air-sea interface. *Ocean-Atmosphere Interactions of Gases and Particles*. Springer,: 55–112.

Glatthor, N.; Höpfner, M.; Baker, I. T.; Berry, J.; Campbell, J. E.; Kawa, S. R.; Krysztofiak, G.; Leyser, A.; Sinnhuber, B. M.; Stiller, G. P.; Stinecipher, J. & Clarmann, T. v. (2015): Tropical sources and sinks of carbonyl sulfide observed from space. *Geophysical Research Letters,*: 10082–10090.

Glatthor, N.; Höpfner, M.; Leyser, A.; Stiller, G. P.; von Clarmann, T.; Grabowski, U.; Kellmann, S.; Linden, A.; Sinnhuber, B. M.; Krysztofiak, G. & Walker, K. A. (2016): Global carbonyl sulfide (OCS) measured by MIPAS/Envisat during 2002–2012. *Atmos. Chem. Phys. Discuss.* **2016** ACPD,: 1–34.

Hattori, S.; Schmidt, J. A.; Mahler, D. W.; Danielache, S. O.; Johnson, M. S. & Yoshida, N. (2012): Isotope Effect in the Carbonyl Sulfide Reaction with O(3P). *The Journal of Physical Chemistry A* **116** (14): 3521–3526.

Ho, D. T.; Zappa, C. J.; McGillis, W. R.; Bliven, L. F.; Ward, B.; Dacey, J. W. H.; Schlosser, P. & Hendricks, M. B. (2004): Influence of rain on air-sea gas exchange: Lessons from a model ocean. *Journal of Geophysical Research-Oceans* **109** (C8)

Ho, D. T.; Law, C. S.; Smith, M. J.; Schlosser, P.; Harvey, M. & Hill, P. (2006): Measurements of air-sea gas exchange at high wind speeds in the Southern Ocean: Implications for global parameterizations. *Geophysical Research Letters* **33** (16): L16611.

Hoffmann, E. H.; Tilgner, A.; Schrodner, R.; Brauera, P.; Wolke, R. & Herrmann, H. (2016): An advanced modeling study on the impacts and atmospheric implications of multiphase dimethyl sulfide chemistry. *Proceedings of the National Academy of Sciences of the United States of America* **113** (42): 11776–11781.

Hynes, A. J.; Wine, P. & Nicovich, J. (1988): Kinetics and mechanism of the reaction of hydroxyl with carbon disulfide under atmospheric conditions. *The Journal of Physical Chemistry* **92** (13): 3846–3852.

Jones, B. M. R.; Burrows, J. P.; Cox, R. A. & Penkett, S. A. (1982): OCS formation in the reaction of OH with CS_2. *Chemical Physics Letters* **88** (4): 372–376.

Jones, B. M. R.; Cox, R. A. & Penkett, S. A. (1983): Atmospheric chemistry of carbon disulphide. *Journal of Atmospheric Chemistry* **1** (1): 65–86.

Junge, C. E.; Manson, J. E. & Chagnon, C. W. (1961): A worl-wide stratospheric aerosol layer. *Science* **133** (346): 1478–1479.

Kettle, A. J. (2002): Global budget of atmospheric carbonyl sulfide: Temporal and spatial variations of the dominant sources and sinks. *Journal of Geophysical Research* **107** (D22)

Kettle, A. J.; Rhee, T. S.; von Hobe, M.; Poulton, A.; Aiken, J. & Andreae, M. O. (2001): Assessing the flux of different volatile sulfur gases from the ocean to the atmosphere. *Journal of Geophysical Research: Atmospheres* **106** (D11): 12193–12209.

Kettle, A. (2000): Extrapolations of the Flux of Dimethylsulfide, Carbon Monooxide, Carbonyl Sulfide and Carbon Disulfide from the Oceans. PhD thesis.

Khalil, M. A. K. & Rasmussen, R. A. (1984): Global Sources, Lifetime s and Mass Balances of Carbonyl Sulfide (OCS) and Carbon-Disulfide (CS_2) in the Earth's Atmosphere. *Atmospheric Environment* **18** (9): 1805–1813.

Kieber, D. J.; Jiao, J.; Kiene, R. P. & Bates, T. S. (1996): Impact of dimethylsulfide photochemistry on methyl sulfur cycling in the equatorial Pacific Ocean. *Journal of Geophysical Research: Oceans* **101** (C2): 3715–3722.

Kiene, R. P.; Linn, L. J. & Bruton, J. A. (2000): New and important roles for DMSP in marine microbial communities. *Journal of Sea Research* **43** (3–4): 209–224.

Kim, K. & Andreae, M. (1987): Carbon disulfide in seawater and the marine atmosphere over the North Atlantic. *Journal of Geophysical Research: Atmospheres* **92** (D12): 14733–14738.

Kim, K. H. & Andreae, M. O. (1992): Carbon disulfide in the estuarine, coastal and oceanic environments. *Marine Chemistry* **40**: 179–197.

Kloster, S.; Feichter, J.; Maier-Reimer, E.; Six, K. D.; Stier, P. & Wetzel, P. (2006): DMS cycle in the marine ocean-atmosphere system, a global model study. *Biogeosciences* **3** (1) BG,: 29–51.

Kock, A.; Schafstall, J.; Dengler, M.; Brandt, P. & Bange, H. W. (2012): Sea-to-air and diapycnal nitrous oxide fluxes in the eastern tropical North Atlantic Ocean. *Biogeosciences* **9** (3): 957–964.

Kreidenweis, S. M. & Seinfeld, J. H. (1988): Nucleation of sulfuric acid-water and methanesulfonic acid-water solution particles: implications for the atmospheric chemistry of organosulfur species. *Atmospheric Environment (1967)* **22** (2): 283–296.

Kremser, S.; Thomason, L. W.; von Hobe, M.; Hermann, M.; Deshler, T.; Timmreck, C.; Toohey, M.; Stenke, A.; Schwarz, J. P.; Weigel, R.; Fueglistaler, S.; Prata, F. J.; Vernier, J.-P.; Schlager, H.; Barnes, J. E.; Antuña-Marrero, J.-C.; Fairlie, D.; Palm, M.; Mahieu, E.; Notholt, J.; Rex, M.; Bingen, C.; Vanhellemont, F.; Bourassa, A.; Plane, J. M. C.; Klocke, D.; Carn, S. A.; Clarisse, L.; Trickl, T.; Neely, R.; James, A. D.;

Rieger, L.; Wilson, J. C. & Meland, B. (2016): Stratospheric aerosol—Observations, processes, and impact on climate. *Reviews of Geophysics* **54**: 278–335.

Krysztofiak, G.; Te, Y. V.; Catoire, V.; Berthet, G.; Toon, G. C.; Jegou, F.; Jeseck, P. & Robert, C. (2015): Carbonyl Sulphide (OCS) Variability with Latitude in the Atmosphere. *Atmosphere-Ocean* **53** (1): 89–101.

Kuai, L.; Worden, J. R.; Campbell, J. E.; Kulawik, S. S.; Li, K.-F.; Lee, M.; Weidner, R. J.; Montzka, S. A.; Moore, F. L.; Berry, J. A.; Baker, I.; Denning, A. S.; Bian, H.; Bowman, K. W.; Liu, J. & Yung, Y. L. (2015): Estimate of carbonyl sulfide tropical oceanic surface fluxes using Aura Tropospheric Emission Spectrometer observations. *Journal of Geophysical Research: Atmospheres* **120** (20): 11, 012–11, 023.

Lana, A.; Bell, T. G.; Simo, R.; Vallina, S. M.; Ballabrera-Poy, J.; Kettle, A. J.; Dachs, J.; Bopp, L.; Saltzman, E. S.; Stefels, J.; Johnson, J. E. & Liss, P. S. (2011): An updated climatology of surface dimethlysulfide concentrations and emission fluxes in the global ocean. *Global Biogeochemical Cycles* **25**

Launois, T.; Belviso, S.; Bopp, L.; Fichot, C. G. & Peylin, P. (2015): A new model for the global biogeochemical cycle of carbonyl sulfide - Part 1: Assessment of direct marine emissions with an oceanic general circulation and biogeochemistry model. *Atmos. Chem. Phys.* **15** (5): 2295–2312.

Likens, G. E. & Bormann, F. H. (1974): Acid Rain: A Serious Regional Environmental Problem. *Science* **184** (4142): 1176–1179.

Liss, P. S. & Slater, P. G. (1974): Flux of gases across air-sea interface. *Nature* **247** (5438): 181–184.

Liss, P.; Marandino, C. A.; Dahl, E.; Helmig, D.; Hintsa, E. J.; Hughes, C.; Johnson, M. T.; Moore, R. M.; Plane, J. M.; Quack, B.; Singh, H. B.; Stefels, J.; Glasow, R. v. & Williams, J. (2014): Short-Lived Trace Gases in the Surface Ocean and the Atmosphere. *Ocean-Atmosphere Interactions of Gases and Particles*. Ed. by M. T. J. Peter Liss. Springer Earth System Sciences.

Marandino, C. A.; De Bruyn, W. J.; Miller, S. D. & Saltzman, E. S. (2008): DMS air/sea flux and gas transfer coefficients from the North Atlantic summertime coccolithophore bloom. *Geophysical Research Letters* **35** (23)

Mayewski, P.; Lyons, W.; Spencer, M.; Twickler, M.; Buck, C. & Whitlow, S. (1990): An ice-core record of atmospheric response to anthropogenic sulphate and nitrate. *Nature* **346** (6284): 554–556.

McGillis, W. R.; Edson, J. B.; Hare, J. E. & Fairall, C. W. (2001): Direct covariance air-sea CO_2 fluxes. *Journal of Geophysical Research-Oceans* **106** (C8): 16729–16745.

Montzka, S. A.; Calvert, P.; Hall, B. D.; Elkins, J. W.; Conway, T. J.; Tans, P. P. & Sweeney, C. (2007): On the global distribution, seasonality, and budget of atmospheric carbonyl sulfide (COS) and some similarities to CO_2. *Journal of Geophysical Research* **112** (D9)

Osthoff, H. D.; Bates, T. S.; Johnson, J. E.; Kuster, W. C.; Goldan, P.; Sommariva, R.; Williams, E. J.; Lerner, B. M.; Warneke, C.; de Gouw, J. A.; Pettersson, A.; Baynard, T.; Meagher, J. F.; Fehsenfeld, F. C.; Ravishankara, A. R. & Brown, S. S. (2009): Regional variation of the dimethyl sulfide oxidation mechanism in the summertime marine boundary layer in the Gulf of Maine. *Journal of Geophysical Research-Atmospheres* **114**

Pos, W. H.; Riemer, D. D. & Zika, R. G. (1998): Carbonyl sulfide (OCS) and carbon monoxide (CO) in natural waters: evidence of a coupled production pathway. *Marine Chemistry* **62** (1–2): 89–101.

Preiswerk, D. & Najjar, R. G. (2000): A global, open-ocean model of carbonyl sulfide and its air-sea flux. *Global Biogeochemical Cycles* **14** (2): 585–598.

Quinn, P. K. & Bates, T. S. (2011): The case against climate regulation via oceanic phytoplankton sulphur emissions. *Nature* **480** (7375): 51–56.

Rodhe, H. (1999): Human impact on the atmospheric sulfur balance. *Tellus A: Dynamic Meteorology and Oceanography* **51** (1): 110–122.

Saltzman, E. S.; Savoie, D. L.; Zika, R. G. & Prospero, J. M. (1983): *Methane sulfonic acid in the marine atmosphere.*

Sandoval-Soto, L.; Stanimirov, M.; von Hobe, M.; Schmitt, V.; Valdes, J.; Wild, A. & Kesselmeier, J. (2005): Global uptake of carbonyl sulfide (COS) by terrestrial vegetation: Estimates corrected by deposition velocities normalized to the uptake of carbon dioxide (CO2). *Biogeosciences* **2** (2): 125–132.

Sheng, J.-X.; Weisenstein, D. K.; Luo, B.-P.; Rozanov, E.; Stenke, A.; Anet, J.; Bingemer, H. & Peter, T. (2015): Global atmospheric sulfur budget under volcanically quiescent

conditions: Aerosol-chemistry-climate model predictions and validation. *Journal of Geophysical Research: Atmospheres* **120** (1): 2014JD021985.

Simo, R.; Archer, S. D.; Gilpin, L. & Stelfox-Widdicombe, C. E. (2002): Coupled dynamics of dimethylsulfoniopropionate and dimethylsulfide cycling and the microbial food web in surface waters of the North Atlantic. *Limnology and Oceanography* **47** (1): 53–61.

Six, K. D.; Kloster, S.; Ilyina, T.; Archer, S. D.; Zhang, K. & Maier-Reimer, E. (2013): Global warming amplified by reduced sulphur fluxes as a result of ocean acidification. *Nature Clim. Change* **3** (11): 975–978.

Solomon, S.; Daniel, J. S.; Neely, R. R.; Vernier, J.-P.; Dutton, E. G. & Thomason, L. W. (2011): The Persistently Variable 'Background' Stratospheric Aerosol Layer and Global Climate Change. *Science* **333** (6044): 866–870.

Solomon, S.; Kinnison, D.; Bandoro, J. & Garcia, R. (2015): Simulation of polar ozone depletion: An update. *Journal of Geophysical Research: Atmospheres* **120** (15): 7958–7974.

Staubes, R. & Geogrii, H.-W. (1993): Biogenic sulfur compounds in seawater and the atmosphere of the Antarctic region. *Tellus* **45B**: 127–137.

Stefels, J. (2000): Physiological aspects of the production and conversion of DMSP in marine algae and higher plants. *Journal of Sea Research* **43** (3): 183–197.

Stefels, J.; Steinke, M.; Turner, S.; Malin, G. & Belviso, S. (2007): Environmental constraints on the production and removal of the climatically active gas dimethylsulphide (DMS) and implications for ecosystem modelling. *Biogeochemistry* **83** (1-3): 245–275.

Stickel, R.; Chin, M.; Daykin, E.; Hynes, A.; Wine, P. & Wallington, T. (1993): Mechanistic studies of the hydroxyl-initiated oxidation of carbon disulfide in the presence of oxygen. *The Journal of Physical Chemistry* **97** (51): 13653–13661.

Sunda, W.; Kieber, D.; Kiene, R. & Huntsman, S. (2002): An antioxidant function for DMSP and DMS in marine algae. *Nature* **418** (6895): 317–320.

Suntharalingam, P.; Kettle, A. J.; Montzka, S. M. & Jacob, D. J. (2008): Global 3-D model analysis of the seasonal cycle of atmospheric carbonyl sulfide: Implications for terrestrial vegetation uptake. *Geophysical Research Letters* **35** (19): L19801.

Tsai, W. T. & Liu, K. K. (2003): An assessment of the effect of sea surface surfactant on global atmosphere-ocean CO_2 flux. *Journal of Geophysical Research-Oceans* **108** (C4)

Uher, G. & Andreae, M. O. (1997): The diel cycle of carbonyl sulfide in marine surface waters: field study results and a simple model. *Atmospheric Geochemistry* **2**: 313–344.

Ulshöfer, V.; Uher, G. & Andreae, M. O. (1995): Evidence for a winter sink of atmospheric carbonyl sulfide in the northeast Atlantic Ocean. *Geophysical Research Letters* **22** (19): 2601–2604.

Von Hobe, M.; Cutter, G. A.; Kettle, A. J. & Andreae, M. O. (2001): Dark production: A significant source of oceanic COS. *Journal of Geophysical Research* **106** (C12): 31217.

Von Hobe, M.; Najjar, R.; Kettle, A. & Andreae, M. (2003): Photochemical and physical modeling of carbonyl sulfide in the ocean. *Journal of Geophysical Research* **108** (C7)

Walker, C. F.; Harvey, M. J.; Smith, M. J.; Bell, T. G.; Saltzman, E. S.; Marriner, A. S.; McGregor, J. A. & Law, C. S. (2016): Assessing the potential for dimethylsulfide enrichment at the sea surface and its influence on air-sea flux. *Ocean Science* **12** (4): 1033–1048.

Wang, Y.; Deutscher, N. M.; Palm, M.; Warneke, T.; Notholt, J.; Baker, I.; Berry, J.; Suntharalingam, P.; Jones, N.; Mahieu, E.; Lejeune, B.; Hannigan, J.; Conway, S.; Mendonca, J.; Strong, K.; Campbell, J. E.; Wolf, A. & Kremser, S. (2016): Towards understanding the variability in biospheric CO_2 fluxes: using FTIR spectrometry and a chemical transport model to investigate the sources and sinks of carbonyl sulfide and its link to CO2. *Atmos. Chem. Phys.* **16** (4): 2123–2138.

Wanninkhof, R.; Asher, W. E.; Ho, D. T.; Sweeney, C. & McGillis, W. R. (2009): Advances in Quantifying Air-Sea Gas Exchange and Environmental Forcing. *Annual Review of Marine Science* **1**: 213–244.

Watts, S. F. (2000): The mass budgets of carbonyl sulfide, dimethyl sulfide, carbon disulfide and hydrogen sulfide. *Atmospheric Environment* **34** (5): 761–779.

Weiss, P.; Andrews, S.; Johnson, J. E. & Zafiriou, O. (1995): Photoproduction of carbonyl sulfide in south Pacific Ocean waters as a function of irradiation wavelength. *Geophysical Research Letters* **22** (3): 215–218.

Whelan, M. & COSANOVA-Team (2017): Synthesis of using OCS as a new tracer to constrain terrestrial gross primary production [working title]. *in preparation.*

Wine, P. H.; Chameides, W. L. & Ravishankara, A. R. (1981): Potential role of CS_2 photooxidation in tropospheric sulfur chemistry. *Geophysical Research Letters* **8** (5): 543–546.

Wurl, O.; Miller, L.; Röttgers, R. & Vagle, S. (2009): The distribution and fate of surface-active substances in the sea-surface microlayer and water column. *Marine Chemistry* **115** (1): 1–9.

Xie, H.; Moore, R. M. & Miller, W. L. (1998): Photochemical production of carbon disulphide in seawater. *Journal of Geophysical Research: Oceans* **103** (C3): 5635–5644.

Xie, H.; Scarratt, M. G. & Moore, R. M. (1999a): Carbon disulphide production in laboratory cultures of marine phytoplankton. *Atmospheric Environment* **33** (21): 3445–3453.

Xie, H.; Scarratt, M. G. & Moore, R. M. (1999b): Carbon disulphide production in laboratory cultures of marine phytoplankton. *Atmospheric Environment* **33** (21): 3445–3453.

Zeng, Z.; Altarawneh, M. & Dlugogorski, B. Z. (2017): Atmospheric oxidation of carbon disulfide (CS2). *Chemical Physics Letters* **669**: 43–48.

Zepp, R. G. & Andreae, M. O. (1994): Factors affecting the photochemical production of carbonyl sulfide in seawater. *Geophysical Research Letters* **21** (25): 2813–2816.

Zhang, W.; Perrie, W. & Vagle, S. (2006): Impacts of winter storms on air-sea gas exchange. *Geophysical Research Letters* **33** (14)

Zhou, X. & Mopper, K. (1997): Photochemical production of low-molecular-weight carbonyl compounds in seawater and surface microlayer and their air-sea exchange. *Marine Chemistry* **56** (3): 201–213.

2
Methods

The research questions addressed in this thesis cover a range of scales, from local scale process understanding to global oceanic emissions and atmospheric impact. Hence, the applied methods reflect these different scales. In the following, new measurement techniques, databases and models, both applied and newly developed, will be described.

2.1 In-situ measurements of OCS and CS_2

2.1.1 A new underway measurement system for OCS

As OCS concentration in surface seawater can have strong diurnal variations, a method to monitor this high temporal variation requires continuous measurements at high temporal resolution. Additionally, the technique should be as automated as possible to minimize the effort of measurements covering full diurnal cycles. In order to enable such measurements onboard steaming vessels, a method for trace gas measurements was developed for OCS. The core of the system is a DLT-100 Trace Gas Analyzer for OCS and additionally CO_2 and CO (Los Gatos, USA), connected to an equilibration system which is supplied with seawater onboard the vessel. Previously, OCS has been analysed discretely using gas chromatographs (GC) coupled to different detectors (for example flame-photometric detection, FPD). Improvements to a previously developed continuous GC-FPD measurement system (Von Hobe et al., 2008) are the use of the novel OCS Analyzer which enables (i) a higher temporal resolution, (ii) a longer time span between calibrations and, (iii) reduced dependency on gas supply, as the new detector does not need any carrier gas.

Off-axis integrated cavity output spectroscopy

The DLT-100 trace gas analyzer operates with the method of off-axis integrated cavity output spectroscopy (OA-ICOS) and had been used for atmospheric measurements previously. The method makes use of the reduction in light intensity of a continuous laser beam that passes through an absorptive medium. The medium, i.e. a gas mixture containing the gas of interest, is located in a cavity with a highly reflective mirror at each side. The optical path length of the laser beam is extend to hundreds of meters using these mirrors, which increases the signal intensity. Gases absorb a defined energy of electromagnetic radiation to reach an excited state, which causes the light from the laser in the cavity to diminish. As the absorption differs in magnitude and wavelength among different gases, the gases can be identified due to the location of the absorption peak and the concentration can be determined due to the peak area. The advantage of off-axis ICOS compared to conventional laser spectroscopy is the non-perpendicular entry of the laser beam into the cavity (Schrade, 2011). The reflected laser beams thus do not extinguish because of interference when they travel through the cavity with an offset, compared to conventional laser spectroscopy, where the length of the cavity needs to be exactly mode-matched to the laser frequency and is thus much more prone to misalignments.

The measured absorption A(λ) is proportional to the amount of gas c in the cavity, the path length L and the molar absorption coefficient ϵ. It can be determined according to the Lambert-Beer-Law (eq. 2.1):

$$A(\lambda) = -ln\left(\frac{I_\upsilon}{I_0}\right) = -\epsilon \cdot c \cdot L \tag{2.1}$$

with I_υ and I_o being the outgoing and incoming light intensity, respectively. The analyzer is operated at a measurement resolution of 1 Hz averaged to 2 minutes, thereby achieving a precision of 15 ppt. The detection limit is ca. 100 ppt for OCS, which translates at a temperature range of 15-26° to a concentration of 2.8.-2.1 pmol L^{-1}. The system was operated on board in a climatised laboratory to minimize temperature changes. The pressure in the cell remained constant between 59.9966 and 60.0652 Torr while the ambient temperature changed between 32.2347 and 37.5080 °C, but variations between pressure and temperature were only weakly correlated (R^2=0.47). Details on drift and standard calibration can be found in chapter 4.

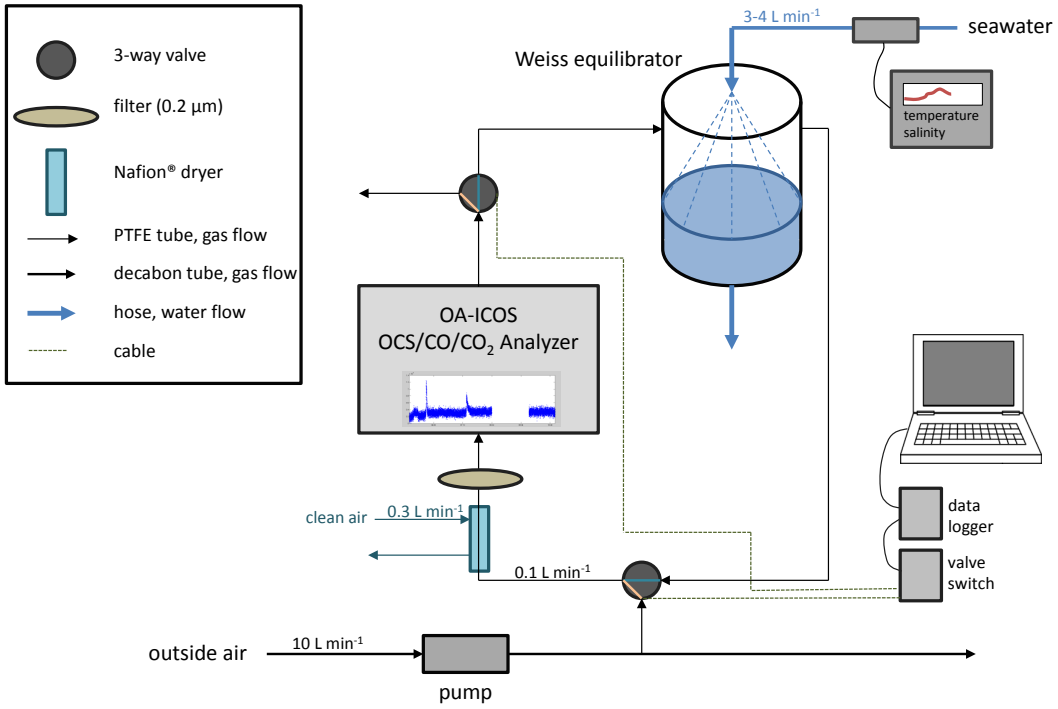

Figure 2.1: Set-up for continuous OCS measurements onboard the research vessels SONNE I and SONNE II.

The equilibration system

As the instrument can only measure in the gas phase, pre-treatment of seawater samples is required. Two different equilibration systems were tested in this thesis: a Weiss-type showerhead equilibrator and a membrane equilibrator. The Weiss-equilibrator was manufactured specifically for such applications at GEOMAR and has been applied successfully during several cruises in N_2O measurement set-ups (Arévalo-Martínez et al., 2013). A plexiglas chamber of 25 cm height and 15 cm diameter is filled with water until a 3 L headspace is reached. Seawater is supplied through a plate with holes at the top of the chamber, leading to a dispersion of the water into small droplets in the gaseous headspace. The droplets ensure a large air-water interface to enhance equilibration time. The second equilibrator was a membrane equilibrator (LiquiCel®, 3M) where water and gas phase are brought in contact over a large surface area (>5m^2) by hollow fiber membranes (material: polyethylene, polypropylene) that enable gas exchange. However, the efficiency of the equilibration with the membrane equilibrator was not sufficient as indicated by a dependency of the OCS mixing ratio at the equilibrator's outlet from (1) the OCS mixing ratio entering the

equilibrator, and (2) the water flow. The OCS mixing ratios at the equilibrator's outlet differed significantly when laboratory air (500 ppt) or clean air (below detection limit) was used at the inlet of the equilibrator (2-sided Welch test, p=2.2x10^{-16}, Fig. 2.2). Also, increasing the water flow from 2.9 to 4.9 L min^{-1} increased the measured OCS concentration for both gas streams tested by up to 40%. The equilibrator could not be operated with a water flow larger than 4.9 L min^{-1}, so a potential complete equilibration at larger water flows could not be tested. Therefore, the Weiss-equilibrator with the recirculation method described in the following was used.

The Weiss-equilibrator was continuously pumped with a flow rate of 3-5 L seawater min^{-1} from the moonpool of the vessel (Fig. 2.1). The equilibrated air was supplied at a flow rate of 100 ml min^{-1} to the cavity of the OCS analyzer, where the concentration of OCS in the gas phase is determined. Applying Henry's law of partitioning between air and water, the concentration in the water can be calculated (eq. 2.2).

$$c_w = \frac{H_T}{c_a} \tag{2.2}$$

As the solubility and thus H depends on temperature, it was logged in the equilibrator or the water supply directly and H_T is adapted by an Arrhenius-relationship (eq. 5.7):

$$H_T = 0.022 \cdot e^{2100 \cdot (\frac{1}{T} - \frac{1}{298})} \tag{2.3}$$

To prevent any water damage, a 0.2 μ filter (Pall Acro, NY, USA) is installed after the outlet of the equilibrator. The gas stream is dried with a Nafion® (Gasmet Ansyco, Germany) drier to reduce the relative humidity from 100% saturation to below the detection limit. The Nafion® drier was supplied with a 200-300 ml min^{-1} counterflow either with air from a clean air generator or from compressed synthetic air.

The equilibration time of the Weiss-equilibrator used had been tested for N_2O previously (Arévalo-Martínez et al., 2013). As the solubility of OCS (Henry constant 0.022 mol kg^{-1} bar^{-1}, (De Bruyn et al., 1995)) is comparable to that of N_2O (Henry constant 0.025 mol kg^{-1} bar^{-1}, (Weiss & Price, 1980)), a similar equilibration time of 2.5 min^{-1} is assumed here.

Several rubber materials are known to emit OCS and thus lead to contaminations. All materials have been tested for contamination, and PTFE or glass has been used as often as possible.

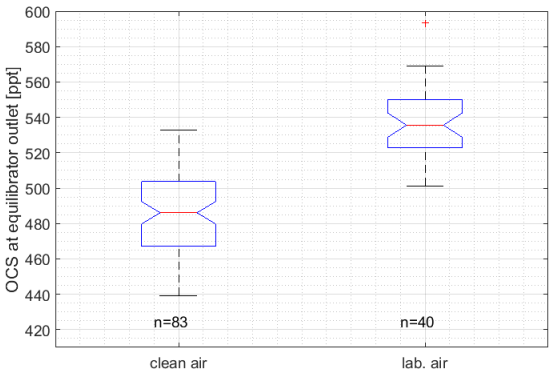

Figure 2.2: Comparison of the effect of the inlet gas stream on the OCS mixing ratio at the outlet of the membrane equilibrator. The OCS content of the gas stream entering the membrane equilibrator (clean air: OCS below detection limit, <100 ppt) and laboratory air (ca. 500 ppt OCS) had a significant effect of the OCS mixing ratio measured at the outlet of the membrane equilibrator (2-sided Welch test, p=2.2x10^{-16}).

2.1.2 A profiling pump for continuous depth profiles of OCS

Moving the water inlet through the water column brings the advantage of high resolution measurements from the horizontal to the vertical dimension. Continuous profiles enable the resolution of small scale gradients and covariation to other environmental parameters of interest. Therefore, a submersible pumping system was developed and deployed on the ASTRA-OMZ cruise (October 2014) in the Peruvian upwelling area.

The system consisted of a Lowara 1GSL03C-L4C submersible pump connected to a Teflon hose of 25mm diameter, which was connected to the Kevlar-wire of the ship's own winch during deployment (Fig. 2.3a). The length of the hose was 150 m, and thus deeper than the mixed layer depth encountered during that cruise. Additional weights attached at the pumphead (ca. 70 kg) reduced horizontal drifting by subsurface currents. To obtain the exact depth below surface, a temperature and pressure was logged near the pump inlet. On the ship's deck, the hose was connected to a manifold outlet, which included a direct overflow, supplies for 2 equilibrators and an additional sampling outlet, where further discrete samples were taken.

A time difference of 2:46 mins (±4.9s) between the hose in- and outlet was determined when the pump was switched on during two profiles. The spatial resolution of the profile is determined by the lowering speed together with the equilibration time (2.5 mins) in the equilibrator. With a lowering speed of 0.1 m s^{-1}, the spatial resolution is 15 m. This low resolution could be improved by using other types of equilibrators to lower the equilibration time in the future. During the four deployments of the ASTRA-OMZ cruise (see chapter

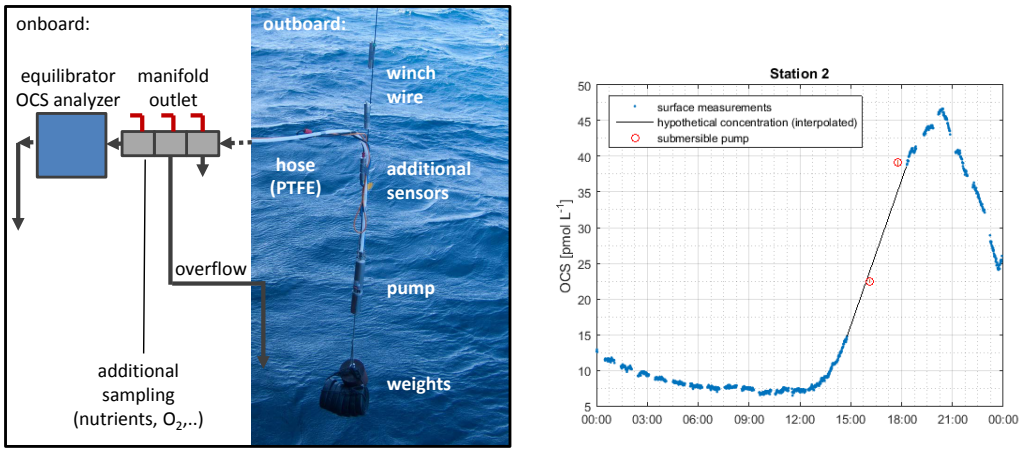

(a) Profiling pump set-up. **(b)** Contamination test.

Figure 2.3: The profiling pump set-up (a) and a test during deployment for possible contamination (b). Measurements with the profiling pump (red circles) and with the continuous surface underway system at the same (5 m) depth.

5), the pump inlet was held at a constant depth level for 10 minutes at 5-6 different depth during each profile, in order to reach complete stabilization of the signal.

Special care was taken to avoid contamination. The fact that concentrations below the detection limit (<100 ppt) were reached limits the upper range of possible contamination. Additionally, contamination against the surface measurement system described in section 2.1.1 at an inlet depth of 5 m was performed by pumping with the submersible pumping set-up in the up and down cast at the same inlet depth. No systematic offset was found, deviations from a hypothetical concentration obtained from a linear interpolation between the surface concentrations before and after the pump profiles were -2.4 pmol L^{-1} and 4.2 pmol L^{-1} respectively.

Four depth profiles up to 136 m depth were obtained with the profiling pump, and the profiling pump proved to be a promising tool for continuous measurements with a large requirement of water supply. Technical modifications in the future should include easier handling on board as well as a reduced equilibration time to increase the resolution of the profiles without further decreasing the lowering speed.

2.1.3 Measurements of CS_2 with GC-MS

No continuously operating systems exist for CS_2. Therefore, discrete samples were analysed for CS_2 concentration using a gas chromatograph coupled to a mass spectrometer (GC/MS; Agilent 7890A/Agilent 5975C; inert XL MSD with triple axis detector) running in single

ion mode. Compounds were transported with helium as carrier gas through the column (SUPEL-Q-Plot length: 30 m, diameter: 0.32 mm) of the gas chromatograph, where they are separated according to their polarity and boiling point. For detection in the MS, positive ions were generated by electron ionization (EI) at a current of 70 eV for acceleration, and mass separated afterwards with a quadrupole mass selector. The $\frac{m}{z}$ of 76 is used for detection of CS_2, as it has the strongest relative intensity in the mass spectrum of possible fragments (NIST, 2017). The ratio of $\frac{m}{z}$ of 76 and 78 (ca. 0.08) was recorded to prove the pure signal of CS_2. This ratio should be stable and consistent with the theoretical mass spectrum (NIST, 2017) if no interference with other ions at one of the two $\frac{m}{z}$ ratios occurs, which would indicate a contamination by altering the ratio.

Seawater was sampled bubble free in 50 mL transparent glass vials and analysed within one hour after sampling. PTFE coated lids were used to avoid contamination by rubber seals according to Drews (2015). Volatile compounds were stripped by purging with helium at a flow rate of 70 mL min^{-1} for 15 minutes. The gases were preconcentrated in a trap cooled by liquid nitrogen and injected into the GC-MS after heating the trap with hot water. The measurement of one sample consisted of running the same temperature program twice (resulting in Fig. 2.4a), where in the first run, a gaseous deuterated internal standard (isoprene-d5 and DMS-d3) is measured from a sample loop. Afterwards, the sample from the cooled trap is injected. Under this set-up, the retention time of CS_2 was 4.9 min.

Reproducibility of measurements was tested with repeatedly measuring samples taken at the same time and place. The mean difference of 5 samples was within 3.3% of the average concentration. The detection limit was determined from measuring MilliQ water three times, and adding three times the standard deviation of the peak areas of these measurements to the average. The detection limit is thus a molar amount of 0.3 pmol, which translates for the sample volume of 50 mL to a concentration of 5.8 pmol L^{-1}.

The concentrations were determined with a 3-5 point calibration from a gravimetrically prepared liquid CS_2 standard in ethylene glycol (see example in Fig. 2.4b). These standard calibrations were carried out daily during the cruise.

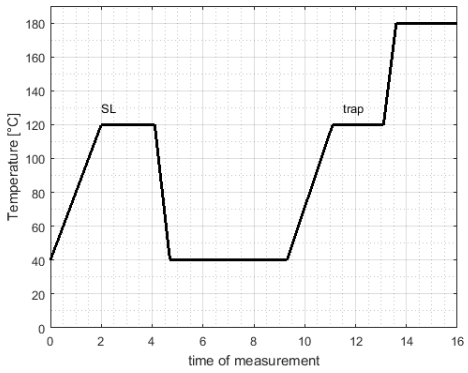

(a) Temperature program GC-MS for measurements of CS_2.

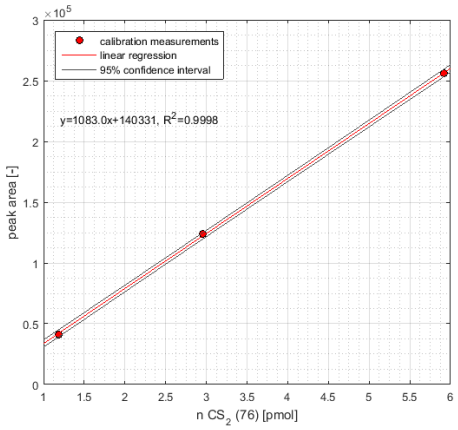

(b) Example of a 3-point calibration for CS_2.

Figure 2.4: Specifications for CS_2 measurements with GC-MS, (a) the temperature program including an internal standard (sample loop, SL) and the sample previously trapped in liquid nitrogen (trap), (b) an example of a 3-point calibration for CS_2 using a gravimetrically produced standard.

2.2 A new database for marine measurements of OCS and CS_2

To validate model simulations of the global surface concentrations of OCS and CS_2, a database including available data in a homogeneously structured and quality controlled way is crucial. For this purpose, a database of available observations was compiled from new, own data and previously published measurements in this thesis. Only shipbased measurements from the surface ocean and the marine boundary layer were considered, aircraft data was excluded. As a minimum, metainformation on geolocation, including water depth, dates (at least year, month, day and hour of day) and the measurement method was required for the data to be considered. Additional data, such as publications, cruises and environmental parameters (temperature, salinity, meteorological conditions including irradiance, wind speed, pressure, humidity and rain, as well as biological parameters such as chlorophyll *a* concentration), were added if available.

The database included all available measurements no matter in which temporal resolution they were taken. A flag was attributed to each database entry ranging from 1 (resolution in minutes) to 8 (yearly data). The temporal resolution of measurements is important for comparing or interpreting OCS data, because it displays strong diurnal cycles in some regions. To interpolate and obtain diurnal means, data base entries with flags 1, 2, 3 and 4 can be used.

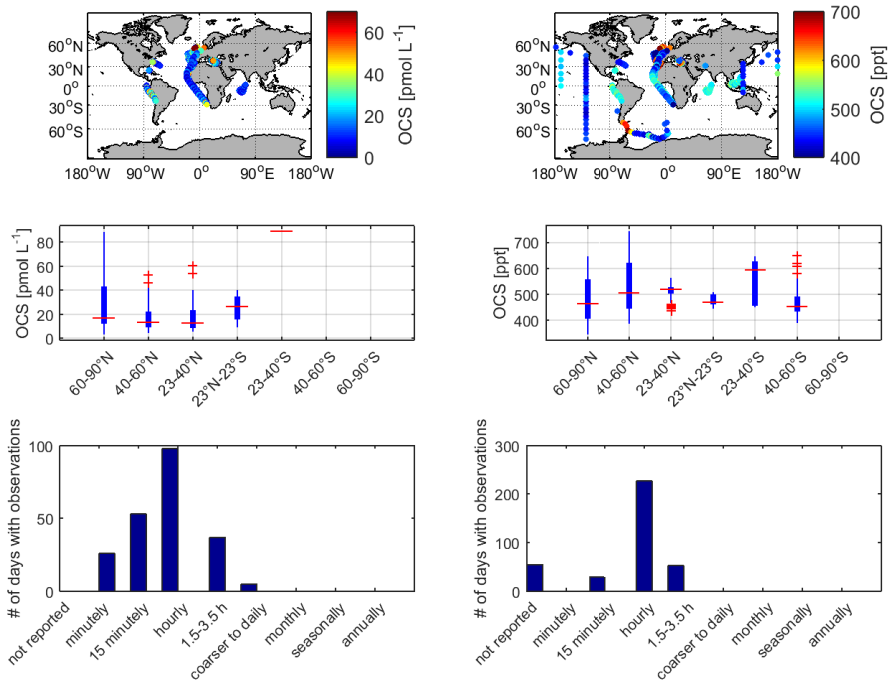

Figure 2.5: Metadata of OCS from the database as of January 2017. The database contains sea surface (left column) and atmospheric boundary layer (right column) measurements of OCS in varying temporal resolution (lower panels).

As of January 2017, the database consists of 24364 entries for OCS water concentrations from 17 cruises. The majority of measurements is located in the Northern hemisphere in the East Atlantic (Fig. 2.5, left panels). Two Atlantic transects from the North Sea to South Africa with hourly measurements are available. Mainly surface measurements were taken, but 26 depth profiles are also available from the BATs time series station (Cutter et al., 2004) and 4 depth profiles from the Peruvian upwelling region (see chapter 5). In total, the mean sea surface concentration is 21.4±20.27 pmol L^{-1}, with a range from 2.4 to 331.1 pmol L^{-1}. The observations for atmospheric boundary layer mixing ratios for OCS comprise 10695 observations, including observations from the Atlantic, Pacific, Indian and Southern Ocean (Fig. 2.5, right panels). The global average is 568.4±89 ppt and ranges from 289.6 to 828.9 ppt.

Less measurements are available for CS_2 in the surface ocean (1263 entries as of January 2017). Most of the observations come from four Atlantic transects, but data is also available from the Pacific and the Southern Ocean (Fig. 2.6). In total, data from seven cruises with a mean of 11.56±13.3 pmol L^{-1} and a range from 1.1 to 154.8 pmol L^{-1} is available. For the atmospheric boundary layer, the database comprises currently only data from Atlantic

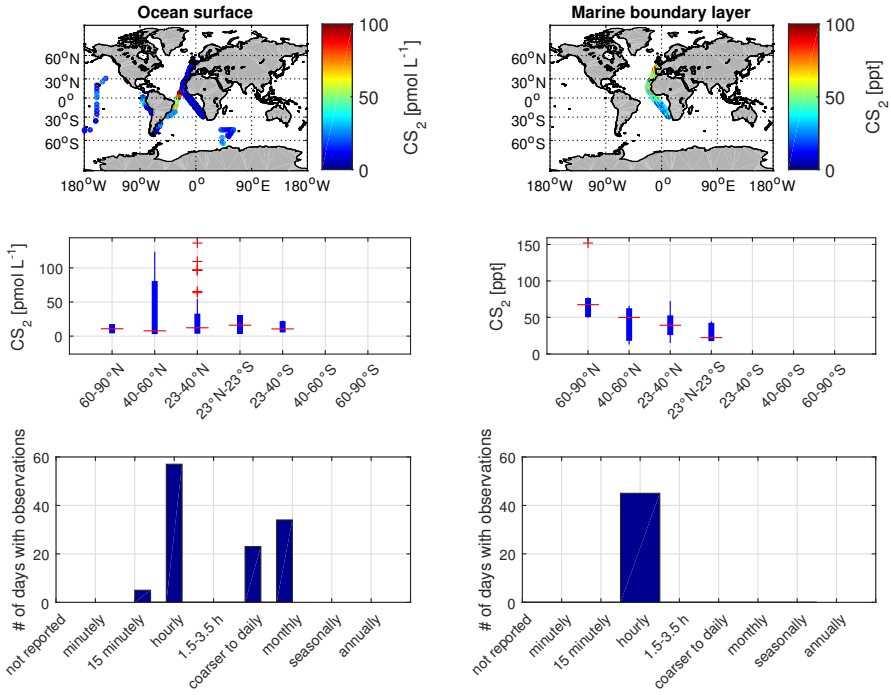

Figure 2.6: Metadata of CS_2 from the database as of January 2017. The database contains sea surface (left column) and atmospheric boundary layer (right column) measurements of CS_2 in varying temporal resolution (lower panels).

transects, in total 841 observations. Mixing ratios in the boundary layer are on average 45.3±22.8 ppt, ranging from below the detection limit to 275.7 ppt.

2.3 Box and 1D models for OCS and CS_2

2.3.1 Parameterizations for OCS

Parameterizations of reaction rates determining OCS concentrations in seawater from previously published studies were implemented in a box and a 1D water column model in this thesis. These processes include hydrolysis, air-sea exchange, dark production and photoproduction. A new parameterization of photoproduction was developed here, which is described in section 2.3.3 and chapter 4.

Hydrolysis describes an efficient loss process that depends on temperature and pH (Elliott et al., 1989). The parameterization for hydrolysis describes acidic and alkaline

degradation of OCS by the reactions 2.4 and 2.5:

$$OCS + H_2O \rightleftharpoons H_2S + CO_2 \tag{2.4}$$

$$OCS + OH^- \rightleftharpoons HS^- + CO_2 \tag{2.5}$$

In both the box and the 1D water column model, hydrolysis was parametrized as a first order kinetic reaction including the rate constant k_h according to Eq. 2.6-2.8 according to Elliott et al. (1989):

$$\frac{dC_{OCS}}{dt} = [OCS] \cdot k_h \tag{2.6}$$

$$k_h = exp\left(24.3 - \frac{10450}{SST}\right) + exp(22.8 - \frac{6040}{SST}) \cdot \frac{K}{a[H^+]} \tag{2.7}$$

$$-log_{10}K = \frac{3046.7}{SST} + 3.7685 + 0.0035486 \cdot \sqrt{SSS} \tag{2.8}$$

where $a[H^+]$ is the proton activity and K the ion product of seawater (Dickinson & Riley, 1979). This parameterization by Elliott et al. (1989) still provides the most comprehensive rate tested over a wide temperature and pH range, but under artificial conditions with much higher OCS concentrations than present in the ocean. Radford-Knoery & Cutter (1994) confirmed the rate and its temperature dependency under environmental conditions, but for a more narrow temperature range. A parameterization by Kamyshny et al. (2003) yielded slightly lower rates, especially at higher temperatures. At temperatures around 30°, the rate constants differ by a factor of 3 (Fig. 2.7).

Air-sea fluxes were calculated by multiplying the concentration gradient across the sea surface by the wind speed based transfer velocity (Eq. 3.1) in both models. The transfer velocity k was parametrized according to Nightingale et al. (2000). (Eq. 2.9):

$$k_{600} = (0.222 \cdot U_{10}^2 + 0.333 \cdot U_{10}) \cdot \left(\frac{Sc_{OCS}}{600}\right)^{0.5} \tag{2.9}$$

The transfer velocity k_{600} (600 is the Schmidt number of CO_2) was adapted for OCS with the respective Schmidt number Sc_{OCS}, i.e. the ratio of the kinematic viscosity of seawater (UNESCO, 1981) and the diffusion coefficient of OCS derived from its molar volume (Wilke & Chang, 1955). The concentration gradient was obtained as the difference between the actual concentration present in seawater and the corresponding equilibrium concentration at the given temperature and salinity. The equilibration concentration was derived from the Henry constant of OCS and its temperature dependency described by De Bruyn et al. (1995).

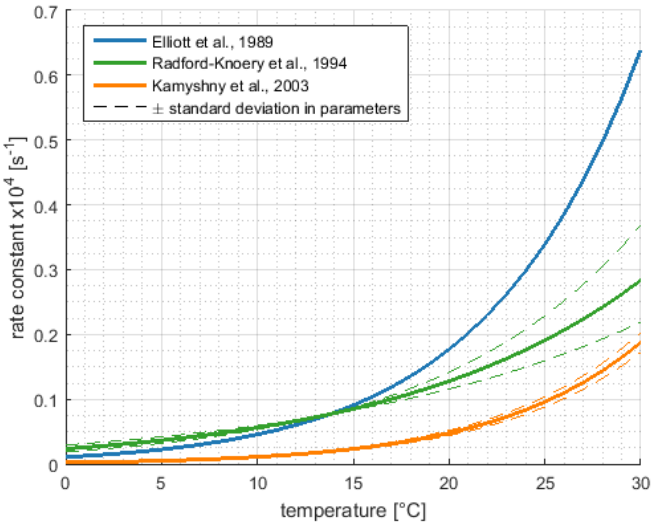

Figure 2.7: Hydrolysisrates for OCS from Elliott et al. (1989) and Radford-Knoery & Cutter (1994) and Kamyshny et al. (2003).

Light-independent production has only been quantified in one field study spanning several cruises to the Atlantic Ocean (Von Hobe et al., 2001). It has been derived from stable surface nighttime concentrations resulting from the equilibrium between loss by hydrolysis and light-independent production, normalized to an absorption of a_{350} of CDOM (Eq. 2.10).

$$\frac{dC_{OCS}}{dt} = a_{350} \cdot 10^{-6} \cdot exp\left(55.8 - \frac{16200}{SST}\right) \tag{2.10}$$

The Von Hobe et al. (2001) parameterization (Eq. 4.2) was used for the box model, whereas for the 1D water column model, a new parameterization was derived for the Peruvian upwelling regime (chapter 5).

The photoproduction term probably is the most difficult to parametrize, because of the spectral characteristics of the required parameters radiation, CDOM absorption and apparent quantum yield. Generally, the photoproduction Π is calculated according to Eq. 2.11:

$$\Pi = E \cdot \Phi \cdot a_{CDOM} \tag{2.11}$$

with E being the spectral irradiance, Φ the apparent quantum yield of OCS (AQY) and a_{CDOM} the absorption by CDOM. Full spectral AQY are available only from a few locations, including the open Pacific Ocean (Weiss et al., 1995), the gulf of Mexico and the North Sea (Zepp & Andreae, 1994), as well as the Sargasso Sea (Cutter et al., 2004). Often,

photoproduction rates are wavelength integrated and calculated with an integrated light spectrum (often UV as this is the range of the largest AQY), a specific absorption wavelength or wavelength range (often 350nm), and an integrated photoproduction rate constant p_{int}, which reflects the integrated AQY (Eq. 2.12).

$$\frac{dC_{OCS}}{dt} = p_{int} a_{350} UV \tag{2.12}$$

Wavelength integrated and wavelength resolved photoproduction rates have been tested and compared for cruises in the Atlantic and found to be reasonable substitutes for each other (von Hobe et al., 2003). Therefore, the integrated approach was used in both models. p_{int} was either fitted in an inverse set-up (1D water column model) or a newly developed parameterization was used (global box model).

The newly developed parameterization for p_{int} is based on CDOM, as von Hobe et al. (2003) found a linearly increasing relationship between p_{int} and CDOM for OCS surface measurements in the Atlantic Ocean. With the photoproduction rate constant p_{int} dependent on a_{350} (proxy for CDOM) in equation 4.8, the overall photoproduction rate becomes a second-order process with respect to CDOM. No global parameterization for p_{int} existed in dependence on CDOM/a_{350}. Thus, a first step to parametrize the photoproduction rate constant was made in this thesis, including in-situ production rate constants from the Indian, Pacific and Atlantic Ocean. The procedure is described in detail in chapter 4.

2.3.2 Parameterizations for CS_2

Processes are less well constrained for CS_2 compared to OCS, and less parameterizations are available from literature for use in models. Photoproduction and evidence for a biological production pathway have been shown in incubation studies (Xie et al., 1999a,b). Chemical degradation seems to be of minor importance (Elliott, 1990), which leaves air-sea exchange as the dominant sink at the surface (Kettle, 2000a).

Air-sea exchange was computed in the same way as for OCS with eq. 3.1 and eq. 2.9, using the Nightingale et al. (2000) parameterization for the transfer velocity k in the 1D water column model. While Elliott (1990) found lifetimes of CS_2 with respect to reactions with the H_2O_2 and OH radical in the order of years, Kettle (2000b) needed a much faster sink, on the order of tens of days, to explain observed concentrations. The mechanism and dependencies of such a degradation process are unknown. In the 1D water column model for CS_2, the chemical sink of CS_2 was therefore calculated according to eq. 2.13:

$$\frac{dC}{dt} = [CS_2] \cdot k_{deg} \tag{2.13}$$

with $[CS_2]$ being the concentration of CS_2 and k_{deg} being the rate constant of the unknown degradation process 8.38e-7 s^{-1} (Kettle, 2000a).

Only one AQY is currently available for the photoproduction of CS_2 (Xie et al., 1998) in the Atlantic, which has some similarities to OCS. However, in this thesis, the photoproduction rate constant p_{int} was estimated by parameter optimization for the 1D water column models according to eq. 2.12.

2.3.3 A simple box model to simulate sea surface concentrations

Box models are useful tools to simulate processes and trace gas concentrations in a simple, cost-effective way. They allow for quantitative conclusions despite simplifications and generalizations that have to be made to reduce complexity. Here, an existing box model (latest version von Hobe et al. (2003)) was further developed by implementing a new parameterization for the photoproduction rate constant and using satellite CDOM data. This version was applied globally for the first time.

The box model approach implies two simplifications. First, the mixed layer is treated as one single box with a uniform concentration of OCS. Second, horizontal mixing and lateral transfer are neglected. These assumptions will hold in regions with warm SST, as the short lifetime of OCS inhibits large-scale transport, and in regions with shallow mixed layers, where a constant concentration profile can develop. These conditions are usually encountered in the tropics to temperate regions, where the time series of measurements on which the box model was based were made. These assumptions might not be valid in higher latitudes, where cold temperatures lead to longer lifetimes. Modeled concentration hot-spots might be too narrow with such a neglection of the lateral transport. A box model is more cost efficient as a 3D model at the expense of the simplifications described above. Still, it provides useful information to constrain marine emissions of OCS, after the validation by comparison to independent measurements.

The box model simulated OCS concentration as the prognostic variable, which is governed by four processes: photoproduction, dark production, hydrolysis and air-sea exchange (Fig. 2.8). It is forced by meteorological parameters (global radiation, wind speed), oceanographic parameters (sea surface temperature, salinity, pH, mixed layer depth) and biogeochemical parameters (CDOM absorption at 350 nm, dry air mole fraction of OCS in the marine boundary layer). It can be run in the forward and in the inverse mode, the latter to enable parameter optimization for the photoproduction rate constant p_{int} in eq. 2.12.

The global box model uses an integrated photoproduction rate constant p_{int} (Eq. 2.12) matching the specific simplifications for UV light (i.e. Eq. 2.14) and CDOM absorption (i.e.

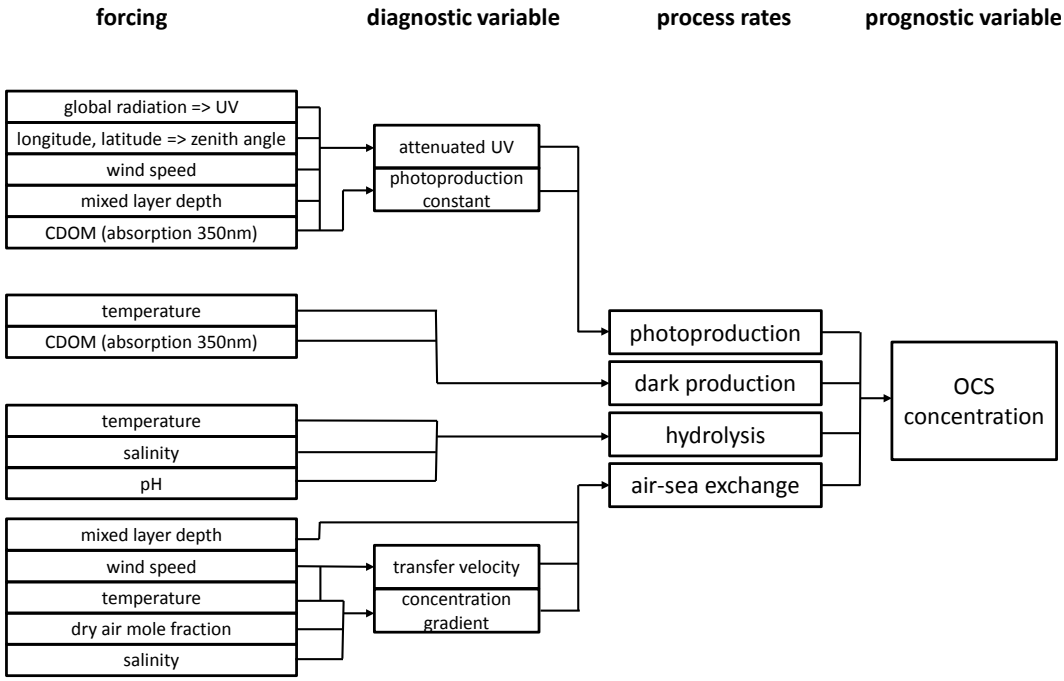

Figure 2.8: Set-up of the simple mixed layer box model for carbonyl sulfide (OCS) including forcing parameters, diagnostic variables, processes and the simulated prognostic variable.

using only the absorption at 350 a_{350}). The amount of UV light at the sea surface is derived from global radiation I [W m^{-2}] by Eq. 2.14 (Najjar et al., 1995):

$$UV = 2.85 \cdot 10^{-4} \cdot I \cdot cos^2\theta \tag{2.14}$$

where cos θ is the zenith angle. The UV light intensity was corrected for attenuation below the sea surface according to Sikorski & Zika (1993). UV light intensity was then calculated in the respective depth of the mixed layer in 1m steps, including attenuation by CDOM at 350nm and pure seawater.

In this thesis, the model was first applied to two cruises to the tropical Indian and the tropical East Pacific (see chapter 4) in inverse mode to estimate photoproduction rate constants needed to explain observed concentrations. For parameter optimization, a Levenberg-Marquardt optimization routine was used. The resulting photoproduction rate constants were then linearly regressed to CDOM absorption at 350 nm (a_{350}, see section 2.3.1) to obtain a new parameterization for P_{int} that incorporates data from different oceanic regions. The global box model was then run in forward mode including the new

parameterization.

2.3.4 1D water column models for OCS and CS_2

Understanding and quantifying (co-)variation of concentrations with depth requires a higher complexity than a simple mixed layer box model can provide. Additional physical processes such as the transport of gases by diapycnal mixing can be considered by extending the model dimension to the vertical water column. Both biogeochemical source and sink terms, as well as physical transport, are needed to provide a complete picture for trace gas cycling. For the purpose of quantitatively exploring depth profiles of the trace gases OCS and CS_2 together with other relevant biogeochemical parameters, a 1D water column model for both gases is presented here for the first time.

The physical processes are handled by the general ocean turbulence model GOTM (Burchard et al., 2006, available at www.gotm.net), which is a one dimensional water column model that simulates hydrodynamic and thermodynamic processes related to vertical mixing (Umlauf et al., 2005). The core of the model solves the transport equations for momentum, heat and salt (Umlauf et al., 2005), including a hydrodynamic and several turbulent models. GOTM is used as the physical host model for the newly developed biogeochemical models for OCS and CS_2. These models are coupled to GOTM by the framework for aquatic biogeochemical models (FABM) (Bruggeman & Bolding, 2014). Therein, local biogeochemical source and sink terms are provided for the prognostic trace gas variables (Fig. 2.9).

GOTM is forced by meteorological parameters, i.e. air temperature, air pressure, u and v components of wind speed, relative air humidity and cloud cover. Sea surface radiation is calculated as a function of day of the year and geographic location, and is corrected by cloud cover. The model simulation was run in a fully nudged set-up in this study to produce conditions as encountered during the field measurements under a steady state assumption. An inverse set-up to estimate photoproduction rate constants is developed as described in section 2.3.3. Details on the set-up of the simulation can be found in chapter 5.

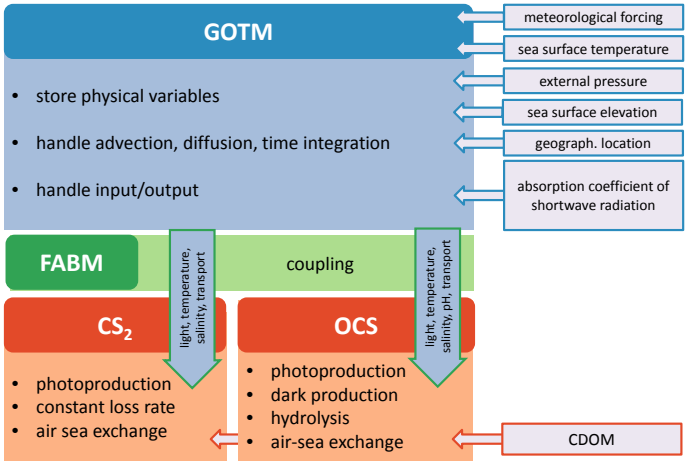

Figure 2.9: Model set-up for the 1D water column models for OCS and CS_2. GOTM serves as the physical host model for the local biogeochemical models for OCS and CS_2, which depend on physical variables for processes and transport on GOTM. This coupling is handled by FABM. Figure after (Bruggeman & Bolding, 2014).

2.4 The global atmospheric 3D chemistry climate model EMAC

EMAC is the *E*CHAM5/*M*ESSy2 *A*tmospheric *C*hemistry model described in Jöckel et al. (2010) and Joeckel et al. (2006). It is a numerical model system with a modular set-up, where tropospheric and middle atmospheric processes, as well as their interaction with other geophysical spheres, are simulated. Within the system, the *M*odular *E*arth *S*ubmodel *S*ystem MESSy2 acts as the interface to connect numerous submodels for physical and chemical atmospheric processes and reactions. ECHAM5 is the 5^{th} generation of an atmospheric global circulation model (A-GCM) developed from the weather forecast model *EC*MWF at the Max-Planck-Institute for Meteorology in *Ham*burg for climate study applications (Roeckner et al., 2006; Roeckner et al., 2003). Within EMAC, the atmospheric chemistry is calculated using the submodel MECCA (Module Efficiently Calculating the Chemistry of the Atmosphere; Sander et al., 2005, 2011) connected via the MESSy submodel system. Therein, basic gas phase, aqueous and heterogeneous chemistry is calculated for O_3, CH_4, HO_x, NO_x, non-methane hydrocarbons, halocarbons and sulfur compounds.

In the context of this thesis, EMAC is used to assess the influence of calculating oceanic emissions online during model simulation, as opposed to prescribing fluxes from the ocean surface. The latter neglects the feedback of atmospheric concentration changes on the

concentration gradient across the surface, making the simulated emissions inconsistent with the concentration of the gas in the marine boundary layer. To calculate emissions online, the submodule AIRSEA (Pozzer et al., 2006) is used. A detailed description of the simulation set-ups can be found in chapter 3. Here, the general model evaluations, relevant for the simulation including oceanic emissions of DMS and halocarbons, are described.

Simulated temperature in the middle atmosphere largely agrees within 2K to observations, and cold biases in wintertime in the lower polar stratosphere as e.g. present in the previous version of ECHAM (MAECHAM4/CHEM) were reduced (Jöckel et al., 2010). In line with previous versions, the warm bias during wintertime in middle latitudes and a slight cold bias at high latitudes still exist (Jöckel et al., 2010). Temperature affects the reaction rates and, thus, the atmospheric lifetime of trace gases, with potential feedbacks on the concentration gradient and thus emissions. However, the global tropospheric lifetimes of the gases considered in our study were consistent with independently calculated lifetimes (see chapter 3). This consistency indicates that the existing temperature biases do not interfere with the results in our study.

The scale of convective clouds is too small to be resolved in global A-GCMs, such as EMAC, and, thus, needs to be parameterized. The choice of the convection scheme has a major influence on the modeled trace gas distribution (Tost et al., 2010). The mismatch between observation and simulation due to unresolved convective processes increases with decreasing lifetime of the gas up to 100%, and can have local variations (Tost et al., 2010). While this mismatch can explain differences between observed and simulated atmospheric mixing ratios of trace gases, it does not interfere the comparison between online (prescribed water concentration) and offline (prescribed emissions) emissions, as the same convection scheme was chosen for both of the runs.

References

Arévalo-Martínez, D. L.; Beyer, M.; Krumbholz, M.; Piller, I.; Kock, A.; Steinhoff, T.; Körtzinger, A. & Bange, H. W. (2013): A new method for continuous measurements of oceanic and atmospheric N2O, CO and CO_2: performance of off-axis integrated cavity output spectroscopy (OA-ICOS) coupled to non-dispersive infrared detection (NDIR). *Ocean Sci.* **9** (6): 1071–1087.

Bruggeman, J. & Bolding, K. (2014): A general framework for aquatic biogeochemical models. *Environmental Modelling & Software* **61**: 249–265.

Burchard, H.; Bolding, K.; Kühn, W.; Meister, A.; Neumann, T. & Umlauf, L. (2006): Description of a flexible and extendable physical–biogeochemical model system for the water column. *Journal of Marine Systems* **61** (3): 180–211.

Cutter, G. A.; Cutter, L. S. & Filippino, K. C. (2004): Sources and cycling of carbonyl sulfide in the Sargasso Sea. *Limnology and Oceanography* **49** (2): 555–565.

De Bruyn, W.; Swartz, E.; Hu, J.; Shorter, J.; Davidovits, P.; Worsnop, D.; Zahniser, M. & Kolb, C. (1995): Henrys law solubilities and Setcheniw coefficients for biogenic reduced sulphur species obtained from gas-liquid uptake measurements. *Journal of Geophysical Research Atmosphere* **100**: 7245–7251.

Dickinson, A. G. & Riley, J. (1979): The estimation of acid dissociation constants in seawater media from potentiometric titrations with strong base. *Mar. Chem.* **7**: 89–99.

Drews, M. (2015): Isoprene and sulphur-containing compounds in seawater: detection, optimisation and application. CAU Kiel, Germany, Master thesis.

Elliott, S. (1990): Effect of hydrogen peroxide on the alkaline hydrolysis of carbon disulfide. *Environmental Science & Technology* **24** (2): 264–267.

Elliott, S.; Lu, E. & Rowland, F. S. (1989): Rates and mechanisms for the hydrolysis of carbonyl sulfide in natural waters. *Environmental Science & Technology* **23** (4): 458–461.

Jöckel, P.; Kerkweg, A.; Pozzer, A.; Sander, R.; Tost, H.; Riede, H.; Baumgaertner, A.; Gromov, S. & Kern, B. (2010): Development cycle 2 of the Modular Earth Submodel System (MESSy2). *Geosci. Model Dev.* **3** (2): 717–752.

Joeckel, P.; Tost, H.; Pozzer, A.; Bruehl, C.; Buchholz, J.; Ganzeveld, L.; Hoor, P.; Kerkweg, A.; Lawrence, M. G.; Sander, R.; Steil, B.; Stiller, G.; Tanarhte, M.; Taraborrelli, D.; Van Aardenne, J. & Lelieveld, J. (2006): The atmospheric chemistry

general circulation model ECHAM5/MESSy1: consistent simulation of ozone from the surface to the mesosphere. *Atmospheric Chemistry and Physics* **6**: 5067–5104.

Kamyshny, A.; Goifman, A.; Rizkov, D. & Lev, O. (2003): Formation of Carbonyl Sulfide by the Reaction of Carbon Monoxide and Inorganic Polysulfides. *Environmental Science & Technology* **37** (9): 1865–1872.

Kettle, A. (2000a): Extrapolations of the Flux of Dimethylsulfide, Carbon Monooxide, Carbonyl Sulfide and Carbon Disulfide from the Oceans. PhD thesis.

Kettle, A. (2000b): Extrapolations of the Flux of Dimethylsulfide, Carbon Monooxide, Carbonyl Sulfide and Carbon Disulfide from the Oceans. PhD thesis.

Najjar, R.; Erickson, D. & Madronich, S. (1995): Modeling the air-sea fluxes of gases formed from the decomposition of dissolved organic matter: Carbonyl sulfide and carbon monoxide. *The role of Nonliving Organic Matter in the Earth's Carbon Cycle*. Ed. by R. Zepp & C. Sonnyag. John Wiley & Sons,: 107–132.

Nightingale, P. D.; Malin, G.; Law, C. S.; Watson, A. J.; Liss, P. S.; Liddicoat, M. I.; Boutin, J. & Upstill-Goddard, R. C. (2000): In situ evaluation of air-sea gas exchange parameterizations using novel conservative and volatile tracers. *Global Biogeochemical Cycles* **14** (1): 373–387.

NIST (2017): *mass spectrum (electron ionization) carbon disulfide*.

Pozzer, A.; Jöckel, P.; Sander, R.; Williams, J.; Ganzeveld, L. & Lelieveld, J. (2006): Technical Note: The MESSy-submodel AIRSEA calculating the air-sea exchange of chemical species. *Atmos. Chem. Phys.* **6** (12): 5435–5444.

Radford-Knoery, J. & Cutter, G. A. (1994): Biogeochemistry of dissolved hydrogen sulfide species and carbonyl sulfide in the western North Atlantic Ocean. *Geochimica et Cosmochimica Acta* **58** (24): 5421–5431.

Roeckner, E.; Brokopf, R.; Esch, M.; Giorgetta, M.; Hagemann, S.; Kornblueh, L.; Manzini, E.; Schlese, U. & Schulzweida, U. (2006): Sensitivity of simulated climate to horizontal and vertical resolution in the ECHAM5 atmosphere model. *Journal of Climate* **19** (16): 3771–3791.

Roeckner, E.; Bäuml, G.; Bonaventura, L.; Brokopf, R.; Esch, M.; Giorgetta, M.; Hagemann, S.; Kirchner, I.; Kornblueh, L. & Manzini, E. (2003): The atmospheric general circulation model ECHAM 5. PART I: Model description.

Schrade, S. (2011): Ground based measurements of Carbon Dioxide and other climatically relevant trace gases using Off-Axis Integrated-Cavity-Output-Spectroscopy (ICOS). RWTH Aachen, Germany, Diploma thesis.

Sikorski, R. J. & Zika, R. G. (1993): Modeling mixed-layer photochemistry of H2O2: Optical and chemical modeling of production. *Journal of Geophysical Research: Oceans* **98** (C2): 2315–2328.

Tost, H.; Lawrence, M. G.; Brühl, C.; Jöckel, P. & Team, G. (2010): Uncertainties in atmospheric chemistry modelling due to convection parameterisations and subsequent scavenging. *Atmospheric Chemistry and Physics* **10** (4): 1931–1951.

Umlauf, L.; Burchard, H. & Bolding, K. (2005): *GOTM - scientific documentation.* Tech. rep.

UNESCO (1981): The Practical Salinity Scale 1978 and the International Equation of State of Seawater 1980. *UNESCO Technical Papers in Marine Science* **36**

Von Hobe, M.; Cutter, G. A.; Kettle, A. J. & Andreae, M. O. (2001): Dark production: A significant source of oceanic COS. *Journal of Geophysical Research* **106** (C12): 31217.

Von Hobe, M.; Kuhn, U.; Van Diest, H.; Sandoval-Soto, L.; Kenntner, T.; Helleis, F.; Yonemura, S.; Andreae, M. & Kesselmeier, J. (2008): Automated in situ analysis of volatile sulfur gases using a Sulfur Gas Analyser (SUGAR) based on cryogenic trapping and gas-chromatographic separation. *International Journal of Environmental Analytical Chemistry* **88** (5): 303–316.

Von Hobe, M.; Najjar, R.; Kettle, A. & Andreae, M. (2003): Photochemical and physical modeling of carbonyl sulfide in the ocean. *Journal of Geophysical Research* **108** (C7)

Weiss, P.; Andrews, S.; Johnson, J. E. & Zafiriou, O. (1995): Photoproduction of carbonyl sulfide in south Pacific Ocean waters as a function of irradiation wavelength. *Geophysical Research Letters* **22** (3): 215–218.

Weiss, R. F. & Price, B. A. (1980): Nitrous-oxide solubility in water and seawater. *Marine Chemistry* **8** (4): 347–359.

Wilke, C. & Chang, P. (1955): Some measurements of diffusion in liquids. **59**: 5.

Xie, H.; Moore, R. M. & Miller, W. L. (1998): Photochemical production of carbon disulphide in seawater. *Journal of Geophysical Research: Oceans* **103** (C3): 5635–5644.

Xie, H.; Scarratt, M. G. & Moore, R. M. (1999a): Carbon disulphide production in laboratory cultures of marine phytoplankton. *Atmospheric Environment* **33** (21): 3445–3453.

Xie, H.; Scarratt, M. G. & Moore, R. M. (1999b): Carbon disulphide production in laboratory cultures of marine phytoplankton. *Atmospheric Environment* **33** (21): 3445–3453.

Zepp, R. G. & Andreae, M. O. (1994): Factors affecting the photochemical production of carbonyl sulfide in seawater. *Geophysical Research Letters* **21** (25): 2813–2816.

3

Modelling marine emissions: the influence of prescribed water concentration vs. prescribed emissions

published as: *Lennartz, S. T., Krysztofiak, G., Marandino, C. A., Sinnhuber, B. M., Tegtmeier, S., Ziska, F., Hossaini, R., Krüger, K., Montzka, S. A., Atlas, E., Oram, D. E., Keber, T., Bönisch, H., and Quack, B.: Modeling marine emissions and atmospheric distributions of halocarbons and dimethyl sulfide: The influence of prescribed water concentration vs. prescribed emissions, Atmos. Chem. Phys., 15, 11753-11772, 10.5194/acp-15-11753-2015, 2015.*

Abstract. Marine produced short-lived trace gases such as dibromomethane (CH_2Br_2), bromoform ($CHBr_3$), methyliodide (CH_3I) and dimehtyl sulfide (DMS) significantly impact tropospheric and stratospheric chemistry. Describing their marine emissions in atmospheric chemistry models as accurately as possible is necessary to quantify their impact on ozone depletion and the Earth's radiative budget. So far, marine emissions of trace gases have mainly been prescribed from emission climatologies, thus lacking the interaction between the actual state of the atmosphere and the ocean. Here we present simulations with the chemistry climate model EMAC with online calculation of emissions based on surface water concentrations, in contrast to directly prescribed emissions. Considering the actual state of the model atmosphere results in a concentration gradient consistent with model real-time conditions at the ocean surface and in the atmosphere, which determine the direction and magnitude of the computed flux. This method has a number of conceptual and practical benefits, as the modeled emission can respond consistently to changes in

sea surface temperature, surface wind speed, sea ice cover and especially atmospheric mixing ratio. This online calculation could enhance, dampen or even invert the fluxes (i.e. deposition instead of emissions) of very short lived substances (VSLS). We show that differences between prescribing emissions and prescribing concentrations (-28 % for CH_2Br_2 to +11% for $CHBr_3$) result mainly from consideration of the actual, time-varying state of the atmosphere. The absolute magnitude of the differences depends mainly on the surface ocean saturation of each particular gas. Comparison to observations from aircraft, ships and ground stations reveals that computing the air-sea flux interactively leads in most of the cases to more accurate atmospheric mixing ratios in the model compared to the computation from prescribed emissions. Calculating emissions online also enables effective testing of different air-sea transfer velocity (k) parameterizations, which was performed here for eight different parameterizations. The testing of these different k values is of special interest for DMS, as recently published parameterizations derived by direct flux measurements using eddy covariance measurements suggest decreasing k values at high wind speeds or a linear relationship with wind speed. Implementing these parameterizations reduces discrepancies in modeled DMS atmospheric mixing ratios and observations by a factor of 1.5 compared to parameterizations with a quadratic or cubic relationship to wind speed.

3.1 Introduction

The oceans emit large amounts of halogen (Penkett et al., 1985; Quack & Wallace, 2003) and sulfur containing substances (Bates et al., 1992; Watts, 2000) that influence atmospheric chemistry. Organic bromine and iodine in the atmosphere is largely supplied by oceanic emissions of Very Short Lived Substances (VSLS) such as dibromomethane (CH_2Br_2), bromoform ($CHBr_3$) and methyliodide (CH_3I)(Hossaini et al., 2013; Lovelock & Maggs, 1973). Also, a large fraction of the atmospheric sulfur loading is due to oceanic emissions of OCS, CS_2, H_2S and dimethyl sulfide (DMS, CH_3SCH_3), the latter being the major compound transporting sulfur from the ocean to the atmosphere (Sheng et al., 2015; Watts, 2000). Thus, we focus on DMS in this study.

Assessing marine emissions of VSLS is crucial, as they significantly influence the Earth's atmosphere in both the troposphere and the stratosphere. In the troposphere, bromine containing VSLS such as $CHBr_3$ and CH_2Br_2 contribute to ozone destruction and alter the oxidative capacity (Salawitch, 2006; von Glasow et al., 2004). Oceanic CH_3I is the main organic iodine compound in the atmosphere (Lovelock & Maggs, 1973), and impacts tropospheric oxidative capacity and ozone destruction (Chameides & Davis, 1980; Saiz-Lopez et al., 2012). Iodine oxides, which can be product gases of CH_3I are likely to contribute to nucleation and growth of secondary marine aerosol production (O'Dowd & De Leeuw, 2007). DMS emitted to the troposphere is a precursor of secondary organic aerosol and potentially cloud condensation nuclei and thus influences the radiative budget (Charlson et al., 1987). Halogenated VSLS also enhance stratospheric ozone depletion (Sinnhuber & Meul, 2015) and thus contribute to the ozone-driven radiative forcing of climate (Hossaini et al., 2015). Despite the short lifetime of CH_3I (4-7 days) compared to the bromocarbons (6-120 days), there is potential for a small fraction of marine produced CH_3I to be transported to the stratosphere where it also contributes to ozone depletion (Solomon et al., 1994; Tegtmeier et al., 2013). DMS has a shorter lifetime of 11 min to 46 h (Barnes et al., 2006; Osthoff et al., 2009) compared to CH_3I. Despite the short lifetime, there is potential even for the very short lived DMS to be transported to the tropical tropopause layer (TTL) in convective hot spot regions (Marandino et al., 2013a,b).

The impact of marine VSLS emissions on atmospheric chemistry has been studied in chemistry-climate and transport models (e.g. Kerkweg et al., 2006b; Liang et al., 2010; Ordonez et al., 2012; Salawitch et al., 2005; Sinnhuber et al., 2009). Therein, marine emissions of the VSLS have mainly been based on prescribed boundary layer mixing ratios (Aschmann et al., 2009) or emission scenarios (Hossaini et al., 2013; Liang et al., 2010; Ordonez et al., 2012; Warwick et al., 2006). However, prescribing emissions in

atmospheric models lacks the impact of the atmospheric boundary layer mixing ratio on the concentration gradient. This concentration gradient at the interface between ocean and atmosphere directly influences the emissions, as it determines the direction and magnitude of the flux. The lack of potential feedbacks can result in a modeled atmospheric surface concentration inconsistent with the oceanic surface concentration.

Here, we evaluate a conceptually different way of considering marine emissions in chemical climate models that is based on a consistent concentration gradient between ocean and atmosphere. In contrast to previous approaches of either specifying atmospheric surface mixing ratios or specifying sea-to-air fluxes, water concentrations are prescribed and emissions are calculated online. Thus, the concentration gradient at the interface and the emissions are consistent with the atmospheric boundary layer and the ocean surface, and the emissions can respond to the actual state of the atmosphere. The approach is applied to established concentration climatologies of short lived halocarbons (CH_2Br_2, $CHBr_3$, CH_3I) and sulfur compounds (DMS) that share common characteristics such as supersaturation in the surface ocean and marine production. For the halocarbons, this set-up is applied for the first time and uses surface ocean concentration climatologies derived from observations by Ziska et al. (2013). Oceanic DMS emissions have been evaluated in coupled ocean-atmosphere models (Cameron-Smith et al., 2011; Kloster et al., 2006) or modeled online during a test for the implementation of different submodels (Kerkweg et al., 2006a). In our study, the focus lies on how to consider oceanic emissions in an stand-alone atmospheric model, and uses the most updated DMS concentrations available (Lana et al., 2011). Additionally, we compare the output of the two methods with observations from aircraft and ship campaigns.

Prescribing water concentrations and calculating emissions online enables convenient testing of different air-sea gas exchange parameterizations. Air-sea gas exchange is calculated as the product of the concentration gradient between air and water at the surface and the transfer velocity. The latter needs to be parameterized, and many different parameterizations have been published (see e.g. Wanninkhof et al., 2009, for a summary) for a summary). Most parameterizations relate the transfer velocity to wind speed (e.g. Ho et al., 2006; Liss & Merlivat, 1986; Nightingale et al., 2000; Wanninkhof & McGillis, 1999), but others take the effect of bubble mediated transfer (Asher & Wanninkhof, 1998) or enhancement by rain (Ho et al., 1997, 2004) into account. Testing a variety of different parameterizations on prescribed water concentrations to calculate atmospheric abundances provides information on the uncertainties of global emission estimates.

The experimental set-up consists of two steps: First, we prescribed surface water concentrations in the chemistry climate model EMAC (ECHAM5/MESSy for Atmospheric

Chemistry) (Jöckel et al., 2010; Joeckel et al., 2006)and air-sea exchange of VSLS was then calculated online by the submodel AIRSEA (Pozzer et al., 2006). The model results are then evaluated and compared to a simulation where the difference results from prescribed VSLS emissions (PE). To compare the simulation set-up with prescribed emissions to the set-up with prescribed water concentrations, we used the same concentration climatologies that were used to create the emission climatologies. In our study, these concentration and corresponding emission climatologies were published by Ziska et al. (2013) for the halocarbons and Lana et al. (2011) for DMS. The modeled atmospheric mixing ratios of the gases are compared to measurements from time series of ground based stations, ship and aircraft campaigns in order to identify whether the online calculation is simulating the atmospheric mixing ratios more accurately. In a second step, we use the coupled module to test the sensitivity of the global emissions to eight different, frequently used or recently published, transfer velocity parameterizations.

3.2 Model set-up and data description

3.2.1 The atmosphere-chemistry model EMAC

The ECHAM5/MESSy Atmospheric Chemistry (EMAC) model is a global atmospheric chemistry climate model described in Jöckel (2006) and Jöckel et al. (2010). ECHAM5/MESSy includes submodels describing processes of the troposphere and middle atmosphere as well as interaction with land and human influences. Air-sea gas exchange is calculated in EMAC with the submodule AIRSEA, as described by Pozzer et al. (2006). The numerical simulations were nudged towards the European Centre for Medium-Range Weather Forecasts (ECMWF), ERA-Interim reanalysis (Dee et al., 2011) every 6 hours (temperature, divergence, vorticity, surface pressure). The resolution of the EMAC atmosphere was 2.8°x2.8° (T42) and 39 vertical hybrid pressure levels up to 0.01 hPa (L39). The effect of resolution on the results tested with a finer resolution (T106) was only minor (see S-Tab. 2, supplementary material). The atmospheric model as well as the submodel AIRSEA uses a time step of 600 s. The convective transport follows the scheme of Tiedtke (1989) and the tracer advection is described in Lin & Rood (1996). An overview of these nudged simulation set-ups can be found in section 3.2.3.

The simulations include the four very short lived species CH_2Br_2, $CHBr_3$, CH_3I and DMS and simplified atmospheric loss reactions for them. The loss reactions include:

1. oxidation with OH, O(1D), Cl and photolysis for $CHBr_3$ and CH_2Br_2 following the

reactions rates by Sander et al. (2011),

2. oxidation with OH, Cl and photolysis for CH_3I Sander et al. (2011)
3. and oxidation with OH and O(3P) for DMS (Sander et al., 2011).

EMAC uses monthly mean concentrations of OH, developed and evaluated for the TRANSCOM-CH4 model intercomparison project, and discussed in detail by Patra et al. (2014). Monthly mean photolysis rates for VSLS were calculated by the TOMCAT CTM which has been used extensively to examine the tropospheric chemistry of VSLS (e.g. Hossaini et al., 2013). These fields were provided at a horizontal resolution of 2.8 x 2.8 degrees (longitude x latitude) and on 60 vertical levels (surface to 60 km). TOMCAT calculates photolysis rates online using the code of Hough (1988) which considers both direct and scattered radiation. Within TOMCAT, this scheme is supplied with surface albedo, monthly mean climatological cloud fields and ozone and temperature profiles. The photolysis rates have recently been used and evaluated as part of the ongoing TRANSCOM-VSLS model intercomparison project (http://www.transcom-vsls.com).

The simulated atmospheric lifetimes in our set-up generally agree well with published estimates for these gases, indicating that the basic assumption of the simplified chemistry applied here is valid. The local mean tropical (20°N-20°S) lifetime of CH2Br2 in the troposphere in our model study is 143 days and thus lies below 167 days, which was found in Hossaini et al. (2010). The mean tropospheric tropical lifetime of $CHBr_3$ is 20 days in our study, which is consistent within 10% with a recent reevaluation of $CHBr_3$ lifetime by Papanastasiou et al. (2014), together with a recent reevaluation of the reaction of OH with $CHBr_3$ by Orkin et al. (2013). The local lifetime of CH_3I in our study is 3 days which is in accordance with the study of Tegtmeier et al. (2013). The tropical lifetime of DMS in our study ranges between less than 1 day and up to 3 days, and is thus within but at the higher end of the range of 11 min to 46 hr (Barnes et al., 2006; Osthoff et al., 2009).

3.2.2 Parameterizations of air-sea gas exchange

In this study, the AIRSEA submodel (Pozzer et al., 2006) and its approach for air-sea gas exchange was adopted, using the two layer model (Liss & Slater, 1974). Marine emissions F of gases are calculated as the product of the concentration gradient between air and water concentration of the gas (Δc) and the transfer velocity k (Eq. 3.1), which needs to be parameterized.

$$F = k \cdot \Delta c = k \cdot (c_w - H \cdot c_{air}) \tag{3.1}$$

with c_w being the water concentration, H the Henry-constant (dimensionless, water over air) and cair the concentration of the gas in air which was taken from the modelled atmosphere in the respective time step. Henry constants and their temperature dependencies are taken from Moore et al. (1995) for the halocarbons and De Bruyn et al. (1995) for DMS.

The transfer velocity k comprises air- (k_{air}) and water-side (k_w) transfer velocities (Eq. 3.2) in all parameterizations with the Henry constant H, air temperature T_{air} and the ideal gas constant R:

$$k = \left(\frac{1}{k_w} + \frac{R \cdot H \cdot T_{air}}{k_{air}} \right)^{-1} \tag{3.2}$$

The water-side transfer velocity k_w is often parametrized in relation to wind speed with linear (e.g. Liss & Merlivat, 1986), quadratic (e.g. Ho et al., 2006) or cubic (e.g. Wanninkhof & McGillis, 1999) dependencies. Differences between these parameterizations arise from different techniques to determine k_w. The k_w parameterizations tested in our study result from tracer release experiments in wind tanks (Liss & Merlivat, 1986), from deliberate tracer techniques in the open ocean (Ho et al., 2006; Nightingale et al., 2000) or from direct flux measurements using eddy covariance (Bell et al., 2013; Marandino et al., 2009; Wanninkhof & McGillis, 1999). Additional drivers of gas exchange, e.g. bubble mediated transfer (e.g. Asher & Wanninkhof, 1998) and enhancement in the presence of rain (e.g. Ho et al., 2004) are discussed. Bubble mediated transfer has been suggested to be influential for gases with low solubilities, since they more quickly escape from the liquid phase into the bubbles. Asher & Wanninkhof (1998) reanalysed data from a dual tracer experiment and found a better fit when bubble mediated gas transfer was considered in the flux calculations. Bubbles are more easily transported to the surface and released to the atmosphere, thereby adding to the total flux. Rain is believed to increase the flux under calm wind conditions due to an alteration of the sea surface, which was tested in a dual tracer experiment in the laboratory (Ho et al., 2004). Other factors that are known to influence air-sea gas exchange, such as the presence of surfactants, but parameterizations including that effect are only marginally explored (Tsai & Liu, 2003) and require global distributions of surfactants that are currently not available. First steps of including surfactants in global models are currently discussed (Burrows et al., 2014; Elliott et al., 2014).

For sparingly soluble gases, k_w dominates the transfer velocity, and k_{air} is often neglected as a simplification. For more soluble gases, McGillis et al. (2000) found that considering k_{air} alters the flux to the atmosphere significantly when low temperatures or moderate wind speeds prevail. The parameterizations of k_{air} according to Kerkweg et al. (2006b, , eq. 3 and 4 therein) assumes a dependency on the friction velocity and surface wind speed, and is considered in the AIRSEA submodel.

The transfer velocity needs to be adapted to each gas by scaling it with the dimensionless Schmidt number in water for k_w and the Schmidt number in air for k_{air} divided by the Schmidt number that the specific parameterization was normalized to, which is in most cases either 600 or 660. The Schmidt number is the ratio of the diffusion coefficient of the compound to the kinematic viscosity of the surrounding medium. Following the approach of the AIRSEA submodel, the Schmidt number in water is estimated by scaling the CO_2 Schmidt number in water (Wanninkhof, 1992; Wilke & Chang, 1955), while the Schmidt number in air is calculated from air viscosity and diffusivity of the gas in air (Lyman et al., 1990).

3.2.3 Experimental Set-up

Prescribed concentrations and prescribed emissions

The experimental set-up consists of two steps: First, we compare emissions and atmospheric mixing ratios from prescribed water concentrations (PWC) with those derived from prescribed emissions (PE)(Fig. 3.1). For the PWC and PE set-up, two different submodels are used to calculate the emissions in EMAC: In the PE approach, emission climatologies are prescribed offline using the submodel OFFLEM (Kerkweg et al., 2006b). For the PWC set-up, emissions (or depositions) are calculated online using the submodel AIRSEA (Pozzer et al., 2006). Details of the simulation set-ups for the simulation 1 (PWC) and 2 (PE) can be found in Tab. 3.1. Both simulations cover a period of 24 years (1990-2013) to average out interannual variabilities in emissions and to ensure that the model output can be subsampled specifically at the times of atmospheric observations specified in section3.2.4.

In simulation 1 (PWC), we prescribe water concentration climatologies for the halocarbons from Ziska et al. (2013, , Z13), and for DMS from Lana et al. (2011, pp. , L11). The assumption of constant water concentrations despite loss by emissions is justified by the relatively small emissions compared to the absolute amount of gas in the oceanic mixed layer and the fast production of the compounds in water (Hepach et al., 2015; Hopkins & Archer, 2014). The modelled emissions from the PWC set-up are compared to the original Z13 & L11 emission climatologies. In the same manner, resulting atmospheric mixing ratios in the PWC simulation are compared to atmospheric concentrations from the PE set-up with prescribed emissions from Z13 & L11. The emission climatology from Z13 is based on constant water and atmospheric concentrations extrapolated from 5,000 measurements, using 6-hourly ERA-Interim wind, pressure and sea surface temperature fields and the Nightingale et al. (2000, , N00) parameterization for water-side transfer velocity. The L11 concentration climatology is based on 40,000 measurements and surface

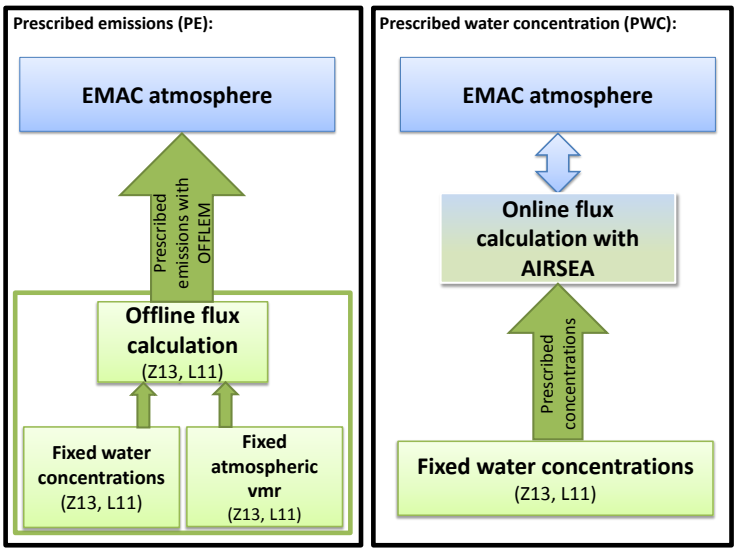

Figure 3.1: Schematic overview of the set-up of prescribed emissions (PE, left panel) and online calculated fluxes based on prescribed water concentrations (PWC, right panel) implemented in EMAC. Climatologies of fixed water and atmospheric concentrations in Ziska et al. (2013; Z13) and Lana et al. (2011; L11) were used to compute a global emission estimate, and the resulting interannual mean emission climatology is prescribed in EMAC using the submodule OFFLEM (PE, left panel). Calculating emissions online based on prescribed concentration (Z13, L11) considers the current state of the atmosphere during the calculation of emissions in the submodule AIRSEA (PWC, right panel).

wind data for the emission climatologies from the NCEP/NCAR reanalysis project with a water-side transfer velocity parametrized according to Nightingale et al. (2000) and an air-side transfer velocity according to Kondo (1975). The climatologies, prescribing emissions and concentrations of the gases of interest (CH_2Br_2, $CHBr_3$, CH_3I and DMS) were regridded to the T42 grid of EMAC with ncregrid (Jöckel, 2006), which is in all four cases coarser than the original grid described in Z13 & L11 (1°x1° in both). It has to be noted that this leads to a smoothing of small, local hotspots, but we assume this to be negligible since we compare emissions on a global scale.

Besides the concentrations taken from the climatologies Z13/L11, the air-sea calculation requires information on sea surface temperature, salinity and wind. The mean sea surface temperature in the model for simulation 1 (1990-2013) was 15.95°C, 15.82°C in Z13 and 16.22 °C in L11. The mean wind speed in the EMAC simulations (PWC, PE) was 7.51 m s^{-1}, which is slightly larger than the wind speed used to calculate the emission climatologies in Z13 (EMAC is 4.7% larger) and L11 (EMAC is 2.7% larger). Sea surface salinity is prescribed with a constant value of 0.4 mol L^{-1} in our model simulations as opposed to spatially varying salinity in Z13 & L11. A two-year simulation comparing the effects of a constant

Table 3.1: Set-up of model simulations evaluated in this study. PWC=prescribed water concentration, PE=prescribed emissions, AIRSEA=submodel for online calculation of emissions, OFFLEM=submodel for prescribing emissions.

	Abbrev.	k_w-Parameterization	Emission calculation submodule	Rain effect	White cap coverage	Period
1	PWC	Nightingale et al. (2000) prescribed emissions, no online calculation	PWC, AIRSEA	No	No	1990-2013
2	PE	k_w in original publications N00	PE, OFFLEM	No	No	1990-2013
3	LM86	Liss & Merlivat (1986)	PWC, AIRSEA	No	No	2010-2011
4	W99	Wanninkhof & McGillis (1999)	PWC, AIRSEA	No	No	2010-2011
5	N00	Nightingale et al. (2000)	PWC, AIRSEA	No	No	2010-2011
6	H06	Ho et al. (2006)	PWC, AIRSEA	No	No	2010-2011
7	H06r	Ho et al. (2006)	PWC, AIRSEA	Yes	No	2010-2011
8	H06w	Ho et al. (2006)	PWC, AIRSEA	No	Yes	2010-2011
9	B13m	Bell et al. (2013) modified, only DMS	PWC, AIRSEA	No	No	2010-2011
10	M09	Marandino et al. (2009)	PWC, AIRSEA	No	No	2004-2013

salinity versus the Z13 climatology revealed a low effect on global emissions (<3%), which is in accordance with findings of Ziska et al. (2013). Compared to the calculation of the Schmidt number in the publications by Z13 & L11, the submodel AIRSEA uses a different empirical, temperature dependent equation to calculate the Schmidt number. In AIRSEA, the Schmidt number of CO_2 at the respective temperature is calculated and then adapted with the molar volume to the Schmidt number of the gas of interest (Hayduk & Laudie, 1974; Wilke & Chang, 1955). In Z13, the Schmidt number is calculated by averaging the diffusion coefficient according to Hayduk & Laudie (1974) and Wilke & Chang (1955) and then dividing by the dynamic viscosity of seawater at varying temperatures and a constant salinity of 35. In L11, the Schmidt number is calculated according to Saltzman et al. (1993). The resulting differences are negligible at sea surface temperatures higher than 10°C and grow largest at 0°C, where they are still less than 15%. Since the Schmidt number is then normalized to the Schmidt-number of CO_2, the resulting difference becomes small and does not lead to significant differences in the global emission estimates of all four compounds. Differences in other influential input parameters for emission calculation between our PWC set-up and Z13 & L11 are thus small, ensuring that differences in emissions between PWC and Z13 & L11 can be attributed to the consideration of the actual state of the atmosphere in the PWC set-up.

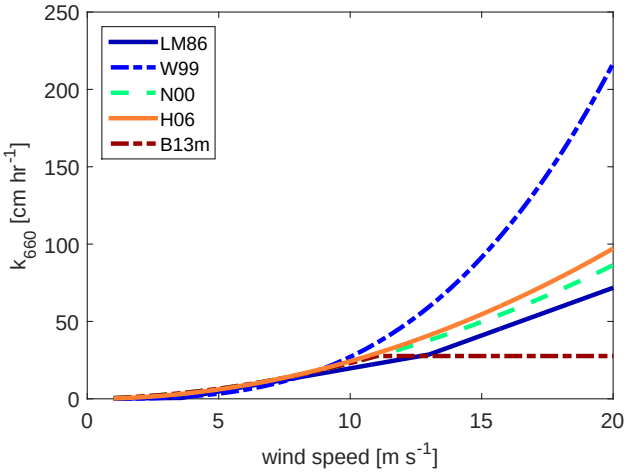

Figure 3.2: Parameterizations for water-side transfer velocity of air-sea gas exchange k_w for a Schmidt number of 660 that are tested in this study: the linear parameterization LM96 (Liss and Merlivat, 1986), the cubic parameterization W99 (Wanninkhof and McGillis, 1999), the quadratic parameterization N00 (Nightingale et al., 2000) and H06 (Ho et al., 2006), the parameterization modified according to Bell et al. (2013, B13m) with a leveling off at wind speeds higher than 11 m s^{-1}, and the linear parameterization M09 (Marandino et al., 2009).

Transfer velocity parameterizations

In the second part of the study, we test the sensitivity of the global emissions towards eight different transfer velocity parameterizations. These tests cover a two year time span (2010-2011) with one year (2009) as spin-up. The simulations 3-6 (Tab. 3.1) test the impact of different water-side transfer velocity parameterization related to wind speed. The parameterizations tested in this study are illustrated in Fig. 3.2. With increasing wind speed, the differences between the transfer velocity parameterizations grow larger; hence testing these parameterizations yields a range of global emission estimates that reflects this uncertainty. Parameterizations and the general description of air-sea gas exchange calculation are described in section 3.2.2.

Tab. 3.1 provides an overview of all performed simulations. Simulation 3 uses the 3-step linear parameterization of Liss & Merlivat (1986, pp. , LM86), simulation 4 the cubic relationship by Wanninkhof & McGillis (1999, , W99), simulation 5 the quadratic parameterization by Nightingale et al. (2000, , N00), and simulation 6 the quadratic transfer velocity parameterization by Ho et al. (2006, , H06)). The effect of rain (simulation 7 in Tab. 3.1) was tested adding the Ho et al. (1997) rain effect parameterization to the H06 transfer velocity parameterization (see Pozzer et al., 2006, , eq. 10 and 11). White cap coverage according to Asher & Wanninkhof (1998, , A98) considers bubble mediated gas exchange

and is used in simulation 8. The different parameterizations (LM86, W99, N00, H06) were available from the AIRSEA version of Pozzer et al. (2006). The N00 parameterization was normalized to the Schmidt number of 600 as in the original publication by Nightingale et al. (2000), while 660 was used in Z13.

Two additional simulations including only DMS were performed to test the effect of two recently published parameterizations of k_w. These two parameterizations have been derived from in-situ DMS eddy covariance measurements and deviate from previously published parameterizations. Bell et al. (2013) observed that the transfer velocity does not increase at wind speeds higher than 11 m s^{-1}. Marandino et al. (2009) found a linear dependency between wind speed and the transfer velocity k_w for DMS. Both simulations cover the period of 2004-2013, since observations from this period were available for comparison. These two parameterizations for k_w were added to the submodule code of AIRSEA (for equations see Tab. 3.2). The modification of the code included a parameterization based on results of the study from Bell et al. (2013, , B13m) with a conservative approach, in which the N00 parameterization was used at wind speeds below 11 m s^{-1} and kept constant at higher wind speeds to account for the missing increase of k_w with increasing wind speed. Finally, the parameterization by Marandino et al. (2009, pp. , M09) was used in simulation 10 for the same period as B13m. Both newly implemented parameterizations are part of the most recent release MESSy 2.52.

3.2.4 Observational data

Simulated atmospheric mixing ratios of the trace gases from PWC and PE are compared to observations from ship campaigns, aircraft campaigns and ground based time series stations.

Twenty-three aircraft campaigns providing halocarbon data are considered in order to create annual zonal mean climatologies of these trace gases. The combined data set ranges from 90°N to 75°S, transecting from the surface to the upper troposphere/lower stratosphere over land and ocean from 1992 to 2012 (see S-Tab. 3.7 for details on the aircraft campaigns). Many of the more recent data sets are inter-calibrated (see e.g. Brinckmann et al., 2012; Hall et al., 2014; Sala et al., 2014; Wisher et al., 2014). The latitudinal and longitudinal distributions and names of the aircraft campaigns are illustrated in Fig. 3.3. The measurements were averaged in zonal 10° wide latitude bins with a vertical extent ranging from 10 to 50 hPa (10 hPa in boundary layer and TTL region). Most of the measurements are located around 30°N of latitude with more than 150 points per bin. The tropical region (20°N – 20°S) has an average of 50 points per bin. S-Fig. 3.12 in the supplementary material illustrates the numbers of the measurements per bin. For the comparison of measured and

Table 3.2: Integrated global emissions during 2010-2011 for sensitivity tests using different parameterizations for the transfer velocity k_w (simulations 3-6, same as in Tab. 1) and the effects of rain (simulation 7), bubble mediated transfer parametrized using white cap coverage (simulation 8) and parameterizations recently suggested for DMS (simulation 9 and 10). Equations for the parameterizations using wind speed u are given for the Schmidt number (subscript after k) as in the original publications listed. u= wind speed at 10 m above sea level in m s^{-1}. k is given in cm hr^{-1}.

Nr.	Parameterization		CH_2Br_2 Gg yr^{-1}	$CHBr_3$ Gg yr^{-1}	CH_3I Gg yr^{-1}	DMS Gg yr^{-1}
		for u≤3.6, k_{660}=*0.17u*				
3	Liss & Merlivat (1986)	for 3.6≤u≤13, k_{660}=*2.85u-9.65*	53.74	189.10	151.88	33.38
		for 13≤u, k_{660}=*5.9u*				
4	Wanninkhof & McGillis (1999)	k_{660}=*0.0283*u^3	53.38	211.17	223.52	45.22
5	Nightingale et al. (2000)	k_{600}=*0.0283*u^3	63.04	238.46	209.73	45.49
6	Ho et al. (2006)	k_{600}=*0.266*u^2	62.71	236.10	213.47	45.91
7	Ho et al. (2006)+rain	–	65.08	249.66	225.67	48.70
8	white cap coverage	–	62.76	238.51	197.44	42.53
9	Bell et al. (2013), modified	for u≤11, k_{600}=*0.22*u^2*+0.333u*	–	–	–	40.63
		for u>11, k_{600}=*30.283*				
10	Marandino et al. (2009)	k_{720}=*1.92u-1.0**	–	–	–	42.45
	Mean (simulation 3-6)		59.47	218.71	199.65	42.5

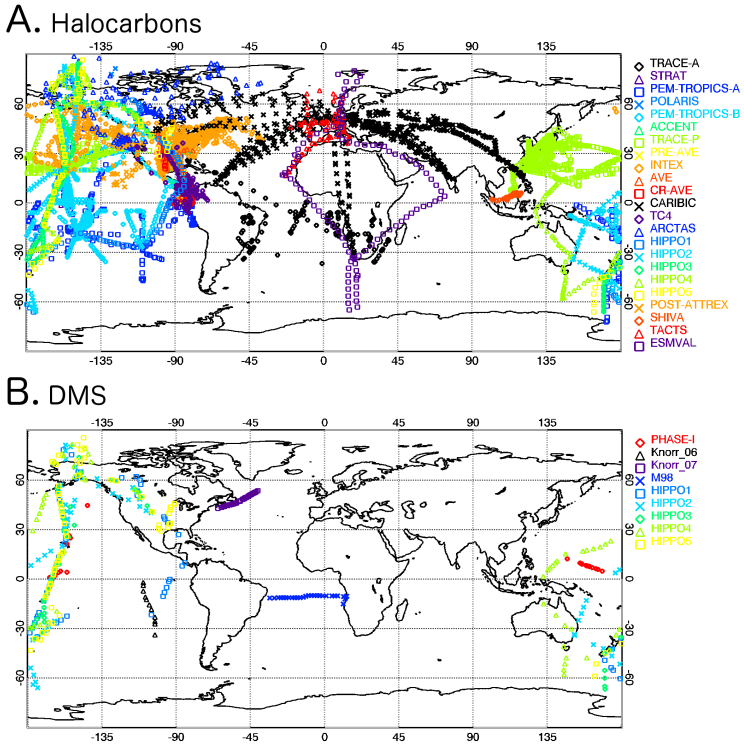

Figure 3.3: Locations of atmospheric data for comparison with model output used in this study. Panel A shows locations of atmospheric measurements from 23 aircraft campaigns considered for comparison with halocarbon simulations. Panel B shows location of measurements in the atmospheric boundary layer from ships (PHASE-1, Knorr-06, Knorr-07, M98) and from aircraft campaigns (HIPPO 1-5) measurements, considered for comparison with DMS simulations.

modelled data, the EMAC output of simulations 1 and 2 is first sampled at the same location as the aircraft measurements (longitude, latitude, altitude and time) by linear interpolation. Then, the same process of averaging per bin as for the measurements is applied to the model output.

Nine coastal ground stations from NOAA/ESRL, where halocarbons have been measured by the NOAA global flask sampling network starting from 1990-2004 were chosen for comparison due to their location close to the coast (Tab. 3.3). These data are currently available at the HalOcAt database (https://halocat.geomar.de/). Two time series stations situated distant to the coast (Park Falls, Wisconsin, Niwot Ridge Forest, Colorado, both USA) were chosen to assess to contribution of marine halocarbon emissions to the atmospheric mixing ratio over land. Monthly means of the time series were compared to monthly means of simulation 1 and 2 for the PWC and PE set-up.

DMS was directly compared to measurements from ship campaigns in the marine bound-

Table 3.3: Metadata of the ground based time series stations of halocarbons (NOAA) considered in this study. For DMS, the data from time series of Cape Grim and Amsterdam Island was considered.

Nr.	Abbr.	Station Name	Latitude	Longitude	Elevation [m]	Period
1	ALT	Alert, CA	82.45°N	62.51°W	210	1992-2011
2	AMS	Amsterdam Island	37.80°S	77.54°E	55	1990-1999
3	SUM	Summit, Greenland	72.58°N	38.48°W	3209	2004-2011
4	BRW	Barrow, Alaska	71.32°N	156.6°W	27	1993-2011
5	MHD	Mace Head, Ireland	53.33°N	9.90°W	42	1998-2011
6	LEF	Park Falls, Wisconsin	45.95°N	90.27°W	868	1996-2011
7	THD	Trinidad Head, Calif.	41.05°N	124.15°W	120	2002-2011
8	NWR	Niwot Ridge Forest, Colorado	40.03°N	105.55°W	3475	1993-2011
9	KUM	Cape Kumuhaki, Hawaii	19.5°N	154.8°E	39	1995-2011
10	MLO	Mauna Loa, Hawaii	19.53°N	155.58°W	3433	1993-2011
11	CGO	Cape Grim, Tasmania	40.68°S	144.69°E	164	1993-2011
12	PSA	Palmer Station, Antarc.	64.92°S	64.00°E	15	1997-2011
13	SPO	South Pole	90.00°S	59.00°E	2837	1993-2011

ary layer, because only few data from ground based time series stations is available. Campaigns chosen were PHASE-I (2004, Marandino et al., 2007), 2 campaigns on RV Knorr (Marandino et al., 2007, 2008), and M98 on RV Meteor (2009, Zavarsky, pers. communication 2014) to ensure a broad spatial coverage (Fig. 3.3). Additionally, DMS data from 2 time series stations, Cape Grim, Australia, 1990-1993 (Ayers et al., 1995), and Amsterdam Island in the Indian Ocean, 1990-1999 (Sciare et al., 2000), was used for comparison (Tab. 3.3). Upper air atmospheric concentrations of DMS were compared to aircraft measurements from the HIAPER Pole-to-Pole observation (HIPPO) campaigns 1-5 (Wofsy et al., 2012), again subsampling the model output for time and location of the observations.

3.3 Results and Discussion

3.3.1 Global emissions based on prescribed concentrations

The long-term mean of global emissions (1990-2013, simulation 1 in Tab. 3.1) based on PWC is different from the offline calculated emission climatologies for all four gases. The magnitude of this difference varies between the gases +11% ($CHBr_3$) to -28% (CH_2Br_2) (Tab. 3.4). The global spatial pattern of the PWC emissions is similar to the spatial patterns in Z13 & L11 (Fig. 3.4 and 3.5). Although global emissions for CH_2Br_2 were reduced in the PWC set-up compared to the Z13 scenario, they still lie in the range of previously published

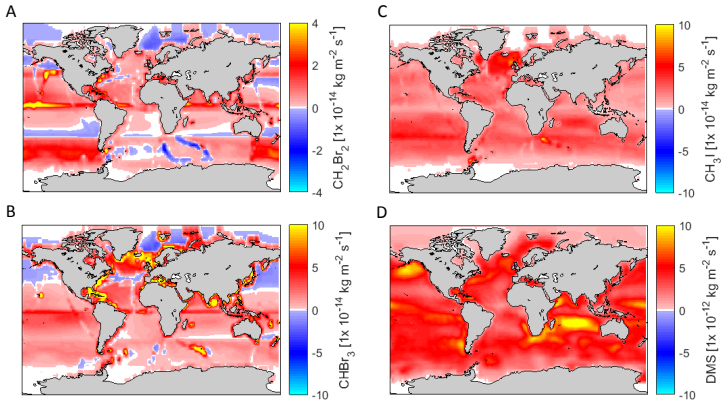

Figure 3.4: Emissions from prescribed water concentrations (PWC; N00 parameterization for k_w) for the trace gases dibromomethane (CH_2Br_2, panel A), bromoform ($CHBr_3$, panel B), methyliodide (CH_3I, panel C) and dimethyl sulfide (DMS, panel D), annual mean of the period 1990-2013 (simulation 1, Tab. 3.1).

estimates (61.8 – 112.7 Tg yr^{-1}, Tab. 3.4). The global PWC emissions for $CHBr_3$ are 11% higher than that from Z13, but still 47-60% lower than top-down approaches by Warwick et al. (2006), Liang et al. (2010) and Ordonez et al. (2012). The PWC $CHBr_3$ emissions lie at the lower end of emission scenarios, closest to Z13. The same holds for CH_3I, where emissions are 2% higher compared to Z13 but still 18% lower than the published estimate from Bell et al. (2002). Emission estimates in PWC are closest to Z13 and thus at the lower end of the range of published global emission estimates. DMS emissions in PWC compared to L11 were 17% lower (Tab. 3.4)

The main differences between PE and PWC result from considering the actual state of the atmosphere when calculating emissions from PWC, since the atmospheric mixing ratio of the gas has a direct feedback on its emissions through the concentration gradient (Eq. 3.1). Higher atmospheric concentrations lead to lower marine emissions (or can even lead to deposition) and vice versa. In the PWC set-up where the actual concentration gradient between the ocean surface concentration and the model's atmospheric mixing ratio is considered, the emissions thus respond consistently to this feedback. The most obvious example for that is the global emission of DMS. In L11, an atmospheric concentration of 0 ppt is assumed justified by the high super saturation in the water and the short lifetime of DMS. In the PWC approach in our study, the atmospheric mixing ratio is always higher than 0 ppt, on average 133 (±125) ppt, and this is likely the main reason for the resulting 17% reduction in the modelled flux vs. L11 (Fig. 3.5).

Considering the actual state of the atmosphere leads to altered concentration gradients

Table 3.4: Integrated global fluxes from this study (PWC: prescribed water concentrations, N00: k_w-parameterization of Nightingale et al. (2000) compared to previously published emission estimates. Note that Ziska et al. (2013, , Z13) is a bottom-up approach and the water concentrations were used in the online flux calculations for the halocarbons; Lana et al. (2011, pp. ,L11) DMS water concentrations were used for DMS online calculations. Ordonez et al. (2012, ,O12), Liang et al. (2010, pp. ,L10) and Warwick et al. (2006, , W06) are top-down approaches, Bell et al. (2002, , B02) is an oceanic mixed-layer bottom-up model approach for CH_3I.*units converted, in original publication: k_{720}=0.46u-0.24 [m day^{-1}]

	CH_2Br_2 (Gg yr^{-1})					$CHBr_3$ (Gg yr^{-1})					CH_3I (Gg yr^{-1})			DMS (Tg yr^{-1})	
	This study	Z13	O12.	L10	W06	This study	Z13	O12	L10.	W06	This study	Z13	B02	This study	L11
90°-50°N	1.3	-4.0	1.6	1.3	0.3	26.7	44.8	13.3	9.4	0.9	13.4	20.3	14.0	2.1	2.3
20°-50°N	12.5	16.5	15.3	14.9	10.5	49.0	33.9	123.2	108.1	27.9	36.8	40.5	89.9	7.2	8.5
20°N-20°S	32.2	38.4	41.1	34.3	84.5	108.5	94.1	286.9	249.0	517.4	63.3	59.3	91.2	18.0	21.1
20°-50°S	7.8	19.3	7.7	9.7	16.5	41.4	42.0	98.0	70.5	43.8	80.7	67.7	82.4	13.9	16.5
50°-90°S	9.1	17.2	0.9	1.6	0.9	12.8	0.1	7.0	11.6	2.4	15.5	17.0	14.9	4.2	6.0
Total	63.0	87.4	66.6	61.8	112.7	238.4	214.9	528.4	448.6	592.4	209.7	204.8	291.7	45.5	54.4

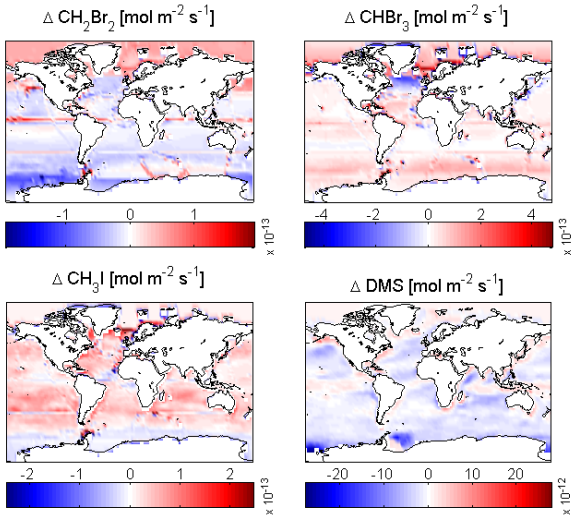

Figure 3.5: Differences (PWC-PE) in emissions between PWC (simulation 1, Tab. 3.1, 2010-2011) and PE (simulation 2, Tab. 3.1, 2010-2011). Red indicates a larger flux in the PWC set-up, blue a larger one in the PE set-up.

and thus emissions for any gas in the PWC set-up, but the impact on global emissions depends on the specific characteristics and global distribution of the gas in the surface ocean. For example, the impact of the PWC approach on global emissions for CH_2Br_2 (28% difference between PWC and Z13) is larger than that for CH_3I (2% difference) (Tab. 3.4). This difference can be explained by the saturation of the two gases: CH3I is mainly oversaturated in the surface ocean with a mean saturation ratio (actual concentration divided by equilibrium concentration) of 18.2 in Z13. CH_2Br_2 with a mean saturation ratio of 2 is concentrated closer to equilibrium. The distance from equilibrium is thus larger for CH_3I than for CH_2Br_2. Changes in atmospheric mixing ratio therefore affect the concentration gradient for CH_2Br_2 more than for CH_3I. For $CHBr_3$ with a similar global ocean surface saturation ratio as CH2Br2, a drastic change in emissions between PWC and Z13 can be seen in the Southern hemisphere (50°-90°S, Tab. 3.4), where the emissions increase two orders of magnitude in the PWC compared to Z13. The Z13 emission climatology displays a latitudinal band of elevated atmospheric mixing ratios around 60°S, which result in this region being a sink for atmospheric $CHBr_3$. In our PWC set-up, atmospheric mixing ratios in this region are not as elevated and hence PWC leads to larger emissions. In general, gases that are concentrated close to equilibrium in the surface ocean respond more strongly to changes in atmospheric concentrations and thus to the

PWC set-up than more supersaturated gases.

Comparing integrated regional fluxes, the halocarbons display the largest differences in the polar regions (Tab. 3.4). Besides dynamic atmospheric concentrations that may alter emissions in the PE set-up, two other reasons for differences in this specific set-up apply for the halocarbons. First, no sea ice is considered in Z13 whereas EMAC uses prescribed sea-ice in our PWC set-up. L11 considers sea-ice. When sea ice is present in the model EMAC/AIRSEA, the flux is reduced by the fraction of surface that is covered by it. This may lead to the lower flux estimations in our PWC set-up and may partly explain e.g. the reduced emissions in the Arctic for $CHBr_3$. Furthermore, our PWC approach takes into account air-side transfer velocity (Eq. 3.2) instead of only the water-side transfer velocity as Z13, which can control the flux of more soluble gases at low temperatures and thus decrease emissions ((McGillis et al., 2000)). At high latitudes (60-90°N and S), where low temperatures and high winds prevail, the transfer velocity can be reduced by up to 68% (CH_2Br_2), 32% ($CHBr_3$) and 61% (CH_3I) using k_{air} in the PWC set-up. L11 takes the k_{air} and sea-ice into account, thus this difference does not apply.

3.3.2 Atmospheric mixing ratios based on PWC and PE

The atmospheric mixing ratios in EMAC sustained by emissions either from PWC or PE are compared to available atmospheric observations from aircraft campaigns (halocarbons, DMS), ground based time series stations from NOAA/ESRL (halocarbons) and ship campaigns (DMS). The model output of simulations 1 and 2 (Tab. 3.1,) was subsampled at the times and locations of the observations. A scatterplot for direct comparison between model output and observations is provided in the supplements in S-Fig. 3.13.

The largest difference between PWC and PE in the atmospheric mixing ratio is again found for CH_2Br_2 in the southern hemisphere (Fig. 3.6), where the PWC set-up yields lower emissions and therefore also lower atmospheric mixing ratios. For CH_2Br_2, atmospheric mixing ratios globally decrease on average by 28% compared to the PE set-up, which is the same percentage as the reduction in the global emissions. Concentrations derived from these reduced fluxes generally agree better with the measurements, even though Arctic emissions still seem to be underestimated in the model compared to the observations. A possible explanation for this underestimation could be emissions of VSLS from sea ice that are not considered in the model, as e.g. Karlsson et al. (2013) observed elevated CH_2Br_2 in brines on top of sea ice. Mixing ratios of CHBr3 are similar in the PWC and PE set-up (difference globally only 1.2%), but both do not show the same pattern as the measurements: For both set-ups, atmospheric mixing ratios are underestimated in the southern hemisphere up to the northern tropics (Fig. 3.6). The same is evident for CH_3I, where PWC and PE

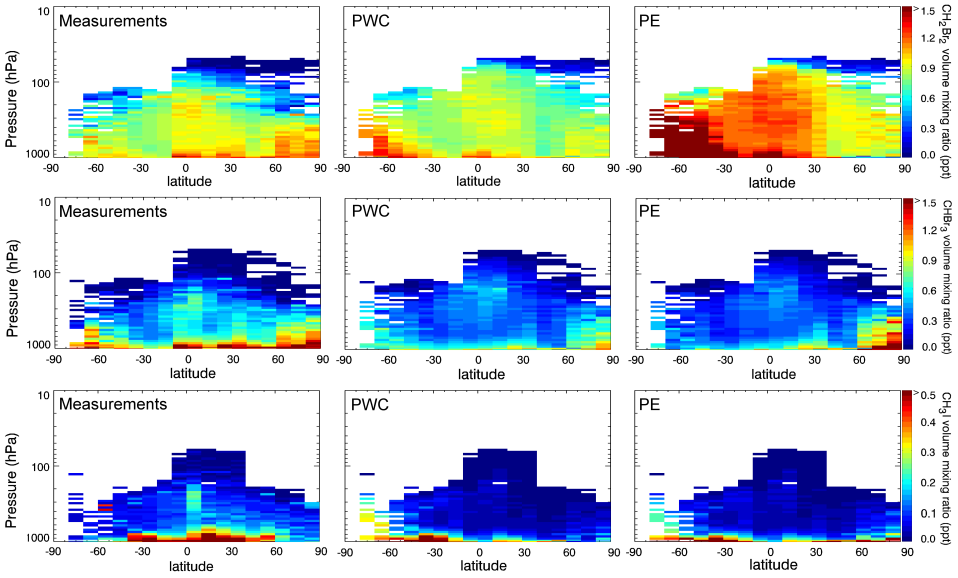

Figure 3.6: Atmospheric mixing ratios (in ppt) of the trace gases dibromomethane (CH_2Br_2, upper row), bromoform ($CHBr_3$, middle row), and methyliodide (CH_3I, lower row) derived from measurements (see Fig. 3 for locations of aircraft campaigns) and EMAC-runs with prescribed water concentrations and prescribed emissions. Model output was subsampled at locations and times of observations and binned for direct comparison.

also vary only slightly, while both set-ups underestimate atmospheric CH3I concentration in the tropics. Since atmospheric concentrations were derived from emissions based on the Z13/L11 water concentration climatology in the PWC set-up, negative discrepancies to atmospheric observations indicate regions where the concentration climatologies lack hotspots and can thus identify missing oceanic source regions. For all three halocarbons, the concentration climatologies seem to represent water concentrations that are too low in the northern hemisphere and the tropics to explain the observed atmospheric mixing ratios. It has to be noted that coastal areas are large source regions of halocarbon emissions with global contributions of up to 70% (Ziska et al., 2013), which might be underrepresented in our modelled approach and thus might at least partly explain these missing sources.

Modeled concentrations matched observations from NOAA/ESRL ground stations in most of the cases better in the PWC set-up compared to PE. The agreement between simulation and measurements increases with the atmospheric lifetime of the gases: modelled mixing ratios for CH_2Br_2, with the longest lifetime of the tested gases, reflect the observed seasonality at all 12 stations well (Fig. 3.7). The modelled seasonality of the atmospheric mixing ratios is similar in both the PWC and PE set-ups, indicating that the main fluctuations at these locations comes from seasonality in atmospheric transport and chemistry rather

than from seasonality in emissions, since emissions are constant in PE. For all stations except for Mace Head, PWC yields atmospheric mixing ratios closer to the measurements for CH_2Br_2, reducing overestimations of modelled atmospheric mixing ratios compared to measurements of up to 75% as e.g. at the South Pole. Discrepancies between observations and model simulations are larger in most of the ground based stations for $CHBr_3$ (lifetime 20 days in our simulation) than for CH_2Br_2, and again PWC yields equally well or more accurate mixing ratios than PE compared to the measurements (Fig. 3.8). However, the observed seasonality is not well reflected in either the PWC or the PE set-up. This mismatch indicates that a further seasonality in the sources is required, which can e.g. be accounted for by introducing a seasonality in the water concentrations prescribed. This finding is opposite to findings from Liang et al. (2010), who concluded that atmospheric $CHBr_3$ mixing ratios are mainly driven by transport and atmospheric chemistry. Furthermore, the good agreement between model and observations at continental sites away from the coast (Park Falls, Wisconsin, USA, Niwot Ridge Forest, Colorado, USA) for CH_2Br_2 and $CHBr_3$ indicates that the ocean is the dominant source of these compounds also over land. CH_3I, the gas with the shortest lifetime in the range of a few days, shows the largest discrepancies between modeled mixing ratios and observations (Fig. 3.9). The PWC set-up yields mixing ratios in the range of the observations for only 2 stations (Alert, Canada and Barrow, Alaska, USA), and in most of the stations, the seasonality was not well reflected in the model runs. CH_3I seasonality in water concentrations has previously been observed (Shi et al., 2014), indicating that seasonally resolved water concentrations are needed to reproduce atmospheric concentrations of the shortest lived compounds in a more accurate way. Oceanic emissions in PE and PWC were too large to explain atmospheric mixing ratios at stations in high latitudes (Summit, Mace Head, Cape Grim, Palmer Station, South Pole), but too low to explain atmospheric mixing ratios in lower latitudes (Park Falls, Trinidad Head, Niwot Ridge, Cape Kumuhaki, Mauna Loa), which agrees with findings from aircraft campaigns (Fig. 3.6).

Four ship campaigns were chosen for comparison of DMS, since long-term measurements of atmospheric mixing ratios of DMS are not available. In addition, no observations from time series stations are available, which makes an analysis of seasonality as done for the halocarbons difficult. Simulation with both the PWC (N00) and the PE approach overestimate DMS mixing ratios in the marine boundary layer from ship campaigns (see positive mean bias in Tab. 3.5). However, the PWC reduces discrepancies within both ship and aircraft campaigns by a factor of 2 (Tab. 3.5), as the mixing ratio is overestimated by a factor of 0.61 in PWC as opposed to 1.31 in PE. The observed seasonality of DMS mixing ratios at Amsterdam island is well reflected in the simulations except for the summer

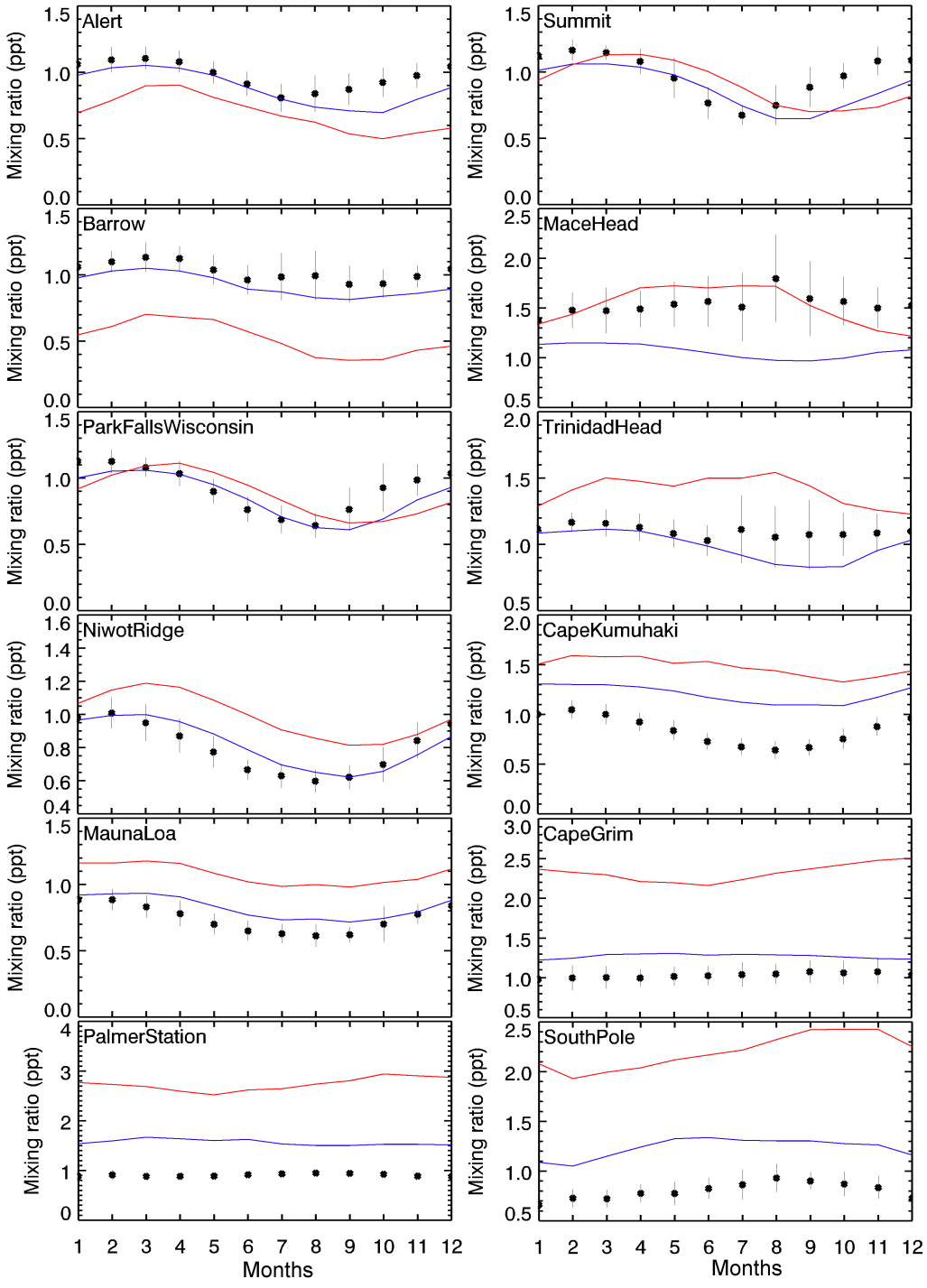

Figure 3.7: Mean seasonal variation of CH_2Br_2 mixing ratios (in ppt) using model output based on prescribed emissions (PE in red) and prescribed water concentration (PWC in blue), subsampled at the location of the NOAA ground based time series stations. Black dots indicate the long term monthly means of the time series at the specific locations (±standard deviation of the monthly means), vertical lines indicate the corresponding standard deviations. Monthly time series of at least 7 years were averaged, the exact periods are listed in table 2.

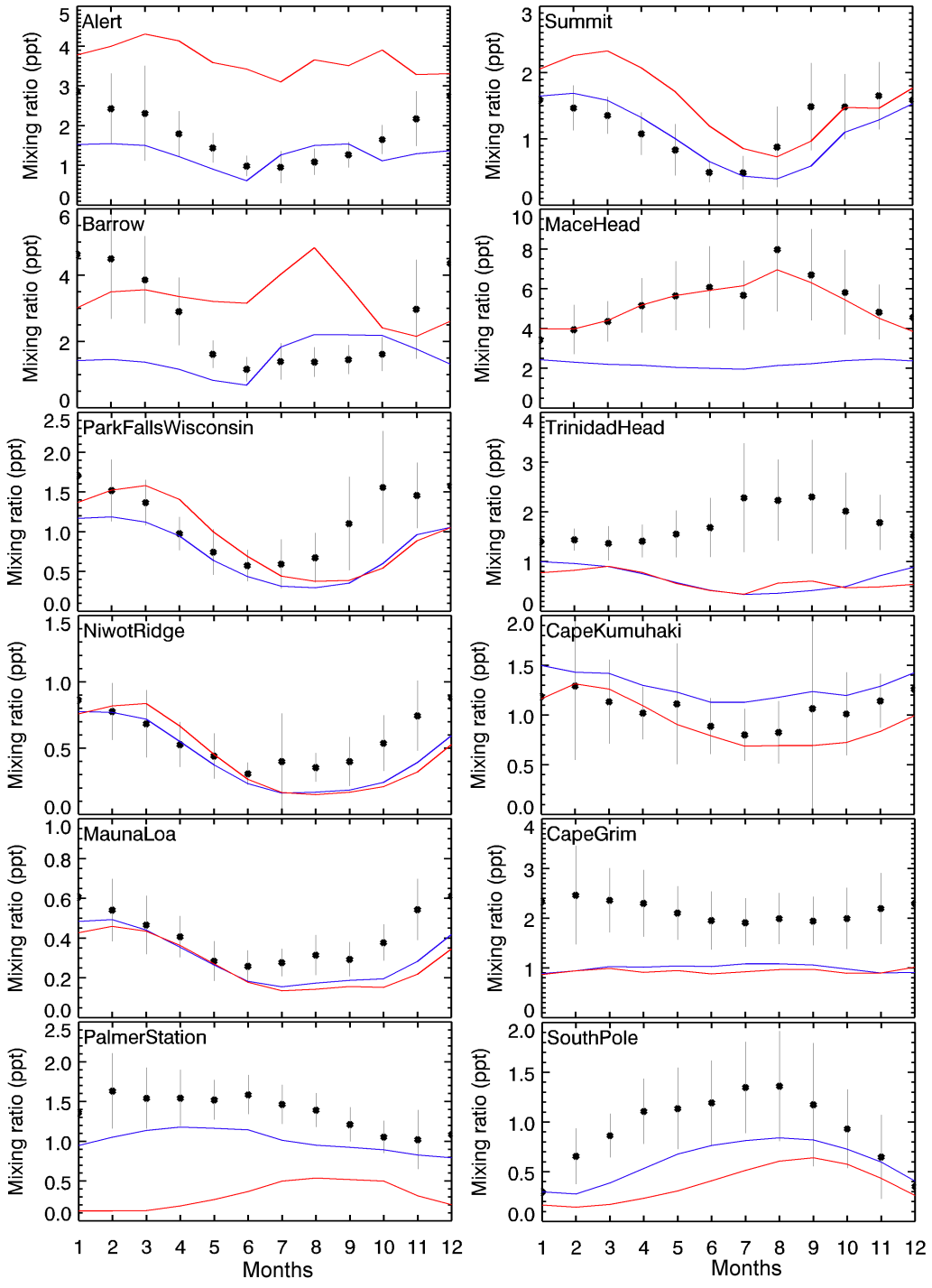

Figure 3.8: Same as Fig. 7 for $CHBr_3$.

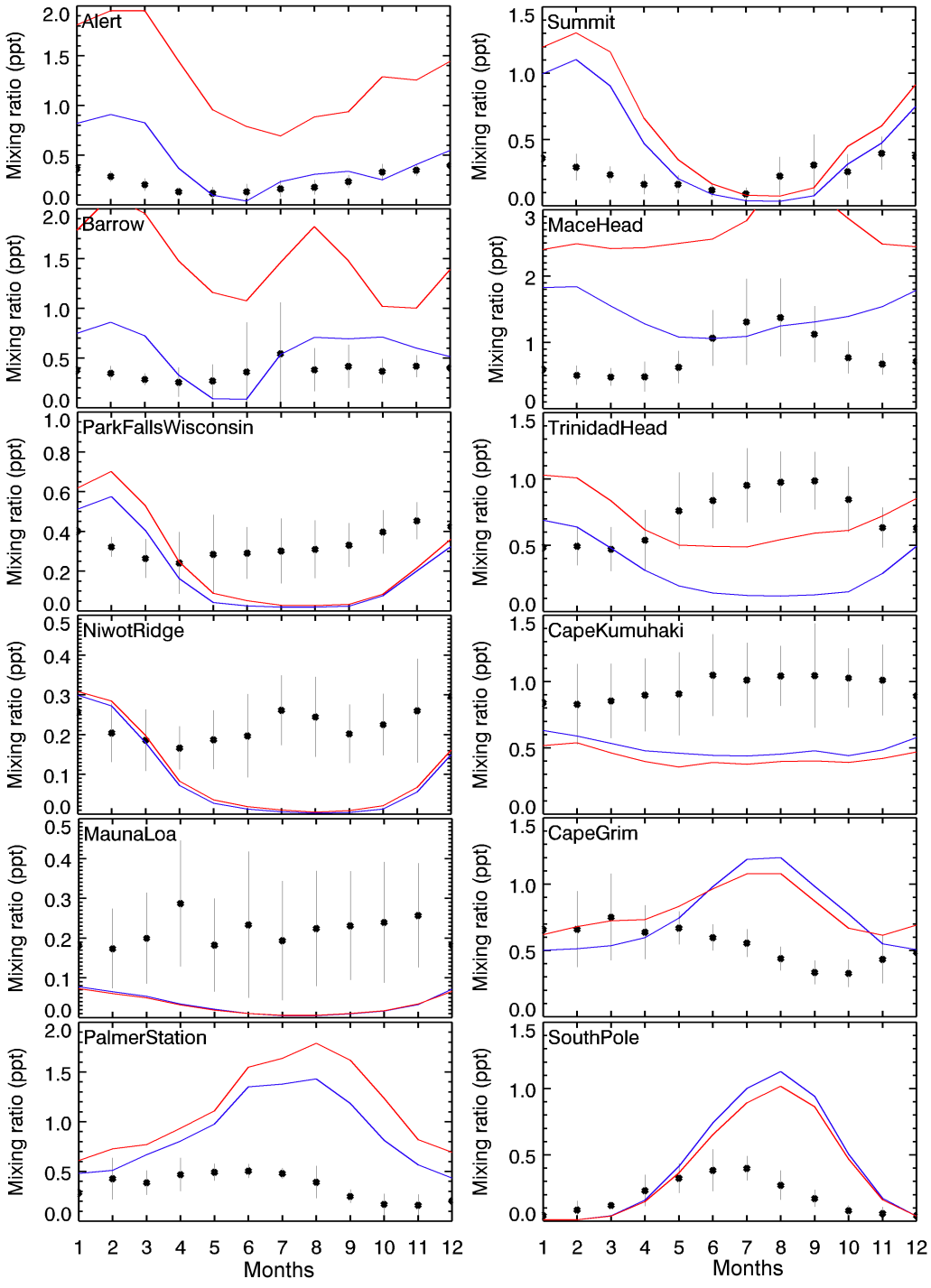

Figure 3.9: Same as Fig. 7 for CH_3I.

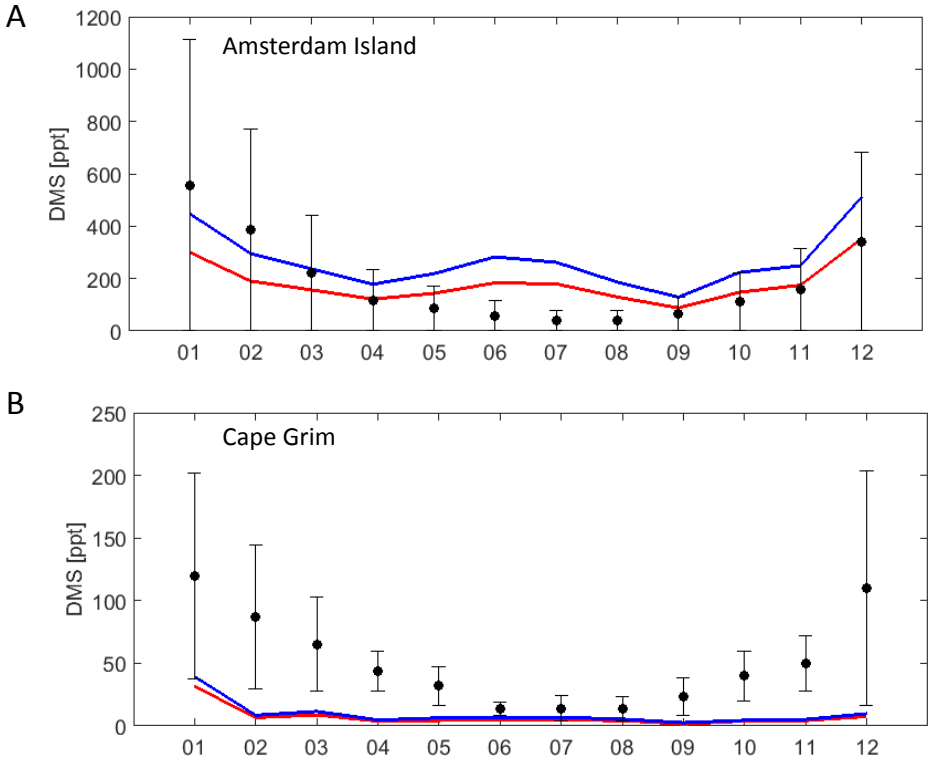

Figure 3.10: Same as Fig. 7 for DMS.

months, where PWC and PE overestimate the monthly mean by a factor of up to 4.6 (PWC) and 6.7 (PE) (Fig. 3.10). At Amsterdam Island, the simulated annual mean atmospheric mixing ratio of 180.7 ppt in the PWC set-up agrees very well with observed annual mean of 181.2 ppt, whereas the simulated annual mean in the PE set-up is 268.5 ppt. At Cape Grim, the results of the two set-ups do not differ that much, and both simulations underestimate the mixing ratios measured during austral summer.

An overall comparison of the agreement of both set-ups with observations is summarized in a Taylor-diagram (Fig. 3.11). This diagram is a statistical summary that shows how well two patterns match each other with regard to their correlation, variance and root-mean-square difference (Taylor, 2001)). The closer a point of a specific set-up is located to the reference point of observations (here 1.0 on x-axis), the more the simulation resembles the observed measurements. PWC simulations increased the agreement with observations for CH_2Br_2, especially the correlation (0.4 in PE to 0.6 in PWC), and for DMS (0.53 in PE to 0.65 in PWC), but only very slightly for $CHBr_3$ and CH_3I. Centered statistics for all compounds can be found in Tab. 3.5. (Yu et al., 2006) listed in the supplementary material.

Table 3.5: Error metrics for the comparison of model output from PWC (simulation 1) and PE (simulation 2) for all of the compounds including all aircraft campaigns and ship observations, illustrated in S-Fig. 2. Determination of error metrics according to Yu et al. (2006).

	CH_2Br_2 PE	CH_2Br_2 PWC	$CHBr_3$ PE	$CHBr_3$ PWC	CH_3I PE	CH_3I PWC	DMS PE	DMS PWC
Mean bias [ppt]	0.24	-0.036	-0.23	-0.24	-0.14	-0.14	86.21	42.12
Mean absolute gross error [ppt]	0.30	0.15	0.31	0.31	0.15	0.16	102.9	67.39
RMSE [ppt]	0.381	0.21	0.53	0.53	0.26	0.26	236.2	135.8
Fractional bias [ppt]	0.26	0.0001	-0.23	-0.20	-0.89	-0.96	0.23	0.10
Fractional absolute error [ppt]	0.31	0.20	0.56	0.56	1.13	1.19	1.23	1.18
normalized mean bias factor[-]	0.27	-0.04	-0.49	-0.53	-1.71	-1.96	1.31	0.64

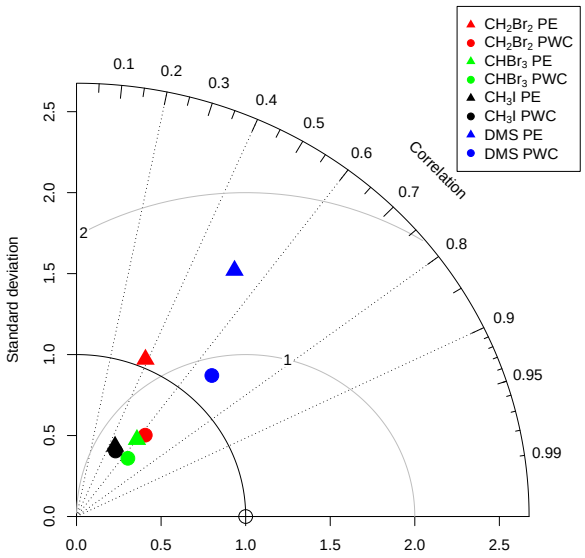

Figure 3.11: Taylor-Diagram of PE (prescribed emissions, triangles) compared to PWC (prescribed water concentrations, circles) runs using the same parameterization for k_w (N00) for comparison. The Taylor diagram relates model simulations to observations according to their root-mean square error (given as the distance to the reference point, x-axis 1.0), correlation and standard deviation. Simulations located closest to the reference point agree best with observations.

3.3.3 Comparison of different transfer velocity (k_w) parameterizations

A large uncertainty of global emission estimates is related to different parameterizations of the transfer velocity in Eq. 3.1. Calculating emissions online enables a simple way of testing different transfer velocity parameterizations, which was realized here with eight 2-year simulations described in Tab. 3.1 (simulations 3-10).

The largest sensitivity for the emissions of all gases is introduced by different parameterizations of the water-side transfer velocity kw tested in simulations 3-6 (Tab. 3.2). The 4 parameterizations that were tested (simulation 3-6, Tab. 3.1) comprised linear (LM86, simulation 3), cubic (W99, simulation 4) and quadratic (N00, simulation 5, H06, simulation 6) relations to wind speed. The resulting global emission estimates in these parameterizations range between 53.7 to 65.1 Gg yr^{-1} for CH_2Br_2, 189.0 to 249.7 Gg yr^{-1} for $CHBr_3$, 151.9 to 225.7 Gg yr^{-1} for CH_3I and 33.4 to 48.7 Tg yr^{-1} for DMS (Tab. 3.2). As expected, the linear kw-parameterization (LM86) yields the lowest global emission estimates, since it produces the lowest k_w-values (Fig. 3.2). The N00 parameterization produces highest global fluxes for $CHBr_3$ and CH_2Br_2, but not for DMS and CH_3I, where the highest fluxes were obtained by H06 (DMS) and W99 (CH_3I) (Tab. 3.2). The fact that different parameterizations lead to highest global estimates for different gases is explained by the varying spatial distribution of concentration hot spots and regional variations of wind.

The k_w parameterization in simulation 7 increases the flux under calm conditions due to precipitation. This increase ranged from 4% (CH_2Br_2) to 6% (DMS) (Tab. 3.2) when compared to the reference flux using H06 alone (simulation 6, Tab. 3.2). Additional flux due to precipitation is inversely correlated to the Schmidt number, so that under identical conditions, increasing flux would be added in the order $CHBr_3$> CH_2Br_2 > DMS > CH_3I. The global flux estimations compared to the reference run do not increase in this order (Tab. 3.2), but DMS>$CHBr_3$ CH_3I>CH_2Br_2. This non-uniform response among the gases is explained by the globally and regionally varying distance from equilibrium for the four gases, which together with regional precipitation patterns leads to variations in the emissions increased by rain. The parametrization based on white-cap coverage (A98) also has small but ambivalent effects on the global flux for the different compounds (simulation 8, Tab. 3.2). Compared to the mean of all nonlinear parameterizations for each gas, global emissions were higher when the white cap coverage parameterization was used for $CHBr_3$ (4%) and CH_2Br_2 (2%) but lower for CH_3I (-8%) and DMS (-6%)(Tab. 3.2).

The parameterizations tested only for DMS are both derived from eddy covariance measurements at sea. Both parameterizations changed the global emissions by -4.4% (B13m) and -1.2% (M09) compared to the average flux of simulation 3-6 (Tab. 3.2). Although the

modelled atmospheric mixing ratios at the time and location of observations is for both of the parameterizations higher than the observations, discrepancies between simulated and observed mixing ratios were reduced compared to the N00 parameterization by a factor of 1.4 (B13m) and 1.2 (M09).

3.4 Summary and conclusions

Two different ways of considering marine emissions of trace gases in global atmospheric chemistry models are discussed here for the halocarbons CH_2Br_2, $CHBr_3$, CH_3I and the sulfur containing compound DMS. In contrast to prescribing emissions (PE) from oceanic and atmospheric concentration climatologies in the model, prescribing water concentrations (PWC) with an online calculation of emissions results in a consistent concentration gradient between ocean and atmosphere. The approach of modeling emissions online was successfully applied for the very short-lived halocarbons for the first time. The approach is based on the submodel AIRSEA coupled to EMAC by Pozzer et al. (2006). The method has a number of conceptual and practical advantages, as in this framework the modelled flux can respond in a consistent way to changes in sea surface temperature, surface wind speed, possible sea ice cover and marine atmospheric mixing ratios in the model.

Global emission estimates of the four gases differ between +11% ($CHBr_3$) and -28% (CH_2Br_2) between PWC and PE, when the transfer velocity k_w is parametrized according to Nightingale et al. (2000) in both set-ups. Prescribing water concentrations instead of emissions has the strongest effect for gases close to equilibrium in the surface ocean such as CH_2Br_2 (28% reduced emissions in PWC compared to PE), as its emissions are most sensitive to atmospheric concentrations. In contrast, only 2% difference is found for the highly supersaturated gas CH_3I. Considering PWC reduces the global emissions of DMS by 17%. Comparison to observations revealed that PWC compared to PE reproduces observations slightly ($CHBr_3$, CH_3I) or much (CH_2Br_2, DMS) better for measurements made at ground based time series stations, aircraft campaigns and ship cruises. Even though it is clear that more data for all compounds are needed globally, the PWC set-up can be used to identify oceanic regions where more measurements will be needed to improve the global emission estimate. For example, there are clear discrepancies in the northern hemisphere for CHBr3 and the tropics for CH_3I.

Global emission estimates display a large sensitivity towards the parameterization of the transfer velocity k_w, with relative differences between 15.6% (CH_2Br_2) and 35.9% (CH_3I) compared to the mean global emissions of the four tested simulations including k_w parameterizations according to Liss & Merlivat (1986, pp. , LM86), Wanninkhof & McGillis

(1999, , W99), Nightingale et al. (2000, , N00) and Ho et al. (2006, , H06). Sensitivity towards rain or bubble mediated transfer was generally low (<10% change in global emission estimate). Two parameterization adapting results that have recently been suggested for DMS (Bell et al., 2013; Marandino et al., 2009, , M09 and B13m) produced both a lower global emission estimate, which at the same time reduced discrepancies between simulated and observed atmospheric mixing ratios and yielded simulated atmospheric mixing ratios closer to observations than simulated mixing ratios with the N00 parameterization.

In summary, prescribing water concentrations instead of prescribing emissions in global atmospheric chemistry models leads to a consistent concentration gradient between ocean and atmosphere, and enables convenient testing of different air-sea gas exchange parameterizations. Based on the results of our comparison between the PE and PWC, prescribing concentrations leads to more consistent emissions and mainly more accurate reproduction of observations of atmospheric mixing ratios of the VSLS described here.

3.5 Acknowledgments

This work was supported through the German Federal Ministry of Education and Research through the project ROMIC-THREAT (BMBF-FK01LG1217A and 01LG1217B). Additional funding for C. Marandino and S. Lennartz came from the Helmholtz Young Investigator Group of C. Marandino, TRASE-EC (VH-NG-819), from the Helmholtz Association through the President's Initiative and Networking Fund and the GEOMAR Helmholtz-Zentrum für Ozeanforschung Kiel. We thank A. Pozzer for advice on the use of AIRSEA and valuable comments on the manuscript. Thanks to Donald R. Blake from the University of California, Irvine for advice and the data access. Thanks to A. Lana for providing emission and concentration fields of DMS and to A. C. Zavarsky for atmospheric DMS measurements on the Meteor 98 cruise. We thank Prabir Patra for his help and for providing the OH field used in the EMAC simulations. NOAA measurements were supported in part by NOAA's Atmospheric Chemistry, Carbon Cycle and Climate Program of its Climate program Office. Data on halocarbon mixing ratios from aircraft campaigns were obtained from the ESPO NASA archive and from the EOL-NCAR database. We acknowledge operational, technical and scientific support provided by NCAR's Earth Observing Laboratory, sponsored by the National Science Foundation. University Frankfurt would like to thank DLR for organizing and funding the ESMVal campaign and DFG (grant. Nr. 367/8 and EN367/11) for funding the TACTS campaign and the measurements.

3.6 Appendix: Supplementary figures

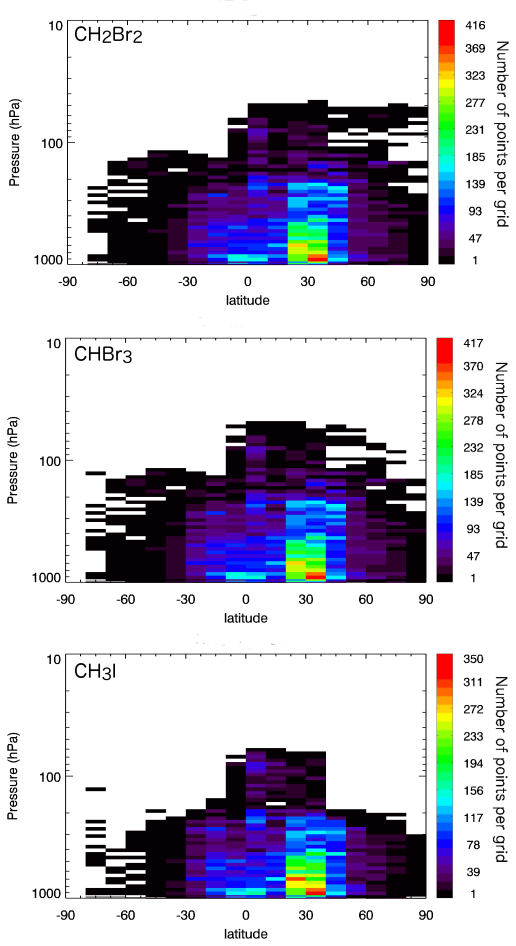

Figure 3.12: Numbers of measurement per 10° latitude bin for Figure 7.

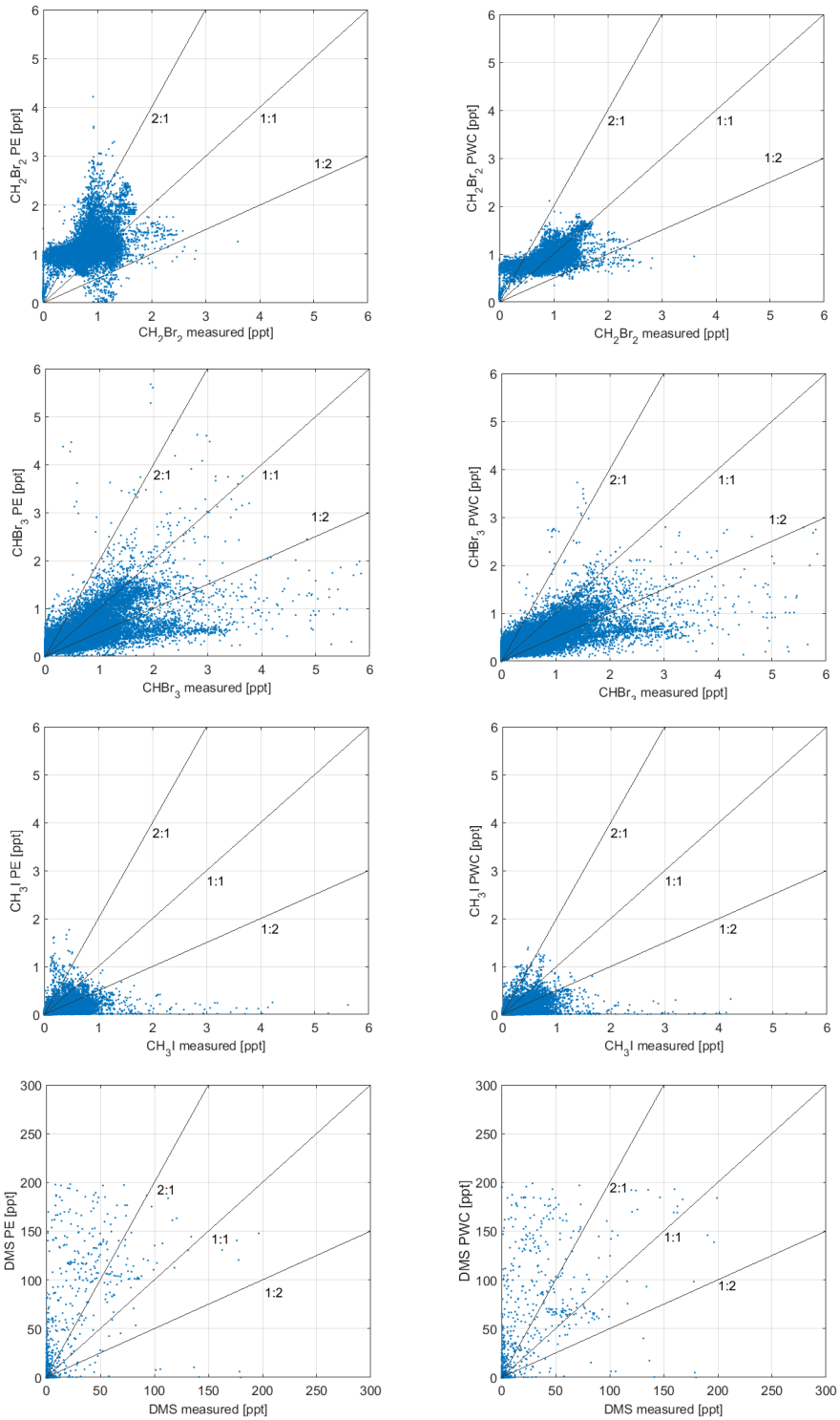

Figure 3.13: Scatterplots for direct comparison between model output of simulations 1 (PWC) and 2 (PE) and observations. The model was subsampled at time and location of observations. For the halocarbons, observations from 23 aircraft campaigns as illustrated in fig. 3a were used to create this scatterplot. For DMS, observations from ship and aircraft campaigns as described in figure 3b were taken into account

3.7 Appendix: Supplementary tables

Table 3.6: Global averages for the year 2012 as a comparison for the resolution of grid T42 and T106 using the prescribed emission and concentration climatologies described in section and the k_w-parameterization according to Nightingale et al. (2000). k_w = water side transfer velocity of air-sea gas exchange, vmr= volume mixing ratio.

	T42 PWC	**T42 PE**	**T106 PWC**	**T106 PE**
wind 10m [m s^{-1}]	6.31		6.31	
k_w CH_2Br_2 [m s^{-1}]	$2.5x10^{-5}$		$2.3x10^{-5}$	
k_w $CHBr_3$ [m s^{-1}]	$2.3x10^{-5}$		$2.2x10^{-5}$	
k_w CH_3I [m s^{-1}]	$2.6x10^{-5}$		$2.5x10^{-5}$	
k_w DMS [m s^{-1}]	$2.5x10^{-5}$		$2.4x10^{-5}$	
surface vmr CH_2Br_2 [mol mol^{-1}]	$1.1x10^{-12}$	$1.56x10^{-12}$	$1.0x10^{-12}$	$1.5x10^{-12}$
surface vmr $CHBr_3$ [mol mol^{-1}]	$8.9x10^{-13}$	$9.38x10^{-13}$	$8.8x10^{-13}$	$9.40x10^{-13}$
surface vmr CH_3I [mol mol^{-1}]	$5.4x10^{-13}$	$6.25x10^{-13}$	$5.0x10^{-13}$	$6.0x10^{-13}$
surface vmr DMS [mol mol^{-1}]	$1.4x10^{-10}$	$2.13x10^{-10}$	$1.3x10^{-10}$	$2.0x10^{-10}$
flux CH_2Br_2 [mol m^{-2} s^{-1}]	$2.2x10^{-14}$		$2.2x10^{-14}$	
flux $CHBr_3$ [mol m^{-2} s^{-1}]	$5.9x10^{-14}$		$5.9x10^{-14}$	
flux CH_3I [mol m^{-2} s^{-1}]	$9.2x10^{-14}$		$8.8x10^{-14}$	
flux DMS [mol m^{-2} s^{-1}]	$4.5x10^{-11}$		$4.3x10^{-11}$	

Table 3.7: Overview of data of the aircraft campaigns (halocarbons, DMS) used in this study.

Campaign	Date	Altitude range [km]	Location	PI/Reference
TRACE-A	1992/09-1992/10	0-12	Atlantic Ocean	D. Blake/ Blake et al. (2003)
STRAT	1996/02-1996/12	14-21	East Pacific	E. Atlas
PEM-TROPICS-A	1996/08-1996/10	0-11	Tropical Pacific Ocean	E. Atlas/D. Blake
POLARIS	1997/09	15-21	East Pacific	E. Atlas
PEM-TROPICS-B	1999/03-1999/04	0-12	Tropical Pacific Ocean	E. Atlas/D. Blake
ACCENT	1999/09	15-16	Central America	E. Atlas
TRACE-P	2001/02-2001/04	0-12	West Pacific	E. Atlas/D. Blake
PRE-AVE	2001/01-2004/02	8-19	Central America	E. Atlas
INTEX	2004/07-2006/05	0-11	Pacific/USA/Atlantic	D. Blake
AVE	2006/06	15-19	Central America	E. Atlas
CR-AVE	2006/01-2006/02	2-19	Central America	E. Atlas/ Ashfold et al. (2012)
CARIBIC	2006/10-2009/10	9-14	Cent. America, S.E. Asia, E. Pacific	D. Oram/ Wisher et al. (2014)
TC4	2007/07-2007/08	0-18	Central America	E.Atlas/D.Blake/ Ashfold et al. (2012)
ARCTAS	2008/04-2008/07	0-11	Canada	D. Blake
HIPPO-1	2009/01	0-14	East Pacific	E. Atlas/ Wofsy et al. (2012)
HIPPO-2	2009/11	0-14	Pacific Ocean	E. Atlas/ Wofsy et al. (2012)
HIPPO-3	2010/03-2010/04	0-14	Pacific Ocean	E. Atlas/ Wofsy et al. (2012)
HIPPO-4	2011/06-2011/07	0-14	Pacific Ocean	E. Atlas/ Wofsy et al. (2012)
HIPPO-5	2011/08-2011/09	0-14	West Pacific	E. Atlas/ Wofsy et al. (2012)
POST-ATTREX	2011/11	13-19	East Pacific	E. Atlas
SHIVA	2011/11-2011/12	0-13	South China Sea	A. Engel/ Sala et al. (2014)
ESMVAL	2012/09	0-15	Africa	A. Engel
TACTS	2012/08-2012/09	0-15	North Africa	A. Engel

3.8 Appendix: Equations to compute error metrics

Error metrics are computed according to Yu et al. (2006) with N=number of data pairs observation and model output, M=model output and O=observation.

Mean bias:

$$B_{mb} = \frac{1}{N}\sum(M_i - O_i) = \overline{M} - \overline{O} \tag{3.3}$$

Mean absolute gross error:

$$E_{MAGE} = \frac{1}{N}\sum|M_i - O_i| \tag{3.4}$$

Root mean square error:

$$E_{RMSE} = [\frac{1}{N}\sum(M_i - O_i)^2]^{\frac{1}{2}} \tag{3.5}$$

Fracitonal bias:

$$B_{fb} = \frac{1}{N}\sum\frac{(M_i - O_i)}{(M_i - O_i)/2} \tag{3.6}$$

Fractional absolute error:

$$E_{fae} = \frac{1}{N}\sum\frac{|M_i - O_i|}{(M_i - O_i)/2} \tag{3.7}$$

Normalized mean bias factor:

$$B_{nmbf} = \frac{\overline{M}}{\overline{O}} - 1 for \overline{M} \geq \overline{O} \tag{3.8}$$

$$B_{nmbf} = 1 - \frac{\overline{M}}{\overline{O}} for \overline{O} \geq \overline{M} \tag{3.9}$$

References

Aschmann, J.; Sinnhuber, B.-M.; Atlas, E. L. & Schauffler, S. M. (2009): Modeling the transport of very short-lived substances into the tropical upper troposphere and lower stratosphere. *Atmospheric Chemistry and Physics* **9** (23): 9237–9247.

Asher, W. E. & Wanninkhof, R. (1998): The effect of bubble-mediated gas transfer on purposeful dual-gaseous tracer experiments. *Journal of Geophysical Research: Oceans* **103** (C5): 10555–10560.

Ashfold, M. J.; Harris, N. R. P.; Atlas, E. L.; Manning, A. J. & Pyle, J. A. (2012): Transport of short-lived species into the Tropical Tropopause Layer. *Atmospheric Chemistry and Physics* **12** (14): 6309–6322.

Ayers, G. P.; Bentley, S. T.; Ivey, J. P. & Forgan, B. W. (1995): Dimethylsulfide in marine air at Cape Grim, 41° S. *Journal of Geophysical Research-Atmospheres* **100** (D10): 21013–21021.

Barnes, I.; Hjorth, J. & Mihalopoulos, N. (2006): Dimethyl Sulfide and Dimethyl Sulfoxide and Their Oxidation in the Atmosphere. *Chemical Reviews* **106** (3): 940–975.

Bates, T. S.; Lamb, B. K.; Guenther, A.; Dignon, J. & Stoiber, R. E. (1992): Sulfur emissions to the atmosphere from natural sources. *Journal of Atmospheric Chemistry* **14** (1-4): 315–337.

Bell, N.; Hsu, L.; Jacob, D. J.; Schultz, M. G.; Blake, D. R.; Butler, J. H.; King, D. B.; Lobert, J. M. & Maier-Reimer, E. (2002): Methyl iodide: Atmospheric budget and use as a tracer of marine convection in global models. *Journal of Geophysical Research: Atmospheres* **107** (D17): 4340.

Bell, T. G.; De Bruyn, W.; Miller, S. D.; Ward, B.; Christensen, K. H. & Saltzman, E. S. (2013): Air-sea dimethylsulfide (DMS) gas transfer in the North Atlantic: evidence for limited interfacial gas exchange at high wind speed. *Atmospheric Chemistry and Physics* **13** (21): 11073–11087.

Blake, N. J.; Blake, D. R.; Simpson, I. J.; Meinardi, S.; Swanson, A. L.; Lopez, J. P.; Katzenstein, A. S.; Barletta, B.; Shirai, T.; Atlas, E.; Sachse, G.; Avery, M.; Vay, S.; Fuelberg, H. E.; Kiley, C. M.; Kita, K. & Rowland, F. S. (2003): NMHCs and halocarbons in Asian continental outflow during the Transport and Chemical Evolution over the Pacific (TRACE-P) Field Campaign: Comparison with PEM-West B. *Journal of Geophysical Research-Atmospheres* **108** (D20)

Brinckmann, S.; Engel, A.; Bönisch, H.; Quack, B. & Atlas, E. (2012): Short-lived brominated hydrocarbons – observations in the source regions and the tropical tropopause layer. *Atmos. Chem. Phys.* **12** (3): 1213–1228.

Burrows, S. M.; Ogunro, O.; Frossard, A. A.; Russell, L. M.; Rasch, P. J. & Elliott, S. M. (2014): A physically based framework for modeling the organic fractionation of sea spray aerosol from bubble film Langmuir equilibria. *Atmospheric Chemistry and Physics* **14** (24): 13601–13629.

Cameron-Smith, P.; Elliott, S.; Maltrud, M.; Erickson, D. & Wingenter, O. (2011): Changes in dimethyl sulfide oceanic distribution due to climate change. *Geophysical Research Letters* **38**

Chameides, W. L. & Davis, D. D. (1980): Iodine - its possible role in tropospheric photochemistry. *Journal of Geophysical Research-Oceans and Atmospheres* **85** (NC12): 7383–7398.

Charlson, R. J.; Lovelock, J. E.; Andreae, M. O. & Warren, S. G. (1987): Oceanic phytoplankton, atmospheric sulfur, cloud albedo and climate. *Nature* **326** (6114): 655–661.

De Bruyn, W.; Swartz, E.; Hu, J.; Shorter, J.; Davidovits, P.; Worsnop, D.; Zahniser, M. & Kolb, C. (1995): Henrys law solubilities and Setcheniw coefficients for biogenic reduced sulphur species obtained from gas-liquid uptake measurements. *Journal of Geophysical Research Atmosphere* **100**: 7245–7251.

Dee, D. P.; Uppala, S. M.; Simmons, A. J.; Berrisford, P.; Poli, P.; Kobayashi, S.; Andrae, U.; Balmaseda, M. A.; Balsamo, G.; Bauer, P.; Bechtold, P.; Beljaars, A. C. M.; van de Berg, L.; Bidlot, J.; Bormann, N.; Delsol, C.; Dragani, R.; Fuentes, M.; Geer, A. J.; Haimberger, L.; Healy, S. B.; Hersbach, H.; Holm, E. V.; Isaksen, L.; Kallberg, P.; Köhler, M.; Matricardi, M.; McNally, A. P.; Monge-Sanz, B. M.; Morcrette, J. J.; Park, B. K.; Peubey, C.; de Rosnay, P.; Tavolato, C.; Thepaut, J. N. & Vitart, F. (2011): The ERA-Interim reanalysis: configuration and performance of the data assimilation system. *Quarterly Journal of the Royal Meteorological Society* **137** (656): 553–597.

Elliott, S.; Burrows, S. M.; Deal, C.; Liu, X.; Long, M.; Ogunro, O.; Russell, L. M. & Wingenter, O. (2014): Prospects for simulating macromolecular surfactant chemistry at the ocean-atmosphere boundary. *Environmental Research Letters* **9** (6)

Hall, B. D.; Engel, A.; Mühle, J.; Elkins, J. W.; Artuso, F.; Atlas, E.; Aydin, M.; Blake, D.; Brunke, E. G.; Chiavarini, S.; Fraser, P. J.; Happell, J.; Krummel, P. B.; Levin, I.; Loewenstein, M.; Maione, M.; Montzka, S. A.; O'Doherty, S.; Reimann, S.; Rhoderick,

G.; Saltzman, E. S.; Scheel, H. E.; Steele, L. P.; Vollmer, M. K.; Weiss, R. F.; Worthy, D. & Yokouchi, Y. (2014): Results from the International Halocarbons in Air Comparison Experiment (IHALACE). *Atmos. Meas. Tech.* **7** (2): 469–490.

Hayduk, W. & Laudie, H. (1974): Prediction of diffusion coefficients for nonelectrolytes in dilute aqueous solutions. *AIChE Journal* **20** (3): 611–615.

Hepach, H.; Quack, B.; Raimund, S.; Fischer, T.; Atlas, E. L. & Bracher, A. (2015): Halocarbon emissions and sources in the equatorial Atlantic Cold Tongue. *Biogeosciences* **12** (21): 6369–6387.

Ho, D. T.; Bliven, L. F.; Wanninkhof, R. & Schlosser, P. (1997): The effect of rain on air-water gas exchange. *Tellus Series B-Chemical and Physical Meteorology* **49** (2): 149–158.

Ho, D. T.; Zappa, C. J.; McGillis, W. R.; Bliven, L. F.; Ward, B.; Dacey, J. W. H.; Schlosser, P. & Hendricks, M. B. (2004): Influence of rain on air-sea gas exchange: Lessons from a model ocean. *Journal of Geophysical Research-Oceans* **109** (C8)

Ho, D. T.; Law, C. S.; Smith, M. J.; Schlosser, P.; Harvey, M. & Hill, P. (2006): Measurements of air-sea gas exchange at high wind speeds in the Southern Ocean: Implications for global parameterizations. *Geophysical Research Letters* **33** (16): L16611.

Hopkins, F. E. & Archer, S. D. (2014): Consistent increase in dimethyl sulfide (DMS) in response to high CO2 in five shipboard bioassays from contrasting NW European waters. *Biogeosciences* **11** (18): 4925–4940.

Hossaini, R.; Chipperfield, M. P.; Monge-Sanz, B. M.; Richards, N. A. D.; Atlas, E. & Blake, D. R. (2010): Bromoform and dibromomethane in the tropics: a 3-D model study of chemistry and transport. *Atmospheric Chemistry and Physics* **10** (2): 719–735.

Hossaini, R.; Chipperfield, M. P.; Montzka, S. A.; Rap, A.; Dhomse, S. & Feng, W. (2015): Efficiency of short-lived halogens at influencing climate through depletion of stratospheric ozone. *Nature Geosci* **8** (3): 186–190.

Hossaini, R.; Mantle, H.; Chipperfield, M. P.; Montzka, S. A.; Hamer, P.; Ziska, F.; Quack, B.; Krüger, K.; Tegtmeier, S.; Atlas, E.; Sala, S.; Engel, A.; Bönisch, H.; Keber, T.; Oram, D.; Mills, G.; Ordonez, C.; Saiz-Lopez, A.; Warwick, N.; Liang, Q.; Feng, W.; Moore, F.; Miller, B. R.; Marécal, V.; Richards, N. A. D.; Dorf, M. & Pfeilsticker, K. (2013): Evaluating global emission inventories of biogenic bromocarbons. *Atmos. Chem. Phys.* **13** (23): 11819–11838.

Hough, A. (1988): *The calculation of photolysis rates for use in global tropospheric modelling studies*. UKAEA Atomic Energy Research Establishment Environmental and Medical Sciences Division.

Jöckel, P. (2006): Technical note: Recursive rediscretisation of geo-scientific data in the Modular Earth Submodel System (MESSy). *Atmos. Chem. Phys.* **6** (11): 3557–3562.

Jöckel, P.; Kerkweg, A.; Pozzer, A.; Sander, R.; Tost, H.; Riede, H.; Baumgaertner, A.; Gromov, S. & Kern, B. (2010): Development cycle 2 of the Modular Earth Submodel System (MESSy2). *Geosci. Model Dev.* **3** (2): 717–752.

Joeckel, P.; Tost, H.; Pozzer, A.; Bruehl, C.; Buchholz, J.; Ganzeveld, L.; Hoor, P.; Kerkweg, A.; Lawrence, M. G.; Sander, R.; Steil, B.; Stiller, G.; Tanarhte, M.; Taraborrelli, D.; Van Aardenne, J. & Lelieveld, J. (2006): The atmospheric chemistry general circulation model ECHAM5/MESSy1: consistent simulation of ozone from the surface to the mesosphere. *Atmospheric Chemistry and Physics* **6**: 5067–5104.

Karlsson, A.; Theorin, M. & Abrahamsson, K. (2013): Distribution, transport, and production of volatile halocarbons in the upper waters of the ice-covered high Arctic Ocean. *Global Biogeochemical Cycles* **27** (4): 1246–1261.

Kerkweg, A.; Buchholz, J.; Ganzeveld, L.; Pozzer, A.; Tost, H. & Jöckel, P. (2006a): Technical Note: An implementation of the dry removal processes dry Deposition and Sedimentation in the Modular Earth Submodel System (MESSy). *Atmos. Chem. Phys.* **6** (12): 4617–4632.

Kerkweg, A.; Sander, R.; Tost, H. & Joeckel, P. (2006b): Technical note: Implementation of prescribed (OFFLEM), calculated (ONLEM), and pseudo-emissions (TNUDGE) of chemical species in the Modular Earth Submodel System (MESSy). *Atmospheric Chemistry and Physics* **6**: 3603–3609.

Kloster, S.; Feichter, J.; Maier-Reimer, E.; Six, K. D.; Stier, P. & Wetzel, P. (2006): DMS cycle in the marine ocean-atmosphere system &; a global model study. *Biogeosciences* **3** (1): 29–51.

Kondo, J. (1975): Air-sea bulk transfer coefficients in diabatic conditions. *Boundary-Layer Meteorology* **9** (1): 91–112.

Lana, A.; Bell, T. G.; Simo, R.; Vallina, S. M.; Ballabrera-Poy, J.; Kettle, A. J.; Dachs, J.; Bopp, L.; Saltzman, E. S.; Stefels, J.; Johnson, J. E. & Liss, P. S. (2011): An updated

climatology of surface dimethlysulfide concentrations and emission fluxes in the global ocean. *Global Biogeochemical Cycles* **25**

Liang, Q.; Stolarski, R. S.; Kawa, S. R.; Nielsen, J. E.; Douglass, A. R.; Rodriguez, J. M.; Blake, D. R.; Atlas, E. L. & Ott, L. E. (2010): Finding the missing stratospheric Bry: a global modeling study of $CHBr_3$ and CH_2Br_2. *Atmos. Chem. Phys.* **10** (5): 2269–2286.

Lin, S. J. & Rood, R. B. (1996): Multidimensional flux-form semi-Lagrangian transport schemes. *Monthly Weather Review* **124** (9): 2046–2070.

Liss, P. S. & Slater, P. G. (1974): Flux of gases across air-sea interface. *Nature* **247** (5438): 181–184.

Liss, P. & Merlivat, L. (1986): *Air-sea gas exchange rates: Introduction and synthesis.*

Lovelock, J. E. & Maggs, R. J. (1973): Halogenated hydrocarbons in and over the Atlantic. *Nature* **241** (5386): 194–196.

Lyman, W.; Reehl, W. & Rosenblatt, D. (1990): *Handbook of chemical property estimation methods.* Washington DC, USA: American Chemical Society.

Marandino, C. A.; De Bruyn, W. J.; Miller, S. D. & Saltzman, E. S. (2007): Eddy correlation measurements of the air/sea flux of dimethylsulfide over the North Pacific Ocean. *Journal of Geophysical Research-Atmospheres* **112** (D3)

Marandino, C. A.; De Bruyn, W. J.; Miller, S. D. & Saltzman, E. S. (2008): DMS air/sea flux and gas transfer coefficients from the North Atlantic summertime coccolithophore bloom. *Geophysical Research Letters* **35** (23)

Marandino, C. A.; De Bruyn, W. J.; Miller, S. D. & Saltzman, E. S. (2009): Open ocean DMS air/sea fluxes over the eastern South Pacific Ocean. *Atmospheric Chemistry and Physics* **9** (2): 345–356.

Marandino, C. A.; Tegtmeier, S.; Krueger, K.; Zindler, C.; Atlas, E. L.; Moore, F. & Bange, H. W. (2013a): Dimethylsulphide (DMS) emissions from the western Pacific Ocean: a potential marine source for stratospheric sulphur? *Atmospheric Chemistry and Physics* **13** (16): 8427–8437.

Marandino, C. A.; Tegtmeier, S.; Kruger, K.; Zindler, C.; Atlas, E. L.; Moore, F. & Bange, H. W. (2013b): Corrigendum: Dimethylsulphide (DMS) emissionsfrom the West Pacific Ocean: a potential marine source for stratospheric sulphur? (vol 13, pg 8427, 2013). *Atmospheric Chemistry and Physics* **13** (17): 8813–8814.

McGillis, W. R.; Dacey, J. W. H.; Frew, N. M.; Bock, E. J. & Nelson, R. K. (2000): Water-air flux of dimethylsulfide. *Journal of Geophysical Research: Oceans* **105** (C1): 1187–1193.

Moore, R. M.; Geen, C. E. & Tait, V. K. (1995): Determination of Henry Law constants for a suite of naturally-occurring halogenated methanes in seawater. *Chemosphere* **30** (6): 1183–1191.

Nightingale, P. D.; Malin, G.; Law, C. S.; Watson, A. J.; Liss, P. S.; Liddicoat, M. I.; Boutin, J. & Upstill-Goddard, R. C. (2000): In situ evaluation of air-sea gas exchange parameterizations using novel conservative and volatile tracers. *Global Biogeochemical Cycles* **14** (1): 373–387.

O'Dowd, C. D. & De Leeuw, G. (2007): Marine aerosol production: a review of the current knowledge. *Philosophical Transactions of the Royal Society a-Mathematical Physical and Engineering Sciences* **365** (1856): 1753–1774.

Ordonez, C.; Lamarque, J. F.; Tilmes, S.; Kinnison, D. E.; Atlas, E. L.; Blake, D. R.; Sousa Santos, G.; Brasseur, G. & Saiz-Lopez, A. (2012): Bromine and iodine chemistry in a global chemistry-climate model: description and evaluation of very short-lived oceanic sources. *Atmos. Chem. Phys.* **12** (3): 1423–1447.

Orkin, V. L.; Khamaganov, V. G.; Kozlov, S. N. & Kurylo, M. J. (2013): Measurements of Rate Constants for the OH Reactions with Bromoform ($CHBr_3$), $CHBr_2Cl$, $CHBrCl_2$, and Epichlorohydrin (C_3H_5ClO). *The Journal of Physical Chemistry A* **117** (18): 3809–3818.

Osthoff, H. D.; Bates, T. S.; Johnson, J. E.; Kuster, W. C.; Goldan, P.; Sommariva, R.; Williams, E. J.; Lerner, B. M.; Warneke, C.; de Gouw, J. A.; Pettersson, A.; Baynard, T.; Meagher, J. F.; Fehsenfeld, F. C.; Ravishankara, A. R. & Brown, S. S. (2009): Regional variation of the dimethyl sulfide oxidation mechanism in the summertime marine boundary layer in the Gulf of Maine. *Journal of Geophysical Research-Atmospheres* **114**

Papanastasiou, D. K.; McKeen, S. A. & Burkholder, J. B. (2014): The very short-lived ozone depleting substance CHBr3 (bromoform): revised UV absorption spectrum, atmospheric lifetime and ozone depletion potential. *Atmos. Chem. Phys.* **14** (6): 3017–3025.

Patra, P. K.; Krol, M. C.; Montzka, S. A.; Arnold, T.; Atlas, E. L.; Lintner, B. R.; Stephens, B. B.; Xiang, B.; Elkins, J. W.; Fraser, P. J.; Ghosh, A.; Hintsa, E. J.; Hurst, D. F.; Ishijima, K.; Krummel, P. B.; Miller, B. R.; Miyazaki, K.; Moore, F. L.; Muehle, J.; O'Doherty, S.; Prinn, R. G.; Steele, L. P.; Takigawa, M.; Wang, H. J.; Weiss, R. F.; Wofsy,

S. C. & Young, D. (2014): Observational evidence for interhemispheric hydroxyl-radical parity. *Nature* **513** (7517): 219–+.

Penkett, S. A.; Jones, B. M. R.; Rycroft, M. J. & Simmons, D. A. (1985): An interhemispheric comparison of the concentrations of bromine compounds in the atmosphere. *Nature* **318** (6046): 550–553.

Pozzer, A.; Jöckel, P.; Sander, R.; Williams, J.; Ganzeveld, L. & Lelieveld, J. (2006): Technical Note: The MESSy-submodel AIRSEA calculating the air-sea exchange of chemical species. *Atmos. Chem. Phys.* **6** (12): 5435–5444.

Quack, B. & Wallace, D. W. R. (2003): Air-sea flux of bromoform: Controls, rates, and implications. *Global Biogeochemical Cycles* **17** (1): 1023.

Saiz-Lopez, A.; Plane, J. M. C.; Baker, A. R.; Carpenter, L. J.; von Glasow, R.; Martin, J. C. G.; McFiggans, G. & Saunders, R. W. (2012): Atmospheric Chemistry of Iodine. *Chemical Reviews* **112** (3): 1773–1804.

Sala, S.; Boenisch, H.; Keber, T.; Oram, D. E.; Mills, G. & Engel, A. (2014): Deriving an atmospheric budget of total organic bromine using airborne in situ measurements from the western Pacific area during SHIVA. *Atmospheric Chemistry and Physics* **14** (13): 6903–6923.

Salawitch, R. J.; Weisenstein, D. K.; Kovalenko, L. J.; Sioris, C. E.; Wennberg, P. O.; Chance, K.; Ko, M. K. W. & McLinden, C. A. (2005): Sensitivity of ozone to bromine in the lower stratosphere. *Geophysical Research Letters* **32** (5)

Salawitch, R. J. (2006): Atmospheric chemistry: Biogenic bromine. *Nature* **439** (7074): 275–277.

Saltzman, E. S.; King, D. B.; Holmen, K. & Leck, C. (1993): Experimental determination of the diffusion coefficient of dimethylsulfide in water. *Journal of Geophysical Research - Oceans* **98** (C9): 16481–16486.

Sander, R.; Baumgaertner, A.; Gromov, S.; Harder, H.; Joeckel, P.; Kerkweg, A.; Kubistin, D.; Regelin, E.; Riede, H.; Sandu, A.; Taraborrelli, D.; Tost, H. & Xie, Z. Q. (2011): The atmospheric chemistry box model CAABA/MECCA-3.0. *Geoscientific Model Development* **4** (2): 373–380.

Sciare, J.; Mihalopoulos, N. & Dentener, F. J. (2000): Interannual variability of atmospheric dimethylsulfide in the southern Indian Ocean. *Journal of Geophysical Research-Atmospheres* **105** (D21): 26369–26377.

Sheng, J.-X.; Weisenstein, D. K.; Luo, B.-P.; Rozanov, E.; Stenke, A.; Anet, J.; Bingemer, H. & Peter, T. (2015): Global atmospheric sulfur budget under volcanically quiescent conditions: Aerosol-chemistry-climate model predictions and validation. *Journal of Geophysical Research: Atmospheres* **120** (1): 2014JD021985.

Shi, Q.; Petrick, G.; Quack, B.; Marandino, C. & Wallace, D. (2014): Seasonal variability of methyl iodide in the Kiel Fjord. *Journal of Geophysical Research-Oceans* **119** (3): 1609–1620.

Sinnhuber, B. M.; Sheode, N.; Sinnhuber, M.; Chipperfield, M. P. & Feng, W. (2009): The contribution of anthropogenic bromine emissions to past stratospheric ozone trends: a modelling study. *Atmos. Chem. Phys.* **9** (8): 2863–2871.

Sinnhuber, B.-M. & Meul, S. (2015): Simulating the impact of emissions of brominated very short lived substances on past stratospheric ozone trends. *Geophysical Research Letters* **42** (7): 2449–2456.

Solomon, S.; Garcia, R. R. & Ravishankara, A. R. (1994): On the role of iodine in ozone depletion. *Journal of Geophysical Research-Atmospheres* **99** (D10): 20491–20499.

Taylor, K. E. (2001): Summarizing multiple aspects of model performance in a single diagram. *Journal of Geophysical Research-Atmospheres* **106** (D7): 7183–7192.

Tegtmeier, S.; Krüger, K.; Quack, B.; Atlas, E.; Blake, D. R.; Boenisch, H.; Engel, A.; Hepach, H.; Hossaini, R.; Navarro, M. A.; Raimund, S.; Sala, S.; Shi, Q. & Ziska, F. (2013): The contribution of oceanic methyl iodide to stratospheric iodine. *Atmospheric Chemistry and Physics* **13** (23): 11869–11886.

Tiedtke, M. (1989): A comprehensive mass flux scheme for cumulus parameterization in large-scale models. *Monthly Weather Review* **117** (8): 1779–1800.

Tsai, W. T. & Liu, K. K. (2003): An assessment of the effect of sea surface surfactant on global atmosphere-ocean CO_2 flux. *Journal of Geophysical Research-Oceans* **108** (C4)

Von Glasow, R.; von Kuhlmann, R.; Lawrence, M. G.; Platt, U. & Crutzen, P. J. (2004): Impact of reactive bromine chemistry in the troposphere. *Atmospheric Chemistry and Physics* **4**: 2481–2497.

Wanninkhof, R. (1992): Relationship between wind-speed and gas-exchange over the ocean. *Journal of Geophysical Research-Oceans* **97** (C5): 7373–7382.

Wanninkhof, R. & McGillis, W. R. (1999): A cubic relationship between air-sea CO_2 exchange and wind speed. *Geophysical Research Letters* **26** (13): 1889–1892.

Wanninkhof, R.; Asher, W. E.; Ho, D. T.; Sweeney, C. & McGillis, W. R. (2009): Advances in Quantifying Air-Sea Gas Exchange and Environmental Forcing. *Annual Review of Marine Science* **1**: 213–244.

Warwick, N. J.; Pyle, J. A.; Carver, G. D.; Yang, X.; Savage, N. H.; O'Connor, F. M. & Cox, R. A. (2006): Global modeling of biogenic bromocarbons. *Journal of Geophysical Research: Atmospheres* **111** (D24): D24305.

Watts, S. F. (2000): The mass budgets of carbonyl sulfide, dimethyl sulfide, carbon disulfide and hydrogen sulfide. *Atmospheric Environment* **34** (5): 761–779.

Wilke, C. & Chang, P. (1955): Some measurements of diffusion in liquids. **59**: 5.

Wisher, A.; Oram, D. E.; Laube, J. C.; Mills, G. P.; van Velthoven, P.; Zahn, A. & Brenninkmeijer, C. A. M. (2014): Very short-lived bromomethanes measured by the CARIBIC observatory over the North Atlantic, Africa and Southeast Asia during 2009-2013. *Atmospheric Chemistry and Physics* **14** (7): 3557–3570.

Wofsy, S. C.; Daube, B. C.; Jimenez, R.; Kort, E.; Pittman, J. V.; Park, S.; Commane, R.; Xiang, B.; Santoni, G.; Jacob, D.; Fisher, J.; Pickett-Heaps, C.; Wang, H.; Wecht, K.; Wang, Q.-Q.; B.Stephens, B.; Shertz, S.; Watt, A.; Romashkin, P.; Campos, T.; Haggerty, J.; Cooper, W. A.; Rogers, D.; Beaton, S.; Hendershot, R.; Elkins, J. W.; Fahey, D. W.; Gao, R. S.; Moore, F.; Montzka, S. A.; Schwarz, J. P.; Perring, A. E.; Hurst, D.; Miller, B. R.; Sweeney, C.; Oltmans, S.; D.Nance; Hintsa, E.; Dutton, G.; Watts, L. A.; Spackman, J. R.; Rosenlof, K. H.; Ray, E. A.; Hall, B.; Zondlo, M. A.; Diao, M.; Keeling, R.; Bent, J.; Atlas, E. L.; Lueb, R. & Mahoney., M. J. (2012): *HIPPO Combined Discrete Flask and GC Sample GHG, Halo-, Hydrocarbon Data (R20121129).*

Yu, S.; Eder, B.; Dennis, R.; Chu, S.-H. & Schwartz, S. E. (2006): New unbiased symmetric metrics for evaluation of air quality models. *Atmospheric Science Letters* **7** (1): 26–34.

Ziska, F.; Quack, B.; Abrahamsson, K.; Archer, S. D.; Atlas, E.; Bell, T.; Butler, J. H.; Carpenter, L. J.; Jones, C. E.; Harris, N. R. P.; Hepach, H.; Heumann, K. G.; Hughes, C.; Kuss, J.; Krüger, K.; Liss, P.; Moore, R. M.; Orlikowska, A.; Raimund, S.; Reeves, C. E.; Reifenhäuser, W.; Robinson, A. D.; Schall, C.; Tanhua, T.; Tegtmeier, S.; Turner, S.; Wang, L.; Wallace, D.; Williams, J.; Yamamoto, H.; Yvon-Lewis, S. & Yokouchi, Y. (2013): Global sea-to-air flux climatology for bromoform, dibromomethane and methyl iodide. *Atmos. Chem. Phys.* **13** (17): 8915–8934.

4

Direct oceanic emissions are unlikely to account for the missing source of OCS

published as:
Lennartz, S. T., Marandino, C. A., von Hobe, M., Cortes, P., Quack, B., Simo, R., Booge, D., Pozzer, A., Steinhoff, T., Arevalo-Martinez, D. L., Kloss, C., Bracher, A., Röttgers, R., Atlas, E., and Krüger, K.: Direct oceanic emissions unlikely to account for the missing source of atmospheric carbonyl sulfide, Atmos. Chem. Phys., 17, 385-402, 10.5194/acp-17-385-2017, 2017.

Abstract. The climate active trace-gas carbonyl sulfide (OCS) is the most abundant sulfur gas in the atmosphere. A missing source in its atmospheric budget is currently suggested, resulting from an upward revision of the vegetation sink. Tropical oceanic emissions have been proposed to close the resulting gap in the atmospheric budget. We present a bottom-up approach including (i) new observations of OCS in surface waters of the tropical Atlantic, Pacific and Indian oceans and (ii) a further improved global box model to show that direct OCS emissions are unlikely to account for the missing source. The box model suggests an undersaturation of the surface water with respect to OCS integrated over the entire tropical ocean area and, further, global annual direct emissions of OCS well below that suggested by top-down estimates. In addition, we discuss the potential of indirect emission from CS_2 and dimethyl sulfide (DMS) to account for the gap in the atmospheric budget. This bottom-up estimate of oceanic emissions has implications for using OCS as a proxy for global terrestrial CO_2 uptake, which is currently impeded by the inadequate quantification of atmospheric OCS sources and sinks.

4.1 Introduction

Carbonyl sulfide (OCS) is the most abundant reduced sulfur compound in the atmosphere. It enters the atmosphere either by direct emissions, e.g., from oceans, wetlands, anoxic soils or anthropogenic emissions, or indirectly via oxidation of the short-lived precursor gases dimethyl sulfide (DMS) and carbon disulfide (CS_2) (Chin & Davis, 1993; Kettle, 2002; Watts, 2000). Both precursor gases are naturally produced in the oceans, and CS_2 has an additional anthropogenic source (Campbell et al., 2015; Kettle, 2002; Stefels et al., 2007). With direct and indirect marine emissions combined, the ocean is considered as the dominant source of atmospheric OCS (Chin & Davis, 1993; Kettle, 2002; Watts, 2000). The most important sink of atmospheric OCS is uptake by terrestrial vegetation (Brown & Bell, 1986; Campbell et al., 2008; Protoschill-Krebs & Kesselmeier, 1992) and oxic soils, while chemical loss by photolysis and reaction with the hydroxyl radical (OH) in the atmosphere are minor loss processes (Chin & Davis, 1993; Kettle, 2002; Watts, 2000). While tropospheric volume mixing ratios show a distinct annual cycle (Montzka et al., 2007), the interannual to decadal variation is low (Kremser et al., 2015; Montzka et al., 2007). Accurate accounts of sources and sinks of atmospheric OCS are crucial for two reasons.

- First, OCS is climate-relevant because it influences the radiative budget of the Earth as a greenhouse gas and by contributing significant amounts of sulfur to the stratospheric aerosol layer (Brühl et al., 2012; Crutzen, 1976; Notholt et al., 2003; Turco et al., 1980) that exerts a cooling effect (Kremser et al., 2016; Turco et al., 1980). The two opposite effects are currently in balance (Brühl et al., 2012), but future changes in atmospheric circulation, as well as the magnitude and distribution of OCS sources and sinks, could change that. Hence, a better understanding of the tropospheric budget is needed to predict the effect of OCS in future climate scenarios (Kremser et al., 2016).

- Second, OCS has recently been suggested as a promising tool to constrain terrestrial CO_2 uptake, i.e., gross primary production (GPP), as it is taken up by plants in a similar way as CO_2 (Asaf et al., 2013). GPP, a major global CO_2 flux, can only be inferred from indirect methods, because the uptake of CO_2 occurs along with a concurrent release by respiration. Unlike CO_2, OCS is irreversibly degraded within the leaf. GPP can thus be estimated based on the uptake ratio of OCS and CO_2, from the leaf to regional scale (Asaf et al., 2013) or even global scale (Beer et al., 2010), under the condition that other sources are negligible or well quantified. The

Table 4.1: OCS missing source estimates derived from top-down approaches: the listed studies used an increased vegetation sink and an a priori direct and indirect ocean flux to estimate the magnitude of the missing source. Assigning the missing source to oceanic emissions results in the total ocean flux listed here. Fluxes are given in Gg S per year.

Reference	A priori ocean flux	Missing source	Total ocean flux
Suntharalingam et al. (2008)	235	230	465
Berry et al. (2013)	276	600	876
Kuai et al. (2015)	289	800	1089
Glatthor et al. (2015)	276	714	992

magnitude of terrestrial biogeochemical feedbacks on climate has been suggested to be similar to that of physical feedbacks (Arneth et al., 2010). In order to reduce existing uncertainties, it is thus crucial to better constrain single processes in the carbon cycle, especially GPP.

Nonetheless, current figures for tropospheric OCS sources and sinks carry large uncertainties (Kremser et al., 2016). While the budget has been previously considered closed (Kettle, 2002), a recent upward revision of the vegetation sink (Berry et al., 2013; Sandoval-Soto et al., 2005; Suntharalingam et al., 2008) led to a gap, i.e., a missing source in the atmospheric budget of 230–800 Gg S per year (Berry et al., 2013; Glatthor et al., 2015; Kuai et al., 2015; Suntharalingam et al., 2008) (Table 4.1), with the most recent estimates at the higher end of the range. This revision of vegetation uptake was suggested to (i) take into account the different deposition velocities of CO_2 and OCS within the leaf and base it on GPP instead of net primary production (Sandoval-Soto et al., 2005) as well as (ii) to better reproduce observed seasonality of OCS mixing ratios in several atmospheric models (Berry et al., 2013; Glatthor et al., 2015; Kuai et al., 2015). Based on independent top-down approaches using MIPAS (Glatthor et al., 2015) and TES (Kuai et al., 2015) satellite observations, FTIR measurements (Wang et al., 2016), and NOAA ground-based time series stations and the HIPPO aircraft campaign (Berry et al., 2013; Kuai et al., 2015), the missing source of OCS was suggested to originate from the (tropical) ocean, most likely from the region of the Pacific warm pool. Other potential sources such as advection of air masses from Asia have been discussed (Glatthor et al., 2015) but not tested. If the ocean was to account for the missing source, the total top-down oceanic source strength would then be the a priori oceanic flux plus the missing source estimate of each inverse model simulation (Table 4.1). This addition would imply a 200–380 % increase in the a priori estimated oceanic source. If oceanic direct and indirect emissions were to account for the total missing source, an

ocean source strength of 465–1089 Gg S yr^{-1} would be required (Table 4.1).

OCS and its atmospheric precursors are naturally produced in the ocean. In the surface open ocean, OCS is present in the lower picomolar range, and has been measured on numerous cruises in the Atlantic (Flöck & Andreae, 1996; Ulshöfer & Andreae, 1998; Ulshöfer et al., 1995; Von Hobe et al., 1999), including three latitudinal transects (Kettle et al., 2001; Xu, 2001), the Indian Ocean (Mihalopoulos et al., 1992), the Pacific Ocean (Weiss et al., 1995a) and the Southern Ocean (Staubes & Geogrii, 1993). Measurements in tropical latitudes, where the missing source is assumed to be located, have previously been performed in the Indian Ocean (Mihalopoulos et al., 1992) and during the Atlantic transects (Kettle et al., 2001; Xu, 2001). OCS is produced photochemically from chromophoric dissolved organic matter (CDOM) (Andreae & Ferek, 2002; Ferek & Andreae, 1984) and by a not fully understood light-independent production that has been suggested to be linked to radical formation (Flöck et al., 1997; Pos et al., 1998). Dissolved OCS is efficiently hydrolyzed to CO_2 and H_2S at a rate depending on pH and temperature (Elliott et al., 1989). CS_2 has been measured in the Pacific and Atlantic oceans in a range of 7.2–27.5 pmol L^{-1} (Xie et al., 1998) and during two Atlantic transects (summer and winter) in a range of 4–40 pmol L^{-1} (Xu, 2001). It is produced photochemically (Xie et al., 1998) and biologically (Xie et al., 1999), and no significant loss process other than air–sea gas exchange has been identified (Xie et al., 1998). DMS is present in the lower nanomolar range in the surface ocean and has been extensively studied in several campaigns, summarized in a climatology by Lana et al. (2011). DMS is biogenically produced and consumed in the surface ocean, as well as photo-oxidized and ventilated by air–sea exchange (Stefels et al., 2007).

Available bottom-up estimates of the global oceanic OCS fluxes from shipboard observations range from −16 to 320 Gg S yr^{-1} (Table 4.2). However, the highest estimates were biased, because mainly summertime and daytime observations of water concentrations were considered. With the discovery of the seasonal oceanic sink of OCS during wintertime (Ulshöfer et al., 1995) and a pronounced diel cycle (Ferek & Andreae, 1984), direct oceanic emissions were corrected downwards.

Only recently, OCS emissions have been estimated with the biogeochemical ocean model NEMO-PISCES (Launois et al., 2015a) at a magnitude of 813 Gg S yr^{-1}, sufficient to account for the missing source. This oceanic emission inventory had been used to constrain GPP based on OCS on a global scale (Launois et al., 2015b). However, the oceanic OCS photoproduction in the ocean model included a parameterization for OCS photoproduction derived from an experiment in the North Sea (Uher & Andreae, 1997a), which might not be representative for the global ocean, as indicated by photoproduction constants that were an order of magnitude lower in the Atlantic ocean compared to the German Bight (Uher &

Table 4.2: Global oceanic emission estimates of OCS: direct ocean emission estimates of OCS from bottom-up approaches. Uncertainties are given in parentheses as in the original paper either as range or ± standard deviation. * Units deviate from original paper, converted to Gg S for comparison.

Reference	Emitted S as OCS (Gg S yr^{-1})
Extrapolated from measurements	
Rasmussen et al. (1982)	320 (±160)*
Ferek & Andreae (1983)	245*
Johnson & Harrison (1986)	110–210*
Mihalopoulos et al. (1992)	230 (110–210)*
Chin & Davis (1993)	160 (85–340)*
Weiss et al. (1995b)	−16 (−10–30)*
Ulshöfer & Andreae (1998)	41–80*
Watts (2000)	53 (±80)*
Xu (2001)	53*
Model simulations	
Kettle (2002)	41 (±154)
Launois et al. (2015a)	813 (573–3997)
This study	130 (±80)

Andreae, 1997b).

Here, we present new observations in all three tropical ocean basins, two of them measured with unprecedented precision and time resolution. Direct fluxes were inferred from continuous OCS measurements in the tropical Pacific and Indian oceans, covering a range of regimes with respect to CDOM content, ultraviolet (UV) radiation and sea surface temperature (SST). These observations are used to further constrain and validate a biogeochemical box model which had previously been shown to reproduce OCS concentration in the Atlantic Ocean reasonably well (Von Hobe et al., 2001). The box model is now updated from its previous global application (Kettle, 2002) by adding and further developing the most recent process parameterizations to estimate the global source strength of direct OCS emissions. The emission estimate is further complemented by discussing the potential of indirect OCS emissions, i.e., the emissions of short-lived precursor gases CS_2 and DMS, to account for the gap in the budget.

4.2 Methods

4.2.1 Study sites

Several cruises were conducted to measure the trace gases OCS (OASIS, TransPEGASO, ASTRA-OMZ) and CS_2 (TransPEGASO, ASTRA-OMZ). Cruise tracks are depicted in Fig. 4.1. The OASIS cruise onboard RV *SONNE I* to the Indian Ocean started from Port Louis, Mauritius, to Malé, Maldives, in July and August 2014, where mainly oligotrophic waters were encountered. TransPEGASO was an Atlantic transect starting in Gibraltar and leading to Buenos Aires, Argentina, and Punta Arenas, Chile. It took place in October and November 2014 and covered a variety of biogeochemical regimes. ASTRA-OMZ onboard RV *SONNE II* started in Guayaquil, Ecuador, and ended in Antofagasta, Chile, in October 2015. Although 2015 was an El Niño year, upwelling together with high biological production was still encountered during the cruise (Stramma et al., 2016).

4.2.2 Measurement setup for trace gases

OCS was measured during two cruises onboard the RV *SONNE I* (OASIS) and *SONNE II* (ASTRA-OMZ) with a continuous underway system similar to the one described in Arévalo-Martínez et al. (2013), at a measurement frequency of 1 Hz. The system consisted of a Weiss-type equilibrator, through which seawater is pumped from approximately 5 m below the surface with a flow of 3–4 L min^{-1}. The air from the equilibrator headspace was Nafion-dried and continuously pumped into an OCS analyzer (model DL-T-100, Los Gatos Research) that uses the off-axis integrated cavity output spectroscopy (OA-ICOS) technique. The instrument used onboard is a prototype of a commercial instrument (`www.lgrinc.com/documents/OCS_Analyzer_Datasheet.pdf`), developed by Los Gatos Research (LGR) in collaboration with Forschungszentrum Jülich GmbH (Schrade, 2011). Data were averaged over 2 min, achieving a precision of 15 ppt. OCS mixing ratios in the marine boundary layer (MBL) were determined by pumping outside air ca. 50 m from the ship's deck to the OCS analyzer (pump: KNF Neuberger, Germany). A measurement cycle consisted of 50 min water sampling and 10 min air sampling, where the first 3 min after switching until stabilization of the signal were discarded.

Before and after the cruise the analyzer was calibrated over a range of concentrations using permeation devices. Both calibrations were consistent. However, during calibration the output of the internal spectral retrieval differed significantly from post-processing of the recorded spectra, which matched the known concentrations (this offset is not present in the commercial instruments). The calibration data were thus used to derive a correction

function. After correction all data stayed within 5 % of the standards. The calibration scale of the permeation devices was 5 % below the NOAA scale. As the OCS analyzer measured CO_2 simultaneously, and CO_2 standards were available during the cruise, drift of the instrument was tested by measuring CO_2 standard gases before and after the cruise and found to be less than 1 % of the signal. Special care was taken to avoid contamination, and all materials used were tested for contamination before use.

During OASIS, the mirrors inside the cavity of the OCS analyzer were not completely clean, which led to a reduced signal. To correct the data, an attenuation factor was determined from simultaneous CO_2 measurements, because no OCS standard was available onboard, and OASIS data were corrected accordingly.

An independent quality check of the data was performed by comparing volume mixing ratios of the MBL from the OCS analyzer with samples from air canisters sampled during both cruises and measured independently (de Gouw et al., 2009; Schauffler et al., 1998). The calibrated (and attenuation corrected for OASIS) OA-ICOS data were on average 5 % lower than the air canister samples, which reflects the 5 % difference between the calibration at Forschungszentrum Jülich and the NOAA scale.

During ASTRA-OMZ, CS_2 was directly measured onboard within 1 h of collection using a purge and trap system attached to a gas chromatograph and mass spectrometer (GC/MS; Agilent 7890A/Agilent 5975C; inert XL MSD with triple axis detector) running in single-ion mode. The discrete surface seawater samples (50 mL) were taken each hour to every 3 h from the same pump system as for continuous OCS measurements. CS_2 was stripped by purging with helium (70 mL min^{-1}) for 15 min. The gas stream was dried using a Nafion membrane dryer (Perma Pure) and CS_2 was preconcentrated in a trap cooled with liquid nitrogen. After heating the trap with hot water, CS_2 was injected into the GC/MS. Retention time for CS_2 (m/z 76, 78) was 4.9 min. The analyzed data were calibrated each day using gravimetrically prepared liquid CS_2 standards in ethylene glycol. During purging, 500 μL gaseous deuterated DMS (d3-DMS) and isoprene (d5-isoprene) were added to each sample as an internal standard to account for possible sensitivity drift between calibrations.

During the TransPEGASO cruise onboard RV *Hesperides*, surface ocean OCS and CS_2 were measured in discrete seawater samples by purge and trap and gas chromatography with mass spectrometry detection (GC-MSD). Samples were collected every day at 09:00 and 15:00 local time in glass bottles without headspace and analyzed within 1 h. Aliquots of 25 mL were withdrawn with a glass syringe and filtered through GF/F during injection into the purge and trap system (Stratum, Teledyne Tekmar). The water was heated to 30 °C and volatiles were stripped by bubbling with 40 mL min^{-1} of ultrapure helium for 12 min and trapped in a U-shaped VOCARB 9 trap at room temperature. After flash thermal desorption,

volatiles were injected into an Agilent 5975T LTM GC-MSD equipped with an Agilent LTM DB-VRX column (20 m × 0.18 mm OD × 1 μm) maintained at 30 °C. Retention times for OCS (m/z 60) and CS_2 (m/z 76) were 1.3 and 2.7 min, respectively. Peak quantification was achieved with respect to gaseous (OCS in N_2) and liquid (CS_2 in methanol and water) standards that were analyzed in the same way. Samples were run in duplicates. Detection limits were 1.8 pM (OCS) and 1.4 pM (CS_2), and precision was typically around 5 %.

The systems are each calibrated against a standard, but they had not been directly intercompared. Still, our measurements are consistent with previous measurements using independent methods as discussed in Sects. 4.3.2 and 4.3.3.

4.2.3 Calculation of air–sea exchange

Fluxes F of all gases were calculated with Eq. (4.1):

$$F = k_w \cdot \Delta c, \tag{4.1}$$

where k_w is the gas transfer velocity in water (i.e., physical constraints on exchange) and ΔC the air–sea concentration gradient (i.e., the chemical constraint on exchange). The air-side transfer velocity (Liss & Slater, 1974) for OCS was calculated to be 7 orders of magnitude smaller and was therefore neglected. The concentration gradient was determined using the temperature dependent Henry constant (De Bruyn et al., 1995) and the measurements in the surface water and MBL for OASIS and ASTRA-OMZ. During TransPEGASO, no atmospheric volume mixing ratio was measured, and a value of 500 ppt was assumed (Montzka et al., 2007). As air volume mixing ratios of OCS vary over the course of a year, we performed a sensitivity test for a scenario of 450 and 550 ppt and found mean deviations of +7.8 and −7.8 %, respectively. The transfer velocity k_w was determined using a quadratic parameterization based on wind speed (Nightingale et al., 2000) which was directly measured onboard (10 min averages). Furthermore, k_w was corrected for OCS and CS_2 by scaling it with the Schmidt number calculated from the molar volume of the gases (Hayduk & Laudie, 1974). It should be noted that the choice of the parameterization for k_w has a non-negligible influence on the global emission estimate. Linear, quadratic and cubic parameterizations of k_w are available, with differences increasing at high wind speeds on the order of a factor of 2 (Lennartz et al., 2015; Wanninkhof et al., 2009). Evidence suggests that the air–sea exchange of insoluble gases such as CO_2, OCS and CS_2 follows a cubic relationship to wind speed because of bubble-mediated gas transfer (Asher & Wanninkhof, 1998; McGillis et al., 2001). However, this difference between soluble and non-soluble gases is not always consistent (Miller et al., 2009), and too few data are

available for a reliable parameterization at high wind speeds above 12 m s^{-1}, where the cubic and the quadratic parameterizations diverge the most. For reasons of consistency, e.g., for the fitted photoproduction p from previous studies, and the fact that most of the previous emission estimates were computed using a quadratic k_w parameterization, we chose the same quadratic parameterization representing the mean range of observations (Nightingale et al., 2000). For a sensitivity test, we computed the global oceanic emission with a cubic relationship (McGillis et al., 2001), which results in an additional 40 Gg S per year as direct OCS emissions, leaving the missing source still unexplained. However, better constraints on the transfer velocity of insoluble gases would decrease the uncertainty in global oceanic emissions of marine trace gases.

4.2.4 Box model of OCS concentration in the surface ocean

A box model to simulate surface concentration of OCS is further developed from the latest version from von Hobe et al. (2003, termed vH2003), where concentrations along the tracks of five Atlantic cruises have been simulated and compared. The vH2003 model results from successful tests and validation to observations on several cruises to the Atlantic Ocean covering all seasons (i.e., Flöck & Andreae, 1996, in January 1994; Uher & Andreae, 1997b, in April/May 1992; Von Hobe et al., 1999, in June/July 1997; Kettle et al., 2001, in September/October 1998). By comparing photoproduction rate constants of the five cruises to CDOM absorption, von Hobe et al. (2003) suggest a second-order process for photoproduction with the photoproduction rate constant being dependent on the absorption of CDOM in seawater.

In our approach, we test vH2003 along the cruise track of two cruises, include a new way of determining the photoproduction rate constant (see below) and apply it with global climatological input (termed L2016). Kettle (2002) and Kettle (2000, termed K2000) applied a similar version of vH2003 globally, which included an optimized photoproduction constant from Atlantic transect cruise data, an optimized constant light-independent production and a linear regression to obtain CDOM from chlorophyll *a*. In comparison to K2000, we use (i) a new way of determining the photoproduction rate constant incorporating information from three ocean basins, (ii) the most recent parameterization of light-independent production available, and (iii) satellite observations for sea surface CDOM instead of an empirical relationship based on chlorophyll *a*.

Launois et al. (2015a) implemented parameterizations for light-independent production, hydrolysis and air–sea exchange similar to vH2003 in the 3-D global ocean model NEMO-PISCES. The main differences to the approach used here are the lack of accounting for mixing in L2016 (discussed in Sect. 4.3.2, which will theoretically lead to higher simulated

concentrations in our case) and the application of a photoproduction rate constant in our model that incorporates information from three open ocean basins in contrast to one from a study in the North Sea (Launois et al., 2015a).

In L2016, the light-independent production term of OCS was parameterized depending on SST (K) and the absorption coefficient of CDOM at 350 nm wavelength, a_{350} (Von Hobe et al., 2001) (Eq. 4.2).

$$\frac{\mathrm{d}C_{\mathrm{OCS}}}{\mathrm{d}t} = a_{350} \times 10^{-6} \times \exp\left(55.8 - \frac{16\,200}{\mathrm{SST}}\right) \tag{4.2}$$

An overview on symbols and abbreviations used in equations in the following is provided in the Appendix. The parameterization for hydrolysis describes alkaline and acidic degradation of OCS by Reactions (4.3) and (4.4):

$$\mathrm{OCS} + \mathrm{H_2O} \rightleftharpoons \mathrm{H_2S} + \mathrm{CO_2} \tag{4.3}$$

$$\mathrm{OCS} + \mathrm{OH^-} \rightleftharpoons \mathrm{HS^-} + \mathrm{CO_2} \tag{4.4}$$

It was parameterized as a first-order kinetic reaction including the rate constant k_{h} according to Eqs. (4.5 to 4.7):

$$\frac{dC_{OCS}}{dt} = [OCS] \cdot k_h \tag{4.5}$$

$$k_h = exp\left(24.3 - \frac{10450}{SST} + exp(22.8 - \frac{6040}{SST}\right) \cdot \frac{K}{a[H^+]} \tag{4.6}$$

$$-\log_{10} K = \frac{3046.7}{SST} + 3.7685 + 0.0035486 \cdot \sqrt{SSS} \tag{4.7}$$

where $a[H^+]$ is the proton activity and K the ion product of seawater (Dickinson & Riley, 1979). Fluxes were calculated with Eq. (4.1) using the same parameterization for k_{w} as for the emission calculation from measurements described above. Photoproduction was integrated over the mixed layer depth (MLD), assuming a constant concentration of OCS and CDOM throughout the mixed layer, with the photoproduction rate constant p ($\mathrm{mol\,J^{-1}}$), a_{350} ($\mathrm{m^{-1}}$) and UV radiation ($\mathrm{W\,m^{-2}}$) (Sikorski & Zika, 1993) (Eq. 4.8).

$$\frac{\mathrm{d}C_{\mathrm{OCS}}}{\mathrm{d}t} = \int_{-\mathrm{MLD}}^{0} p a_{350} \mathrm{UV} \mathrm{d}z \tag{4.8}$$

MLD was obtained from CTD (conductivity, temperature, depth) profiles and interpolated between these locations (Figs. 4.6 and 4.7 in the Supplement). The photochemically active

radiation that reaches the ocean surface was approximated by Eq. (4.9) (Najjar et al., 1995):

$$\mathrm{UV} = 2.85 \times 10^{-4} \cdot I \cdot \cos^2 \theta, \tag{4.9}$$

with global radiation I (W m^{-2}) and the zenith angle cos θ. The attenuated UV light intensity directly below the surface (Sikorski & Zika, 1993) down to the respective depth of the mixed layer was calculated in 1 m steps, taking into account attenuation by CDOM and pure seawater. As a simplification in this global approach, the box model did not resolve the whole wavelength spectrum, but rather used a_{350} and applied a photoproduction rate constant that takes into account the integrated spectrum. A similar approach had been tested and compared to a wavelength spectrum resolving version by von Hobe et al. (2003).

The rate coefficients for hydrolysis, light-independent production and air–sea exchange are all reasonably well constrained and parameterizations have been derived from dedicated laboratory and field experiments (hydrolysis, air–sea exchange) or from nighttime OCS observations in several regions assuming steady state (dark production; Von Hobe et al., 2001). However, the photoproduction rate constant p is not well constrained and no generally applicable parameterization exists. In the study of von Hobe et al. (2003), a start was made in parameterizing p in terms of CDOM absorption, and they found this to be dependent on the exact model setup used with respect to wavelength integration and mixed layer treatment. To extend the p–CDOM relationship for other ocean basins, we use the two cruises OASIS and ASTRA-OMZ as case studies for parameter optimization of the photoproduction rate constant p. The photoproduction constant p in the case study simulations was fitted individually for periods of daylight $> 100\,\mathrm{W\,m^{-2}}$ (Fig. 4.2, blue lines) with a Levenberg–Marquardt optimization routine in MatLab version 2015a (8.5.0) by minimizing residuals between simulated and hourly averaged measurements. Different starting values were tested to reduce the risk of the fitted p being a local minimum. Together with photoproduction rate constants obtained by a similar optimization procedure by von Hobe et al. (2003, Table 2 therein, termed MLB STC) , a relationship of the photoproduction constant p dependent on a_{350} was established (Fig. 4.3). The resulting linear relationship thus includes values from the Atlantic, Pacific and Indian oceans, making it a good approximation for a globally valid dependence. For the global box model, p was calculated in every time step based on this relationship ($r = 0.71$, Eq. 4.10):

$$p = 3591.3 \cdot a_{350} + 329.4 \tag{4.10}$$

The scatter in Fig. 4.3 likely reflects the inhomogeneity of the water masses across the three oceanic basins considered, as CDOM absorbance is a valid proxy, but carries some

uncertainty in the concentration of the actual precursor.

The model input for simulations of the cruises OASIS and ASTRA-OMZ consisted of measurements made during the respective cruise, including SST and SSS (MicroCAT SBE41) measured every minute, CDOM absorption coefficient (spectrophotometrically measured ca. every 3 h with a liquid capillary cell setup) and the ship's in situ measured meteorological data such as wind speed and global radiation averaged over 10 min (Figs. S1, S2, Tables S1, S2). Forcing data were linearly interpolated to the time step of integration of 2 min.

For the global box model, monthly global meteorological fields with a spatial resolution of $2.8^\circ \times 2.8^\circ$ were used (Table S3, Fig. S3). For global a_{350} at the sea surface, monthly climatological means for absorption due to gelbstoff and detritus a_{443} (gelbstoff representing CDOM) from the MODIS-Aqua satellite (all available data, 2002–2014) (NASA, 2014) were corrected to 350 nm with Eq. (4.11) (Fichot & Miller, 2010; Launois et al., 2015a):

$$a_{350} = a_{443} \cdot \exp(-0.02 \cdot (350 - 443)). \tag{4.11}$$

SST, wind speed, and atmospheric pressure were obtained as monthly climatological means from the same period, i.e., 2002 to 2014, by ERA-Interim (Dee et al., 2011). A diel cycle of global radiation I was obtained by fitting the parable parameters a and b during time of the day t in Eq. (4.12) (Fig. S4),

$$I = -a \cdot t^2 + b, \tag{4.12}$$

to conditions of (i) x axis interceptions in the distance of the sunshine duration and (ii) the integral being the daily incoming energy by ERA-Interim (Dee et al., 2011). Monthly climatologies of mixed layer depths were used from the MIMOC project (Schmidtko et al., 2013). For details of data sources please refer to Tables S1–S3 provided in the Supplement. The time step of the model was set to 120 min, which had been tested to result in negligible ($< 3\,\%$) smoothing.

4.2.5 Assessing the indirect contribution of DMS with EMAC

Model outputs from ECHAM/MESSy Atmospheric Chemistry (EMAC) from the simulation RC1SDbase-10a of the ESCiMo project (Jöckel et al., 2016) are used to evaluate the contribution of DMS on the production of OCS. The model results were obtained with ECHAM5 version 5.3.02 and MESSy version 2.51, with a T42L90MA resolution (corresponding to a quadratic Gaussian grid of approx. 2.8 by 2.8° in latitude and longitude and 90 vertical hybrid pressure levels up to 0.01 hPa). The dynamics of the general circulation model were nudged by Newtonian relaxation towards ERA-Interim reanalysis data. DMS emissions were calculated with the AIRSEA submodel (Pozzer et al., 2006), which takes into account

concentration of DMS in the atmosphere and in the ocean, following a two-layer conceptual model to calculate emissions (Liss & Slater, 1974). While atmospheric concentrations are estimated online by the model (with DMS oxidation), the oceanic concentrations are prescribed as monthly climatologies (Lana et al., 2011). It was shown that such an online calculation of emissions provides the most realistic results when compared to measurements compared to a fixed emission rate (Lennartz et al., 2015). The online-calculated concentrations of DMS and OH were been used to estimate the production of OCS. A production yield of 0.7 % was used for the reaction of DMS with OH (Barnes et al., 1994), using the reaction rate constant suggested by the International Union of Pure and Applied Chemistry (IUPAC) (Atkinson et al., 2004).

4.3 Results and discussion

4.3.1 Observations of OCS in the tropical ocean

OCS was measured in the surface ocean and MBL during three cruises in the tropics. Measurement locations (Fig. 4.1) include oligotrophic open ocean regions in the Indian Ocean (OASIS, 07-08/2014), open ocean and shelf areas in the eastern Pacific (ASTRA-OMZ, 10/2015) and a meridional transect in the Atlantic (TransPEGASO, 10-11/2014). In the Indian and Pacific oceans, continuous underway measurements provided the necessary temporal resolution to observe diel cycles of OCS concentrations in surface water. Dissolved OCS concentrations exhibited diel cycles with maxima 2 to 4 h after local noon (Fig. 4.1), which are a consequence of photochemical production and removal by hydrolysis (Uher & Andreae, 1997b). OCS concentrations also varied spatially. Taking a_{350} as a proxy for CDOM content, we found that daily mean OCS concentrations were higher in CDOM-rich (Table 4.3, 28.3 ± 19.7 pmol OCS L^{-1}, a_{350}: 0.15 ± 0.03 m^{-1}) than in CDOM-poor waters (Table 4.3, OASIS: 9.1 ± 3.5 pmol OCS L^{-1}, a_{350}: 0.03 ± 0.02 m^{-1}). Samples during TransPEGASO were measured with gas chromatography–mass spectrometry twice a day (around 08:00–10:00 and 15:00–17:00 local times). Therefore, the full diel cycles could not be reconstructed and potential variations of OCS with CDOM absorption were overlaid by diel variations. Nevertheless, the observed range of OCS concentrations in the Atlantic corresponds well to the observations from the eastern Pacific and Indian Ocean (Table 4.3) and is consistent with measurements from a previous Atlantic meridional transect (AMT-7) cruise (Kettle et al., 2001) (1.3–112.0 pmol OCS L^{-1}, mean 21.7 pmol OCS L^{-1}).

Air–sea fluxes calculated from surface concentrations and mixing ratios of OCS as a function of wind speed generally follow the diel cycle of the surface ocean concentration.

Table 4.3: Average, standard deviation and range of parameters observed during the cruises OASIS (Indian Ocean, 2014), ASTRA-OMZ (Pacific Ocean, 2015) and TransPEGASO (Atlantic Ocean, 2014).

		Average (±SD)	Min.	Max.
OASIS (Indian Ocean)				
OCS sea surface concentration	($pmol\,L^{-1}$)	9.1 (±3.5)	5.1	20.7
OCS flux	($g\,S\,d^{-1}\,km^{-2}$)	−0.25 (±0.5)	−1.6	1.5
SST	(°C)	27.0 (±1.4)	22.2	32.0
Salinity	(–)	34.9 (±0.3)	34.3	35.4
Wind speed	($m\,s^{-1}$)	7.6 (±2.1)	0.2	14.5
$a_{CDOM}(350)$	(m^{-1})	0.03 (±0.02)	n.d.	0.12
ASTRA-OMZ (Pacific Ocean)				
OCS sea surface concentration	($pmol\,L^{-1}$)	28.3 (±19.7)	6.5	133.8
OCS flux	($g\,S\,d^{-1}\,km^{-2}$)	1.5 (±2.1)	−1.5	19.9
CS_2 sea surface concentration	($pmol\,L^{-1}$)	17.8 (±8.9)	6.7	40.1
CS_2 flux	($g\,S\,d^{-1}\,km^{-2}$)	4.1 (±3.2)	0.2	14.4
SST	(°C)	20.1 (±2.9)	15.6	26.9
Salinity	(–)	35.0 (±0.43)	33.4	35.5
Wind speed	($m\,s^{-1}$)	7.4 (±2.0)	0.3	15.5
$a_{CDOM}(350)$	(m^{-1})	0.15 (±0.03)	0.1	0.24
TransPEGASO (Atlantic Ocean)				
OCS sea surface concentration	($pmol\,L^{-1}$)	23.6 (±19.3)	2.6	78.3
OCS flux	($g\,S\,d^{-1}$)	1.3 (±3.5)	−1.7	14.0
CS_2 sea surface concentration	($pmol\,L^{-1}$)	62.5 (±42.1)	23.2	154.8
CS_2 flux	($g\,S\,d^{-1}\,km^{-2}$)	13.7 (±9.8)	0.3	33.9
SST	(°C)	22.6 (±6.3)	7.1	29.6
Salinity	(–)	34.9 (±2.6)	28.4	38.1
Wind speed	($m\,s^{-1}$)	7.4 (±3.1)	0.4	19.0
$a_{CDOM}(350)$	(m^{-1})	0.13 (±0.11)	0.0023	0.45

While supersaturation prevailed during the day, low nighttime concentrations usually led to oceanic uptake of atmospheric OCS. OCS fluxes integrated over one day ranged from -0.024 to $-0.0002\,g\,S\,km^{-2}$ in the open Indian Ocean and from 0.38 to $2.7\,g\,S\,km^{-2}$ in the coastal Pacific. During the observed periods, the ocean was a net sink of atmospheric OCS in the Indian Ocean, whereas it was a net source in the eastern Pacific. Although an assessment of net flux is difficult given the lower temporal resolution during TransPEGASO, calculated emissions were in the same range as the ones measured in the Pacific and Indian Ocean.

The water masses encountered during the cruises to the Indian Ocean (OASIS) and eastern Pacific (ASTRA-OMZ), which are used to constrain the global box model, differ considerably with respect to the properties relevant for OCS cycling and, thus, span a large

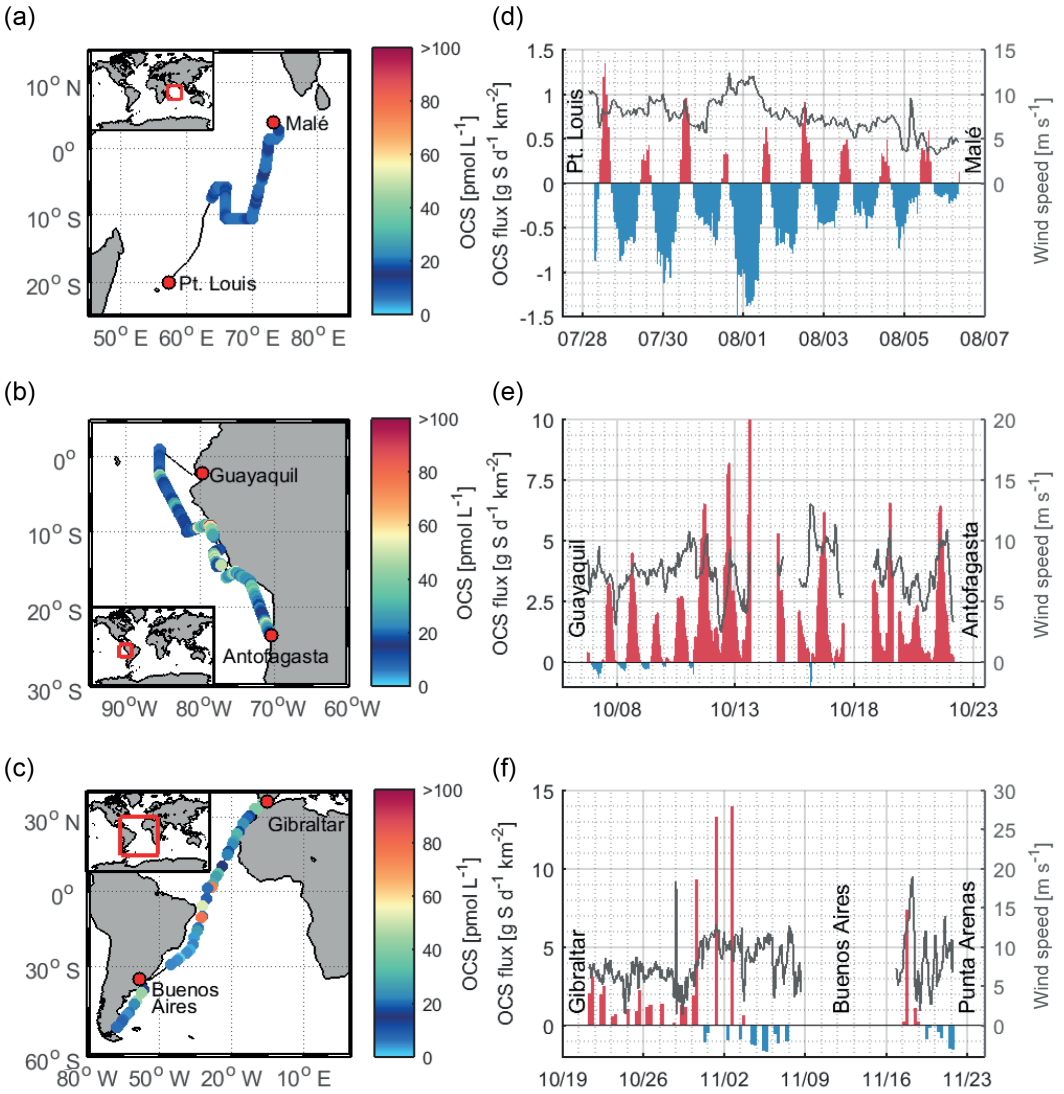

Figure 4.1: Observed OCS water concentrations and calculated emissions: observations of OCS concentrations in the surface ocean during the three cruises **(a)** OASIS, **(b)** ASTRA-OMZ, and **(c)** TransPEGASO as well as the corresponding emissions calculated based on the concentration gradient between water and marine boundary layer **(d–f)**. Outgassing is indicated in red bars; oceanic uptake in blue bars. The grey line shows wind speed measured onboard the vessels. Flux data are shown with different scales on the *y* axes. Data gaps occurred during stays in port and territorial waters or during instrument tests.

range of possible OCS variability. The properties encountered during these two cruises encompass or exceed the ones of the Pacific warm pool (climatological averages, Table 4.4), which is where the location of the missing source has been hypothesized (Glatthor et al., 2015; Kuai et al., 2015). Both higher SST and lower wind speeds (Table 4.4) would decrease

Table 4.4: Comparison of water properties relevant for OCS production and consumption for the cruises OASIS (Indian Ocean, July–August 2014) and ASTRA-OMZ (eastern Pacific, October–November 2015) with the assumed source region in the Pacific warm pool (15° N–15° S, 120–180° E). Data from cruises are in situ measurements; the data for the Pacific warm pool were extracted from climatological monthly means from sources for the global model run as specified in the Supplement.[a] Calculated from an annual mean diurnal cycle based on ERA-Interim sunshine duration and flux. SR: surface radiation, daily integral. [b] Assumed pH = 8.15 for box model simulation.

Parameter	OASIS	ASTRA-OMZ	Pacific warm pool
SST (°C)	27.0 ± 1.0	19.6 ± 2.6	28.9 ± 0.9
SSS ($g\,kg^{-1}$)	35.0 ± 0.3	35.1 ± 0.3	34.5 ± 0.42
Wind speed ($m\,s^{-1}$)	8.2 ± 1.7	7.5 ± 1.8	5.3 ± 0.4
a_{350} (m^{-1})	0.039 ± 0.02	0.146 ± 0.02	0.050 ± 0.08
I ($W\,m^{-2}$)	226.5 ± 303.0	196.4 ± 283.1	206.4 ± 286.6[a]
SR ($J\,m^{-2}$)	$1.9 \times 10^7 \pm 1.7 \times 10^6$	$1.6 \times 10^7 \pm 4.5 \times 10^6$	$8.9 \times 10^6 \pm 1.3 \times 10^6$
pH (–)	8.03 ± 0.01	–[b]	8.07 ± 0.01
MLD (m)	43.3 ± 15.8	18.9 ± 7.5	35.9 ± 14.1

the OCS sea surface concentrations in the ocean, leading to decreased emissions to the atmosphere: higher SSTs favor a stronger degradation by hydrolysis (Elliott et al., 1989), and lower wind speeds decrease the transfer velocity k. Lower integrated daily radiation (SR in Table 4.4) in the Pacific warm pool also points to lower OCS production. Hence, our new OCS observations presented here likely span the range of emission variability in the tropics.

The observed concentrations and calculated emissions are approximately 1 order of magnitude lower than the annual mean surface concentrations and emissions simulated in the 3-D global ocean model NEMO-PISCES (Launois et al., 2015a).

4.3.2 A direct global oceanic emission estimate for OCS

The OCS observations from the Indian and Pacific Ocean were used to improve a box model for simulating OCS concentrations in the surface ocean (Kettle, 2002; Uher & Andreae, 1997a; von Hobe et al., 2003). With the a_{350}-dependent photoproduction constant included, the model reproduced the diel pattern of OCS concentrations in the surface oceans for both cruises (Fig. 4.2, black lines). A slight overestimation of observed concentrations is present for the Indian Ocean cruise OASIS (observed mean concentration: $9.1 \pm 3.5\,pmol\,L^{-1}$; simulated: $10.8 \pm 3.9\,pmol\,L^{-1}$). This overestimation was more pronounced in the eastern Pacific (observed mean: $28.3 \pm 19.7\,pmol\,L^{-1}$; simulated: $47.3 \pm 25.4\,pmol\,L^{-1}$) and can largely be attributed to a lack of downward mixing inherent in the mixed layer box model due to the assumption of the OCS concentration being constant throughout the entire mixed layer.

Table 4.5: Comparison of previous ship campaign measurements with corresponding month and approximate geolocation from the global box model in this study (L2016), taken either from figures or tables as provided in the original references. Note that the box model is based on input data from climatological means that do not fully represent the conditions encountered during the respective cruises. Only observational data with measurements of the full diel cycle were included for comparison. *n*: number of measurements. [a] Converted from ng L^{-1} with a molar mass of OCS of 60.07 g. [b] Converted from ng S L^{-1} with a molar mass of *S* of 32.1 g.

References	**Season**	**Region**	**Mean OCS ± SD** (pmol L^{-1})	*n*	**L2016 mean** (pmol L^{-1})
Mihalopoulos et al. (1992)		open Indian Ocean 20° N–37° S			
	Mar/May 1986	OCEAT II	19.9 ± 0.5[a]	20	11.2 ± 6.3
	Jul 1987	OCEAT III	19.9 ± 1.0[a]	14	17.7 ± 13.1
Staubes & Geogrii (1993)	Nov–Dec 1990	Weddell Sea 40–72° S,72° W–24° E	109[b]	126	66.6 ± 49.8
Ulshöfer et al. (1995)		North Atlantic Ocean			
	Apr/May 1992	47° N 20° W	14.9 ± 6.9	118	42.8 ± 11.3
	Jan 1994	48–50° N, 10–17° W	5.3 ± 1.6	120	8.9 ± 3.2
	Sep 1994	48–50° N, 10–17° W	19.0 ± 8.3	235	33.4 ± 3.5
Flöck & Andreae (1996)	Jan 1994	northeastern Atlantic Ocean 49° N, 12° W	6.7 (4–11)	120	9.6 ± 3.7
Ulshöfer & Andreae (1998)	Mar 1995	western Atlantic 32° N, 64° W	8.1 ± 7.0	323	15.8
Von Hobe et al. (1999)	Jun/Jul 1997	northeastern Atlantic Ocean 30–40° N, 8–15° W	23.6 ± 16.0	940	30.5 ± 12.6
Kettle et al. (2001)	Sep/Oct 1998	Atlantic transect 50° N–60° S, 1–64° W	21.7 ± 19.1	783	22.9 ± 3.2
Von Hobe et al. (2001)	Aug 1999	Sargasso Sea/BATS 32° N, 64° W	8.6 ± 2.8	518	8.1
Xu (2001)	Oct/Nov 1997	Atlantic meridional transect 53° N–34° S, 25° W–20° E	14.8 ± 11.4	306	11.8 ± 12.7
	May/Jun 1998	Atlantic meridional transect 53° N–34° S, 25° W–20° E	18.1 ± 16.1	440	27.8 ± 47.9

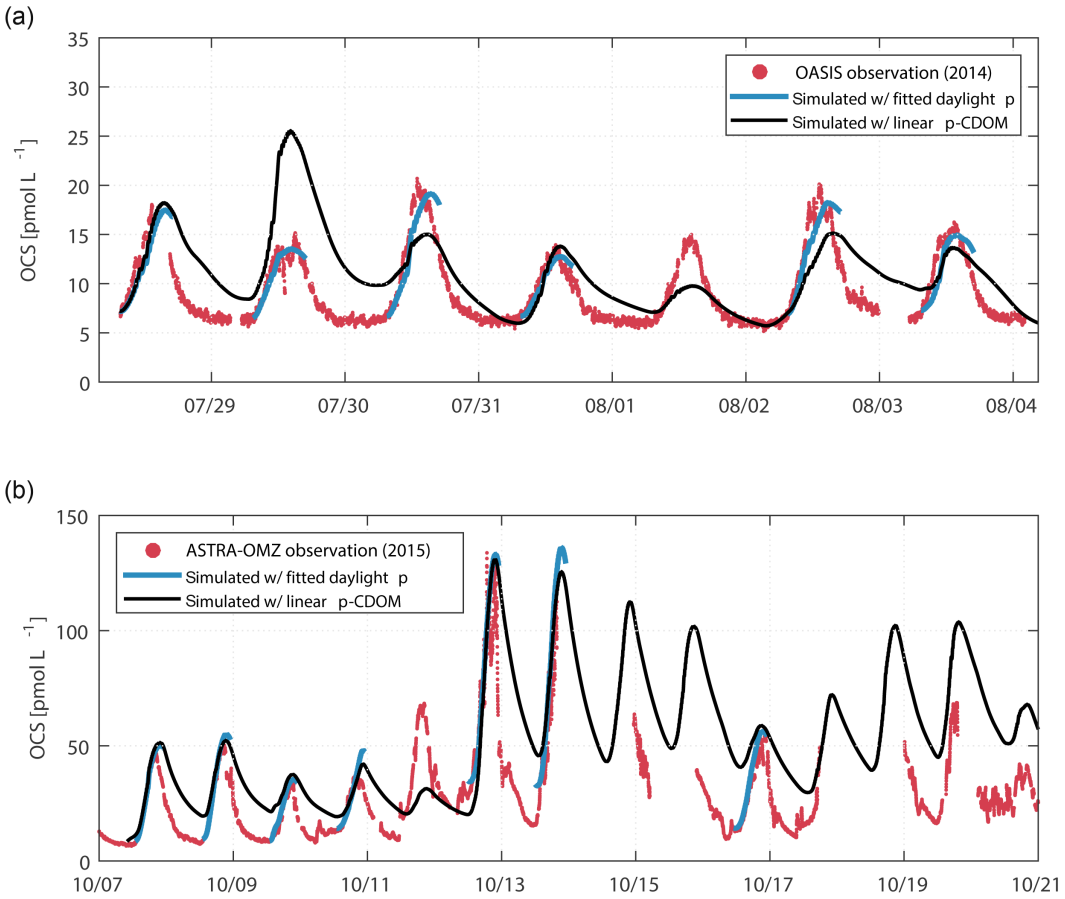

Figure 4.2: Box model simulations compared to observations: comparison of simulated OCS water concentrations against measurements from the OASIS cruise to the Indian Ocean **(a)** and the eastern Pacific Ocean during the ASTRA-OMZ cruise **(b)**. Blue indicates OCS concentrations with a least-squares fit for the photoproduction rate constant p during daylight, fitted individually for days with homogeneous water masses (SST, a_{350}). Black shows the simulation including the p depending on a_{350}, obtained from linear regression of individually fitted p with a_{350} ($r = 0.71$). The time on the x axis is local time (GMT+5 during OASIS 2014, GMT−4 during ASTRA-OMZ 2015).

Using the linear $p - a_{350}$ parameterization for the first time in a global model, the same box model as for the case studies is applied to estimate sea surface concentrations and fluxes of OCS on a global scale (Fig. 4.4). The OCS production is consistent with the global distribution of CDOM absorption (Fig. 4.8), with highest concentrations calculated for coastal regions and higher latitudes. Despite the photochemical hot spot in the tropics (30° N–30° S), degradation by hydrolysis prevents any accumulation of OCS in the surface water, as we calculated the lifetime due to hydrolysis to be only 7 h (Fig. 4.8). The simulated range of water concentrations is too low to sustain emissions in the tropics that could close the atmospheric budget of OCS (Fig. 4.4). With saturation ratios integrated over 1 year,

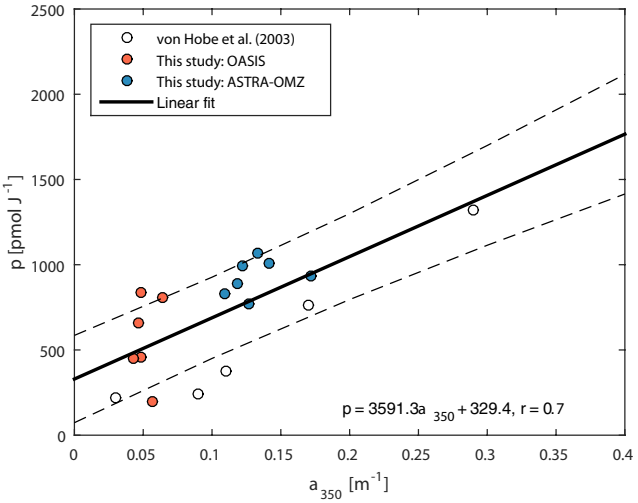

Figure 4.3: Dependence of photoproduction rate constant p on a_{350} including own fits for p (resulting in blue lines in Fig. 2) and fits from a similar study (von Hobe et al., 2003). Dashed lines indicate the 95 % confidence interval.

the tropical ocean (30° N–30° S) is even undersaturated with respect to OCS, taking up 3.0 Gg S yr^{-1}. Globally, the integration over one year yields annual oceanic OCS emissions of 130 Gg S. Our results corroborate the upper limit of an earlier study that used an observation-derived emission inventory (Table 4.1) (Kettle, 2002) but which includes more process-oriented parameterizations as described in Sect. 4.2.4. Clearly, our results from both observations and modeling contradict the latest bottom-up emission estimate from the NEMO-PISCES model (Launois et al., 2015a), and do not support a hot spot of direct OCS emissions in the Pacific Warm Pool or the tropical oceans in general.

Comparison to previous ship-based measurements

The global simulation of OCS surface water concentrations generally reproduced the lower picomolar range of concentrations (Table 4.5), the seasonal pattern of higher concentrations during summer compared to winter (as, for example, in Ulshöfer et al., 1995) and the spatial pattern of higher concentrations in higher latitudes (e.g., Southern Ocean; Staubes & Geogrii, 1993). Given that monthly means of a model simulation driven by climatological data of the input parameters are compared to cruise measurements, the absolute mean deviation of 6.9 pmol L^{-1} and the mean deviation of 3.7 pmol L^{-1} indicate an overall good reproduction of observations (differences between observation and model output were weighted to the number of observations in Table 4.4). It should be noted that, on average, the model overestimates OCS concentrations as indicated by the positive mean error, suggesting

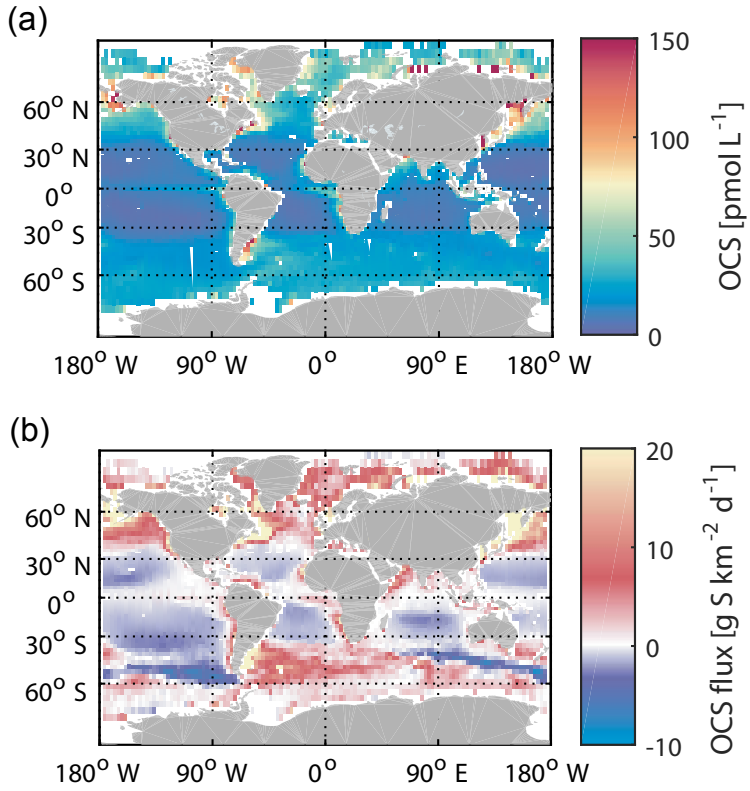

Figure 4.4: Annual mean of surface ocean concentrations of OCS simulated with the box model **(a)** and corresponding emissions **(b)**.

our emission estimate to be an upper limit to direct oceanic OCS emissions in most regions. The largest deviations from observations are found in the Southern Ocean (see Staubes & Geogrii, 1993, in Table 4.4), where the model underestimated observations by 40 %. While there are several explanations for this, i.e., a possible violation of the underlying assumption of a constant OCS production in regions with deep mixed layers such as the Southern Ocean, or the missing satellite data for CDOM during polar nights, it is a clear indication of the need for more observations from high latitudes. However, this underestimation does not interfere with our conclusion drawn for the tropical oceans, where the location of the missing source is derived from top-down approaches.

Uncertainties

Simulated concentrations and fluxes carry uncertainties from input parameters and process parameterizations. One major uncertainty associated with the mixed layer box model approach arises from the fact that it does not adequately account for downward mixing and

vertical concentration gradients within the mixed layer. Under most circumstances, and especially in the tropical open ocean, where hydrolysis greatly exceeds surface outgassing and low a_{350} makes photoproduction extend further down in the water column, the model tends to overestimate the real OCS concentrations, as was shown for our two cruises above. Therefore, we deem the fluxes from our global simulation to represent an upper limit of the true fluxes. Only at high latitudes would we expect more complex uncertainties, because hydrolysis at low temperatures is slow and only photoproduction and loss by outgassing are directly competing at the very surface.

Other uncertainties are associated with the calculation of the photoproduction rate. The wavelength of 443 nm combines the absorption of detritus and CDOM, which could have an impact especially in river plumes, where terrestrial material is transported into the ocean. As it is the CDOM that is important for photochemistry, assuming the 443 nm is purely CDOM would lead to an overestimation of photoproduction and therefore is a conservative estimate. It should also be noted that a single spectral slope from 443 to 350 nm in the global simulation is a simplification. Furthermore, using a wavelength integrated photoproduction rate constant instead of a wavelength-resolved approach, which would take global variations in the CDOM and light spectra into account, is an additional simplification. It has been shown that this does not lead to large differences regionally (von Hobe et al., 2003) but could, potentially, lead to variations globally. Our p–CDOM relationship is a first step for constraining this variability globally in one parameterization, as it incorporates photoproduction rate constants optimized to observations and thus accounting for differences in the light and CDOM spectra. More data from different regions can help to further constrain this relationship in future studies. Despite these simplifications, the simulated concentrations agree very well with previous observations ($n > 4000$, Table 4.4). To test the sensitivity of our box model to the photoproduction rate constant, we performed a sensitivity test with a photoproduction increased by a factor of 5 in the tropical region (30° N–30° S; note that this factor is considerably larger than the uncertainty in the p–CDOM relationship). This leads to an annual mean concentration of 35.1 pmol L^{-1} in the tropics (30° N–30° S), resulting in tropical direct emissions of 160 Gg S as OCS per year. The efficient hydrolysis in warm tropical waters prevents OCS concentrations from accumulating despite the high photoproduction and still results in emissions too low to account for the missing source.

With a mean error of 3.7 pmol L^{-1} in the OCS surface water concentrations added to (subtracted from) the modeled concentration and subsequent calculation of fluxes using annual climatologies for wind, pressure and SST (same data sources as global simulation forcing data), we calculate an uncertainty of 60 %, which translates into a total uncertainty

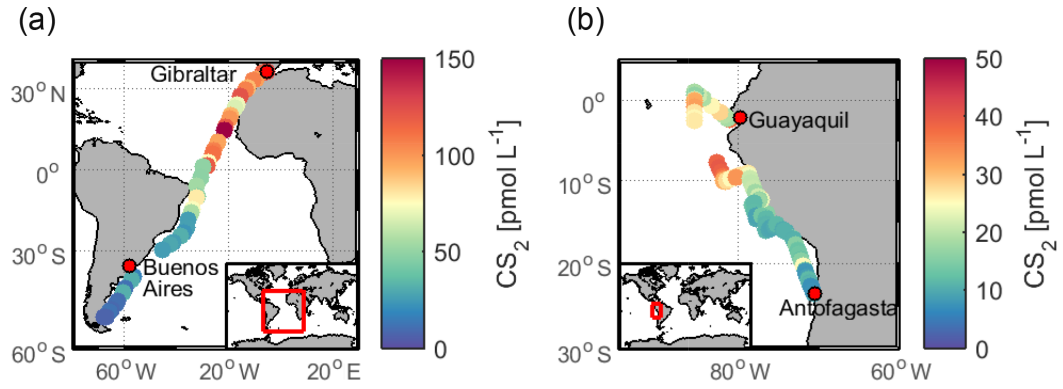

Figure 4.5: Measured concentration of CS_2 in surface waters during **(a)** ASTRA-OMZ in the eastern Pacific Ocean and **(b)** TransPEGASO in the Atlantic Ocean.

in the integrated global flux of 80 Gg S yr^{-1}.

4.3.3 Indirect OCS emissions by DMS and CS_2

A significant contribution to the OCS budget in the atmosphere results from oceanic emissions of DMS and CS_2 that are partially converted to OCS on timescales of hours to days (Chin & Davis, 1993; Kettle, 2002; Watts, 2000). A yield of 0.7 % for OCS is used for the reaction of DMS with OH (Barnes et al., 1994), which results in a global oceanic source of DMS from OCS of 80 (65–110) Gg S yr^{-1} based on the procedure described in Sect. 4.2.5. The uncertainty range of 65–110 Gg S yr^{-1} originated from the uncertainty in oceanic emissions, not the conversion factor. This conversion factor is much more uncertain, as the formation of OCS from DMS involves a complex multi-step reaction mechanism that is not fully understood. It has been shown in laboratory experiments that the presence of NO_x reduces the OCS yield considerably (Arsene et al., 2001), which would make our indirect emission estimate an upper limit. However, the yield was measured under laboratory conditions and may be different and more variable under natural conditions.

DMS emissions do not show a pronounced hot spot in the Pacific warm pool region, but as DMS transports much more sulfur across the air–sea interface than OCS, even low changes in the OCS yield could affect the atmospheric budget of OCS. As the spatial oceanic emission pattern of DMS does not reflect the spatial pattern of the assumed missing source, a locally specific tropospheric change in the conversion yield would be one potential way of bringing the patterns in agreement. While it is possible that the OCS yield could vary under certain conditions (e.g., it cannot be excluded that the low OH concentrations in the broader Pacific warm pool area as suggested by Rex et al. (2014), influence the yield), the (local) increase in the conversion factor would need to be on the order of a factor of 10–100.

For CS_2, the atmospheric reaction pathway producing OCS is better understood with a well-constrained molar conversion ratio of 0.81 (Chin & Davis, 1993). However, the global distribution of oceanic CS_2 concentration, and hence its emissions to the atmosphere, is poorly known. In our study, surface CS_2 concentrations (Fig. 4.5) were on average $17.8 \pm 8.9\,\mathrm{pmol\,L^{-1}}$ during ASTRA-OMZ, and $62.5 \pm 42.1\,\mathrm{pmol\,L^{-1}}$ during TransPEGASO (Table 4.3).
The latter values are higher than previously reported concentrations from the AMT-7 cruise in the central Atlantic (Kettle et al., 2001) ($10.9 \pm 15.2\,\mathrm{pmol\,L^{-1}}$). We extrapolate a weighted mean of the CS_2 emissions from TransPEGASO ($n = 42$, $13.7 \pm 9.8\,\mathrm{g\,S\,d^{-1}\,km^{-2}}$), ASTRA-OMZ ($n = 122$, $4.1 \pm 3.2\,\mathrm{g\,S\,d^{-1}\,km^{-2}}$) and AMT-7 (Kettle et al., 2001) ($n = 744$, $1.6 \pm 1.8\,\mathrm{g\,S\,d^{-1}\,km^{-2}}$) in order to estimate CS_2-derived OCS emissions from the global ocean. According to our extrapolation, $135\,(7–260)\,\mathrm{Gg\,S\,yr^{-1}}$ enters the atmosphere as oceanic CS_2 emissions converted to OCS. The uncertainty range of $7–260\,\mathrm{Gg\,S\,yr^{-1}}$ results from extrapolating the highest and the lowest emissions encountered during the cruises to the global ocean. This number is at the highest end of the range for OCS emissions from globally simulated CS_2 oceanic concentrations (Kettle, 2002; Kettle, 2000), as measured CS_2 concentrations from the cruises ASTRA-OMZ and TransPEGASO are higher than the simulated surface concentrations in Kettle (2000) for the respective month. However, the spatial pattern of higher concentrations and emissions in the tropical region in our measurements agrees well with the spatial pattern simulated in Kettle (2000). Nonetheless, even the extrapolation of the highest measurement would not close the budget for the three largest missing source estimates (Table 4.1).
For oceanic emission estimates used to constrain GPP, quantifying the seasonal cycle of the single contributors is essential. For example, high emissions during oceanic spring and fall blooms could mask OCS uptake by the terrestrial vegetation, and therefore neglecting them could lead to an underestimation of global GPP, with implications for the atmospheric and terrestrial carbon budget.

4.4 Conclusions and outlook

Considering the observational evidence and the modeled global emission estimate of $130 \pm 80\,\mathrm{Gg\,S\,yr^{-1}}$, direct OCS emissions from the oceans are too low to account for the missing atmospheric source. Together with indirect emissions, the oceanic source strength of OCS would add up to $345\,\mathrm{Gg\,S\,yr^{-1}}$, compared to the $465–1089\,\mathrm{Gg\,S\,yr^{-1}}$ required to balance the suggested increase in vegetation uptake. Direct and even additional indirect oceanic emissions of OCS are thus unlikely to balance the budget after the upward revision

of the vegetation sink. Largest uncertainties are associated with the indirect emission estimates, especially in the conversion of DMS to OCS and the global source strength of CS_2.

As our study suggests, the search for an additional source of OCS to the atmosphere should include other sources than oceanic emissions alone. There are indications of other parts of the OCS budget being underestimated, such as domestic coal combustion (Du et al., 2016). Emissions of biomass burning and direct and indirect anthropogenic emissions have been considered in previous estimates (e.g., 315.5 Gg S yr^{-1} in Berry et al., 2013, 224 Gg S yr^{-1} in Kuai et al., 2015, and 219 Gg S yr^{-1} in Glatthor et al., 2015), but a recent anthropogenic emission estimate by Lee & Brimblecombe (2016) increases this number to 598 Gg S yr^{-1}, which would already bring sources and sinks closer to agreement. They attribute the largest direct OCS emissions to biomass and biofuel burning, as well as pulp and paper manufacturing, and the largest CS_2 emissions to the rayon industry. Hence, a hot spot of anthropogenic emissions in the Asian continent might be a potential candidate, together with atmospheric transport, to produce atmospheric mixing ratios as observed by satellite.

A redistribution of the magnitude and seasonality of known sources and sinks could also bring top-down and bottom-up estimates closer together. For example, the general view of oxic soils as a sink for OCS has recently been challenged. Field (Billesbach et al., 2014; Maseyk et al., 2014) and incubation studies (Whelan et al., 2016) show that some oxic soils may shift from OCS uptake to emission depending on the temperature and water content. Furthermore, it has been speculated previously that vegetation uptake might not be solely responsible for the decrease in OCS mixing ratios in fall because of the temporal lag between CO_2 and OCS minimum (Montzka et al., 2007). The observed seasonality in mixing ratios is a superposition of the seasonality of all individual sources and sinks. These seasonalities are currently neglected or associated with a considerable uncertainty. An improved understanding of the seasonality of the individual sources and sinks could help to better constrain the gap in the atmospheric budget. First steps to resolve OCS seasonality in sources and sinks are currently being undertaken, e.g., in the case of anthropogenic emissions (Campbell et al., 2015).

All in all, better constraints on the seasonality and magnitude of the atmospheric OCS sources and sinks are critical for a better assessment of the role of this compound in climate and its application to quantify GPP on a global scale. This study confirms oceanic emission as the largest known single source of atmospheric OCS but shows that its magnitude is unlikely to balance the gap in the atmospheric OCS budget.

4.5 Data availability

All data, including OCS and CS_2 measurements in sea water and the marine boundary layer, as well as OCS model output, are available upon request from the authors (correspondence to S. T. Lennartz, slennartz@geomar.de or C.A. Marandino, cmarandino@geomar.de).

4.6 List of parameters

Symbol/abbreviation	Meaning
a_{350}	absorption coefficient of CDOM at 350 nm
a	fitted parameter in diurnal cycle of I
b	fitted parameter in diurnal cycle of I
c_{air}	concentration in air
C_{OCS}	concentration of OCS in water
F	gas flux
H	Henry constant
I	downwelling solar radiation
K	ion product of seawater
k_{w}	water-side transfer velocity in air–sea gas exchange
MLD	mixed layer depth
p	photoproduction rate constant
SSS	sea surface salinity
SST	sea surface temperature
Sc	Schmidt number
t	time
θ	zenith angle
u_{10}	wind speed at 10 m height
UV	ultraviolet radiation
z	depth

4.7 Acknowledgements

We thank the captain and crew of the research vessels *SONNE* I and II as well as *Hesperides* for assistance during the cruises SO235-OASIS (BMBF – FK03G0235A), SO243-ASTRA-OMZ (BMBF – FK03G0243A) and TransPEGASO. We thank H. W. Bange and A. Körtzinger for providing equipment for the continuous underway system and C. Schlundt for support during CS_2 measurements. This work was supported by the German Federal Ministry of Education and Research through the project ROMIC-THREAT (BMBF-FK01LG1217A

and 01LG1217B) and ROMIC-SPITFIRE (BMBF-FKZ: 01LG1205C). Additional funding for Christa A. Marandino and Sinikka T. Lennartz came from the Helmholtz Young Investigator Group of Christa A. Marandino (TRASE-EC, VH-NG-819), from the Helmholtz Association through the President's Initiative and Networking Fund, and from the GEOMAR Helmholtz-Zentrum für Ozeanforschung Kiel. Kirstin Krüger acknowledges financial support from the EU FP7 StratoClim project (603557), and Pau Cortes and Rafel Simo acknowledge support from the Spanish MINECO through PEGASO (CTM2012-37615). We are grateful for the data provided by ECMWF (ERA-Interim) and NASA (MODIS-Aqua). DKRZ and its scientific steering committee are gratefully acknowledged for providing the HPC and data archiving resources for this consortial project ESCiMo (Earth System Chemistry Integrated Modelling). Elliot Atlas acknowledges support from the NASA Upper Atmosphere Research Program.

4.8 Appendix: Supplementary figures

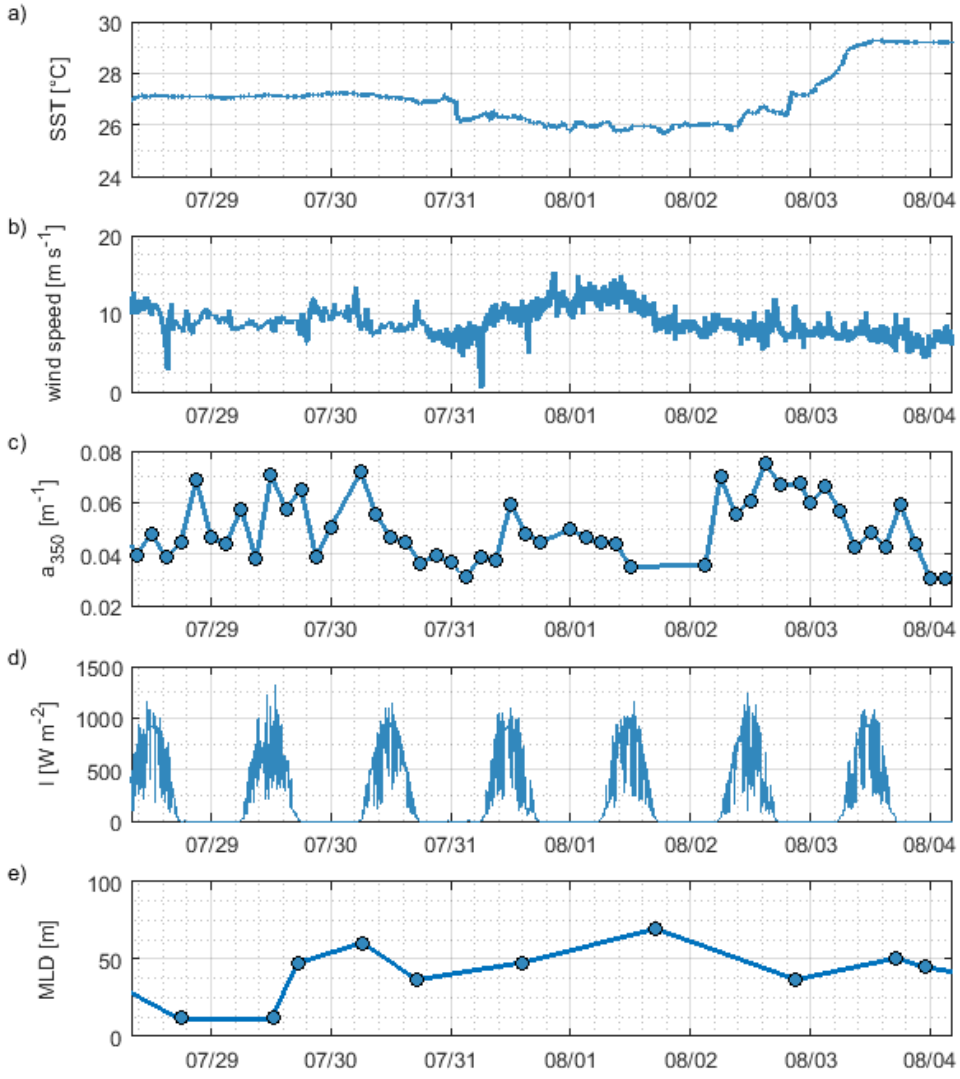

Figure 4.6: Input parameters for case study box model simulation for the OASIS cruise to the Indian Ocean for a) SST, b) wind speed corrected to 10 m height, c) absorption at 350 nm, d) global radiation, e) mixed layer depth; all measured directly onboard RV SONNE I in 2014.

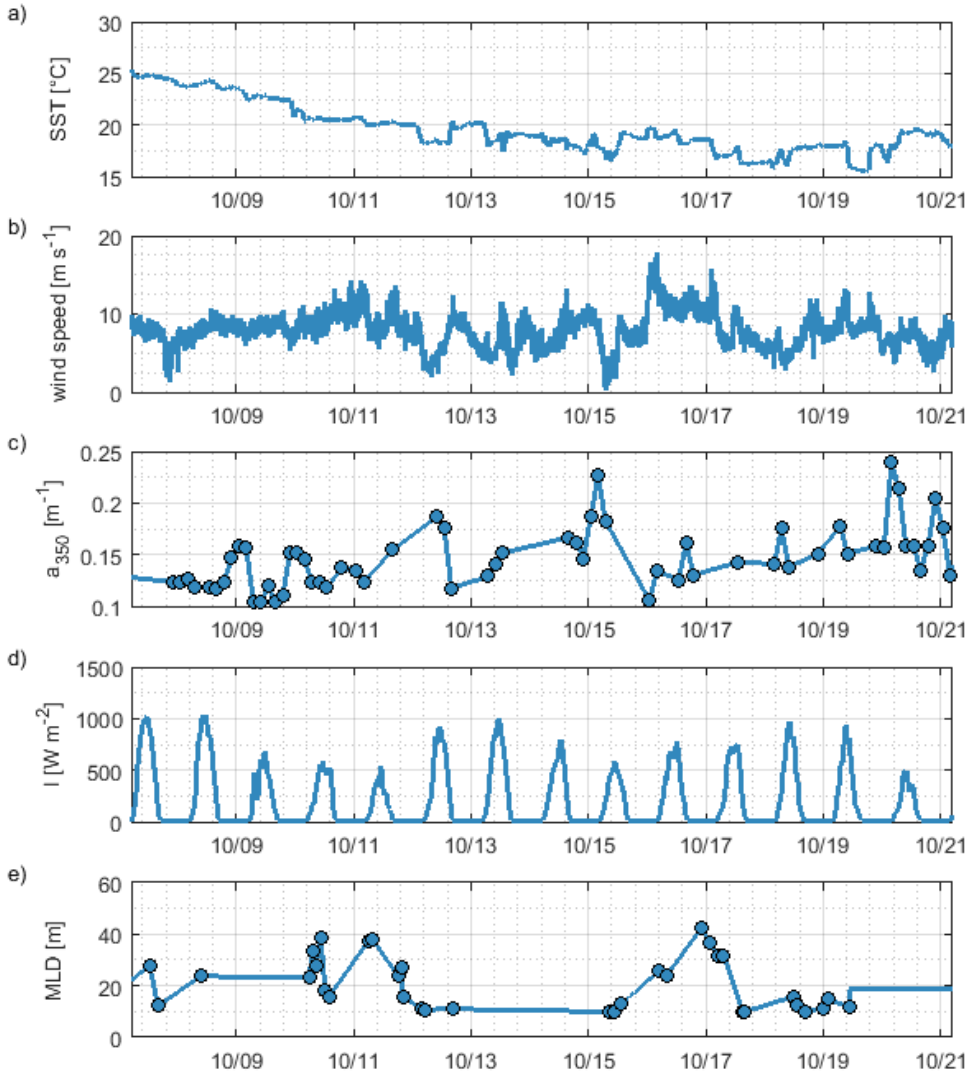

Figure 4.7: Input parameters for case study box model simulation for the ASTRA-OMZ cruise to the eastern Pacific Ocean for a) SST, b) wind speed corrected to 10 m height, c) absorption at 350 nm, d) global radiation, e) mixed layer depth; all measured directly onboard RV SONNE II in 2015.

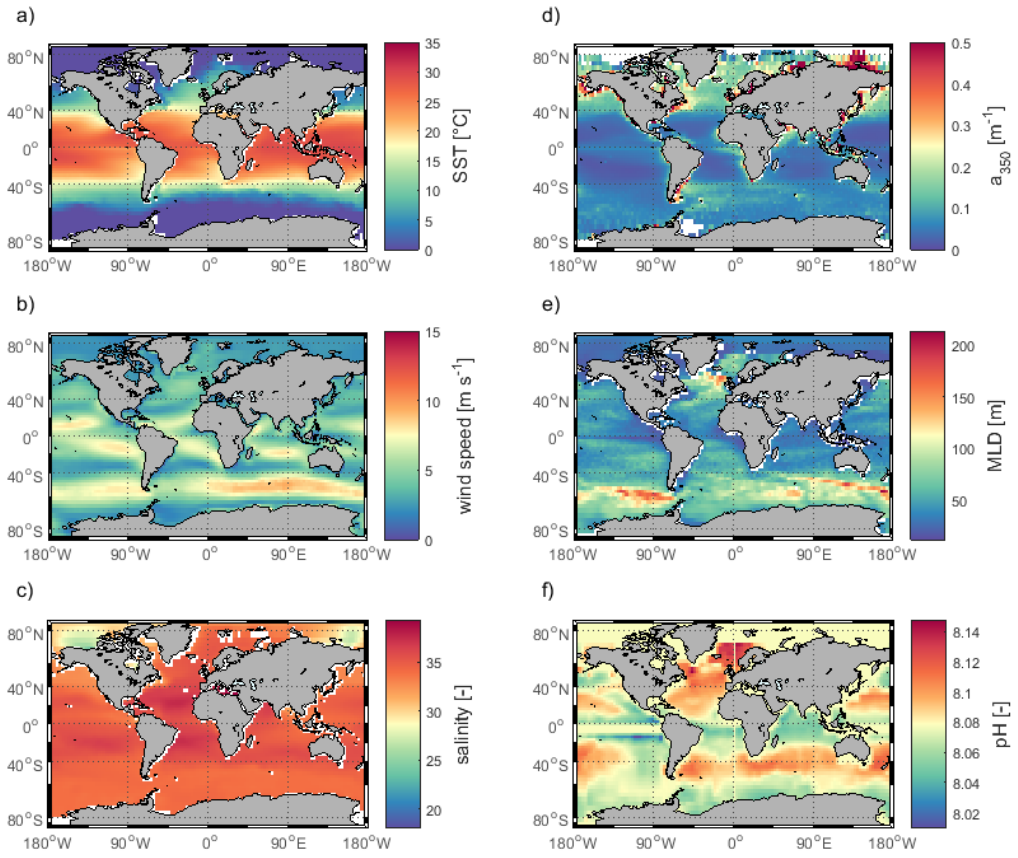

Figure 4.8: Annual mean for input parameters of a) sea surface temperature SST, b) wind speed, c) salinity, d) absorption of CDOM at 350 nm a_{350}, e) mixed layer depth, and f) pH. Details on data sources can be found in Tab. 4.8

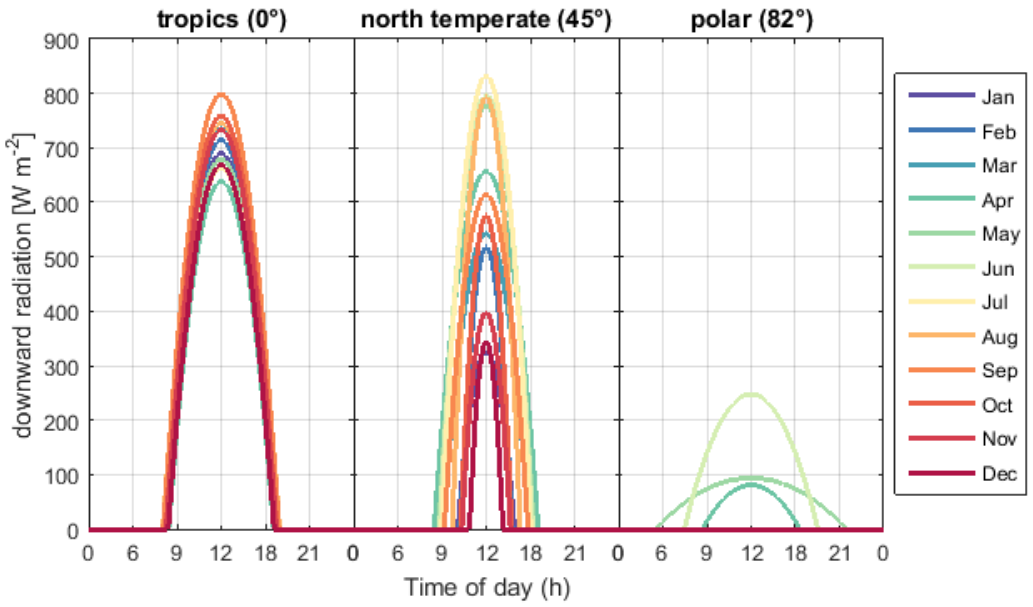

Figure 4.9: Diurnal cycles of downward radiation from the tropics, north temperate and polar regions resulting from fitting a parable to the sunshine duration and downwelling radiance from ERAInterim (Eq. 4.12, Tab. 4.8). Color coding refers to mean monthly diurnal cycles.

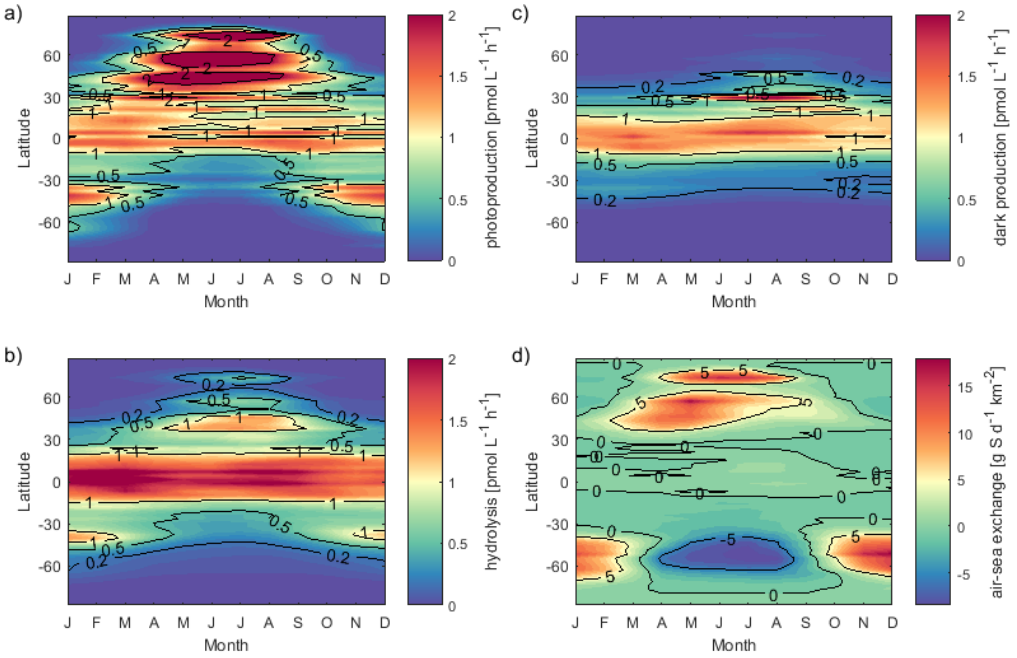

Figure 4.10: Rates of a) photoproduction (average of the mixed layer), b) hydrolysis, c) dark production and d) air sea exchange in the mixed layer for each month and latitude from the box model simulation.

4.9 Appendix: Supplementary tables

Table 4.6: Input parameters for the box model for the OASIS cruise (Indian Ocean). Measurements were linearly interpolated to a time grid of 2 minute resolution.

Parameter	Data source
global radiation	shipboard meteorological equipment, 10 minute mean
CDOM absorption spectrum	measured onboard, ca. 3-hour resolution, LWCC setup (Miller et al., 2002)
sea surface temperature	continuously (every minute) measured at seawater intake for underway system, Seabird MicroCat SBE41
sea surface salinity	continuously (every minute) measured at seawater intake for underway system, Seabird MicroCat SBE41
pH	calculated from dissolved inorganic carbon and alkalinity sampled at seawater intake from underway system, ca. 3-hourly resolution
wind speed	measured onboard, corrected to 10 m height, 10 minute averages
atm. volume mixing ratio of OCS	sampled onboard, ca. 3-hourly resolution, air canister samples analysed at RSMAS (de Gouw et al., 2009; Schauffler et al., 1998)
mixed layer depth	obtained from CTD profiles, using the Lorbacher (Lorbacher et al., 2006) criterion, 1-2 times per day
sea level air pressure	measured onboard, 10 minute averages

Table 4.7: Input parameters for the box model for the ASTRA-OMZ cruise (Pacific Ocean). Measurements were linearly interpolated to a time grid of 2 minute resolution.

Parameter	Data source
global radiation	shipboard meteorological equipment, 10 minute mean
CDOM absorption spectrum	measured onboard, ca. 3-hour resolution, LWCC setup (Miller et al., 2002)
sea surface temperature	continuously (every minute) measured at seawater intake for underway system, Seabird MicroCat SBE41
sea surface salinity	continuously (every minute) measured at seawater intake for underway system, Seabird MicroCat SBE41
pH	mean value of 8.1 assumed (minor sensitivity to pH confirmed in sensitivity tests)
wind speed	measured onboard, corrected to 10 m height, 10 minute averages
atm. volume mixing ratio of OCS	sampled onboard, ca. 3-hourly resolution, air canister samples analysed at RSMAS (de Gouw et al., 2009; Schauffler et al., 1998)
mixed layer depth	obtained from CTD profiles, using the Lorbacher (Lorbacher et al., 2006) criterion, 0-4 times per day
sea level air pressure	measured onboard, 10 minute averages

Table 4.8: Input parameters for the global box model. Data was linearly interpolated to a time grid of 2 h resolution.

Parameter	Data source
Global radiation	Diurnal cycle fitted to downwards radiation and sunshine duration from 2014 ERAInterim reanalysis data (Dee et al., 2011)
CDOM absorption 350 nm	MODIS Aqua satellite data "absorption due to gelbstoff and detritus 443 nm", GIOP model, corrected to 350nm assuming an exponential spectrum, climatological monthly mean 2002-2014 (NASA, 2014)
sea surface temperature	ERAInterim reanalysis, climatology from 2002-2014 synoptic monthly means (Dee et al., 2011)
sea surface salinity	World Ocean Atlas climatology (Antonov et al., 2010)
pH	Takahashi climatology (Takahashi et al., 2014)
wind speed	ERAInterim reanalysis, climatology from 2002-2014 synoptic monthly means atm. volume mixing ratio for OCS assumed 550 ppt
atm. volume mixing ratio for OCS	assumed 550 ppt
mixed layer depth	MIMOC climatology (Schmidtko et al., 2013)
sea level air pressure	ERAInterim reanalysis, climatology from 2000-2014 synoptic monthly means
initial condition	8 pmol L^{-1}
spin-up until stable global mean	2 years

References

Andreae, M. O. & Ferek, R. (2002): Photochemical production of carbonyl sulfide in seawater and its emission to the atmosphere. *Global Biogeochemical Cycles* **6** (2): 175–183.

Antonov, J.; Seidov, D.; Boyer, T. P.; Locarnini, R.; Mishonov, A.; Garcia, H.; Baranova, O.; Zweng, M. & Johnson, D. (2010): *World Ocean Atlas 2009, Volume 2: Salinity.*

Arévalo-Martínez, D. L.; Beyer, M.; Krumbholz, M.; Piller, I.; Kock, A.; Steinhoff, T.; Körtzinger, A. & Bange, H. W. (2013): A new method for continuous measurements of oceanic and atmospheric N2O, CO and CO_2: performance of off-axis integrated cavity output spectroscopy (OA-ICOS) coupled to non-dispersive infrared detection (NDIR). *Ocean Sci.* **9** (6): 1071–1087.

Arneth, A.; Harrison, S. P.; Zaehle, S.; Tsigaridis, K.; Menon, S.; Bartlein, P. J.; Feichter, J.; Korhola, A.; Kulmala, M.; O'Donnell, D.; Schurgers, G.; Sorvari, S. & Vesala, T. (2010): Terrestrial biogeochemical feedbacks in the climate system. *Nature Geoscience* **3** (8): 525–532.

Arsene, C.; Barnes, I.; Becker, K. H. & Mocanu, R. (2001): FT-IR product study on the photo-oxidation of dimethyl sulphide in the presence of NOx - temperature dependence. *Atmospheric Environment* **35** (22): 3769–3780.

Asaf, D.; Rotenberg, E.; Tatarinov, F.; Dicken, U.; Montzka, S. A. & Yakir, D. (2013): Ecosystem photosynthesis inferred from measurements of carbonyl sulphide flux. *Nature Geoscience* **6** (3): 186–190.

Asher, W. E. & Wanninkhof, R. (1998): The effect of bubble-mediated gas transfer on purposeful dual-gaseous tracer experiments. *Journal of Geophysical Research: Oceans* **103** (C5): 10555–10560.

Atkinson, R.; Baulch, D. L.; Cox, R. A.; Crowley, J. N.; Hampson, R. F.; Hynes, R. G.; Jenkin, M. E.; Rossi, M. J. & Troe, J. (2004): Evaluated kinetic and photochemical data for atmospheric chemistry: Volume I - gas phase reactions of Ox, HOx, NOx and SOx species. *Atmos. Chem. Phys.* **4** (6): 1461–1738.

Barnes, I.; Becker, K. H. & Patroescu, I. (1994): The tropospheric oxidation of dimethyl sulfide: A new source of carbonyl sulfide. *Geophysical Research Letters* **21** (22): 2389–2392.

Beer, C.; Reichstein, M.; Tomelleri, E.; Ciais, P.; Jung, M.; Carvalhais, N.; Rödenbeck, C.; Arain, M. A.; Baldocchi, D. & Bonan, G. B. (2010): Terrestrial gross carbon dioxide uptake: global distribution and covariation with climate. *Science* **329** (5993): 834–838.

Berry, J.; Wolf, A.; Campbell, J. E.; Baker, I.; Blake, N.; Blake, D.; Denning, A. S.; Kawa, S. R.; Montzka, S. A.; Seibt, U.; Stimler, K.; Yakir, D. & Zhu, Z. (2013): A coupled model of the global cycles of carbonyl sulfide and CO_2: A possible new window on the carbon cycle. *Journal of Geophysical Research: Biogeosciences* **118** (2): 842–852.

Billesbach, D. P.; Berry, J. A.; Seibt, U.; Maseyk, K.; Torn, M. S.; Fischer, M. L.; Abu-Naser, M. & Campbell, J. E. (2014): Growing season eddy covariance measurements of carbonyl sulfide and CO2 fluxes: COS and CO_2 relationships in Southern Great Plains winter wheat. *Agricultural and Forest Meteorology* **184**: 48–55.

Brown, K. A. & Bell, J. N. B. (1986): Vegetation—The missing sink in the global cycle of carbonyl sulphide (COS). *Atmospheric Environment (1967)* **20** (3): 537–540.

Brühl, C.; Lelieveld, J.; Crutzen, P. J. & Tost, H. (2012): The role of carbonyl sulphide as a source of stratospheric sulphate aerosol and its impact on climate. *Atmos. Chem. Phys.* **12** (3): 1239–1253.

Campbell, J. E.; Carmichael, G. R.; Chai, T.; Mena-Carrasco, M.; Tang, Y.; Blake, D. R.; Blake, N. J.; Vay, S. A.; Collatz, G. J.; Baker, I.; Berry, J. A.; Montzka, S. A.; Sweeney, C.; Schnoor, J. L. & Stanier, C. O. (2008): Photosynthetic Control of Atmospheric Carbonyl Sulfide During the Growing Season. *Science* **322** (5904): 1085–1088.

Campbell, J. E.; Whelan, M. E.; Seibt, U.; Smith, S. J.; Berry, J. A. & Hilton, T. W. (2015): Atmospheric carbonyl sulfide sources from anthropogenic activity: Implications for carbon cycle constraints. *Geophysical Research Letters* **42** (8): 3004–3010.

Chin, M. & Davis, D. D. (1993): Global sources and sinks of OCS and CS_2 and their distributions. *Global Biogeochemical Cycles* **7** (2): 321–337.

Crutzen, P. J. (1976): The possible importance of CSO for the sulfate layer of the stratosphere. *Geophysical Research Letters* **3** (2): 73–76.

De Bruyn, W.; Swartz, E.; Hu, J.; Shorter, J.; Davidovits, P.; Worsnop, D.; Zahniser, M. & Kolb, C. (1995): Henrys law solubilities and Setcheniw coefficients for biogenic reduced sulphur species obtained from gas-liquid uptake measurements. *Journal of Geophysical Research Atmosphere* **100**: 7245–7251.

De Gouw, J. A.; Warneke, C.; Montzka, S. A.; Holloway, J. S.; Parrish, D. D.; Fehsenfeld, F. C.; Atlas, E. L.; Weber, R. J. & Flocke, F. M. (2009): Carbonyl sulfide as an inverse tracer for biogenic organic carbon in gas and aerosol phases. *Geophysical Research Letters* **36** (5)

Dee, D. P.; Uppala, S. M.; Simmons, A. J.; Berrisford, P.; Poli, P.; Kobayashi, S.; Andrae, U.; Balmaseda, M. A.; Balsamo, G.; Bauer, P.; Bechtold, P.; Beljaars, A. C. M.; van de Berg, L.; Bidlot, J.; Bormann, N.; Delsol, C.; Dragani, R.; Fuentes, M.; Geer, A. J.; Haimberger, L.; Healy, S. B.; Hersbach, H.; Holm, E. V.; Isaksen, L.; Kallberg, P.; Köhler, M.; Matricardi, M.; McNally, A. P.; Monge-Sanz, B. M.; Morcrette, J. J.; Park, B. K.; Peubey, C.; de Rosnay, P.; Tavolato, C.; Thepaut, J. N. & Vitart, F. (2011): The ERA-Interim reanalysis: configuration and performance of the data assimilation system. *Quarterly Journal of the Royal Meteorological Society* **137** (656): 553–597.

Dickinson, A. G. & Riley, J. (1979): The estimation of acid dissociation constants in seawater media from potentiometric titrations with strong base. *Mar. Chem.* **7**: 89–99.

Du, Q.; Zhang, C.; Mu, Y.; Cheng, Y.; Zhang, Y.; Liu, C.; Song, M.; Tian, D.; Liu, P.; Liu, J.; Xue, C. & Ye, C. (2016): An important missing source of atmospheric carbonyl sulfide: Domestic coal combustion. *Geophysical Research Letters*.

Elliott, S.; Lu, E. & Rowland, F. S. (1989): Rates and mechanisms for the hydrolysis of carbonyl sulfide in natural waters. *Environmental Science & Technology* **23** (4): 458–461.

Ferek, R. & Andreae, M. O. (1983): The supersaturation of carbonyl sulfide in surface waters of the pacific oceans off Peru. *Geophysical Research Letters* **10** (5): 393–395.

Ferek, R. & Andreae, M. O. (1984): Photochemical production of carbonyl sulphide in marine surface waters. *Letters to Nature* **1984**: 148–150.

Fichot, C. G. & Miller, W. L. (2010): An approach to quantify depth-resolved marine photochemical fluxes using remote sensing: Application to carbon monoxide (CO) photoproduction. *Remote Sensing of Environment* **114** (7): 1363–1377.

Flöck, O. & Andreae, M. O. (1996): Photochemical and non-photochemical formation and destruction of carbonyl sulfide and methyl mercaptan in ocean waters. *Marine Chemistry* **54**: 11–26.

Flöck, O. R.; Andreae, M. O. & Dräger, M. (1997): Environmentally relevant precursors of carbonyl sulfide in aquatic systems. *Marine Chemistry* **59** (1–2): 71–85.

Glatthor, N.; Höpfner, M.; Baker, I. T.; Berry, J.; Campbell, J. E.; Kawa, S. R.; Krysztofiak, G.; Leyser, A.; Sinnhuber, B. M.; Stiller, G. P.; Stinecipher, J. & Clarmann, T. v. (2015): Tropical sources and sinks of carbonyl sulfide observed from space. *Geophysical Research Letters,*: 10082–10090.

Hayduk, W. & Laudie, H. (1974): Prediction of diffusion coefficients for nonelectrolytes in dilute aqueous solutions. *AIChE Journal* **20** (3): 611–615.

Jöckel, P.; Tost, H.; Pozzer, A.; Kunze, M.; Kirner, O.; Brenninkmeijer, C. A. M.; Brinkop, S.; Cai, D. S.; Dyroff, C.; Eckstein, J.; Frank, F.; Garny, H.; Gottschaldt, K. D.; Graf, P.; Grewe, V.; Kerkweg, A.; Kern, B.; Matthes, S.; Mertens, M.; Meul, S.; Neumaier, M.; Nutzel, M.; Oberlander-Hayn, S.; Ruhnke, R.; Runde, T.; Sander, R.; Scharffe, D. & Zahn, A. (2016): Earth System Chemistry integrated Modelling (ESCiMo) with the Modular Earth Submodel System (MESSy) version 2.51. *Geoscientific Model Development* **9** (3): 1153–1200.

Johnson, J. E. & Harrison, H. (1986): Carbonyl Sulfide Concentrations in the Surface Waters and Above the Pacific Ocean. *Journal of Geophysical Research* **91** (D7): 7883–7888.

Kettle, A. J. (2002): Global budget of atmospheric carbonyl sulfide: Temporal and spatial variations of the dominant sources and sinks. *Journal of Geophysical Research* **107** (D22)

Kettle, A. J.; Rhee, T. S.; von Hobe, M.; Poulton, A.; Aiken, J. & Andreae, M. O. (2001): Assessing the flux of different volatile sulfur gases from the ocean to the atmosphere. *Journal of Geophysical Research: Atmospheres* **106** (D11): 12193–12209.

Kettle, A. (2000): Extrapolations of the Flux of Dimethylsulfide, Carbon Monooxide, Carbonyl Sulfide and Carbon Disulfide from the Oceans. PhD thesis.

Kremser, S.; Jones, N. B.; Palm, M.; Lejeune, B.; Wang, Y.; Smale, D. & Deutscher, N. M. (2015): Positive trends in Southern Hemisphere carbonyl sulfide. *Geophysical Research Letters* **42** (21): 9473–9480.

Kremser, S.; Thomason, L. W.; von Hobe, M.; Hermann, M.; Deshler, T.; Timmreck, C.; Toohey, M.; Stenke, A.; Schwarz, J. P.; Weigel, R.; Fueglistaler, S.; Prata, F. J.; Vernier, J.-P.; Schlager, H.; Barnes, J. E.; Antuña-Marrero, J.-C.; Fairlie, D.; Palm, M.; Mahieu, E.; Notholt, J.; Rex, M.; Bingen, C.; Vanhellemont, F.; Bourassa, A.; Plane, J. M. C.; Klocke, D.; Carn, S. A.; Clarisse, L.; Trickl, T.; Neely, R.; James, A. D.; Rieger, L.; Wilson, J. C. & Meland, B. (2016): Stratospheric aerosol—Observations, processes, and impact on climate. *Reviews of Geophysics* **54**: 278–335.

Kuai, L.; Worden, J. R.; Campbell, J. E.; Kulawik, S. S.; Li, K.-F.; Lee, M.; Weidner, R. J.; Montzka, S. A.; Moore, F. L.; Berry, J. A.; Baker, I.; Denning, A. S.; Bian, H.; Bowman, K. W.; Liu, J. & Yung, Y. L. (2015): Estimate of carbonyl sulfide tropical oceanic surface fluxes using Aura Tropospheric Emission Spectrometer observations. *Journal of Geophysical Research: Atmospheres* **120** (20): 11, 012–11, 023.

Lana, A.; Bell, T. G.; Simo, R.; Vallina, S. M.; Ballabrera-Poy, J.; Kettle, A. J.; Dachs, J.; Bopp, L.; Saltzman, E. S.; Stefels, J.; Johnson, J. E. & Liss, P. S. (2011): An updated climatology of surface dimethlysulfide concentrations and emission fluxes in the global ocean. *Global Biogeochemical Cycles* **25**

Launois, T.; Belviso, S.; Bopp, L.; Fichot, C. G. & Peylin, P. (2015a): A new model for the global biogeochemical cycle of carbonyl sulfide - Part 1: Assessment of direct marine emissions with an oceanic general circulation and biogeochemistry model. *Atmos. Chem. Phys.* **15** (5): 2295–2312.

Launois, T.; Peylin, P.; Belviso, S. & Poulter, B. (2015b): A new model of the global biogeochemical cycle of carbonyl sulfide - Part 2: Use of carbonyl sulfide to constrain gross primary productivity in current vegetation models. *Atmospheric Chemistry and Physics* **15** (16): 9285–9312.

Lee, C.-L. & Brimblecombe, P. (2016): Anthropogenic contributions to global carbonyl sulfide, carbon disulfide and organosulfides fluxes. *Earth-Science Reviews* **160**: 1–18.

Lennartz, S. T.; Krysztofiak, G.; Marandino, C. A.; Sinnhuber, B. M.; Tegtmeier, S.; Ziska, F.; Hossaini, R.; Krüger, K.; Montzka, S. A.; Atlas, E.; Oram, D. E.; Keber, T.; Bönisch, H. & Quack, B. (2015): Modelling marine emissions and atmospheric distributions of halocarbons and dimethyl sulfide: the influence of prescribed water concentration vs. prescribed emissions. *Atmos. Chem. Phys.* **15** (20): 11753–11772.

Liss, P. S. & Slater, P. G. (1974): Flux of gases across air-sea interface. *Nature* **247** (5438): 181–184.

Lorbacher, K.; Dommenget, D.; Niiler, P. P. & Köhl, A. (2006): Ocean mixed layer depth: A subsurface proxy of ocean-atmosphere variability. *Journal of Geophysical Research: Oceans* **111** (C7)

Maseyk, K.; Berry, J. A.; Billesbach, D.; Campbell, J. E.; Torn, M. S.; Zahniser, M. & Seibt, U. (2014): Sources and sinks of carbonyl sulfide in an agricultural field in the Southern Great Plains. *Proceedings of the National Academy of Sciences of the United States of America* **111** (25): 9064–9069.

McGillis, W. R.; Edson, J. B.; Hare, J. E. & Fairall, C. W. (2001): Direct covariance air-sea CO_2 fluxes. *Journal of Geophysical Research-Oceans* **106** (C8): 16729–16745.

Mihalopoulos, N.; Nguyen, B. C.; Putaud, J. P. & Belviso, S. (1992): The oceanic source of carbonyl sulfide (COS). *Atmospheric Environment* **26A** (8): 1383–1394.

Miller, R. L.; Belz, M.; Del Castillo, C. & Trzaska, R. (2002): Determining CDOM absorption spectra in diverse coastal environments using a multiple pathlength, liquid core waveguide system. *Continental Shelf Research* **22** (9): 1301–1310.

Miller, S.; Marandino, C.; De Bruyn, W. & Saltzman, E. S. (2009): Air-sea gas exchange of CO_2 and DMS in the North Atlantic by eddy covariance. *Geophysical Research Letters* **36** (15)

Montzka, S. A.; Calvert, P.; Hall, B. D.; Elkins, J. W.; Conway, T. J.; Tans, P. P. & Sweeney, C. (2007): On the global distribution, seasonality, and budget of atmospheric carbonyl sulfide (COS) and some similarities to CO_2. *Journal of Geophysical Research* **112** (D9)

Najjar, R.; Erickson, D. & Madronich, S. (1995): Modeling the air-sea fluxes of gases formed from the decomposition of dissolved organic matter: Carbonyl sulfide and carbon monoxide. *The role of Nonliving Organic Matter in the Earth's Carbon Cycle*. Ed. by R. Zepp & C. Sonnyag. John Wiley & Sons,: 107–132.

NASA (2014): *MODIS-Aqua Ocean Color Data, url: NASA: MODIS-Aqua Ocean Color Data, available at: https://oceancolor.gsfc.nasa.gov/cgi/l3,last access: 30 May 2015, Sensor: Aqua MODIS, product name: Absorption die to gelbstoff and detrital material at 443 nm, GIOP model.*

Nightingale, P. D.; Malin, G.; Law, C. S.; Watson, A. J.; Liss, P. S.; Liddicoat, M. I.; Boutin, J. & Upstill-Goddard, R. C. (2000): In situ evaluation of air-sea gas exchange parameterizations using novel conservative and volatile tracers. *Global Biogeochemical Cycles* **14** (1): 373–387.

Notholt, J.; Kuang, Z.; Rinsland, C. P.; Toon, G. C.; Rex, M.; Jones, N.; Albrecht, T.; Deckelmann, H.; Krieg, J.; Weinzierl, C.; Bingemer, H.; Weller, R. & Schrems, O. (2003): Enhanced Upper Tropical Tropospheric COS: Impact on the Stratospheric Aerosol Layer. *Science* **300** (5617): 307–310.

Pos, W. H.; Riemer, D. D. & Zika, R. G. (1998): Carbonyl sulfide (OCS) and carbon monoxide (CO) in natural waters: evidence of a coupled production pathway. *Marine Chemistry* **62** (1–2): 89–101.

Pozzer, A.; Jöckel, P.; Sander, R.; Williams, J.; Ganzeveld, L. & Lelieveld, J. (2006): Technical Note: The MESSy-submodel AIRSEA calculating the air-sea exchange of chemical species. *Atmos. Chem. Phys.* **6** (12): 5435–5444.

Protoschill-Krebs, G. & Kesselmeier, J. (1992): Enzymatic Pathways for the Consumption of Carbonyl Sulphide (COS) by Higher Plants. *Botanica Acta* **105** (3): 206–212.

Rasmussen, R. A.; Khalil, M. A. K. & Hoyt, S. D. (1982): The oceanic source of carbonyl sulfide (OCS). *Atmospheric Environment* **16** (6): 1591–1594.

Rex, M.; Wohltmann, I.; Ridder, T.; Lehmann, R.; Rosenlof, K.; Wennberg, P.; Weisenstein, D.; Notholt, J.; Kruger, K.; Mohr, V. & Tegtmeier, S. (2014): A tropical West Pacific OH minimum and implications for stratospheric composition. *Atmospheric Chemistry and Physics* **14** (9): 4827–4841.

Sandoval-Soto, L.; Stanimirov, M.; von Hobe, M.; Schmitt, V.; Valdes, J.; Wild, A. & Kesselmeier, J. (2005): Global uptake of carbonyl sulfide (COS) by terrestrial vegetation: Estimates corrected by deposition velocities normalized to the uptake of carbon dioxide (CO2). *Biogeosciences* **2** (2): 125–132.

Schauffler, S. M.; Atlas, E. L.; Flocke, F.; Lueb, R. A.; Stroud, V. & Travnicek, W. (1998): Measurements of bromine containing organic compounds at the tropical tropopause. *Geophysical Research Letters* **25** (3): 317–320.

Schmidtko, S.; Johnson, G. C. & Lyman, J. M. (2013): MIMOC: A global monthly isopycnal upper-ocean climatology with mixed layers. *Journal of Geophysical Research-Oceans* **118** (4): 1658–1672.

Schrade, S. (2011): Ground based measurements of Carbon Dioxide and other climatically relevant trace gases using Off-Axis Integrated-Cavity-Output-Spectroscopy (ICOS). RWTH Aachen, Germany, Diploma thesis.

Sikorski, R. J. & Zika, R. G. (1993): Modeling mixed-layer photochemistry of H2O2: Optical and chemical modeling of production. *Journal of Geophysical Research: Oceans* **98** (C2): 2315–2328.

Staubes, R. & Geogrii, H.-W. (1993): Biogenic sulfur compounds in seawater and the atmosphere of the Antarctic region. *Tellus* **45B**: 127–137.

Stefels, J.; Steinke, M.; Turner, S.; Malin, G. & Belviso, S. (2007): Environmental constraints on the production and removal of the climatically active gas dimethylsulphide (DMS) and implications for ecosystem modelling. *Biogeochemistry* **83** (1-3): 245–275.

Stramma, L.; Fischer, T.; Grundle, D. S.; Krahmann, G.; Bange, H. W. & Marandino, C. A. (2016): Observed El Niño conditions in the eastern tropical Pacific in October 2015. *Ocean Sci.* **12** (4): 861–873.

Suntharalingam, P.; Kettle, A. J.; Montzka, S. M. & Jacob, D. J. (2008): Global 3-D model analysis of the seasonal cycle of atmospheric carbonyl sulfide: Implications for terrestrial vegetation uptake. *Geophysical Research Letters* **35** (19): L19801.

Takahashi, T.; Sutherland, S. C.; Chipman, D. W.; Goddard, J. G.; Ho, C.; Newberger, T.; Sweeney, C. & Munro, D. R. (2014): Climatological distributions of pH, pCO_2, total CO_2, alkalinity, and $CaCO_3$ saturation in the global surface ocean, and temporal changes at selected locations. *Marine Chemistry* **164** (0): 95–125.

Turco, R. P.; Whitten, R. C.; Toon, O. B.; Pollack, J. B. & Hamill, P. (1980): OCS, stratospheric aerosols and climate. *Nature* **283** (5744) 10.1038/283283a0,: 283–285.

Uher, G. & Andreae, M. O. (1997a): Photochemical production of carbonyl sulfide in North Sea water: A process study. *Limnology and Oceanography* **42** (3): 432–442.

Uher, G. & Andreae, M. O. (1997b): The diel cycle of carbonyl sulfide in marine surface waters: field study results and a simple model. *Atmospheric Geochemistry* **2**: 313–344.

Ulshöfer, V. & Andreae, M. O. (1998): Carbonyl Sulfide (COS) in the Surface Ocean and the Atmospheric COS Budget. *Atmospheric Geochemistry* **3**: 283–303.

Ulshöfer, V.; Uher, G. & Andreae, M. O. (1995): Evidence for a winter sink of atmospheric carbonyl sulfide in the northeast Atlantic Ocean. *Geophysical Research Letters* **22** (19): 2601–2604.

Von Hobe, M.; Cutter, G. A.; Kettle, A. J. & Andreae, M. O. (2001): Dark production: A significant source of oceanic COS. *Journal of Geophysical Research* **106** (C12): 31217.

Von Hobe, M.; Kettle, A. J. & Andreae, M. O. (1999): Carbonyl sulphide in and over seawater: summer data from the northeast Atlantic Ocean. *Atmospheric Environment* **33**: 3503–3514.

Von Hobe, M.; Najjar, R.; Kettle, A. & Andreae, M. (2003): Photochemical and physical modeling of carbonyl sulfide in the ocean. *Journal of Geophysical Research* **108** (C7)

Wang, Y.; Deutscher, N. M.; Palm, M.; Warneke, T.; Notholt, J.; Baker, I.; Berry, J.; Suntharalingam, P.; Jones, N.; Mahieu, E.; Lejeune, B.; Hannigan, J.; Conway, S.; Mendonca, J.; Strong, K.; Campbell, J. E.; Wolf, A. & Kremser, S. (2016): Towards understanding the variability in biospheric CO_2 fluxes: using FTIR spectrometry and a chemical transport model to investigate the sources and sinks of carbonyl sulfide and its link to CO2. *Atmos. Chem. Phys.* **16** (4): 2123–2138.

Wanninkhof, R.; Asher, W. E.; Ho, D. T.; Sweeney, C. & McGillis, W. R. (2009): Advances in Quantifying Air-Sea Gas Exchange and Environmental Forcing. *Annual Review of Marine Science* **1**: 213–244.

Watts, S. F. (2000): The mass budgets of carbonyl sulfide, dimethyl sulfide, carbon disulfide and hydrogen sulfide. *Atmospheric Environment* **34** (5): 761–779.

Weiss, P.; Andrews, S.; Johnson, J. E. & Zafiriou, O. (1995a): Photoproduction of carbonyl sulfide in south Pacific Ocean waters as a function of irradiation wavelength. *Geophysical Research Letters* **22** (3): 215–218.

Weiss, P.; Johnson, J. E.; Gammon, R. & Bates, T. (1995b): Reevaluation of the open ocean source of carbonyl sulfide to the atmosphere. *Journal of Geophysical Research* **100** (D11): 23083–23092.

Whelan, M. E.; Hilton, T. W.; Berry, J. A.; Berkelhammer, M.; Desai, A. R. & Campbell, J. E. (2016): Carbonyl sulfide exchange in soils for better estimates of ecosystem carbon uptake. *Atmos. Chem. Phys.* **16** (6): 3711–3726.

Xie, H.; Moore, R. M. & Miller, W. L. (1998): Photochemical production of carbon disulphide in seawater. *Journal of Geophysical Research: Oceans* **103** (C3): 5635–5644.

Xie, H.; Scarratt, M. G. & Moore, R. M. (1999): Carbon disulphide production in laboratory cultures of marine phytoplankton. *Atmospheric Environment* **33** (21): 3445–3453.

Xu, X. (2001): Investigations into the tropospheric cycle of COS: atmospheric distribution, air-sea and air-vegetation exchanges. PhD thesis.

5

OCS and CS_2 production and loss processes in the eastern tropical South Pacific

Lennartz, S.T., Marandino, C.A., von Hobe, M., Fischer, T., Bittig, H., Booge, D., Goncalves-Araujo, R., Ksionzek, K., Koch, B.P., Bracher, A., Röttgers, R., Quack, B., manuscript in prep.

Abstract. Oceanic emissions significantly contribute to the atmospheric budget of the climate relevant trace gases carbonyl sulfide (OCS) and carbon disulfide (CS_2), but the magnitude of global marine emissions is associated with high uncertainties. These uncertainties arise from 1) scarcity of measurements especially below the mixed layer for both gases, 2) lacking process quantification under environmental conditions across various biogeochemical ocean regimes for OCS, and 3) insufficient process understanding of production and loss of CS_2 in the water column. Here we present for the first time combined measurements and model simulations for both gases simultaneously, which extend down to 140 m water depth in the highly productive eastern tropical South Pacific (ETSP). Trace gas measurements are complemented by analysis of specific fractions of the dissolved organic matter pool relevant for the photochemical production. Using a newly developed water column model, we derive daily integrated surface photoproduction rates in the range of 43.2 to 194.4 pmol L^{-1} d^{-1} for OCS and 4.8 to 35.7 pmol L^{-1} d^{-1} for C_S, representing an upper end of previously reported rates for OCS and first derived photoproduction rates of CS_2 under environmental conditions. A ratio of 1:5 between the apparent quantum yield of CS_2 and OCS at open ocean and shelf stations confirmed a stable ratio across different biogeochemical regimes. In addition, we show first evidence of the occurrence of a subsurface CS_2 degradation process, for which a reaction mechanism remains unknown.

5.1 Introduction

Oceanic emissions play a dominant role in the atmospheric budget of the climate relevant trace gases carbonyl sulfide (OCS) and carbon disulfide (CS_2)(Chin & Davis, 1993; Kremser et al., 2016; Watts, 2000). OCS is the most abundant sulfur gas in the atmosphere (Kremser et al., 2016; Sheng et al., 2015), and CS_2 is its most important precursor gas. Both gases influence the climate directly (OCS) or indirectly (CS_2 by oxidation to OCS in the atmosphere). Both are weak greenhouse gases, and in addition, OCS is the major supplier of stratospheric aerosols in volcanically quiescent periods (Brühl et al., 2012), which exert a cooling effect and catalyze ozone depletion in high latitudes (Kremser et al., 2016; Solomon et al., 2015). Furthermore, OCS has been suggested as a proxy to constrain global terrestrial gross primary production, which requires well quantified sources and sinks of OCS (Campbell et al., 2017). However, the atmospheric budgets of OCS currently highly uncertain, as known sinks (ca. 1200 Gg S yr^{-1}) exceed known sources by 600-800 Gg S per year. Oceanic emissions of OCS and CS_2 from the tropical Pacific and Indian Ocean have been suggested as the missing source (Glatthor et al., 2015; Kuai et al., 2015), while the total amount of direct OCS emissions from the ocean is still debated (Launois et al., 2015; Lennartz et al., 2017). Oceanic emissions of CS_2 are even more uncertain due to scarcity of data.

Both gases are produced naturally in the ocean, and process understanding and quantification of OCS sources and sinks is higher than for CS_2. Several chemical and physical processes determine the concentration of OCS in seawater, which are briefly reviewed in the following. OCS is photochemically produced in the surface ocean from UV radiation (280-340 nm) and chromophoric dissolved organic matter (CDOM) (Uher & Andreae, 1997). Despite the similar shape in apparent quantum yields (AQY, in-situ photoproduction rate constant), the absolute AQY varied across one order of magnitude for different locations between several studies (Cutter et al., 2004; Weiss et al., 1995; Zepp & Andreae, 1994). Possible sulfur-containing precursors involved in the reaction most likely include a thiol group to form thiyl radicals. Experimental evidence exists for cysteine, methyl mercaptan, gluthathione (Flöck et al., 1997), methionine, dimethyl sulfide (Zepp & Andreae, 1994), and to a very minor degree dimethylsulfoxide and dimethylsulfoniopropionate (Zepp & Andreae, 1994). To date, the most detailed reaction mechanism for OCS formation is suggested by Pos et al. (1998), who showed evidence for a coupled production pathway of OCS and CO from incubation studies. Their suggested mechanism requires 1) a source for a carbonyl group, 2) a thiyl or sulfhydryl-radical and 3) potentially the catalyzation by metal complexes, all of which are present in marine environments. Furthermore, OCS is

produced in a light-independent reaction termed dark production including sulfur containing precursors, such as cysteine and glutathione (Flöck & Andreae, 1996; Von Hobe et al., 2001). They suggested a production process involving thiyl-radicals formed by O_2 or metal complexes. Radford-Knoery & Cutter (1994) found a covariance of OCS with nitrite in the water column, and suggested that dark production might be coupled to microbial processes during organic matter remineralization. It is currently unclear, whether the main dark production process in the oxic water column is due to microbial respiration or radical formation. The reaction rate of hydrolysis, yielding CO_2 and sulfide, increases strongly with temperature, which is well quantified by a comprehensive laboratory study across a wide temperature range (Elliott et al., 1989) and shows a lifetime on the order of few hours. This rate has been confirmed by seawater incubation studies (Radford-Knoery & Cutter, 1994). At the ocean surface, OCS is exchanged with the atmosphere, but this loss process is of minor importance compared to hydrolysis. Finally, physical transport also affects OCS distribution in the water column, which has so far not been addressed specifically for OCS.

Production and loss processes for CS_2 are less well constrained compared to OCS. Photochemical incubation studies indicate that the AQY of CS_2 has a similar wavelength-dependence as OCS, but only a quarter of the magnitude compared to OCS in the open Pacific Ocean (Xie et al., 1998). It is currently unclear whether both AQY covary on larger spatial scales, as simultaneous assessment of both gases are not available. Laboratory studies indicate that cystine, cysteine and, to a lesser extent, methionine are precursors for CS_2 photochemistry, with a mechanism similar to the production mechanism of OCS (Xie et al., 1998). Evidence for biological production comes from incubation studies performed by Xie et al. (1999), who showed CS_2 production for some, but not all of the tested phytoplankton species. This biological production was supported by observed subsurface concentration peaks below the mixed layer coincident with a chlorophyll *a* maximum (Xie et al., 1999). Laboratory experiments indicated that CS_2 is hydrolyzed, and oxidized by H_2O_2, but with corresponding lifetimes on the order of years (Elliott, 1990). In contrast to this proposed lifetime, Kettle (2000) derived a sink additional to air-sea exchange with a lifetime on the order of weeks, but no underlying mechanism for such a sink is currently known. CS_2 is less soluble than OCS, and, since atmospheric concentrations of CS_2 are very low due to fast oxidation to OCS in the atmosphere, the ocean is generally supersaturated with CS_2. Outgassing to the atmosphere appears, thus, the most important sink for CS_2 in the mixed layer (Kettle, 2000). With the absence of a strong chemical sink in the water column, physical transport processes might become relatively more important for CS_2 than they are for the OCS, but have not been specifically addressed so far.

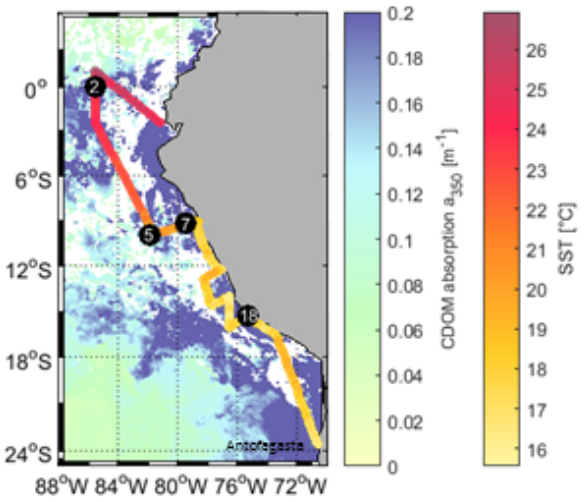

Figure 5.1: Sea surface temperature (SST) along the cruise track of ASTRA-OMZ (SO243) against monthly composite of absorption of CDOM/detritus detected by the Moderate Resolution Imaging Spectroradiometer (MODIS) instrument on board the Aqua satellite (AquaMODIS), converted to 350 nm. Station numbers of profiles with model simulations are indicated by black circles

Much of the mechanistic process understanding is derived from incubation studies, which provide a useful tool to manipulate single factors and thus determine key parameters, but represent simplified, artificial settings. Therefore, *in-situ* observations from various biogeochemical regimes are needed to assess the influence of identified key parameters under natural conditions. Most of the currently available field measurements were taken in the Northern Atlantic and adjacent seas, and have covered mainly surface waters. Here, we present for the first time a combined approach of measurements and modelling of both gases in the water column of the Eastern Tropical South Pacific (ETSP). Observations of the gases are complemented by measurements of specific fractions of the dissolved organic matter pool relevant for photochemistry (chromophoric and fluorescent dissolved organic matter, CDOM and FDOM) and sulfur-containing precursors (dissolved organic sulfur, DOS). This systematic, process-specific approach allows us to 1) determine production rates of both gases in the ETSP, 2) assess covariations of photoproduction rates of both gases with respect to suggested similar production mechanisms, 3) assess the influence of different fractions of the DOM pool on the production rates, 4) discuss plausible reaction mechanisms with respect to reaction pathways determined by incubation studies, and 5) assess the variation of OCS and CS_2 concentration in the water column as a result of their source and sink processes.

5.2 Methods

5.2.1 Study area

The cruise ASTRA-OMZ on RV SONNE started in Guayaquil, Ecuador, on the 05.10.2015 and reached the destination Antofagasta on 22.10.2015 (Fig. 5.1). It covered several transects from the open ocean to the coastal shelf between 10 and 17°S. Biogeochemical properties of the area under investigation are influenced by a complex system of surface and subsurface currents. These hydrographic conditions encountered during this specific cruise have been described previously and are summarized here (Stramma et al., 2016). In the coastal and shelf region off Peru, nutrient rich and oxygen depleted water is upwelled from the Peru-Chile Undercurrent, which results in very high biological productivity. The coastal area off Peru, thus, belongs to one of the four major global eastern boundary upwelling systems (Chavez et al., 2008). Connected to the upwelling zone, a large oxygen minimum zone expands into the Pacific Ocean at depths between 100 and 900 m, resulting from weak ventilation and strong respiration (Karstensen et al., 2008). The cruise took place during the onset of one of the four strongest El Nino events since 1950, which had an impact on the hydrographic conditions encountered during the cruise (Stramma et al., 2016). As a consequence, a weakening of the Equatorial Undercurrent (EUC) led to warmer temperatures and lower nutrient concentrations in the Northern part of the cruise track east of the Galapagos Islands (close to station 2). Around 9°S (stations 5 and 7), typical El Nino conditions occurred, i.e. upwelling of lighter, warmer and more oxygenated water, compared to neutral conditions (Stramma et al., 2016). At the southernmost transect, the El Nino influence was weaker and cold, oxygen poor water was upwelled. OCS and CS_2 profiles were taken at stations 2, 5, 7 and 18. Station 2 was located in the open ocean, station 7 at the shelf and station 18 closest to coastal waters. At station 5, an anticyclonic mesoscale eddy was indicated by sea surface height anomalies, which has formed around the 5^{th} of August near the shelf at 10°S (pers. communication L. Stramma, 2016). At station 18, several subsequent CTD casts indicated high internal wave activities with a vertical water displacement of ca. 50 m.

5.2.2 Measurements of trace gases

OCS concentrations were determined with an off-axis integrated cavity output spectrometer for OCS (OA-ICOS, Los Gatos Inc., USA) coupled to a Weiss-type equilibrator (Lennartz et al., 2017). The Weiss-type equilibrator is constantly supplied with 2-4 L min^{-1} of seawater from the hydrographic shaft (moon pool) of the ship (5 m below surface) and brings

the concentration in the headspace of the equilibration chamber to equilibrium with the concentration in seawater. The sample gas stream from the headspace of the equilibrator is filtered (Pall Acro Filter, 0.2 μm) and dried (Nafion® dryer, Gasmet Perma Pure) before entering the cavity of the OCS analyzer. The outlet of the OCS analyzer is connected to the Weiss-equilibrator, as this recirculation method keeps the concentration gradient between water and gas phase small and thus enables rapid equilibration (Arévalo-Martínez et al., 2013). OCS calibrations using standards from permeation tubes (Fine Metrology, Italy) were performed before and after the cruise, showing good agreement to each other. Additionally, independent samples for comparison measured with GC-MS (de Gouw et al., 2009; Schauffler et al., 1998) reflected only the 5% different between the NOAA scale and the perm tube standards, but was otherwise consistent (Lennartz et al., 2017).

Depth profiles of OCS were obtained using a newly developed submersible pumping system. A rotary pump (Lowara, Xylem) connected to a 1" PTFE hose supplied the Weiss-equilibrator with 2-4 L seawater min^{-1}. With an equilibration time of 2.5 min (Arévalo-Martínez et al., 2013) and a lowering speed of 6 m min^{-1}, the spatial resolution of the profiles equates to 15 m. Therefore, the pump inlet was held at a constant depth for 10-15 min to ensure full equilibration at 4-6 depths during each profile.

During ASTRA-OMZ, CS_2 was measured with a purge and trap system attached to a gas chromatograph and mass spectrometer (GC/MS; Agilent 7890A/Agilent 5975C; inert XL MSD with triple axis detector) running in single-ion mode (Lennartz et al., 2017). 50 mL samples were taken in 1 to 3 hour intervals from the same underway system as for continuous OCS measurements. After purging for 15 min with helium (70 mL min^{-1}), the gas stream was dried with a Nafion® membrane drier (Gasmet Perma Pure) and trapped with liquid nitrogen for preconcentration. Hot water was used to heat the trap and inject CS_2 into the GC/MS. The retention time for CS_2 (m/z=76, 78) was 4.9 min. The analyzed data were calibrated daily using gravimetrically prepared liquid CS_2 standards in ethylene glycol. During purging, 500 μL gaseous deuterated DMS (d3-DMS) and isoprene (d5-isoprene) were added to each sample as an internal standard to account for possible sensitivity drift between calibrations. Discrete samples from depth profiles were obtained from the rosette sampler connected to a CTD.

For dimethyl sulfoxide (DMSO) and dimethylsulfoniopropionate (DMSP) analysis, 50 mL purged seawater samples were spiked with 3 pellets of sodium hydroxide to convert DMSP into DMS and transported to Kiel. Samples were analyzed using a purge and trap system coupled to a gas-chromatograph (GC; Agilent 7820A; WCOT fused Silica, 30 m x 0.32 mm i.d., Varian Capillary Columns) and a flame photometer detector (FPD; Agilent H9261) (Simo et al., 1996). Triplicates of 2-10 mL were extracted from each sample and DMSP was measured

as DMS. After the analysis the samples triplicates were used and cobalt-doped sodium borohydride was added to reduce DMSO to DMS which was measured immediately after addition. The amount of DMS in each sample was quantified by performing calibrations, using gravimetrically prepared liquid DMS standards in ethylene glycol.

5.2.3 Measurements of ancillary parameters

Dissolved organic matter

CDOM was sampled from CTD Niskin bottles or the underway system in a 3-hour interval, filtered (0.2 μm) and analyzed with a liquid waveguide capillary cell (LWCC, Ocean Optics) photometer (Miller et al., 2002). The spectrum was recorded for wavelengths between 270 to 700 nm at a resolution of 2 nm. The absorption coefficient was determined according to the Lambert-Beer-Law. The slope of the absorption spectrum was determined by fitting an *e*-function to the spectral range of 270-700 nm.

Fluorescent dissolved organic matter (FDOM) was recorded in Excitation-Emission-Matrices (EEMs) with a UV-vis-spectrophotometer (Hitachi F2700) from filtered (0.2 µm, <200 mbar below atmospheric pressure) seawater samples. Excitation wavelengths ranged from 220 nm to 550 nm with a resolution of 10 nm. Emission wavelengths were recorded from 250 nm to 550 nm in 1 nm resolution at a voltage of 400 or 800 V. For both voltages, calibration curves with quinine sulfate (5 to 30 ppb) in sulfuric acid were measured with R^2 of 0.9991 and 0.9971, respectively. EEMs were blank subtracted and Raman normalized (Murphy et al., 2013). The values are reported here in quinine sulfate QS units (QS). A parallel factor analysis (PARAFAC) was performed using the drEEM Toolbox (Murphy et al., 2013; Stedmon & Bro, 2008) to separate the superimposed optical signals of different fluorophores ('components') in the EEMs. The separated fluorophores allow for the identification of molecule classes such as humic or protein-like substances. The conversion factor between QS units and Raman units was 0.3540 and 0.4256 respectively.

Solid phase extractable dissolved organic sulfur (SPE-DOS) was sampled from the underway system or from submersible pump profiles directly into glass bottles and filtered through pre-combusted GF/F filters (Whatman, 450°C for >5h) at maximum 200 mbar below atmospheric pressure. Aliquots for dissolved organic carbon (DOC) analysis were stored in HDPE-bottles at -20°C. For SPE-DOS, the filtered samples were acidified to pH 2 (hydrochloric acid, suprapur, Merck), extracted according to Dittmar et al. (2008)(PPL, 1g, Mega Bond Elut, Varian) and stored at -20°C until further analysis. For analysis, the PPL-cartridges were eluted with 5 mL of methanol (LiChrosolv, Merck). SPE-DOS was quantified with an inductively coupled plasma sector field mass spectrometer (ICP-MS, Element 2, Thermo

Fisher Scientific) equipped with a desolvation nebulizer (Apex Q, Elemental Scientific), a platinum guard electrode, nickel sampler and skimmer cones as specified in (Ksionzek et al., 2016).

Underwater short wave radiation

Underwater optical light fields were assessed through downwelling irradiance profiles obtained with the hyperspectral radiometer RAMSES ACC-VIS (TriOS GmbH, Germany). The instruments cover a wavelength range of 305 nm to 950 nm with an optical resolution of 3.3 nm and a spectral accuracy of 0.3 nm. Measurements were collected with sensor-specific automatically adjusted integration times (between 4 ms and 8 s). Radiometric profiles were collected prior or after CDOM/FDOM sampling except at station 7 where sampling took place at night only. At each profile, measurements of downwelling irradiance (E_d) were performed. The E_d sensor was equipped with inclination and pressure sensors. To avoid ship shadow, the ship was oriented such that the sun was illuminating the side where the measurements have taken place. During the acquisition of the profiles, stops (of about 60 s) were performed within a 2 m depth interval until 30 m and then 5 m down to the maximum depth until which light could be measured. The irradiance profiles were corrected for incident sunlight using simultaneously obtained E_d, measured above the surface without ship's shading with another hyperspectral radiometer (RAMSES ACC-VIS, TriOS GmbH, Germany). These data were then averaged and interpolated in discrete intervals of 1 m following the NASA protocols (Mueller et al., 2003). Then the euphotic depth Zeu at each station was calculated from the in situ PAR profiles as the depth where PAR(z) 0.01 of PAR(z=0m).

Determination of gas diffusivity with microstructure profiles

To estimate fluxes into and out of the mixed layer, a surface volume is defined with its base set as the mixed layer depth (MLD) plus 10 m, following Hummels et al. (2013). The diapycnal and vertical advective fluxes are determined in a 'transition zone' to the mixed layer, which is centered at 10 m below MLD. The MLD is defined here as the depth where the density has increased by an amount equivalent to a 0.5 K temperature decrease compared to the surface to avoid unintended detection of diurnal warm layers as MLD (Schlundt et al., 2014).

The diapycnal mixing flux, $\Phi_{dia,base}$ [pmol m^3 s^1], which transports the gas across the pycnocline is defined as in eq. 5.1:

$$\Phi_{dia,base} \approx \rho \cdot K_\rho \cdot \frac{\partial c}{\partial z} \tag{5.1}$$

where $\frac{\partial c}{\partial z}$ [nmol kg^{-1} m^{-1}] is the vertical gradient of gas concentration across the transition zone which was determined from discrete profiles taken at the same stations as the microstructure profiles, K_ρ [m^2 s^{-1}] is the diapycnal diffusion coefficient estimated from the average dissipation rate of turbulent kinetic energy in the transition zone, as measured by a microstructure probe (Hummels et al., 2013), and ρ [kg m^{-3}] is the water density in the transition zone.

The microstructure profiles were performed with a tethered profiler (type MSS 90D of Sea& Sun Technology). The MSS profiler records small-scale fluctuations of the water velocity with airfoil sensors, which can be used to estimate the turbulent diffusivity K across density surfaces. Diapycnal gas fluxes can be estimated for vertical intervals that are limited by two depths, where gas concentration is known, by multiplying the average K by the average gas gradient in that depth interval. The average gas gradient is approximated by the difference of the two limiting concentrations divided by their distance. Uncertainties of fluxes have been calculated by error propagation from measurement uncertainties of the gas concentrations (0.1 μM for single values) and the average K values (typically 6% for a 10 m interval, e.g.). There are additional uncertainties not quantified, e.g. from the approximation of the average gas gradient, or from the assumption of other gas transport processes than diapycnal mixing to be negligible. More details on the methodology to estimate diapycnal fluxes and flux divergences of dissolved substances from microstructure measurements and concentration profiles can be found in Fischer et al. (2013) and Schlundt et al. (2014).

The vertical component of the advective flux Φ_{adv} describes the transport related to upwelling (eq. 5.2):

$$\Phi_{adv} \approx \rho \cdot \omega_{base} \cdot (c_{base} - < c_{boundary} >) \tag{5.2}$$

where ω_{base} [m s^{-1}] is the current velocity normal to the base plane, c_{base} [nmol kg^{-1}] is the gas concentration at the base plane and $c_{boundary}$ [nmol kg^{-1}] is the mean gas concentration of the water column above the base level, further averaged along the horizontal boundary of the budget volume.

5.2.4 Modeling OCS and CS_2 concentration in the water column

The Framework for Aqueous Biogeochemical Modeling (FABM) was used to develop a new submodule in order to simulate concentration-depth profiles of the gases OCS and CS_2 (Bruggeman & Bolding, 2014). FABM provides the frame for a physical host model and a biogeochemical model, wherein the physical host is responsible for tracer transport

and the biogeochemical model provides local source and sink terms. The physical host used here is the General Ocean Turbulence Model (GOTM), which is a 1D water column model simulating hydrodynamic and thermodynamic processes related to vertical mixing (Umlauf et al., 2005). GOTM derives solutions for the transport equations of heat, salt and momentum. A second order model is applied for the turbulence calculating the length scale of turbulence, l, and the turbulent kinetic energy (TKE) from differential transport equations. TKE is described by a $k - \epsilon$ model whereas l is calculated by a dynamic dissipation rate model (Umlauf et al., 2005).

Submodel for OCS

The biogeochemical submodel for OCS in FABM includes parameterizations for photochemical and dark production, loss by hydrolysis and air-sea exchange at the surface, similar to the box model described in Lennartz et al. (2017). The photoproduction rate is calculated as the product of the radiation, rad, the absorption coefficient of CDOM at 350nm, a_{350}, and the integrated apparent quantum yield AQY (eq. 5.3) according to von Hobe et al. (2003):

$$\frac{dC}{dt} = rad \cdot a_{350} \cdot AQY \tag{5.3}$$

a_{350} is prescribed from measurements, and the radiation is obtained from the model-specific light field of the physical host. The absorption within the water column is adapted to match observed radiation profiles (see section 5.2.3). The AQY has not been directly measured and is derived by parameter optimization in an inverse model set-up (see section 5.2.4).

For dark production, a new parameterization is developed and implemented in the model. Dark production rates were determined from measured seawater concentrations at nighttime or at depths excluding photoproduction. The determination of dark production rates relies on the principle that stable concentrations measured in the absence of light are the equilibrium concentrations resulting from dark production and loss by hydrolysis. In steady state, dark production P_D equals loss from hydrolysis L_H, which is the product of the steady-state concentration [OCS] and the rate constant k_h according to eq. 5.4 – 5.6:

$$P_D = L_H = [OCS] \cdot k_h \tag{5.4}$$

The rate constant k_h was calculated according to Elliott et al. (1989), eq. 5.5:

$$k_h = exp\left(24.3 - \frac{10450}{T}\right) + exp\left(22.8 - \frac{6040}{T}\right) \cdot \frac{K_w}{a[H^+]} \tag{5.5}$$

$$-log_{10}K_w = \frac{3046.7}{T} + 3.7685 + 0.0035486 \cdot \sqrt{S} \tag{5.6}$$

with temperature T, salinity S, $a[H^+]$ the proton activity and K_w the ion product of seawater (Dickinson & Riley, 1979).

The temperature dependency of a reaction rate P_D can be described with an Arrhenius-relationship. In its linearized form, the temperature dependency is described by the following equation (eq. 5.7):

$$ln\frac{P_D}{a_{350}} = \frac{a}{T} + b \tag{5.7}$$

with a_{350} being the absorption coefficient of CDOM at 350 nm, T the temperature and a and b coefficients describing the temperature dependency of the reaction. The production rate P_D is normalized to a_{350} (Von Hobe et al., 2001). Developing such a new parameterization for dark production in the ETSP in an approach similar to (Von Hobe et al., 2001) allows for quantitative comparison of the dark production rates and their temperature dependencies between the Atlantic and the Pacific, therefore indicating global variations in this relationship.

Hydrolysis, as defined by the rate constant eq. 5.5, and air sea exchange, using the parameterization by Nightingale et al. (2000) for the transfer velocity k, are identical to the box model of Lennartz et al. (2017).

Submodel for CS_2

The submodel for CS_2 contains a similar formulation of the photochemical production and air-sea exchange as the submodel for OCS. Currently, no experimental evidence for any other loss process is known, but Kettle (2000) inferred an *e*-folding lifetime on the order of 11-13.3 days, which is analogous to a loss rate of 1.05e-6 and 8.7e-7 s^{-1}. This loss rate had been needed in addition to the loss by gas exchange to explain observed concentrations in Kettle (2000), although no mechanism for this process is known. We perform sensitivity studies with an average rate (9.52e-7, equates to 12.15 days lifetime) and with the absence of a sink to determine the probability of a sink in seawater.

Determining photoproduction rates and AQY for OCS and CS_2

Photoproduction rates and AQY for both gases are estimated using an inverse set-up of the GOTM/FABM model based on measured concentration profiles of the gases. The model was completely nudged to represent environmental conditions of temperature, salinity, meteorological conditions and light absorption in the water column, as observed during sampling of the trace gases. Photoproduction rates were estimated, which results

Table 5.1: Simulation set-up for the GOTM/FABM model simulations at 4 stations for the two gases OCS and CS_2. T, S and a_{350} are column averages. n_1,n_2 and A are absorption coefficients for the light profiles according to eq. 5.8. pos.=geographical position,SST=surface temperature, T=water temperature, S=salinity, re. hum.=relative humidity, air press.=air pressure, cloud cov.=cloud coverage.

	Station 2 'open ocean'		Station 5 'eddy'		Station 7 'shelf'		Station 18 'coastal shelf'	
	OCS	CS_2	OCS	CS_2	OCS	CS_2	OCS	CS_2
pos.	0.0°N 85.5°W	0.0°N 85.5°W	10.0°S 81.9°W	10.0°S 81.9°W	9.2°S 79.5°W	9.2°S 79.5°W	15.3°S 75.3°W	15.3°S 75.3°W
date	10/7/15 16h	10/7/15 23h	10/11/15 3h	10/10/15 19h	10/12/15 9h	10/12/15 3h	10/19/15 20h	10/19/15 18h
depth [m]	100	150	150	150	120	150	117	119
SST [°C]	24.28	20.52	20.64	20.55	20.10	20.06	15.58	15.71
T [°C]	21.05	19.26	17.47	17.61	17.92	17.28	14.73	14.55
S [-]	34.87	34.94	35.12	35.13	35.13	35.14	35.00	34.99
a_{350} [m^{-1}]	0.13	0.13	0.15	0.15	0.14	0.14	0.14	0.14
n_1	8.96	8.96	6.89	6.89	0.02	0.02	4.19	4.19
n_2	15.47	15.47	1.24e7	1.27e7	4.10	4.10	8.04	8.04
A	0.95	0.95	0.99	0.99	0.04	0.04	0.97	0.97
wind u [m s^{-1}]	0.23	0.23	-4.59	-4.59	-2.44	-2.44	-4.51	-4.51
wind v m s^{-1}]	6.54	6.54	7.95	7.95	7.11	7.11	4.83	4.83
rel. hum. [%]	100	100	77.8	77.8	80.9	80.9	87.95	87.95
air press. [hPa]	1011.3	1011.3	1011.9	1011.9	1013.9	1013.9	1016.7	1016.7
cloud cov. [-]	0.1	0.1	0.1	0.1	0.1	0.1	0.1	0.1

directly into an estimate of the AQY, as the AQY is the only unknown parameter in eq. 5.3. A Levenberg-Maquardt-optimization routine in Matlab (2016a) was used to fit the measured concentration profiles of OCS and CS_2. Only concentration measurements in the euphotic zone were used for parameter estimation to exclude any bias in the estimated AQY by subsurface processes. Several (>3) starting values were used to reduce the risk of convergence at a local minimum during parameter optimization.

Model set-up

The goal of the simulations was to use the same physical conditions in temperature, salinity, short wave radiation and meteorology as encountered during profiling, and repeat them until the model reaches a steady daily average OCS level and diel cycle (<1 pmol L^{-1} change in daily average)(Tab. 5.1). Only the light field varied over the course of the day in the cycle defined by the geographical position of the measured profile. To ensure a similar light field in the model as encountered during measurement of the profiles, the absorption coefficients to force the model were taken from radiation profiles measured at the same station (except station 7, see below) and day (see section 5.2.3). Therefore, eq. 5.8 was fitted to the observed profiles rad integrated over the wavelength range 300-400 nm:

$$rad(z) = rad(0) \cdot \left(A \cdot exp\left(-\frac{z}{n_1}\right)\right) + (1 - A) \cdot exp\left(-\frac{z}{n_2}\right) \tag{5.8}$$

The fitted parameters n_1, n_2 and A define the absorption of light in the water column according to Paulson & Simpson (1977), and are required as forcing parameters in GOTM. The wavelength range of 300-400 nm was chosen as it reflects the range of the maximum production for both gases (Weiss et al., 1995; Xie et al., 1998). At station 7, no irradiance profile was available. Therefore, the absorption coefficients of the station 6 nearby, which was similar with respect to the depth of the chlorophyll a maximum, were applied.

The simulation of vertical mixing was tested with a model simulation specifically set up to compare to measurements of the dissipation rate of kinetic energy ϵ [W kg^{-1}] as a measure of turbulent mixing. Therefore, microstructure profiles taken at station 5 were compared to ϵ calculated by GOTM. These runs were initialized and nudged to the temperature and salinity profiles obtained from the microstructure cast. The profiles of ϵ showed good agreement in the variation with depths, and averaged ϵ for three microstructure profiles from station 5 agreed within the standard deviation below the mixed layer. Within the mixed layer, ϵ was slightly overestimated in GOTM, although standard deviations for model simulation and measurements still overlapped. This indicates that simulated concentrations could be too homogeneous within the mixed layer.

5.3 Results

5.3.1 Characterization of dissolved organic matter

The pool of dissolved organic matter (DOM) contains the precursors for photochemical production of OCS and CS_2. Specific fractions of the DOM pool are either defined by

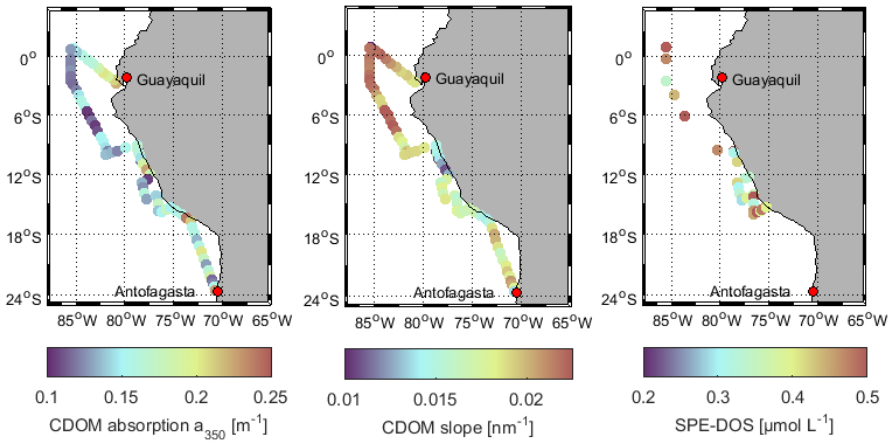

Figure 5.2: Characteristics of the organic matter pool at the ocean surface (5m) along the cruise track of ASTRA-OMZ in the ETSP in October 2015: left: absorption of chromophoric dissolved organic matter CDOM at 350 nm (a_{350}), middle: slope of the CDOM spectrum, and right: concentration of solid phase extractable dissolved organic sulfur (SPE-DOS).

their characteristics (CDOM, FDOM) or particular elements (SPE-DOS). FDOM always forms a part of CDOM, as fluorescence requires the absorption of light prior to reemission. SPE-DOS is purely operationally defined as the amount of sulfur containing molecules that are retained in PPL cartridges due to their polarity, but its relation to CDOM and FDOM is not quantifiable. The amount of CDOM is characterized here by its absorption coefficient at 350nm, a_{350}, to ensure comparability to previous observations in relation to OCS and CS_2. a_{350} during ASTRA-OMZ was generally high (a_{350}=0.15±0.03), as expected in upwelling regions like the ETSP (Nelson & Siegel, 2013). Highest absorption coefficients were found closest to the continent, coinciding with flat slopes of the absorption spectra (Fig. 5.2). The variation in slope is an indication for the relative amount of larger and smaller molecules, since the absorption of larger molecules is higher at higher wavelengths. Therefore, a steep slope indicates a high abundance of molecules with a lower molecular weight (LMW) whereas a flat slopes indicate a larger fraction of molecules with high molecular weight (HMW)(Helms et al., 2008). Accordingly, LMW CDOM was present in the open ocean section of the cruise whereas closer to land, HMW CDOM was more abundant. Four different components of FDOM, representing groups of similarly fluorescing molecules, were isolated and validated with PARAFAC analysis. Components C1 and C4 have their fluorescence peak in the UV part of the EEM. They thus resemble the naturally occurring amino acids tryptophane and tyrosine, which are part of the quickly overturning, labile DOM pool

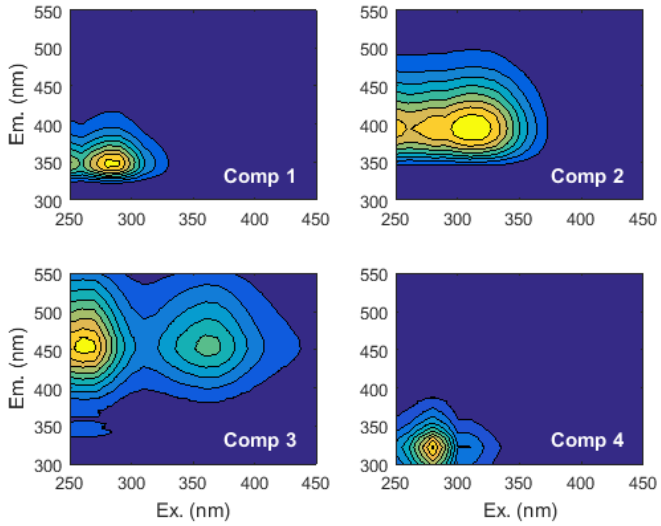

Figure 5.3: FDOM components of PARAFAC analysis validated with split half analysis. C1 and C4 have a fluorescence maximum in the UV range, C2 and C3 in the vis-range and are thus referred to as UV-FDOM and vis-FDOM.

connected to fresh biological production (Jorgensen et al., 2011; Murphy et al., 2008). Components C2 and C3 fluoresce in the visible range (VIS-FDOM) of the EEM (Fig. 5.3). Their fluorescence pattern shows characteristics of humic-like substances which seem to be ubiquitously present in the global oceans and have been found to be enriched in surface waters of upwelling regions (Jorgensen et al., 2011). Both VIS-FDOM components are more abundant at locations where cold water was upwelled (>9°S), and, most likely, reflect DOM from below that reached the surface. SPE-DOS was distributed very heterogeneously along the cruise track, with hot spots near the equator and on the southernmost transect (Fig. 5.2). SPE-DOS concentrations in the water column (not shown) decreased with depth, as also found for the East Atlantic Ocean and the Sargasso Sea (Ksionzek et al., 2016).
In total, the DOM pool can be spatially divided into three major parts:

1. Open Ocean (including station 2): high SPE-DOS, high UV-FDOM and low a_{350} with high slopes, the latter indicating a DOM pool dominated by freshly produced, small, protein-like substances.

2. Transition to shelf (including station 5 and 7): low SPE-DOS, high UV-FDOM, medium a_{350} with medium slope heights.

3. Upwelling (including station 18): high SPE-DOS, high UV-FDOM, high VIS-FDOM,

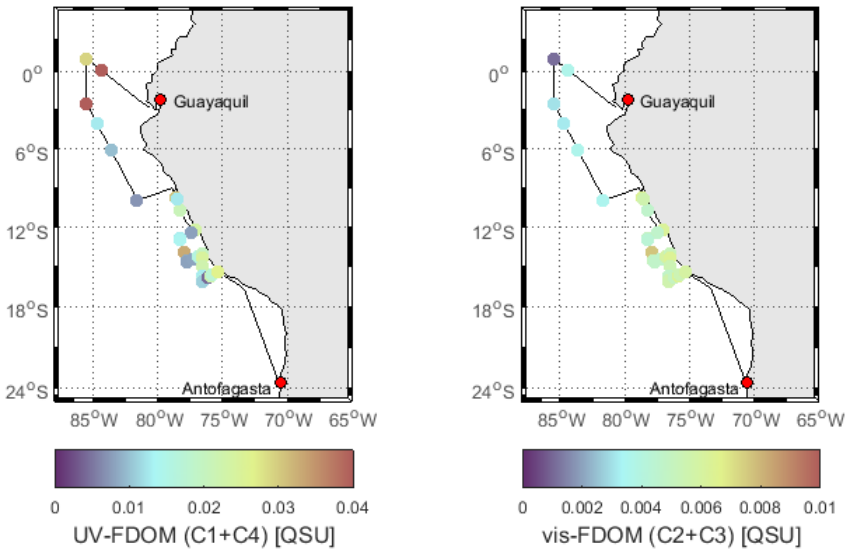

Figure 5.4: UV-FDOM (left, sum of component C1 and C4) and VIS-FDOM (right, sum of component C2 and C3) concentrations along the cruise track of ASTRA-OMZ in the ETSP. Note different color scales.

medium a_{350} with medium slopes, indicating large, humic-like molecules upwelled from subsurface waters.

The cruise track thus covers a large range of variability in DOM fractions that are potentially relevant for photochemical production of sulfur containing gases.

5.3.2 Carbonyl sulfide (OCS)

OCS surface water concentrations ranged from 6.5 to 133.8 (average 28.3±19.7 pmol L^{-1}) with strong diurnal cycles as described in Lennartz et al. (2017). Spatially, concentrations increased towards shelf and coast, and were highest along a shelf transect from 8° to 12° S (Fig. 5.5). The vertical variation of OCS concentrations was investigated at the four stations 2, 5, 7 and 18. The concentrations were decreasing with depth at stations 2, 7 and 18, but their slopes varied (Fig. 5.6). Subsurface concentrations are below 10 pmol L^{-1} from open ocean to the shelf. Differences in surface concentrations in the profiles from highest at station 18 to lowest in station 5 and 7 mainly reflect diurnal variations resulting from photochemical production, as stations 5 and 7 were taken at nighttime, station 2 in the morning hours and station 18 in the afternoon. The shape of the concentration profile for station 5 differed strongly from the other stations. Here the profile had a convex

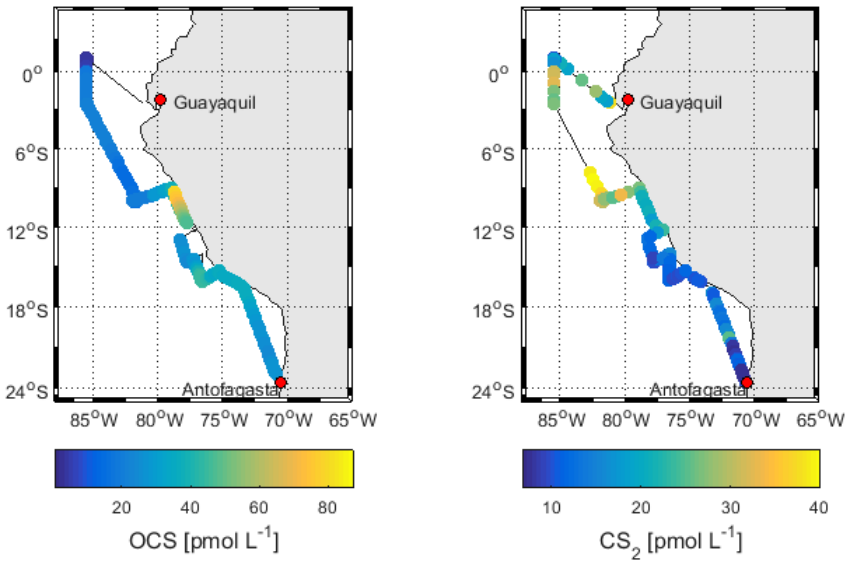

Figure 5.5: Concentrations of OCS (running 24h mean, left), and CS_2 along the cruise track of ASTRA-OMZ (right).

shape down to 75 m, and it was the only station where the concentration increased at lower depths. The diapycnal fluxes of OCS within the water column were derived from measured concentration and microstructure profiles. Overall, OCS that is produced at the surface is usually mixed downwards, although upward fluxes occur at station 5 and 7 in the lowermost budgeted volumes (Fig. 5.7). Converging and diverging fluxes between the budgeted volumes indicate the presence of local source and sink processes, but the fluxes within the water column were small compared to fluxes to the atmosphere and local sources and sinks calculated in the model simulations (see below). The dark production rates at the surface varied between 0.72 and 1.67 pmol L^{-1} h^{-1} along the northern part of the cruise track, and between 0.18 and 0.76 pmol L^{-1} h^{-1} in the four depth profiles below 50 m. The Arrhenius-type temperature dependency shows significantly decreasing dark production rates with decreasing temperature (Pearson's test, p=5.66 x10^{-10}). The same linear relationship is valid for both the dark production at the surface and at depth along the whole cruise track (Fig. 5.9) and is described by the following equation:

$$P_D = a_{350} \dot{e}xp\left(-\frac{14244}{T} - 49.9\right) \tag{5.9}$$

Instead of normalizing to a_{350} (Fig. 5.9, eq. 5.7), other fractions of the DOM pool (VIS-FDOM, SPE-DOS) and dissolved O_2 yielded significant (p<0.05) correlations but explained less of

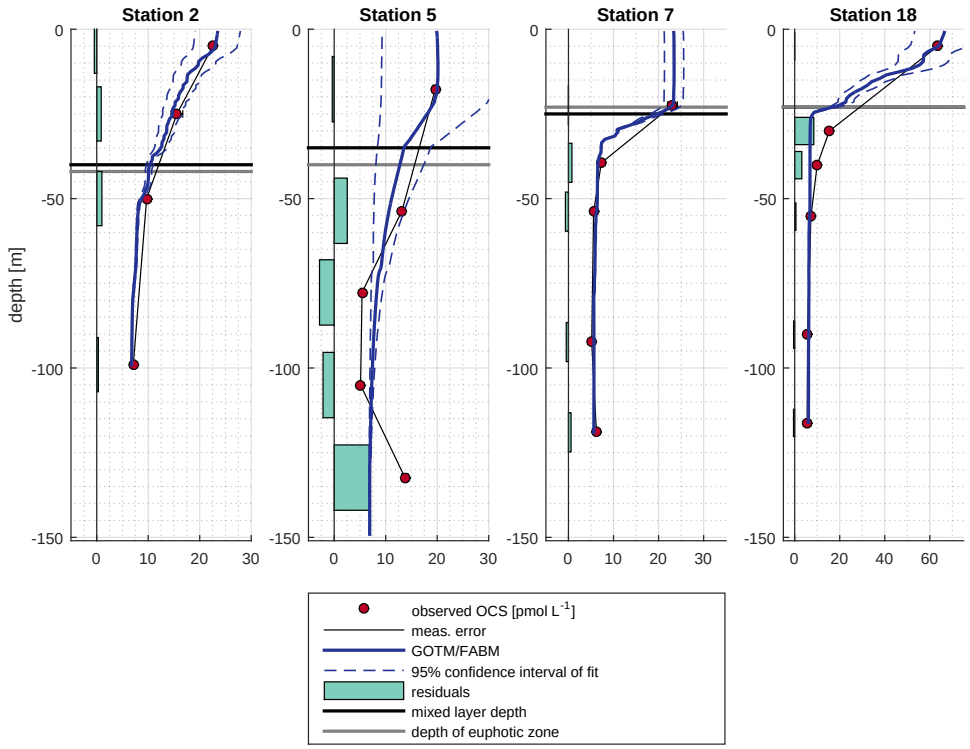

Figure 5.6: Observed (red circles), simulated (blue line) and residual (green bars) concentration profiles of OCS [pmol L^{-1}] at the stations 2, 5, 7 and 18 along the cruise track of ASTRA-OMZ.

the variance than a_{350} (R^2=0.94). At station 5, the dark production rates at two depths did not fit within the Arrhenius relationship, i.e. the depths at 50 and 136 m. In both cases, the dark production rate was larger than predicted for the temperature and the a350 present. OCS concentrations in the water column could be very well reproduced with the model including the processes photoproduction, the new parameterization of dark production (eq. 5.9), hydrolysis and air-sea exchange. The FABM/GOTM simulations for OCS reproduced the concentrations best for stations 2 and 7 with a root mean square error (RMSE) <1 pmol L^{-1}. RMSE for stations 5 and 18 were <4pmol L^{-1}. The model simulations reproduced the different slopes in concentration decline with depth reasonably well for all stations except station 5, using one single AQY (eq. 5.3) estimated for the total water column per station. At station 5, the convex declining with depths as well as the concentration increase at 136 m depth was not reproduced by the model.

The daily averaged photoproduction rates (surface) simulated for the four stations with FABM/GOTM ranged between 1.8 and 8.1 pmol L^{-1} h^{-1} (Fig. 5.8), leading to daily integrated production rates of 43.2 to 194.4 pmol L^{-1} d^{-1}. Generally, profiles from station 2, 7 and 18

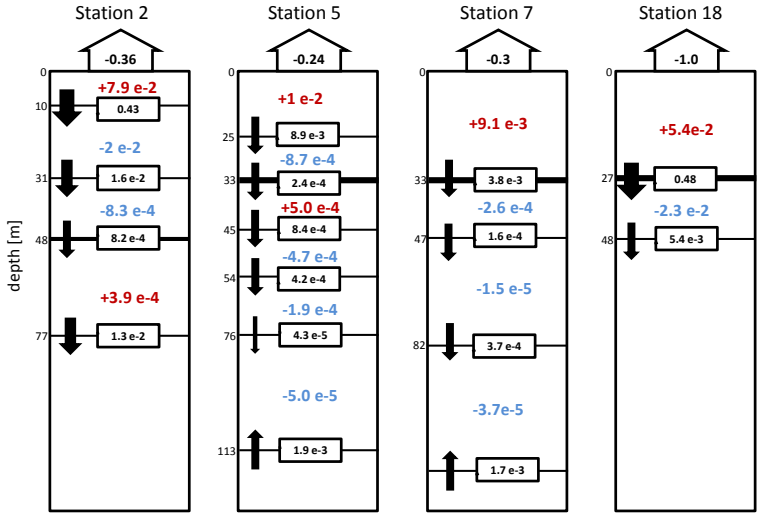

Figure 5.7: OCS fluxes within the water column as calculated using measured concentrations and microstructure profiles. Black arrows indicate fluxes corresponding to the fluxes in pmol s^{-1} m^{-3} given in black boxes respective for reference level. Thick black lines indiacte mixed layer. Local sources (red) and sinks (blue) are given in pmol m^{-3} s^{-1}.

were all consistent with a single estimated AQY per station throughout the water column (Tab. 5.2). Estimated integrated AQY (eq. 5.3) were similar for stations 2, 7, and 18 with an increase towards the continent, where upwelling of cold and oxygen poor water was present. The AQY was substantially smaller at station 5 (Tab. 5.2). The spatial variation of VIS-FDOM C2 explained 91% of the variance in this pattern of AQY. Concentrations of SPE-FOS, DMSP and DMSO showed an opposite spatial pattern, but none of the correlations were significant (p>0.05).

5.3.3 Carbon disulfide (CS_2)

The surface concentration of CS_2 during ASTRA-OMZ was in the lower picomolar range with an average of 17.8±8.9 pmol L^{-1} and did not show strong diurnal cycles. The concentrations measured in the ETSP are considerably higher than observations from an Atlantic transect (Kettle et al., 2001, , average 10.9 pmol L^{-1}, n=744), the North Atlantic (13.4 pmol L^{-1}) and the Pacific (14.6 pmol L^{-1}) (Xie et al., 1999), but lower than during another transect through the Atlantic (Lennartz et al., 2017, , average 62.8 pmol L^{-1}). Coinciding high CS_2 concentrations and high SST confirm a similar positive correlation found in the North Atlantic (Xie et al., 1999). The spatial pattern of sea surface concentrations was opposite to that of OCS, with highest concentrations distant from the shelf/coast and lowest closer

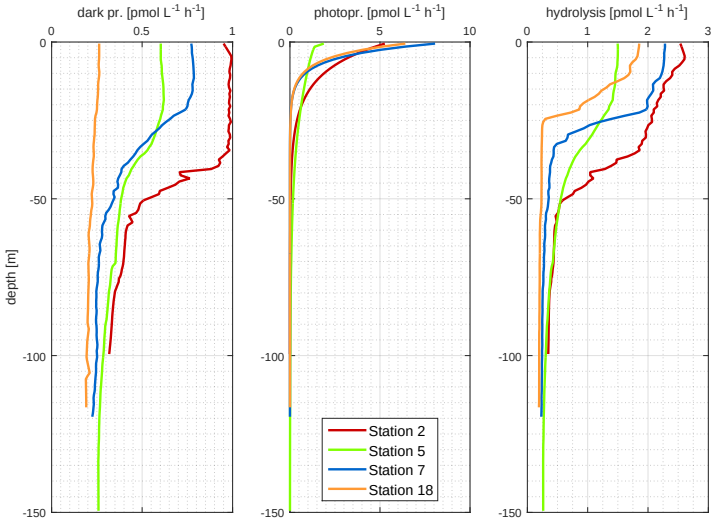

Figure 5.8: Daily averaged profiles of production (dark production and photoproduction) and loss processes (hydrolysis) for stations 2, 5, 7, and 18 during the ASTRA-OMZ cruise as simulated with the FABM/GOTM model.

to the shore. Highest surface concentrations of CS_2 coincided with warm temperatures (Fig. 5.1 and 5.5). The concentration profiles of CS_2 at station 2, 5, 7 and 18 show less variation with depth and a different shape compared to OCS (Fig. 5.10 and 5.6). At station 2, concentrations in the mixed layer showed variations which were not present at other statins where concentrations within the mixed layer were homogeneous. Below the mixed layer, a pronounced peak in CS_2 concentrations was present at stations 5 and 18.

The diapycnal fluxes of CS_2 within the water column reveal highest production at the surface except for station 18, and a flux divergence at the bottom of the mixed layer (Fig. 5.12). Within the water column, CS_2 is redistributed downwards as indicated by the downward fluxes in Fig. 5.12. Small in-situ sinks (station 2, 7, and 18) and in-situ sources (stations 2 and 18) within the water column are required to explain the observed concentration profiles under a steady state assumption. In addition, a small upward flux of CS_2 into the lowermost budgeted volume on station 7 and 18 was present, which were the only profiles which covered the whole water column close to the sediment surface. Based on the assumption that photoproduction is the only production process for CS_2 at the surface, photoproduction rates were estimated in a model simulation with an inverse model set-up. Within the mixed layer, air-sea exchange is the dominant sink, the results are thus not biased by a potential additional sink process. Surface photoproduction rates

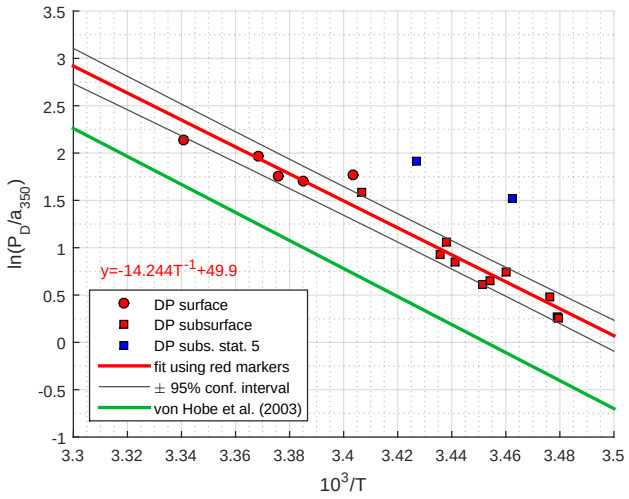

Figure 5.9: Arrhenius-plot of temperature dependency of dark production rates (P_D) normalized to CDOM absorption at 350nm from the ETSP (red markers/line) and for comparison the Arrhenius relationship derived by von Hobe et al. (2003) in the Atlantic Ocean, North Sea and Mediterranean. In this study, dark production rates were derived from stable nighttime concentrations (red circles) and from measurements in vertical profiles below the euphotic zone (red squares). The profile for station 5 showed an untypical shape and is thus excluded (blue squares).

estimated with the inverse model set-up were in the range of 0.7 to 1.49 pmol L^{-1} h^{-1} for station 2, 5, and 7, but only 0.2 pmol L^{-1} h^{-1} for station 18 (daily averages). The spatial pattern in a_{350} explained most of the variance, which is consistent with a stable AQY and similar light conditions among the stations when calculating the photoproduction with eq. 5.3. Indeed, estimated integrated AQY (eq. 5.3) were in a similar range for stations 2, 5 and 7, but considerably lower for station 18 (Tab. 5.2). The overall spatial pattern of these AQY did not show any spatial covariation with the ones for OCS, and the AQY of CS_2 was in a range of 19-37% of the AQY of OCS. Station 5 was the only station where a substantial amount of photoproduction occurred below the mixed layer. The region below the mixed layer is thus a depth where in-situ production of CS_2 occurs, but opposite to the mixed layer, air-sea exchange does not act as the major sink. Therefore, a sensitivity run with an assumed absence of a sink below the mixed layer was performed for station 5 to assess whether an additional sink process is required. With the absence of a sink, the subsurface concentrations were drastically overestimated (>110 pmol L^{-1}). An additional simulation to estimate both AQY and a first-order sink revealed a sink with a lifetime of 30 days for station 5.

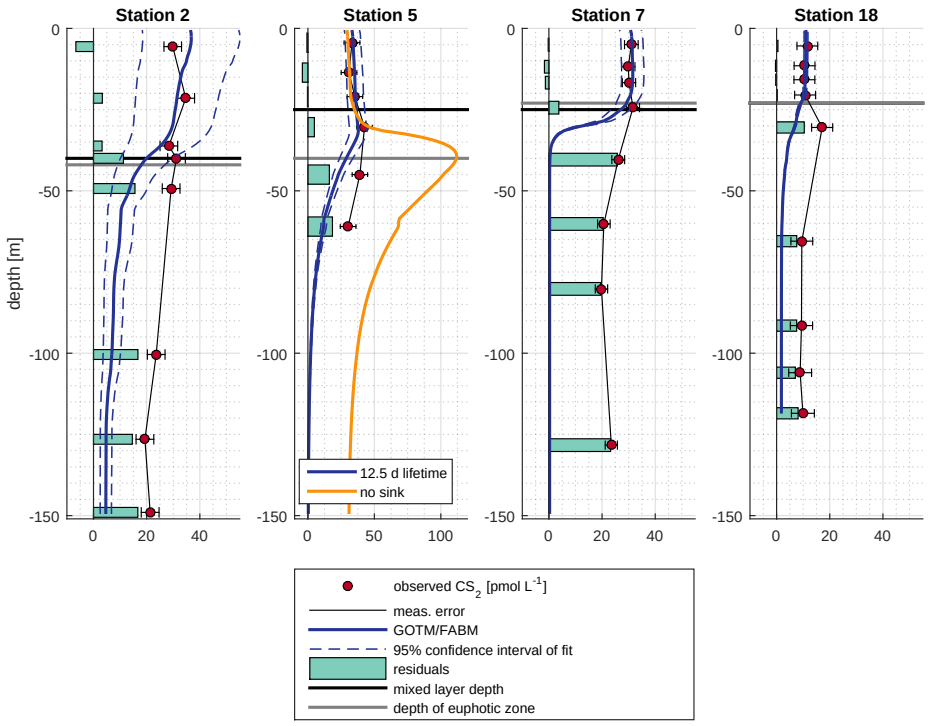

Figure 5.10: Observed (red circles), simulated (blue line) and residuals (green bars) concentration profiles of CS_2[pmol L^{-1}] at the stations 2, 5, 7 and 18 along the cruise track of ASTRA-OMZ.

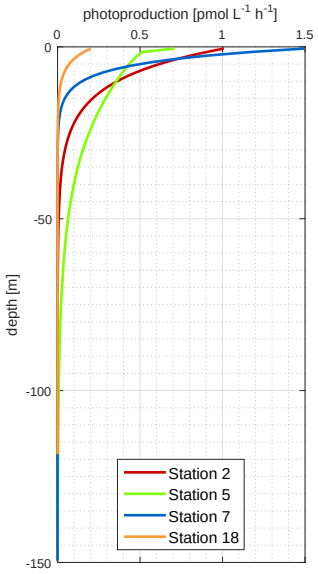

Figure 5.11: Photoproduction rates of CS_2 at stations 2, 5, 7, and 18 as simulated with the FABM/GOTM model.

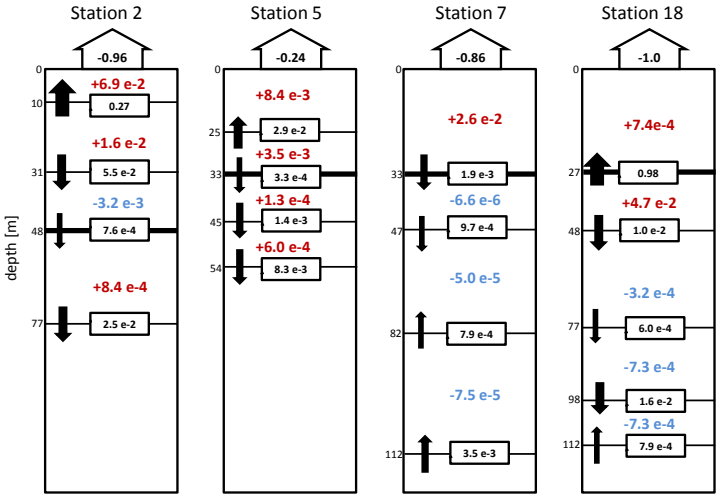

Figure 5.12: CS_2 fluxes within the water column as calculated using measured concentrations and microstructure profiles. Black arrows indicate fluxes corresponding to the fluxes in pmol s^{-1} m^{-3} given in black boxes respective for reference level. Thick black lines indiacte mixed layer. Local sources (red) and sinks (blue) are given in pmol m^{-3} s^{-1}.

5.4 Discussion

5.4.1 Carbonyl sulfide (OCS)

Dark production

The surface production rates found during this cruise are at the upper end of the range of previously reported dark production rates of the open ocean (Flöck & Andreae, 1996; Ulshöfer et al., 1996, 1995; Von Hobe et al., 2001, 1999), but similar to the Mauritanian upwelling region (Von Hobe et al., 1999).These results suggest that highest dark production rates might be encountered in upwelling regions. Upwelling effects both drivers of dark production rates, temperature and a_{350}, in a counteracting way. Cold temperatures decrease dark production rates, whereas higher a_{350} increases them. When the surface water is transported further away at the coasts, these effects switch: Surface temperatures are warmed, and a_{350} decreases slightly decreases because of photobleaching (Nelson & Siegel, 2013). Given the observed spatial pattern of increasing surface dark production rates further away from the coast, the temperature seems to be the dominant controlling factor. Despite the photobleaching at the surface, a_{350} is still high in the ETSP compared to open ocean regions, which is likely to be the reason for increased dark production rates in upwelling regions.

The temperature dependency of the dark production is very similar to the one found by (Von Hobe et al., 2001) in the North Atlantic, North Sea and Mediterranean (Fig. 5.9). However, the overall magnitude of dark production is higher in the ETSP compared to the region covered by Von Hobe et al. (2001). The similar temperature dependency points towards an ubiquitous process across different biogeochemical regimes, as it is very similar for an oligotrophic region like the Sargasso Sea and a nutrient rich and biologically very productive region as in the ETSP. The different magnitude in the dark production rates when normalized to a_{350} most likely indicates that the fraction of the actual precursor (e.g. S-containing and/or radical forming compound) to a_{350} varied between both studies. Unfortunately, no data on DOS is available from the previous study for comparison.

The higher covariation of a_{350} compared to SPE-DOS, VIS FDOM and dissolved O_2 indicates that a chemical property common to most of the CDOM (a_{350}) determines the dark production rate. Molecules that absorb light and are thus part of the CDOM pool often display similar chemical features such as unsaturated bonds and non-bonding orbitals (Coble, 2007). These properties also favor radical stability. Therefore, the higher covariation of CDOM compared to other parameters supports the radical hypothesis for dark production suggested by Pos et al. (1998). While we cannot rule out a microbial process completely,

such a process seems unlikely because of the low influence of parameters such as O_2 that have a large influence on shaping the microbial community.

At 50 and 136 m at station 5, the dark production rate was larger than predicted for the temperature and the a_{350} present. Most likely, the steady-state conditions required for the determination of the dark production rate was violated, possibly because of physical transport processes. Downwelling occurred within this eddy, possibly leading to a nonnegligible, physically caused input of OCS from the surface down to 50 m. No concentration below 136m was measured to determine any physically caused fluxes there, leaving the increase at this depth for this station unexplained. These results thus suggest that mesoscale features such as eddies might influence the distribution of OCS in the water column by vertical physical transport processes.

Photoproduction of OCS

The photoproduction rates of OCS showed some spatial variations with an increase towards shelf and upwelling stations, but error bands in the fitted parameters for the AQY overlapped. This indicates an overall similar AQY for the ETSP. According to eq. 5.3, the variation in the photoproduction rate within the ETSP is hence mainly determined by the amount of CDOM approximated by a_{350}.

The AQY does not show any regional dependence on a_{350}, as had been previously reported (von Hobe et al., 2003), but rather covaries with VIS-FDOM. The covariations allow speculations about the occurrence of possible reaction mechanisms under environmental conditions, that have been reported from laboratory experiments. (Pos et al., 1998) suggested a coupled production pathway of CO and OCS, which would involve a photosensitizer for both substances from the CDOM pool (i.e. an acyl radical formed by photolysed carbonyl groups), a S-containing precursor in the case of OCS (thiyl or sulfhydryl radical) and, potentially, metal redox systems to form these radicals. Incubation studies have confirmed that molecules containing thiol-groups are precursors for OCS in a radical reaction (Flöck & Andreae, 1996; Flöck et al., 1997). Photoproduction of CO in natural waters has been shown to vary not primarily by the amount of carbonyl groups available, but by the aromaticity of the whole molecule that contains the carbonyl group (Stubbins et al., 2008). Therefore, high-aromatic, humic-like substances showed the highest CO production (Stubbins et al., 2008). Similar to production rates of CO in Stubbins et al. (2008), production rates of OCS in our study showed a higher correlation with VIS-FDOM, indicating that humic-like substances play a key role. A coupled production pathway as suggested by Pos et al. (1998) is thus consistent with our data, as the production seems to be coupled to high-aromatic, humic-like substances as would be expected for CO.

Interestingly, the AQY does not seem to covary with any sulfur related parameter tested (SPE-DOS, DMSO, DMSP), opposite to findings of Cutter et al. (2004). The fact that SPE-DOS does not seem to be determine the AQY either 1) confirms that the limiting factor in this reaction is not the sulfur source but the photosensitizer or 2) indicates that the S-containing precursor is very specific and not a major part of the SPE-DOS pool.
The missing correlation to a_{350} opposite to previous findings in von Hobe et al. (2003) is explicable, if a_{350} and VIS-FDOM covaried in the areas investigated in this study. Such a covariance is likely, as the study did not cover any upwelling regions that would introduce major amounts of VIS-FDOM in the surface DOM pool and alter the ratio between a_{350} and VIS-FDOM. Also, the study covered a larger range of a_{350} from 0.03 to 0.29 m^{-1}, which makes an overall correlation more likely. Scaling the AQY to a_{350} might thus be valid for a global relationship spanning a large CDOM (a_{350}) range, but might be regionally improved by using VIS-FDOM. The fact that VIS-FDOM explains the AQY better than a_{350} might be the reason for the large scatter observed in the global AQY-CDOM relationship in Lennartz et al. (2017).

Diapycnal mixing

The diapycnal mixing shows that, in general, downward fluxes of OCS that is produced at the surface. Diapycnal mixing thus acts as a sink in the surface mixed layer. However, fluxes are always two or three orders of magnitude smaller than emissions to the atmosphere, except for station 18. There, diapycnal fluxes were almost half of the air-sea flux, most likely due to low temperatures and low wind speeds, which reduce the relative significance of other sinks (hydrolysis and air-sea exchange) in the mixed layer. In total, neglecting diapycnal fluxes when calculating OCS concentrations in surface mixed layer box models may thus lead to minor overestimations of the concentrations.

At station 7, where observations covered the whole water column down to the sediment surface, very small upward diapycnal fluxes indicate a minor net source at the bottom of the water column. OCS production has been shown for the porewater of sediments (Cutter & Radford-Knoery, 1993), and is a very likely explanation for the observed net source, but the impact of sedimental input on concentrations in the water column is overall only minor.

Modeling of OCS

OCS concentrations could be modeled with the new, regionally valid parameterization of dark production as well as a single AQY within the water column for each station. At stations

Table 5.2: Fitted AQY for stations 2, 5, 7, and 18 with error metrics. RMSE=root mean square error, ME=mean error, AME=absolute mean error.

	Station 2 'open ocean'		Station 5 'eddy'		Station 7 'shelf'		Station 18 'coastal shelf'	
	OCS	CS_2	OCS	CS_2	OCS	CS_2	OCS	CS_2
AQY [pmol J^{-1}]	0.3964	0.0783	0.2086	0.0772	0.4098	0.0762	0.4374	0.0235
lower C.I. [pmol J^{-1}]	0.2840	0.0392	0.0119	0.0638	0.3398	0.0661	0.3385	0.0126
upper C.I. [pmol J^{-1}]	0.5088	0.1174	0.4053	0.0905	0.4797	0.0864	0.5363	0.0144
RMSE [pmol L^{-1}]	0.72	12.28	3.64	10.35	0.57	15.87	3.72	6.13
ME [pmol L^{-1}]	0.43	9.35	0.79	5.7	0.04	11.16	1.87	4.51
AME [pmol L^{-1}]	0.67	11.0	2.96	7.46	0.50	11.98	2.21	4.68

2 and 7, where the steady state assumption is very likely to be valid, RMSE were only minor, indicating that process understanding is high enough to model subsurface concentrations of OCS. At station 5, observed deviations from the typical decreasing concentration profile with depth could not be reproduced with the 1D model. Most likely, this mismatch occurs since the 1D model is not able to reproduce the vertical downwelling introduced by the eddy. At station 18, the general shape was reproduced but concentrations were slightly underestimated. High internal wave activity at this station led to subsurface vertical water displacements of up to 50 m within the water column, which is not reproduced in the 1D model. Therefore, the steady state assumption might have been violated at station 18. However, since the general shape of the profile was well reproduced, the processes parameterizations that have been shown to determine concentrations in mixed layer box models are also applicable to the subsurface water column.

5.4.2 Carbon disulfide (CS_2

Photoproduction of CS_2

CS_2 did not show strong diurnal cycles as would be expected for a photochemically produced compound. This had been shown previously in some locations (Kettle et al., 2001), but not all (Xu, 2001). However, at wind speeds of 8-10 m s^{-1} as encountered during the cruise, air-sea exchange is enough to mask diurnal variations in the surface layer. The modeled

diurnal amplitude is on the order of 1-2 pmol L^{-1}. It is likely that such small amplitudes are masked by spatial heterogeneity and the error associated with the GC-MS measurements of CS_2.

The estimated AQY for CS_2 (eq. 5.3) were stable for stations 2, 5 and 7, but considerably lower for station 18 (Tab. 5.2). The lower surface concentrations closest to the continent are thus a result of smaller photoproduction rates along the shelf. This pattern mirrors the pattern of the slope in absorption spectra (Fig. 5.2), suggesting that concentrations and thus production rates increase with an increasing fraction of smaller, labile molecules. This covariance might indicate that a process related to biological fresh production appears. Xie et al. (1999) found that the species *Chaetoceros calcitrans*, *Phaeodactylum tricornutum*, and *Phaeocystis sp.* produce CS_2, the first two belonging to the groups of diatoms and the latter to the group of haptophytes. However, we compared the CS_2 data to pigment data from diatoms and haptophytes, that were the dominant plankton groups at these stations, and could not detect any positive correlation. It thus seems likely, that the observed CS_2 production is not directly related to these species alone, but either to other species not detected or to photochemical production, with the limiting precursor influenced by fresh biological production.

The ratio between the AQY of CS_2 and OCS is stable at 18-19% for stations 2 and 7, which represent 'open ocean' and 'shelf'. This ratio confirms a ratio of 4:1 between the AQY of OCS and CS_2 derived in a previous study where the CS_2 AQY was measured wavelength resolved by incubation experiments with seawater from the Atlantic Ocean. The ratio is significantly larger at stations 5 and 18, i.e. 37 and 30%, where downwelling (eddy, station 5) and coastal upwelling (station 18) occurred. Both station 5 and 18 therefore display a DOM pool at the surface that is influenced by subsurface DOM. The results suggest that a ratio of 20% between the AQY seems a valid approximation across different biogeochemical regimes, but deviations from this ratio can occur if subsurface DOM reaches the mixed layer.

Gradients within the mixed layer

Concentration gradients within the mixed layer were observed for station 2, but not for stations 5, 7 and 18, where concentrations in the mixed layer were very homogeneous. Station 2 was the only station where a weak stratification was visible in the density profile, indicating a diurnal stratification based on daytime heat influx. This has been previously observed by and it had been speculated that this can affect the distribution of substances in the mixed layer. The mixed layer variations from station 2 confirm such a hypothesis. Most likely, the diurnal stratification suppresses the mixing and thus acts as a small barrier for

photochemically produced CS_2 at the bottom of the mixed layer. The observed peak is thus very likely an accumulation peak as a result of weak stratification within the mixed layer.

Subsurface processes

The strongest subsurface peak directly below the mixed layer is found at stations 5 and 18. The model simulations suggest that a substantial part of the photoproduction still takes place below the mixed layer at station 5 (Fig. 5.10). There, the bottom of the mixed layer acts as a barrier to prevent CS_2 from outgassing, which leads to a physical accumulation of CS_2 and thus a concentration peak in the water column profile. Such a peak is not present for OCS although it is similarly photochemically produced, but its chemical degradation is too fast (lifetimes in the order of hours) to enable accumulation. However, the strong *in-situ* production of CS_2 below the mixed layer at station 5 requires an additional sink process below the mixed layer, as concentrations are drastically overestimated (>110 pmol L^{-1}) when no sink is assumed (Fig. 5.10). To explain the observed concentration, an additional sink with a lifetime on the order of at least 30 days is needed, which corresponds to a first-order reaction rate of 3.8e-7 s^{-1}. Such a sink is smaller than required for the mixed layer model in Kettle (2000) with a lifetime 11-13 days, but substantially larger than found in incubation experiments by Elliott (1990) with a lifetime ca. 1-2 years. However, the experiments of the latter study were performed with artificial seawater, which might not be transferable to environmental conditions. Possibly, the presence of other molecules can catalyze the reaction. Unfortunately, the photoproduction below the mixed layer was only observed for station 5, which was located within the eddy. The eddy already led to changed concentration patterns in the water column for OCS, and we cannot exclude here that previous mixing dynamics during the travel of the eddy might have led to deviations of the concentration profiles. The *in-situ* photoproduction below the mixed layer however requires the presence of a subsurface sink to explain observed concentration patterns.

The evidence for an *in-situ* sink at station 5 points towards the existence of such a significant sink processes also at other stations, which might be masked by a concurrent production process. With an unknown production and an unknown consumption process, subsurface processes for CS_2 are very badly constrained, making it impossible to derive rates from observed profiles. The sink with a lifetime of 30 days at station 5 could also be stronger, if an additional source process occurs at the same time. Quantitative knowledge on either the source or the sink process is needed to derive the other from observed concentration profiles.

Internal fluxes in the water column as budgeted from microstructure profiles indicated an upward flux at the lowermost budgeted volumes for stations 7 which was a magnitude

higher than fluxes across other budgeted volumes in the water column. At station 7, the profiles reached the sediment surface. Therefore, the net source indicated by an inward flux to the lowermost budgeted volume indicates that the flux across the sediment-water interface of CS_2 into the water column might be more significant than for OCS. At station 18, such a flux was not observed at the bottom of the profile, although the profile extended down to the sediment surface. However, high internal wave activity at station 18 led to a large vertical water displacement of up to 50 m. With such a displacement, water that has been in contact to the sediment previously can be brought upwards below the mixed layer. Potentially, this displacement explains the subsurface peak observed at station 18, which leads to a flux into the mixed layer on the order of that of emissions to the atmosphere (Fig. 5.12). This would imply that subsurface processes at the sediment surface can have an influence on mixed layer concentrations and, thus, emissions of CS_2 to the atmosphere.

5.5 Summary and conclusion

Concentrations of OCS and CS_2 were measured at the surface during transects from the equator down to 24°S, and within the water column at four stations in the ETSP. Measurements of photochemically relevant fractions of the DOM pool, microstructure profiles and a newly developed module for a GOTM/FABM model environment for both gases were used to systematically assess processes determining the distribution of the gases in the water column.

For the first time, we show that process parameterizations valid for surface box models can also be used to model subsurface OCS profiles in agreement with observations in an upwelling region. Below the mixed layer, dark production and hydrolysis together with physical transport processes control the distribution of OCS in the water column. The same temperature dependency in dark production found for the ETSP in this study and the Atlantic Ocean with adjacent seas in a previous study indicates that dark production shows a ubiquitous reaction mechanism across different biogeochemical regimes. These findings suggest that dark production can thus be scaled to other locations using a '1-point-correction', where the same temperature trend is used when the offset is known. The inverse set-up of the newly developed 1D water column model proved useful to determine photoproduction rates for OCS. The photoproduction rates were used to derive the quantum yield, which is the parameter that is most difficult to predict when modeling OCS concentrations. A covariation of the AQY for OCS and a DOM pool with a large fraction of upwelled, humic like substances is consistent with a previously reported hypothesis of OCS formation by a radical reaction. The production of OCS seems to be not limited by a

sulfur-containing precursor from within the DOM pool, but rather by radical precursors.

Our results also confirm an upper limit of the AQY of CS_2 on the order of 20% of that of OCS from a previous study in the Atlantic Ocean, showing a surprising similarity in this ratio across various biogeochemical regimes. Furthermore, we provide first field evidence for a significant subsurface sink of CS_2, however, this could only be observed at one out of four stations. The general occurrence of such an additional sink process requires the presence of a subsurface source process to explain observed concentrations, which are relatively stable within the water column. Neither such a source nor a sink process is currently known. With both, subsurface sources and sinks, only poorly constrained, our results call for targeted incubation studies that define the magnitude and drivers for at least one of these processes. Knowledge on at least one of the processes would help to derive missing processes from observed concentration profiles.

References

Arévalo-Martínez, D. L.; Beyer, M.; Krumbholz, M.; Piller, I.; Kock, A.; Steinhoff, T.; Körtzinger, A. & Bange, H. W. (2013): A new method for continuous measurements of oceanic and atmospheric N2O, CO and CO_2: performance of off-axis integrated cavity output spectroscopy (OA-ICOS) coupled to non-dispersive infrared detection (NDIR). *Ocean Sci.* **9** (6): 1071–1087.

Bruggeman, J. & Bolding, K. (2014): A general framework for aquatic biogeochemical models. *Environmental Modelling & Software* **61**: 249–265.

Brühl, C.; Lelieveld, J.; Crutzen, P. J. & Tost, H. (2012): The role of carbonyl sulphide as a source of stratospheric sulphate aerosol and its impact on climate. *Atmos. Chem. Phys.* **12** (3): 1239–1253.

Campbell, E.; Kesselmeier, J.; Yakir, D.; Berry, J. A.; Peylin, P.; Belviso, S.; Vesala, T.; Maseyk, K.; Seibt, U.; Chen, H.; Whelan, M.; Hilton, T.; Montzka, S.; Lennartz, S.; Kuai, L.; Wohlfahrt, G.; Wang, Y.; Blake, N. & Blake, D. (2017): Assessing a New Clue to How Much Carbon Plants Store. *EOS Earth and Space Science News.*

Chavez, F. P.; Bertrand, A.; Guevara-Carrasco, R.; Soler, P. & Csirke, J. (2008): *The northern Humboldt Current System: Brief history, present status and a view towards the future.*

Chin, M. & Davis, D. D. (1993): Global sources and sinks of OCS and CS_2 and their distributions. *Global Biogeochemical Cycles* **7** (2): 321–337.

Coble, P. G. (2007): Marine optical biogeochemistry: the chemistry of ocean color. *Chemical Reviews* **107** (2): 402–418.

Cutter, G. A.; Cutter, L. S. & Filippino, K. C. (2004): Sources and cycling of carbonyl sulfide in the Sargasso Sea. *Limnology and Oceanography* **49** (2): 555–565.

Cutter, G. A. & Radford-Knoery, J. (1993): Carbonyl sulfide in two estuaries and shelf waters of the western North Atlantic Ocean. *Marine Chemistry* **43** (1–4): 225–233.

De Gouw, J. A.; Warneke, C.; Montzka, S. A.; Holloway, J. S.; Parrish, D. D.; Fehsenfeld, F. C.; Atlas, E. L.; Weber, R. J. & Flocke, F. M. (2009): Carbonyl sulfide as an inverse tracer for biogenic organic carbon in gas and aerosol phases. *Geophysical Research Letters* **36** (5)

Dickinson, A. G. & Riley, J. (1979): The estimation of acid dissociation constants in seawater media from potentiometric titrations with strong base. *Mar. Chem.* **7**: 89–99.

Dittmar, T.; Koch, B.; Hertkorn, N. & Kattner, G. (2008): A simple and efficient method for the solid-phase extraction of dissolved organic matter (SPE-DOM) from seawater. *Limnol. Oceanogr. Methods* **6** (6): 230–235.

Elliott, S. (1990): Effect of hydrogen peroxide on the alkaline hydrolysis of carbon disulfide. *Environmental Science & Technology* **24** (2): 264–267.

Elliott, S.; Lu, E. & Rowland, F. S. (1989): Rates and mechanisms for the hydrolysis of carbonyl sulfide in natural waters. *Environmental Science & Technology* **23** (4): 458–461.

Fischer, T.; Banyte, D.; Brandt, P.; Dengler, M.; Krahmann, G.; Tanhua, T. & Visbeck, M. (2013): Diapycnal oxygen supply to the tropical North Atlantic oxygen minimum zone. *Biogeosciences* **10** (7): 5079.

Flöck, O. & Andreae, M. O. (1996): Photochemical and non-photochemical formation and destruction of carbonyl sulfide and methyl mercaptan in ocean waters. *Marine Chemistry* **54**: 11–26.

Flöck, O. R.; Andreae, M. O. & Dräger, M. (1997): Environmentally relevant precursors of carbonyl sulfide in aquatic systems. *Marine Chemistry* **59** (1–2): 71–85.

Glatthor, N.; Höpfner, M.; Baker, I. T.; Berry, J.; Campbell, J. E.; Kawa, S. R.; Krysztofiak, G.; Leyser, A.; Sinnhuber, B. M.; Stiller, G. P.; Stinecipher, J. & Clarmann, T. v. (2015): Tropical sources and sinks of carbonyl sulfide observed from space. *Geophysical Research Letters,*: 10082–10090.

Helms, J. R.; Stubbins, A.; Ritchie, J. D.; Minor, E. C.; Kieber, D. J. & Mopper, K. (2008): Absorption spectral slopes and slope ratios as indicators of molecular weight, source, and photobleaching of chromophoric dissolved organic matter. *Limnology and Oceanography* **53** (3): 955–969.

Hummels, R.; Dengler, M. & Bourlès, B. (2013): Seasonal and regional variability of upper ocean diapycnal heat flux in the Atlantic cold tongue. *Progress in Oceanography* **111**: 52–74.

Jorgensen, L.; Stedmon, C. A.; Kragh, T.; Markager, S.; Middelboe, M. & Sondergaard, M. (2011): Global trends in the fluorescence characteristics and distribution of marine dissolved organic matter. *Marine Chemistry* **126** (1-4): 139–148.

Karstensen, J.; Stramma, L. & Visbeck, M. (2008): Oxygen minimum zones in the eastern tropical Atlantic and Pacific oceans. *Progress in Oceanography* **77** (4): 331–350.

Kettle, A. J.; Rhee, T. S.; von Hobe, M.; Poulton, A.; Aiken, J. & Andreae, M. O. (2001): Assessing the flux of different volatile sulfur gases from the ocean to the atmosphere. *Journal of Geophysical Research: Atmospheres* **106** (D11): 12193–12209.

Kettle, A. (2000): Extrapolations of the Flux of Dimethylsulfide, Carbon Monooxide, Carbonyl Sulfide and Carbon Disulfide from the Oceans. PhD thesis.

Kremser, S.; Thomason, L. W.; von Hobe, M.; Hermann, M.; Deshler, T.; Timmreck, C.; Toohey, M.; Stenke, A.; Schwarz, J. P.; Weigel, R.; Fueglistaler, S.; Prata, F. J.; Vernier, J.-P.; Schlager, H.; Barnes, J. E.; Antuña-Marrero, J.-C.; Fairlie, D.; Palm, M.; Mahieu, E.; Notholt, J.; Rex, M.; Bingen, C.; Vanhellemont, F.; Bourassa, A.; Plane, J. M. C.; Klocke, D.; Carn, S. A.; Clarisse, L.; Trickl, T.; Neely, R.; James, A. D.; Rieger, L.; Wilson, J. C. & Meland, B. (2016): Stratospheric aerosol—Observations, processes, and impact on climate. *Reviews of Geophysics* **54**: 278–335.

Ksionzek, K. B.; Lechtenfeld, O. J.; McCallister, S. L.; Schmitt-Kopplin, P.; Geuer, J. K.; Geibert, W. & Koch, B. P. (2016): Dissolved organic sulfur in the ocean: Biogeochemistry of a petagram inventory. *Science* **354** (6311): 456–459.

Kuai, L.; Worden, J. R.; Campbell, J. E.; Kulawik, S. S.; Li, K.-F.; Lee, M.; Weidner, R. J.; Montzka, S. A.; Moore, F. L.; Berry, J. A.; Baker, I.; Denning, A. S.; Bian, H.; Bowman, K. W.; Liu, J. & Yung, Y. L. (2015): Estimate of carbonyl sulfide tropical oceanic surface fluxes using Aura Tropospheric Emission Spectrometer observations. *Journal of Geophysical Research: Atmospheres* **120** (20): 11, 012–11, 023.

Launois, T.; Belviso, S.; Bopp, L.; Fichot, C. G. & Peylin, P. (2015): A new model for the global biogeochemical cycle of carbonyl sulfide - Part 1: Assessment of direct marine emissions with an oceanic general circulation and biogeochemistry model. *Atmos. Chem. Phys.* **15** (5): 2295–2312.

Lennartz, S. T.; Marandino, C. A.; von Hobe, M.; Cortes, P.; Quack, B.; Simo, R.; Booge, D.; Pozzer, A.; Steinhoff, T.; Arevalo-Martinez, D. L.; Kloss, C.; Bracher, A.; Röttgers, R.; Atlas, E. & Krüger, K. (2017): Direct oceanic emissions unlikely to account for the missing source of atmospheric carbonyl sulfide. *Atmos. Chem. Phys.* **17** (1): 385–402.

Miller, R. L.; Belz, M.; Del Castillo, C. & Trzaska, R. (2002): Determining CDOM absorption spectra in diverse coastal environments using a multiple pathlength, liquid core waveguide system. *Continental Shelf Research* **22** (9): 1301–1310.

Mueller, J. L.; Fargion, G. S.; McClain, C. R.; Pegau, S.; Zanefeld, J.; Mitchell, B. G.; Kahru, M.; Wieland, J. & Stramska, M. (2003): Ocean optics protocols for satellite ocean color sensor validation, revision 4, volume IV: Inherent optical properties: Instruments, characterizations, field measurements and data analysis protocols.

Murphy, K. R.; Stedmon, C. A.; Graeber, D. & Bro, R. (2013): Fluorescence spectroscopy and multi-way techniques. PARAFAC. *Analytical Methods* **5** (23): 6557–6566.

Murphy, K. R.; Stedmon, C. A.; Waite, T. D. & Ruiz, G. M. (2008): Distinguishing between terrestrial and autochthonous organic matter sources in marine environments using fluorescence spectroscopy. *Marine Chemistry* **108** (1): 40–58.

Nelson, N. B. & Siegel, D. A. (2013): The Global Distribution and Dynamics of Chromophoric Dissolved Organic Matter. *Annual Review of Marine Science, Vol 5* **5**: 447–476.

Nightingale, P. D.; Malin, G.; Law, C. S.; Watson, A. J.; Liss, P. S.; Liddicoat, M. I.; Boutin, J. & Upstill-Goddard, R. C. (2000): In situ evaluation of air-sea gas exchange parameterizations using novel conservative and volatile tracers. *Global Biogeochemical Cycles* **14** (1): 373–387.

Paulson, C. A. & Simpson, J. J. (1977): Irradiance measurements in the upper ocean. *Journal of Physical Oceanography* **7** (6): 952–956.

Pos, W. H.; Riemer, D. D. & Zika, R. G. (1998): Carbonyl sulfide (OCS) and carbon monoxide (CO) in natural waters: evidence of a coupled production pathway. *Marine Chemistry* **62** (1–2): 89–101.

Radford-Knoery, J. & Cutter, G. A. (1994): Biogeochemistry of dissolved hydrogen sulfide species and carbonyl sulfide in the western North Atlantic Ocean. *Geochimica et Cosmochimica Acta* **58** (24): 5421–5431.

Schauffler, S. M.; Atlas, E. L.; Flocke, F.; Lueb, R. A.; Stroud, V. & Travnicek, W. (1998): Measurements of bromine containing organic compounds at the tropical tropopause. *Geophysical Research Letters* **25** (3): 317–320.

Schlundt, M.; Brandt, P.; Dengler, M.; Hummels, R.; Fischer, T.; Bumke, K.; Krahmann, G. & Karstensen, J. (2014): Mixed layer heat and salinity budgets during the onset of the 2011 Atlantic cold tongue. *Journal of Geophysical Research: Oceans* **119** (11): 7882–7910.

Sheng, J.-X.; Weisenstein, D. K.; Luo, B.-P.; Rozanov, E.; Stenke, A.; Anet, J.; Bingemer, H. & Peter, T. (2015): Global atmospheric sulfur budget under volcanically quiescent conditions: Aerosol-chemistry-climate model predictions and validation. *Journal of Geophysical Research: Atmospheres* **120** (1): 2014JD021985.

Simo, R.; Grimalt, J. O. & Albaiges, J. (1996): Sequential method for the field determination of nanomolar concentrations of dimethyl sulfoxide in natural waters. *Analytical chemistry* **68** (9): 1493–1498.

Solomon, S.; Kinnison, D.; Bandoro, J. & Garcia, R. (2015): Simulation of polar ozone depletion: An update. *Journal of Geophysical Research: Atmospheres* **120** (15): 7958–7974.

Stedmon, C. A. & Bro, R. (2008): Characterizing dissolved organic matter fluorescence with parallel factor analysis: a tutorial. *Limnology and Oceanography: Methods* **6** (11): 572–579.

Stramma, L.; Fischer, T.; Grundle, D. S.; Krahmann, G.; Bange, H. W. & Marandino, C. A. (2016): Observed El Niño conditions in the eastern tropical Pacific in October 2015. *Ocean Sci.* **12** (4): 861–873.

Stubbins, A.; Hubbard, V.; Uher, G.; Law, C. S.; Upstill-Goddard, R. C.; Aiken, G. R. & Mopper, K. (2008): Relating Carbon Monoxide Photoproduction to Dissolved Organic Matter Functionality. *Environmental Science & Technology* **42** (9): 3271–3276.

Uher, G. & Andreae, M. O. (1997): The diel cycle of carbonyl sulfide in marine surface waters: field study results and a simple model. *Atmospheric Geochemistry* **2**: 313–344.

Ulshöfer, V.; Flöck, O.; Uher, G. & Andreae, M. O. (1996): Photochemical production and air-sea exchange of carbonyl sulfide in the eastern Mediterranean Sea. *Marine Chemistry* **53**: 25–39.

Ulshöfer, V.; Uher, G. & Andreae, M. O. (1995): Evidence for a winter sink of atmospheric carbonyl sulfide in the northeast Atlantic Ocean. *Geophysical Research Letters* **22** (19): 2601–2604.

Umlauf, L.; Burchard, H. & Bolding, K. (2005): *GOTM - scientific documentation.* Tech. rep.

Von Hobe, M.; Cutter, G. A.; Kettle, A. J. & Andreae, M. O. (2001): Dark production: A significant source of oceanic COS. *Journal of Geophysical Research* **106** (C12): 31217.

Von Hobe, M.; Kettle, A. J. & Andreae, M. O. (1999): Carbonyl sulphide in and over seawater: summer data from the northeast Atlantic Ocean. *Atmospheric Environment* **33**: 3503–3514.

Von Hobe, M.; Najjar, R.; Kettle, A. & Andreae, M. (2003): Photochemical and physical modeling of carbonyl sulfide in the ocean. *Journal of Geophysical Research* **108** (C7)

Watts, S. F. (2000): The mass budgets of carbonyl sulfide, dimethyl sulfide, carbon disulfide and hydrogen sulfide. *Atmospheric Environment* **34** (5): 761–779.

Weiss, P.; Andrews, S.; Johnson, J. E. & Zafiriou, O. (1995): Photoproduction of carbonyl sulfide in south Pacific Ocean waters as a function of irradiation wavelength. *Geophysical Research Letters* **22** (3): 215–218.

Xie, H.; Moore, R. M. & Miller, W. L. (1998): Photochemical production of carbon disulphide in seawater. *Journal of Geophysical Research: Oceans* **103** (C3): 5635–5644.

Xie, H.; Scarratt, M. G. & Moore, R. M. (1999): Carbon disulphide production in laboratory cultures of marine phytoplankton. *Atmospheric Environment* **33** (21): 3445–3453.

Xu, X. (2001): Investigations into the tropospheric cycle of COS: atmospheric distribution, air-sea and air-vegetation exchanges. PhD thesis.

Zepp, R. G. & Andreae, M. O. (1994): Factors affecting the photochemical production of carbonyl sulfide in seawater. *Geophysical Research Letters* **21** (25): 2813–2816.

6

Conclusion and Outlook

The goal of this thesis was to quantify marine emissions of sulfur gases, with an emphasis on carbonyl sulfide (OCS), carbon disulfide (CS_2), and dimethyl sulfide (DMS). This goal is motivated by the necessity to better understand feedbacks in the climate system, for which well quantified sources and sinks of these gases to the atmosphere are required. However, their marine emissions are still associated with high uncertainties. The atmospheric budget of OCS includes direct and indirect emissions from the precursor gases DMS and CS_2. Its atmospheric budget currently exhibits a large gap.
In order to assess marine emissions and their feedbacks, coupled oceanic and atmospheric models are required. Four steps are needed for a successful implementation of OCS, CS_2 and DMS in ocean models: 1) availability of field data for validation, 2) process understanding, 3) process quantification, and, 4) the actual implementation and validation of relevant processes in the model. This thesis combines local scale measurements with newly developed sampling systems, database compilations, and local (1D) to global scale (2D and 3D) modeling, to contribute to these steps (Fig. 6.1). Based on the results of this thesis, the research questions raised in section 1.4 can be answered as follows:

I **What is the best method to model marine emissions in atmospheric stand alone 3D models?**
Using commonly applied flux and concentration climatologies of DMS and three halocarbons were used to systematically assess the difference between offline and online calculation of emissions. The results highlight the strong influence of atmospheric mixing ratios on emissions and suggest that interactive online calculation of emissions improves the accuracy of simulated atmospheric mixing ratio for two groups of gases. First, gases concentrated close to equilibrium benefit from the online calculation of emissions based on prescribed climatologies of sea surface trace gas concentrations.

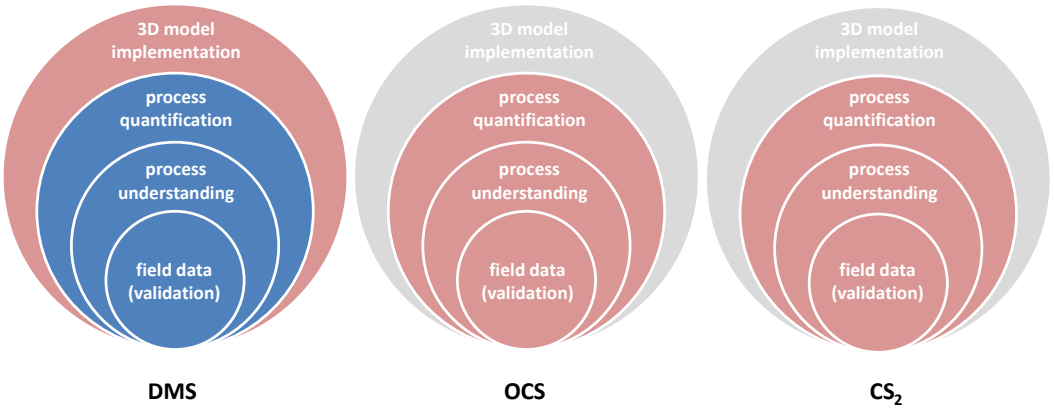

Figure 6.1: Level of previous knowledge and contributions of this thesis towards comprehensively modeling sulfur emissions of OCS, CS_2 and DMS in 3D numerical models. Previous knowledge is indicated by blue circles, fields to which this thesis contributed to previous knowledge are indicated in red and spheres with low level of knowledge are colored in grey.

Their emissions are very sensitive to changes in the atmospheric mixing ratios during the model simulation, and only an online calculation allows for such a feedback. Gases that are concentrated further away from equilibrium did not show a large improvement by prescribing concentrations instead of emissions. For such gases, prescribing flux climatologies is sufficient. Second, calculating emissions online makes a difference for gases which are commonly statically calculated offline with an atmospheric mixing ratio of 0 ppt due to their generally low atmospheric concentration and short lifetime, such as DMS. The results show that for DMS, the marine flux was considerably lower and was more consistent with observations when emissions were calculated online.

II **What is the global marine source strength of OCS?**
The global marine source strength was investigated with respect to the missing tropical source. Only few tropical measurements had been available previously, mostly from Atlantic transect cruises, and are now complemented by new measurements from all three major tropical ocean basins. The measurements show that large areas of the tropical oceans are undersaturated of OCS. Using the new data together with previously reported photoproduction rates led to a new parameterization for global OCS photoproduction, for the first time including information from the Atlantic, the Pacific and the Indian Ocean. Global sea surface concentrations consistent with more than 3000 previous measurements were simulated with a mixed layer box model. The

resulting emissions of 130 (±80) Gg S yr^{-1} confirmed that the global ocean is a major direct source of OCS to the atmosphere, but is very unlikely to account for the enhanced atmospheric mixing ratios in the tropics and, thus, the missing source. Emission estimates of the precursor gases CS_2 and DMS were included, and are also unlikely to account for that missing source. However, the uncertainties in oceanic emissions of CS_2 and in the conversion of DMS to OCS are still large. This study also provides monthly resolved concentration maps for sea surface concentrations of OCS for the use in atmospheric models.

III **Which processes drive the marine biogeochemical cycling of OCS and CS_2?** Water column concentration profiles of both gases in the Eastern Tropical South Pacific (ETSP) were systematically assessed with respect to biogeochemical and physical processes and similarities to other oceanic provinces. OCS could be modeled with good agreement with observations below the mixed layer, indicating that process parameterizations of surface mixed layer box models can be used above and below the mixed layer. A temperature dependency in a light-independent production process of OCS similar to the North Atlantic was found, which promises a validity on global scales. The most uncertain parameter in the determination of the photoproduction rate, the apparent quantum yield (AQY), showed minor variations but was lower in a mesoscale eddy where less humic substances were available, suggesting an influence of the composition of the dissolved organic matter pool on the AQY. Subsurface process understanding of CS_2 was considerably lower, but first field evidence of an *in-situ* sink process below the mixed layer is provided in this study. The AQY for CS_2 was stable across open ocean and shelf regions including spatial variations in the composition of dissolved organic matter. The AQY was considerably lower close to coastal upwelling, coinciding with an altered composition of the dissolved organic matter pool towards low-molecular-weight substances. The low photoproduction rates along the shelf partly explain the observed opposite concentration pattern of CS_2 and OCS. AQY ratios of both substances were remarkably stable on open ocean and shelf stations when compared to previous measurements. Such systematic similarities are promising for global modeling studies of CS_2.

As a result of this thesis, the role of oceanic emissions in the atmospheric budget of OCS is now better constrained, since it is based on a broader spatial data coverage including tropical key regions, and a global mixed-layer model consistent with previous observations. Combining results of all three studies, the complete direct and indirect marine emissions of

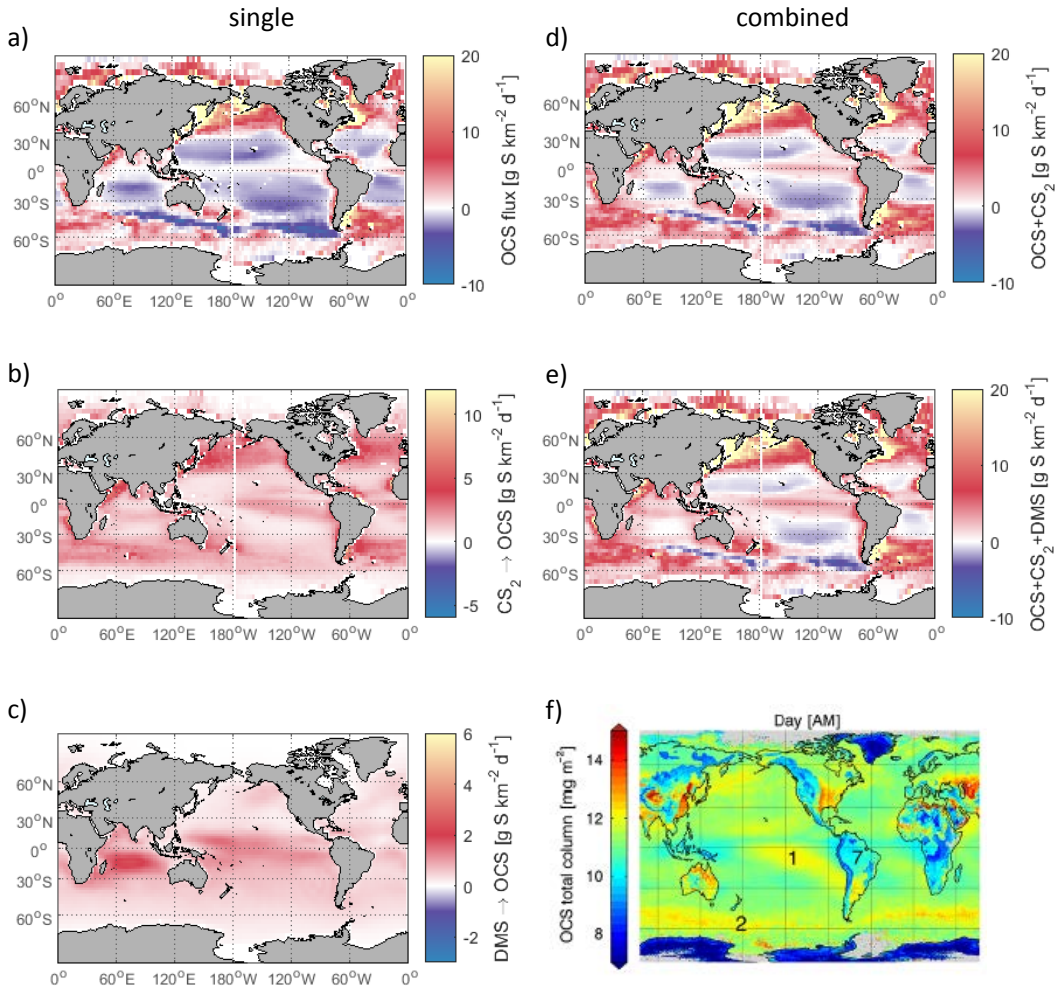

Figure 6.2: Annual mean of direct and indirect emissions of OCS from the global oceans. Left column: Marine emissions of sulfur from a) OCS, b) CS_2 (converted to OCS flux), and c) DMS (converted to OCS). Right column: Combined sulfur fluxes of a) OCS and CS_2, b) OCS, CS_2 and DMS and c) annual total atmospheric column mean of OCS, according to the Infrared Atmospheric Sounding Interferometer (Vincent & Dudhia, 2017).

OCS can be assessed. Direct emissions are taken from the second study's global surface mixed layer box model (130 Gg S yr^{-1}). The contribution of DMS is very uncertain due to a poorly understood conversion to OCS, but is included here for completeness. Using emissions and conversions calculated in the first and second study, the contribution of DMS to the budget of OCS is ca. 80 Gg S yr^{-1}. Making use of the constant AQY ratio between OCS and CS_2 found in the third study, a new model simulation for CS_2 is performed as a

first approximation for global CS_2 emissions from the ocean. While the simulated mean surface concentration of 12.6 pmol L^{-1} matches well with the mean of the database for CS_2 of 11.56 pmol L^{-1}, the stable ratio in AQY is a strong simplification and might need further refinement. The resulting emission estimate for CS_2 is 180 Gg S yr^{-1}, which is slightly higher but still in the range of CS_2 emissions extrapolated from measurements in the second study of this thesis. In total, the direct and indirect emissions amount to 390 Gg S yr^{-1} (including DMS). This total emission estimate is not sufficient to account for the total ocean flux of 600-1000 Gg S yr^{-1} needed if the ocean would account for the whole missing source.

Since the contribution of DMS to the atmospheric budget of OCS is debated, combined OCS surface fluxes are shown with and without DMS included (Fig. 6.2). Comparing emissions to the annual total atmospheric column mean of OCS retrieved from the Infrared Atmospheric Sounding Interferometer reveals similarities in the spatial patterns(Vincent & Dudhia, 2017). In the Southern Ocean, total column concentrations for OCS are elevated (Fig. 6.2, (2)), and coincide with large direct OCS fluxes predicted with the mixed layer box model. The elevated column means in the tropics (Fig. 6.2,(1)) resemble the predicted flux pattern of CS_2. Including DMS increases the flux especially in the tropics, e.g. the Indian and Pacific Ocean, close to where the missing source is suggested to be located. The overall flux, however, is too small to account for the source, when reported conversion factors are used. As these conversion factors are still debated, targeted experimental studies are needed to constrain the contribution of DMS.

Resolving the annual mean fluxes of direct and indirect emissions per latitude reveals that the tropical oceans turn from a sink into a source when indirect emissions are considered (Fig. 6.3). The contribution of DMS using current conversion factors remains small. The seasonality in the globally integrated emissions is driven by direct rather than indirect emissions (Fig. 6.3). This is most likely a result of the location of their main source. Whereas indirect emissions have their main source in the tropics (Fig. 6.2), where conditions such as irradiation are relatively stable yearround, OCS has its major source in the Southern Ocean, where photochemical production mainly takes place during austral summer. This simulated seasonality can be used to further confine the missing source. The missing source in the atmospheric budget of OCS had been inferred from top-down approaches, as an additional source without large seasonality was required to match observed atmospheric mixing ratios (Berry et al., 2013; Glatthor et al., 2015; Kuai et al., 2015). Given that direct marine emissions show a comparably large seasonality, this is a further indication that direct marine emissions are unlikely to account for the missing source.

The improved quantification of oceanic direct and indirect emissions as a result of this

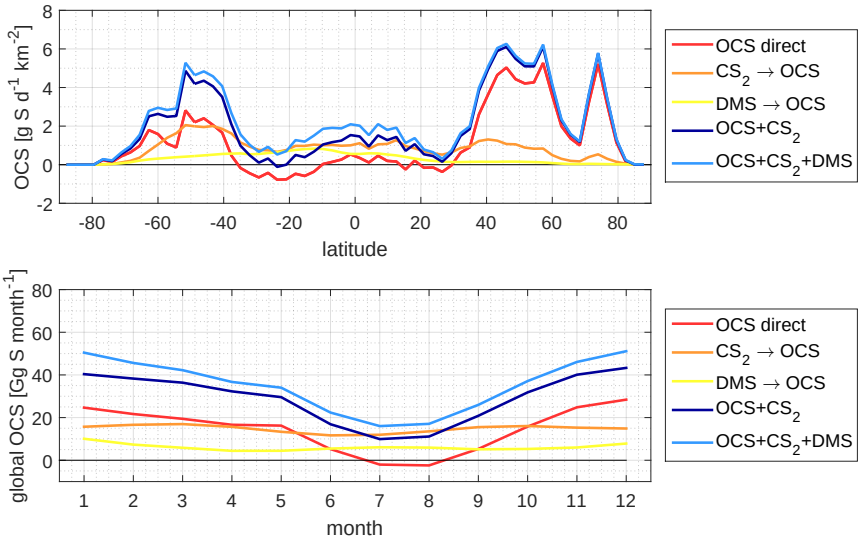

Figure 6.3: Seasonality and latitudinal dependence of global direct and indirect marine OCS emissions. Upper panel: Mean annual emissions per latitude. Lower panel: monthly resolved, globally integrated direct and combined OCS emissions.

thesis is important in two larger contexts. The first context is the climate relevance of these sulfur gases and their involvement in climate feedback mechanisms. The developed global concentration climatologies and box models of OCS and CS_2 can be used in global atmospheric chemistry climate models to assess past and future climates. Past observed variations of the stratospheric aerosol layer can be identified, when the natural background of OCS and its variations are quantified and spatially resolved. In addition, climate feedbacks can be assessed when the mixed layer box model is coupled to an atmospheric climate model. Many processes of OCS and CS_2 in the ocean are linked to environmental parameters that vary under changing climate conditions. OCS and CS_2 are thus likely to be involved in feedback effects. The impact and directions of the feedbacks are, however, not straightforward. Warmer temperatures lead to enhanced degradation of OCS by hydrolysis in seawater, but also enhanced dark production if chromophoric dissolved organic matter (CDOM) is available. The amount and composition of dissolved organic matter strongly influences OCS production rates, and is changing due to altered biological processes and altered mixed layer depths. For CS_2 a strong correlation of surface concentrations to temperature indicates a close relationship, although the mechanism behind this covariation is currently not known. This high sensitivity of process rates towards environmental parameters emphasizes the need for dynamically coupled ocean-atmosphere models to improve climate predictions.

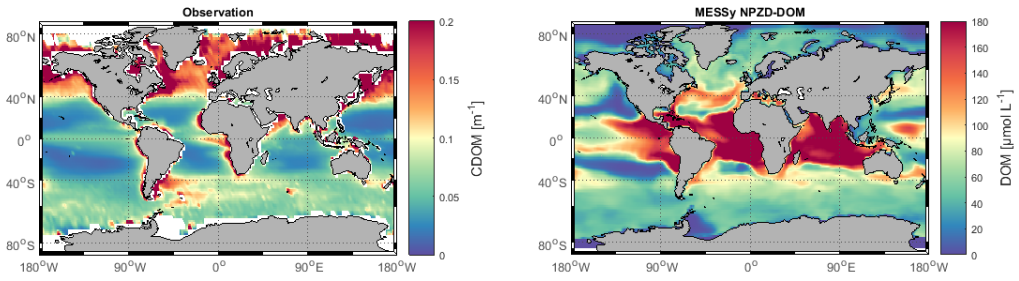

(a) CDOM from Aqua MODIS satellite.

(b) DOM modeled by HAMOCC/MESSy.

Figure 6.4: Comparison of spatial patterns in CDOM and DOM. CDOM in (a) represents the annual mean of Aqua MODIS CDOM data from 2002-2014, transferred to a wavelength of 350nm as described in chapter 4. DOM is the annual mean of 2011-2012 of the NPZD model in HAMOCC/MESSy.

The second context in which the results of this thesis advance understanding is using OCS as a tool to constrain terrestrial gross primary production on a global level. The basic idea of this concept is to infer the vegetational uptake of CO_2 from the uptake of OCS and the uptake ratio of both gases. An accurate quantification of oceanic emissions is needed, because the global vegetational OCS uptake can be derived only if all other sources and sinks in the atmospheric budget of OCS are quantified. The results of this thesis constrain the seasonality of direct and indirect OCS emissions, and thus help to confine the still missing source. Nevertheless, the budget is not yet fully explained and conclusions assuming a well explained budget cannot be fully supported. Previous conclusions based on an overestimated ocean source are likely inconsistent with observations and may need to be revised. This includes previous conclusions to constrain the global terrestrial gross primary production (Launois et al., 2015) and on the historical growth of gross primary production (Campbell et al., 2017). Before such conclusions can be drawn, the budget of OCS, including the seasonality of all major sources and sinks, need to be fully understood.

Next steps towards comprehensively implementing sulfur compounds in 3D ocean models and derive their emissions become apparent from Fig 6.1. Results of this thesis showed that for OCS, process understanding is adequate to implement surface box model parameterization in the full oceanic model realm. Relying on CDOM from satellites proved to be sufficient for the surface mixed layer box model, but is challenging for a 3D model implementation, as satellite data assimilation is not possible for the subsurface. OCS production has been tied to dissolved organic carbon (DOC) or chlorophyll *a* instead of CDOM in the past. Since CDOM on one hand and DOC or chlorophyll *a* on the other hand

exhibit a different spatial pattern (Fig. 6.4), a simple factor conversion is unlikely to be valid. A more process based parameterization for CDOM would help to overcome this problem. Furthermore, the data coverage for predicted concentration hot-spots of OCS should be extended. In this thesis, OCS hot spots are predicted for high latitudes. Observations of full diurnal cycles from these latitudes would further validate the mixed layer box model and reduce uncertainties in the magnitude of emissions.

For CS_2, data coverage and process understanding need to be expanded, both in and below the mixed layer. Latitudinal transects through ocean basins other than the Atlantic Ocean are needed to assess the correlation of concentration and temperatures on a broader spatial scale and help to further constrain the mixed layer box model. Quantification of subsurface sink and light-independent source processes can be achieved for example with incubation studies using isotopically labeled substances. Knowledge on either the source or the sink process would help to derive the other from observed concentration profiles using the 1D water column models developed in this thesis.

In total, the results of this thesis improve the understanding of marine emissions of climate relevant sulfur gases and, thus, reduce uncertainties in their atmospheric budget. The outcome sets the base for future model implementations, in order to assess global questions concerning the climate on our planet including dynamic feedback processes.

References

Berry, J.; Wolf, A.; Campbell, J. E.; Baker, I.; Blake, N.; Blake, D.; Denning, A. S.; Kawa, S. R.; Montzka, S. A.; Seibt, U.; Stimler, K.; Yakir, D. & Zhu, Z. (2013): A coupled model of the global cycles of carbonyl sulfide and CO_2: A possible new window on the carbon cycle. *Journal of Geophysical Research: Biogeosciences* **118** (2): 842–852.

Campbell, E.; Kesselmeier, J.; Yakir, D.; Berry, J. A.; Peylin, P.; Belviso, S.; Vesala, T.; Maseyk, K.; Seibt, U.; Chen, H.; Whelan, M.; Hilton, T.; Montzka, S.; Lennartz, S.; Kuai, L.; Wohlfahrt, G.; Wang, Y.; Blake, N. & Blake, D. (2017): Assessing a New Clue to How Much Carbon Plants Store. *EOS Earth and Space Science News*.

Glatthor, N.; Höpfner, M.; Baker, I. T.; Berry, J.; Campbell, J. E.; Kawa, S. R.; Krysztofiak, G.; Leyser, A.; Sinnhuber, B. M.; Stiller, G. P.; Stinecipher, J. & Clarmann, T. v. (2015): Tropical sources and sinks of carbonyl sulfide observed from space. *Geophysical Research Letters*,: 10082–10090.

Kuai, L.; Worden, J. R.; Campbell, J. E.; Kulawik, S. S.; Li, K.-F.; Lee, M.; Weidner, R. J.; Montzka, S. A.; Moore, F. L.; Berry, J. A.; Baker, I.; Denning, A. S.; Bian, H.; Bowman, K. W.; Liu, J. & Yung, Y. L. (2015): Estimate of carbonyl sulfide tropical oceanic surface fluxes using Aura Tropospheric Emission Spectrometer observations. *Journal of Geophysical Research: Atmospheres* **120** (20): 11, 012–11, 023.

Launois, T.; Belviso, S.; Bopp, L.; Fichot, C. G. & Peylin, P. (2015): A new model for the global biogeochemical cycle of carbonyl sulfide - Part 1: Assessment of direct marine emissions with an oceanic general circulation and biogeochemistry model. *Atmos. Chem. Phys.* **15** (5): 2295–2312.

Vincent, R. A. & Dudhia, A. (2017): Fast retrievals of tropospheric carbonyl sulfide with IASI. *Atmos. Chem. Phys.* **17** (4) ACP,: 2981–3000.

Sinikka T. Lennartz

Curriculum Vitae

Education

12/2013 – 05/2017 **Ph.D. student**
Geomar Helmholtz-Zentrum für Ozeanforschung Kiel
WG Prof. Dr. Christa Marandino

10/2011 – 11/2013 **Geoökologie (M. Sc.)**, *(with distinction)*
Carolo-Wilhelmina Technical University Braunschweig, Germany

10/2007– 07/2010 **Geoökologie/Environmental Management (B. Sc.)**,
Eberhard-Karls-University Tübingen, Germany

06/2006 **Abitur**, Main-Taunus-Gymnasium Hofheim, Germany

Research Visits and further Training

04/2013 – 11/2013 **GEOMAR Helmholtz-Centre for Ocean Research Kiel, Germany**

09/2012 – 11/2012 **Woods Hole Oceanographic Institution**, USA

11/2010 – 01/2011 **ECT Ecotoxicology GmbH**, Flörsheim, Germany

03/2010 – 07/2010 **eawag/ETH Zürich**, Switzerland

07/2009 – 09/2009 **Helmholtz-Centre for Environmental Research Leipzig-Halle GmbH**, Lake Research

08/2006 – 07/2007 **Voluntary Service in Ecology (FÖJ)**
Naturschutzbund Deutschland (NABU), Waterfowl Reservation Wallnau, Fehmarn, Germany

Grants and Awards

2016 Selected participant in the 25^{th} Dissertation Symposium on Chemical Oceanography, HI, USA

2015 Scientific Award of the Annette-Barthelt-Foundation for outstanding master thesis

2013 Award of the Matthäi Foundation for outstanding master studies

10/2011 – 11/2013 Scholarship of Heinrich Böll Foundation

04/2009 – 07/2010 Scholarship of Heinrich Böll Foundation

2006 Award of German Chemical Society for best exam in chemistry on Main-Taunus-Gymnasium, Hofheim

Research Expeditions

11/2015	SO243 ASTRA-OMZ, RV Sonne Guayaquil (Ecuador) – Antofagasta (Chile)
07/2014 – 08/2014	SO235 OASIS, RV Sonne Pt. Louis (Mauritius) – Male (Maledives)
2013	several 1-day cruises to time series station Boknis Eck, SW Baltic Sea
07/2012	RV Walther-Herwig III Bremerhaven (Germany) – Lerwick (U.K.)
09/2011	RV Heincke Cuxhaven (Germany) – Heligoland (Germany)
07/2011 – 08/2011	RV Walther-Herwig III Bremerhaven (Germany) – Bremerhaven (Germany)

List of Publications

Peer-reviewed

Lennartz, S. T., Marandino, C. A., von Hobe, M., Cortes, P., Quack, B., Simo, R., Booge, D., Pozzer, A., Steinhoff, T., Arevalo-Martinez, D. L., Kloss, C., Bracher, A., Röttgers, R., Atlas, E., and Krüger, K.: Direct oceanic emissions unlikely to account for the missing source of atmospheric carbonyl sulfide, **Atmos. Chem. Phys.**, 17, 385-402, 10.5194/acp-17-385-2017, 2017.

Hossaini, R., Patra, P. K., Leeson, A. A., Krysztofiak, G., Abraham, N. L., Andrews, S. J., Archibald, A. T., Aschmann, J., Atlas, E. L., Belikov, D. A., Bönisch, H., Carpenter, L. J., Dhomse, S., Dorf, M., Engel, A., Feng, W., Fuhlbrügge, S., Griffiths, P. T., Harris, N. R. P., Hommel, R., Keber, T., Krüger, K., **Lennartz, S. T.**, Maksyutov, S., Mantle, H., Mills, G. P., Miller, B., Montzka, S. A., Moore, F., Navarro, M. A., Oram, D. E., Pfeilsticker, K., Pyle, J. A., Quack, B., Robinson, A. D., Saikawa, E., Saiz-Lopez, A., Sala, S., Sinnhuber, B. M., Taguchi, S., Tegtmeier, S., Lidster, R. T., Wilson, C., and Ziska, F.: A multi-model intercomparison of halogenated very short-lived substances (transcom-vsls): Linking oceanic emissions and tropospheric transport for a reconciled estimate of the stratospheric source gas injection of bromine, **Atmos. Chem. Phys.**, 16, 9163-9187, 10.5194/acp-16-9163-2016, 2016.

Lennartz, S. T., Krysztofiak, G., Marandino, C. A., Sinnhuber, B. M., Tegtmeier, S., Ziska, F., Hossaini, R., Krüger, K., Montzka, S. A., Atlas, E., Oram, D. E., Keber, T., Bönisch, H., and Quack, B.: Modelling marine emissions and atmospheric distributions of halocarbons and dimethyl sulfide: The influence of prescribed water concentration vs. Prescribed emissions, **Atmos. Chem. Phys.**, 15, 11753-11772, 10.5194/acp-15-11753-2015, 2015.

Boyd, P. W., **Lennartz, S. T.**, Glover, D. M., and Doney, S. C.: Biological ramifications of climate-change-mediated oceanic multi-stressors, **Nature Clim. Change**, 5, 71-79, 10.1038/nclimate2441,2015.

Lennartz, S. T., Lehmann, A., Herrford, J., Malien, F., Hansen, H. P., Biester, H., and Bange, H. W.: Long-term trends at the time series station Boknis Eck (Baltic Sea), 1957–2013: Does climate change counteract the decline in eutrophication? , **Biogeosciences**, 11, 7615-7658, 2014.

In press

Campbell, E., Kesselmeier, J., Yakir, D., Berry, J. A., Peylin, P., Belviso, S., Vesala, T., Maseyk, K., Seibt, U., Chen, H., Whelan, M., Hilton, T., Montzka, S., **Lennartz, S.T.**, Kuai, L., Wohlfahrt, G., Wang, Y., Blake, N., and Blake, D.: Assessing a new clue to how much carbon plants store, EOS Earth and Space Science News, 2017.

In review

Schlundt, C., Marandino, C. A., Tegtmeier, S., **Lennartz, S. T.**, Bracher, A., Cheah, W., Krüger, K., and Quack, B.: Oxygenated volatile organic carbon in the western pacific convective centre: Ocean cycling, air-sea gas exchange and atmospheric transport, Atmos. Chem. Phys. Discuss., 2017, 1-29, 10.5194/acp-2017-9, 2017.

Falk, S., Sinnhuber, B. M., Krysztofiak, G., Jöckel, P., Graf, P., and **Lennartz, S. T.**: Brominated VSLS and their influence on ozone under a changing climate, Atmos. Chem. Phys. Discuss., 2017, 1-24, 10.5194/acp-2017-34, 2017.